TABLE OF CONTENTS

SUMMARY 1 1/A6

INTRODUCTION 2 1/A7

LIST OF SYMBOLS 3 1/A8

DESCRIPTION OF DATA BASE 6 1/A11

PREDICTION PROCEDURE 8 1/A13

Equivalent Jet 9 1/A14
Acoustic Power 10 1/B1
Directivity and Overall Mean Square Pressure 11 1/B2
Spectral Distribution 12 1/B3

DATA COMPARISONS 13 1/B4

Static Case Data 14 1/B5
Wind Tunnel Case Data 16 1/B7

CONCLUSIONS 18 1/B9

REFERENCES 20 1/B11

TABLES 21 1/B12

FIGURES 44 1/E7

APPENDIX A Typical Static Case Spectral Distributions 79 2/B2

APPENDIX B Typical Wind Tunnel Case Spectral Distributions 128 2/E9

Item 830-H-14
NAS1.26:3176
JAN 3 1980
COMPLETED
ORIGINAL

NASA Contractor Report 3176

A Method for Predicting the Noise Levels of Coannular Jets With Inverted Velocity Profiles

James W. Russell

CONTRACT NAS1-13500
OCTOBER 1979

NASA

157

NASA Contractor Report 3176

A Method for Predicting the Noise Levels of Coannular Jets With Inverted Velocity Profiles

James W. Russell
Kentron International, Inc.
Hampton, Virginia

Prepared for
Langley Research Center
under Contract NAS1-13500

National Aeronautics
and Space Administration

**Scientific and Technical
Information Branch**

1979

BLANK PAGE

TABLE OF CONTENTS

SUMMARY 1

INTRODUCTION 2

LIST OF SYMBOLS 3

DESCRIPTION OF DATA BASE 6

PREDICTION PROCEDURE 8

- Equivalent Jet 9
- Acoustic Power 10
- Directivity and Overall Mean Square Pressure 11
- Spectral Distribution 12

DATA COMPARISONS 13

- Static Case Data 14
- Wind Tunnel Case Data 16

CONCLUSIONS 18

REFERENCES 20

TABLES 21

FIGURES 44

APPENDIX A Typical Static Case Spectral Distributions 79

APPENDIX B Typical Wind Tunnel Case Spectral Distributions 128

SUMMARY

This report presents a method for predicting the noise characteristics of a coannular jet exhaust nozzle with an inverted velocity profile. The method equates the coannular jet to a single stream equivalent jet with the same mass flow, energy, and thrust as the coannular jet. The acoustic characteristics of the coannular jet are then related to the acoustic characteristics of the single jet. The method presented in this report also includes forward flight effects by incorporating a forward velocity exponent, a Doppler amplification factor, and a Strouhal frequency shift.

A comparison of the prediction method with the model test data shows that (1) for the static cases the spectral correlations were generally greater than 90 percent and the spectral sound pressure level standard deviations were generally less than 4 dB in the aft arc direction. (2) For the static cases, the predicted overall sound pressure levels were generally within 4 dB of the measured values. (3) This method predicts the acoustic characteristics of coannular nozzles without centerbodies better than coannular nozzles with centerbodies located in the primary stream exhaust where the flow must either overexpand or neck down. (4) For the forward flight cases, the method underpredicts the jet noise by approximately 3 dB in the forward arc, and overpredicts the jet noise by approximately 2 dB in the aft arc. (5) For the low velocity forward flight cases the spectral correlation coefficients were greater than 90 percent and the standard deviations of the spectral sound pressure levels were generally less than 4 dB. (6) For both the static and wind tunnel cases the spectral correlations, sound pressure level deviations, and overall sound pressure level differences between measured and predicted values were not affected by changes in equivalent jet velocity.

It is recommended that (1) the forward flight effect on jet noise be reevaluated using additional data to determine whether the Doppler amplification factor exponent should be greater than unity, and that (2) additional data be obtained at higher jet exhaust temperatures and velocities to reduce extrapolation errors incurred in evaluating noise levels of variable cycle engines.

INTRODUCTION

In recent years, advanced engine designs which employ coannular jet exhausts have been studied for application to supersonic transport configurations. These engines are efficient at both supersonic and subsonic flight speeds. The coannular jet exhaust flow scheme has been shown to significantly reduce the engine jet exhaust noise levels during takeoff and landing operations.

The prediction method presented herein was developed from three extensive sets of coannular jet noise model test data sponsored by NASA Lewis Research Center (refs. 1, 2, and 3). These data have been correlated by S. P. Pao of NASA Langley Research Center (ref. 4), which provides the basis for the prediction method.

Because the coannular jet contains twice as many flow parameters as the single jet, the prediction scheme is more complex than the SAE single jet prediction method (ref. 5). The noise emitted from a coannular jet contains two major components: the premerged noise produced by the secondary flow stream and the noise produced by the portion of the jet plume where the two streams have merged. In the forward direction angles, the premerged noise is predominant. However, in the aft arc, there are two distinct peaks to the jet noise spectral distribution. The low frequency peak is associated with the plume noise of the merged jet, and the high frequency peak is associated with the premerged noise of the secondary or outer flow stream.

The method presented herein equates the coannular jet to a single stream equivalent jet which has the same mass flow, energy flow, and thrust as the coannular jet. The acoustical power of the coannular jet is then derived by computing the power of the single jet and applying a coannular jet noise benefit function. From the acoustic power, the overall sound pressure level in a given direction is defined. Then the spectrum is defined which is composed of the premerged and postmerged jet noise components. The prediction method also includes forward flight effects by incorporating a forward velocity exponent and a Doppler amplification factor. Also, the frequency is shifted in proportion to the relative velocity, which is the difference between the nozzle exit velocity and the forward flight velocity.

The following constraints should be applied to the method presented due to the limited data base. The outer to inner stream nozzle exit area ratio should not be less than 0.4 or greater than 2.5. The outer to inner stream velocity ratio should not be less than 1.0. The equivalent jet velocity should be greater than 0.85 times the local ambient speed of sound. The test data upon which this method is based have a range of equivalent jet velocities from just below the ambient speed of sound to 2.5 times the local ambient speed of sound. This prediction method is designed for obtaining free field unattenuated source noise levels. It should be noted that coannular jet area ratio and radius ratio are not included explicitly due to the limitations of the data base.

LIST OF SYMBOLS

A_e	equivalent fully expanded jet area, m^2
A_1	nozzle exit plane area of primary stream, m^2
A_2	nozzle exit plane area of secondary stream, m^2
c_∞	ambient speed of sound, m/s
$D(\theta)$	directivity function
D_e	equivalent jet diameter, m
D_h	hydraulic diameter of secondary stream, m
dB	decibel
f	one-third octave band frequency, Hz
$G(\theta,\sigma)$	normalized spectral distribution in one-third octave band
H	secondary stream annular exit height, m
$\dot{m}_e$	total mass flow of the equivalent jet, kg/s

$\dot{m}_1$	mass flow of the primary stream, kg/s
$\dot{m}_2$	mass flow of the secondary stream, kg/s
n	number of one-third octave band frequencies
OAPWL	overall sound power level, re: 10^{-12} W
$OASPL(\theta)$	predicted overall sound pressure level, re: 2×10^{-5} N/m^2
$OASPL_m(\theta)$	measured overall sound pressure level, re: 2×10^{-5} N/m^2
$\bar{p}^2(\theta)$	predicted overall mean square pressure, N^2/m^4
$\bar{p}^2(\theta,f)$	one-third octave band predicted mean square pressure, N^2/m^4
$\bar{p}_m{}^2(\theta)$	measured overall mean square pressure, N^2/m^4
$\bar{p}_m{}^2(\theta,f)$	one-third octave band measured mean square pressure, N^2/m^4
p_∞	ambient atmospheric pressure, N/m^2
$P(V_e/c_\infty)$	power deviation factor, W
P_{ISA}	international standard atmospheric pressure, N/m^2
$Q(V_e/c_\infty,V_2/V_1)$	power reduction factor, W
r	radial distance between source and observer, m
R	spectral mean square pressure correlation coefficient
S_1	peak Strouhal number of the first spectral component
S_2	peak Strouhal number of the second spectral component

SD	spectral sound pressure level standard deviation, dB
$SPL(\theta,f)$	predicted one-third octave band sound pressure level, re: 2×10^{-5} N/m^2
$SPL_m(\theta,f)$	measured one-third octave band sound pressure level, re: 2×10^{-5} N/m^2
T_e	total temperature of the equivalent single jet, K
T_{ISA}	international standard atmospheric temperature, K
T_1	total temperature of the primary stream, K
T_2	total temperature of the secondary stream, K
T_∞	ambient air temperature, K
V_a	forward velocity of the jet nozzle, m/s
V_e	fully expanded jet velocity of the equivalent jet, m/s
V_1	fully expanded jet velocity of the primary stream, m/s
V_2	fully expanded jet velocity of the secondary stream, m/s
α'	magnitude of peak mean square pressure of second spectral component relative to first spectral component, N^2/m^4
γ_e	ratio of specific heats for the equivalent jet
γ_1	ratio of specific heats for the primary stream
γ_2	ratio of specific heats for the secondary stream
θ	directivity angle from the inlet axis, deg.

Π	total sound power, W
ρ_∞	ambient air density, kg/m^3
ρ_e	density of equivalent jet, kg/m^3
σ_1	normalized Strouhal number for the first spectral component
σ_2	normalized Strouhal number for the second spectral component
ϕ	directivity angle from flight path, deg.
ω	density exponent

DESCRIPTION OF DATA BASE

The inverted flow profile coannular jet data base was obtained from model scale experimental work (refs. 1, 2, and 3). The static tests of references 1 and 2 consist of 98 separate test conditions with three different nozzle configurations. The first two configurations shown in figures 1 and 2 (models 2 and 3) have area ratios of 0.75 and 1.2 respectively. The third configuration (model 4) has a centerbody within the core flow stream which extends past the core flow nozzle exit plane. The area ratio for model 4 of figure 3 is 0.647. The wind tunnel tests of reference 3 consist of 92 separate test conditions with two different nozzle configurations which have inverted flow profiles. The wind tunnel nozzle configurations (models 7 and 8) have area ratios of 0.75 and 1.2 respectively, and are shown in figures 4 and 5. In all models the core flow exit plane was offset from the secondary flow exit plane.

The acoustic data covered thirty one-third octave bands. All the tests were conducted in outdoor facilities using a polar array of microphones. The table below lists the frequency range, directivity range, and microphone distance for each of the test models.

Model	Forward Velocity	Frequency Range	Range of Directivity Angle	Distance to Microphone
2	0	0.1-80 KHz	60 - 165 degrees	4.57 m
3	0	0.1-80 KHz	60 - 165 degrees	4.57 m
4	0	0.05-40 KHz	30 - 160 degrees	12.2 m
7	30-130 m/s	0.1-80 KHz	70 - 150 degrees	3.05 m
8	30-130 m/s	0.01-80 KHz	70 - 150 degrees	3.05 m

The acoustic data were corrected to remove atmospheric attenuation effects in accordance with ARP 866 (ref. 6). Spherical divergence effects were included to correct the data base to a radius of 45.7 m (150 ft). In the case of model 4, the data were also corrected for ground reflection and attenuation effects using the method of reference 2. The forward flight data of models 7 and 8 of reference 3 already have been corrected for the effects of the wind tunnel flow shear layer on the directivity and intensity. In addition, Doppler frequency shifts were incorporated into the data to account for the relative motion effect between the source and the observer. This effect is included in the prediction but is not present in the wind tunnel.

For all cases used in the development of this prediction method, the secondary stream flow velocity was greater than the primary stream flow velocity. The table below lists the range of temperatures and velocities of each flow stream for each of the models.

	Velocity Range, m/s		Temperature Range, K	
Model	Primary	Secondary	Primary	Secondary
2	294 - 624	310 - 872	381 - 1098	380 - 1133
3	298 - 441	319 - 859	389 - 810	702 - 1089
4	291 - 609	295 - 847	286 - 814	392 - 1097
7	284 - 306	303 - 683	370 - 410	390 - 669
8	297 - 307	430 - 638	339 - 407	396 - 710

The applicability of the prediction method presented herein is limited to the velocity range and temperature range of the model test data base. The maximum secondary flow velocity was 872 m/s for the static cases and 683 m/s for the wind tunnel cases, which is less than the 975 m/s for the secondary flow velocity of a varible cycle engine for an SST design. Similarly, the maximum secondary flow total temperature of the data was 1133 K for the static cases and 710 K for the wind tunel cases, which are considerably less than the variable cycle engine secondary flow temperatures of 1750 K.

PREDICTION PROCEDURE

The noise prediction method presented in this report is based on determining the noise characteristics of a single equivalent jet, which has the same total mass flow, energy flow, and thrust as the coannular jet. First, the overall acoustic power level of the coannular jet must be defined. It was found that for the static case (no forward velocity), that the acoustic power of the coannular jet is sometimes as much as 4.0 dB lower than the overall sound power level of the single equivalent jet. The power of the single equivalent jet for the static case is determined using the current SAE prediction method (ref. 5). A jet noise benefit function is employed to obtain the power level of the coannular jet. For the case with forward velocity, a procedure by Hoch (ref. 7) is employed. This procedure employs a power function to account for changes in source strength and sound convection. Also a Doppler amplification factor is used. Both the Doppler factor and the power function vary with directivity angle. The overall sound pressure level in a given direction at a given radius is computed from the overall sound power level using a directivity index which is independent of forward flight velocity. Finally, the one-third octave band sound pressure level is computed by a two component method. The first component is associated with the secondary stream of the premerged jet. The second component is associated with the post merged region of the fully mixed jet. The one-third octave band spectra is corrected for forward velocity effects by basing the Strouhal numbers on the difference between the jet nozzle velocity and the forward flight velocity.

Equivalent Jet

The single equivalent jet has the same mass flow, energy flow, and thrust as the coannular jet. The mass flow of the single equivalent jet is

$$\dot{m}_e = \dot{m}_1 + \dot{m}_2, \tag{1}$$

where

$$\dot{m} = \rho \; A \; V. \tag{2}$$

The condition of equivalence of mass flow and thrust gives

$$V_e = \frac{\dot{m}_1 \; V_1 + \dot{m}_2 \; V_2}{\dot{m}_1 + \dot{m}_2} \; . \tag{3}$$

Since the gas constant for air is not significantly changed by the addition of a small amount of combustion products, the equivalent temperature can be defined from the total energy flow as

$$T_e = \frac{\dot{m}_1 \left(\frac{\gamma_1}{\gamma_1 - 1}\right) T_1 + \dot{m}_2 \left(\frac{\gamma_2}{\gamma_2 - 1}\right) T_2}{\dot{m}_1 \left(\frac{\gamma_1}{\gamma_1 - 1}\right) + \dot{m}_2 \left(\frac{\gamma_2}{\gamma_2 - 1}\right)} \tag{4}$$

where

$$\frac{\gamma}{\gamma - 1} = \frac{c_p}{R} \; . \tag{5}$$

The equivalent specific heat ratio is defined from the mixing of the gases of each stream, as

$$\frac{\gamma_e}{\gamma_e - 1} = \frac{\dot{m}_1 \left(\frac{\gamma_1}{\gamma_1 - 1}\right) + \dot{m}_2 \left(\frac{\gamma_2}{\gamma_2 - 1}\right)}{\dot{m}_1 + \dot{m}_2} \; . \tag{6}$$

Because the fully expanded jet static pressure is equal to the ambient static pressure, the equivalent jet density is

$$\rho_e = \rho_\infty \left\{ \frac{T_e}{T_\infty} - \frac{\gamma_e - 1}{2} \left(\frac{V_e}{c_\infty} \right)^2 \right\}^{-1} . \tag{7}$$

The equivalent area is (from equation 2)

$$A_e = \frac{\dot{m}_e}{\rho_e V_e} , \tag{8}$$

the equivalent jet diameter is

$$D_e = \left(\frac{4 A_e}{\pi} \right)^{1/2} , \tag{9}$$

and the secondary stream hydraulic diameter is

$$D_h = 2H. \tag{10}$$

Acoustic Power

The jet acoustic power Π is calculated for the single jet using the current SAE prediction method (ref. 5) and applying a coannular jet power benefit function, Q.

$$\Pi = 6.67 \times 10^{-5} \; \rho_\infty \; c_\infty^3 \, A_e \left(\frac{\rho_e}{\rho_\infty} \right)^\omega \left(\frac{V_e}{c_\infty} \right)^8 P \left(\frac{V_e}{c_\infty} \right) Q \left(\frac{V_e}{c_\infty} , \frac{V_2}{V_1} \right) . \tag{11}$$

The density exponent, ω, is the same as in reference 5 and is given as a function of V_e/c_∞ in table 1 and figure 6. The power deviation factor $P(V_e/c_\infty)$ represents the deviation of sound power from the U^8 law of dependence and is shown in table 2 and figure 7. The coannular jet power benefit function $Q(V_e/c_\infty, V_2/V_1)$ is shown in table 3 and figure 8.

The overall sound power level can be obtained from equation 11 as

$$\text{OAPWL} = 10\ \text{Log}_{10} \left\{ \left(\frac{\Pi}{\rho_\infty c_\infty^{\ 3} A_e} \right) \left(\frac{p_\infty}{p_{ISA}} \right) \sqrt{\frac{T_\infty}{T_{ISA}}} \right\} + 197\ \text{dB}. \qquad (12)$$

The effect of forward flight on acoustic power includes the Doppler amplification factor and a velocity exponent. Both of these terms are related to the directivity angle. Therefore the forward velocity effect is included along with the directivity effects in the determination of the mean square pressure.

Directivity and Overall Mean Square Pressure

The mean square pressure at a given observer position relative to the position of the jet is

$$\bar{p}^2(\theta) = \frac{\rho_\infty\ c_\infty}{4\pi r^2} \frac{D(\theta, V_e/c_\infty)}{(1-V_a\ \cos\phi/c_\infty)} \left(\frac{V_e - V_a}{V_e} \right)^{m(\theta)}, \qquad (13)$$

where r is the distance between the source and the observer, and $D(\theta, V_e/c_\infty)$ is the normalized directivity factor and is given in table 4 and figure 9. The forward velocity exponent function $m(\theta)$ was taken from Hoch (ref. 7) and is presented in table 5 and figure 10. The Doppler amplification factor $(1 - V_a/c_\infty \cos\phi)$ depends on the angle between the flight path vector and the vector between the source and observer. This angle, denoted as, ϕ, is different than the directivity angle, θ, when the jet axis is not along the flight path. Figure 11 shows the geometric variables used for computing the overall mean square pressure at a particular directivity angle.

The overall sound pressure level, computed from the mean square pressure, is:

$$\text{OASPL} = 10\ \text{Log}_{10} \left\{ \frac{\bar{p}^2(\theta)}{\rho_\infty^{\ 2}\ c_\infty^{\ 4}} \left(\frac{p_\infty}{p_{ISA}} \right)^2 \right\} + 197\ \text{dB}. \qquad (14)$$

Spectral Distribution

The one-third octave band spectra in a given direction are composed of a single component for directivity angles below 110 degrees where the high velocity, secondary stream jet noise is predominant. At directivity angles equal to or greater than 110°, the one-third octave band spectra consist of two components. The low frequency component is associated with the jet noise from the merged portion of the exhaust, and the high frequency component is associated with the secondary stream flow. Figure 12 shows a diagram of the two component spectra. The peak Strouhal number of the first spectral component $S_1(V_e/c_\infty, \theta)$ applies to all directivity angles. For directivity angles equal to or greater than 110°, there is a second component peak Strouhal number, $S_2(V_e/c_\infty, \theta)$. The values of S_1 and S_2 are listed in tables 6 and 7 and are shown in figures 13 and 14, respectively.

Figure 12 shows that there is a difference in amplitude between the first and second peaks. At directivity angles equal to or greater than 110 degrees, the parameter, α', indicates the relative magnitudes of the mean square pressure of the second peak with respect to the first peak. α' is defined from the parameter, $\alpha(V_e/c_\infty, V_2/V_1, \theta)$ as

$$\alpha' = \alpha \frac{A_2}{A_e} . \tag{15}$$

The values of α are presented in table 8 and figure 15.

The one-third octave band mean square pressure

$$\bar{p}^2(\theta,f) = \bar{p}^2(\theta) \quad G(\theta,\sigma_1) \qquad , \text{ for } \theta < 110°, \tag{16}$$

and

$$\bar{p}^2(\theta,f) = \bar{p}^2(\theta) \left(\frac{G(\theta,\sigma_1)}{1 + \alpha'} + \frac{\alpha' G(\theta,\sigma_2)}{1 + \alpha'} \right) \text{ , for } \theta \geq 110°, \tag{17}$$

where the values of $G(\theta,\sigma)$ are given in table 9 and figure 16. The values of σ_1 and σ_2 are defined from S_1 and S_2 by

$$\sigma_1 = \frac{f\,D_e}{S_1(V_e - V_a)} \left(\frac{T_e}{T_\infty}\right)^{0.4}, \tag{18}$$

and

$$\sigma_2 = \frac{f\,D_h}{S_2(V_e - V_a)} \left(\frac{T_e}{T_\infty}\right)^{0.4}. \tag{19}$$

The forward flight effect is incorporated into equations 18 and 19 in the computation of the peak frequency, the frequency corresponding to a σ value of 1.0. This frequency is dependent on the difference between the nozzle jet exhaust velocity and the aircraft forward flight velocity. A temperature correction factor is included in equations 18 and 19 which corresponds with the frequency shift due to temperature in accordance with the SAE single jet method of reference 5.

The one-third octave band sound pressure level is defined by

$$SPL(\theta,f) = OASPL(\theta) + 10\ \mathrm{Log}_{10}\ G(\theta,\sigma_1),\ \text{for } \theta < 110°, \tag{20}$$

and

$$SPL(\theta,f) = OASPL(\theta) + 10\ \mathrm{Log}_{10} \left(\frac{G(\theta,\sigma_1)}{1 + \alpha'} + \frac{\alpha' G(\theta,\sigma_2)}{1 + \alpha'}\right), \tag{21}$$

for $\theta \geq 110°$.

DATA COMPARISONS

Comparisons were made to evaluate the prediction method against the model test data for 48 static cases from references 1 and 2 and 22 wind tunnel cases from reference 3. The predicted values were corrected to incorporate shock noise as well as jet noise, as shock noise does exist in the model data. The shock noise was predicted over the range of frequencies and directivity angles for each case using Stone's method from reference 8. For each case at each directivity angle for which spectra data are available, the spectral mean square pressure correlation coefficient, the spectral sound pressure level standard deviation, and the overall sound pressure level difference between the measured and predicted values were computed.

The mean square pressure correlation coefficient, R, for a range of n one-third octave band frequencies is

$$R = \frac{\sum_{i=1}^{n} [\bar{p}^2(\theta,i) \quad \bar{p}^2_m(\theta,i)]}{\left\{\sum_{i=1}^{n} [\bar{p}^2(\theta,i)]^2 \quad \sum_{i=1}^{n} [\bar{p}^2_m(\theta,i)]^2\right\}^{1/2}} . \tag{22}$$

The spectral sound pressure level standard deviation, SD, in units of decibels for a range of n one-third octave band frequencies is

$$SD = \left\{\frac{\sum_{i=1}^{n} [SPL(\theta,i) - SPL_m(\theta,i)]^2}{(n - 1)}\right\}^{1/2} \tag{23}$$

The difference between the predicted and measured overall sound pressure level, OASPL, at each directivity angle is

$$\Delta OASPL(\theta) = OASPL(\theta) - OASPL_m(\theta). \tag{24}$$

The data comparison study consists of two parts: the static comparison and the forward flight comparisons.

Static Case Data

The static data comparison consists of evaluating 48 typical data cases. These include 33 cases from reference 1 (models 2 and 3) and 15 cases from reference 2 (model 4). Table 10 lists the flow properties for the 48 cases including equivalent velocity and the ratio of the secondary flow velocity to the primary flow velocity. Table 11 shows the spectral mean square pressure correlation coefficient, the spectral sound pressure level standard deviation, and the difference in overall sound pressure level between the measured and predicted values for each case at nine directivity angles.

The variation of the comparison parameters of table 11 with normalized equivalent velocity are shown on figures 17, 18, and 19, respectively, at directivity angles of 60, 90, 120, and 150 degrees.

Figure 17 shows that at 90 and 120 degrees the correlation coefficient exceeds 90 percent except in 7 cases. At 60 degrees it can be seen that there is considerable discrepancy which is partially attributable to the relatively low jet noise levels. At 150 degrees the model 4 cases generally seem to have a low correlation, whereas only 4 of the model 2 and model 3 cases are below 90 percent. This may be due to the fact that the jet exhaust flow of model 4 overexpands as it flows over the plug surface.

Figure 18 shows the variation of standard deviation of the spectral sound pressure levels with normalized equivalent velocity for the 48 data cases. From figure 18 it can be seen that at 90, 120, and 150 degrees less than 7 cases exceed a standard deviation of 4 dB, whereas at 60 degrees almost a third of the cases exceed a standard deviation of 4 dB. The standard deviation indicates a discrepancy between the measured and predicted values but does not indicate the direction of this discrepancy. Therefore the difference in overall sound pressure levels for these 48 cases were determined.

Figure 19 shows the variation of the difference between predicted and measured overall sound pressure levels with normalized equivalent velocity for the 48 data cases at directivity angles of 60, 90, 120, and 150 degrees. Figure 19 shows that at 90 degrees, the method overpredicts for model 2 and underpredicts for models 3 and 4. At 120 degrees the method underpredicts the noise of model 4, whereas models 2 and 3 appear to not be biased. At 150 degrees the predicted OASPL levels average slightly higher than the measured values, except at the lower equivalent jet velocities, where they are 2 to 4 dB higher. At 60 degrees it can be seen that there is considerable scatter in the OASPL differences. This corresponds to the low jet noise level problems that were seen in figures 17 and 18.

From table 11 and these figures 17, 18, and 19, it can be seen that the prediction method does not correlate better at higher jet velocities than at lower velocities. Also at angles below 90 degrees, there are some large discrepancies between the prediction method and the measured data, which can be partially attributed to the lower levels of jet noise which are produced in the forward arc and thus to the lower difference in noise level between the jet noise and the background noise.

Appendix A shows spectral plots of the measured and predicted sound pressure levels for 16 of the 48 static data cases.

Wind Tunnel Case Data

The wind tunnel or forward flight data comparison consists of evaluating 22 typical data cases of reference 3 (models 7 and 8). Table 12 lists the flow properties for the 22 cases including equivalent velocity and the ratio of the secondary stream velocity to the primary stream velocity. In the wind tunnel test, the microphones are stationary with respect to the nozzle, whereas in forward flight they are not. However, the power level and directivity are affected by the wind tunnel flow velocity which alters the strength and direction of the acoustic waves. Also, the frequency is shifted by the wind tunnel flow. However, the frequency shift defined by equations 18 and 19 has incorporated a Doppler shift. Therefore, to correct from forward flight prediction to wind tunnel prediction, the predicted forward flight frequencies were corrected by the Doppler frequency shift which is

$$f_{\text{wind tunnel}} = f_{\text{forward flight}} \left[1 - V_a/c_\infty \cos(\theta)\right]. \qquad (25)$$

Table 13 shows the spectral mean square pressure correlation coefficient, the spectral sound pressure level standard deviation, and the difference in overall sound pressure level between the measured and predicted values for each case at the nine directivity angles for which measured data are available. Figures 20, 21, and 22 respectively show the variation of these comparison parameters as a function of normalized equivalent velocity at directivity angles of 70, 90, 120, and 150 degrees. Appendix B shows comparisons between the predicted and measured spectral sound pressure level distributions for several typical wind tunnel data cases at directivity angles of 70, 90, 120, and 150 degrees. The spectral plots of Appendix B show that in the high frequency range the measured data rises abnormally. This was attributed to electrical interference and therefore the four highest frequencies were not included in evaluating this prediction method.

From table 13 and figure 20 it can be seen that the correlation coefficients are generally close to or above 90 percent except for the high forward velocity cases. Figures B1, B4, B7, and B8 of Appendix B show typical spectral plots for these high velocity cases. From these four figures, it can be seen that there appears to be something other than jet or shock noise present at the low frequencies. Furthermore, this low frequency interference phenomenon increases as the directivity angle increases and also as the forward velocity increases. Therefore, at the higher forward velocities figure 20 shows that the correlation coefficient is low.

Table 13 and figure 21 show that at the low forward velocities the spectral sound pressure level standard deviation is less than 4 dB except at the directivity angle of 150 degrees where it varies from 4 dB to almost 6 dB. However, at the higher forward velocities the standard deviation is large due to the low frequency interference phenomenon.

From table 13 and figure 22 it can be seen that the method underpredicts the overall sound pressure level at all directivity angles except at 150 degrees where the method overpredicts. The amount of discrepancy in the overall sound pressure level is about 3.5 dB at 70 degrees, 1.5 dB at 90 degrees, 2 dB at 120 degrees, and -2.0 to +2.0 dB at 150 degrees. In general there appears to be no trend in the overall sound pressure level difference with changes in either the jet velocity or forward velocity. Also at a directivity angle of 90 degrees it is anticipated that the overall sound pressure level discrepancy will be at a minimum because the forward velocity effect is reduced to zero in the prediction method per equations 13 and 18.

The prediction method is acceptable at directivity angles of 90 and 120 degrees. At the directivity angle of 70 degrees the method predicts low at all forward flight speeds. At the directivity angle of 150 degrees at the higher flight velocities the prediction method is poor in that it overpredicts the jet noise overall sound pressure level by as much as 3 dB.

In general this prediction method is acceptable for the forward flight cases. However for comparison purposes it should be noted that in reference 3, a least squares fit of the data was made and a forward velocity power index and Doppler amplification factor for noise convection were determined. Using the method of this report the power index of equation 13 shown in table 5 and figure 10 is about the same as the forward velocity power index factor of reference 3. However, the Doppler amplification factor of equation 13 is raised to the first power in the presented prediction method. In the data correlation of reference 3, the Doppler amplification factor is raised to a power of 4 at a directivity angle of 70 degrees and to a power of 10 at a directivity angle of 150 degrees. The value of the Doppler amplification factor exponent also depends on the total pressure ratio. The fact that this Doppler amplification factor exponent is considerably greater than unity and that it was derived from test data correlations indicates that the prediction method presented herein will underpredict the jet noise at directivity angles below 90 degrees, and overpredict the jet noise at directivity angles above 90 degrees. Furthermore, the amount of discrepancy will increase as the forward velocity increases. However, the amount of OASPL discrepancy in the method of this report is generally less than 2 dB at directivity angles of 90, 120 and 150 degrees, which is probably within the range of the model test data scatter.

CONCLUSIONS

For the static case data without the centerbody plug the coannular jet prediction method presented herein yields correlation coefficients above 90 percent at directivity angles of 90, 120, and 150 degrees. For the static case data with the centerbody plug the correlation coefficient is lower at a directivity angle of 150 degrees. One reason for this difference may be due to the overexpansion, or turning, of the flow as it passes over the centerbody plug. The standard deviations for all the nozzle configurations were generally less than 4 dB at directivity angles of 90, 120, and 150 degrees. At the directivity angle of 60 degrees, where the jet noise levels are relatively low and the data may be affected by background noise, the correlation coefficients were sometimes considerably less than 90 percent and the standard deviations sometimes exceed 10 dB. In general the overall sound pressure levels were predicted within 4 dB at directivity angles of 60, 90, and 150 degrees. At 120 degrees the method appeared to underpredict by sometimes more than 6 dB.

For the wind tunnel cases, the coannular jet prediction method presented herein yields correlation coefficients above 90 percent for the lower forward velocities at directivity angles of 70, 90, 120, and 150 degrees. Also at the lower forward velocities, the standard deviations were less than 4 dB at directivity angles of 60, 90, and 120 degrees, and varied from 4 to 6 dB at the directivity angle of 150 degrees. At the higher forward velocities, there appeared to be some low frequency interference phenomenon which increased as the directivity angle increased and as the forward velocity increased. Therefore at the higher forward velocities the correlation coefficient and standard deviation were not good. However this low frequency phenomenon did not affect the SPL values near the peak level, and therefore did not affect the overall sound pressure levels. For the forward velocity cases the difference between the measured and predicted overall sound pressure levels were less than 4 dB at directivity angles of 70, 90, 120, and 150 degrees, except for two cases at 70 degrees.

For the forward flight cases this method underpredicts the jet noise by approximately 3 dB in the forward arc as shown on Figure 22a. Similarly, at the higher directivity angles this method overpredicts the jet noise by approximately 2 dB, as shown on Figure 22d. To correct this a Doppler amplification factor exponent could be employed in addition to the forward velocity exponent.

For both the static and wind tunnel cases changes in equivalent jet velocity did not affect the correlation coefficients, the sound pressure level standard deviations, or the difference between the measured and predicted overall sound pressure levels.

Since, at supersonic jet velocities, a shock noise prediction is included in the jet noise correlation and the results obtained were found to be satisfactory, it is evident that shock noise is present in the model test data.

The applicability of the prediction method presented herein is limited to the velocity range and temperature range of the model test data base.

REFERENCES

1. Kozlowski, H.; and Packman, A. B.: Pratt and Whitney Data Base on Model Coannular Jet, NASA CR-134910, Pratt and Whitney Aircraft Company, February 1977.

2. Allan, R. D.; and Joy, W.: Comprehensive Data Report - Acoustic Tests of Duct-Burning Turbofan Jet Noise Simulation, NASA CR-135236, General Electric Co., November 1977.

3. Kozlowski, Hilary; and Packman, Allan B.: Flight Effects on the Aero/Acoustic Characteristics of Inverted Profile Coannular Nozzles, NASA CR-3018, 1978.

4. Pao, S. P.: A Correlation of Mixing Noise from Coannular Jets with Inverted Flow Profiles, NASA TP-1301, 1979.

5. Aerospace Recommended Practice Procedure 876, Gas Turbine Jet Exhaust Noise Prediction, March 1978.

6. Aerospace Recommended Practice Procedure 866, Standard Values of Atmospheric Absorption as a Function of Temperature and Humidity for use in Evaluating Aircraft Flyover Noise, Society of Automotive Engineers, March 1978.

7. Hoch, R. G.; Duponchel, J. P.; Cocking, B. J.; and Bryce, W. D.: Studies of the Influence of Density on Jet Noise, Paper presented at the First International Symposium on Airbreathing Engines, Marseille, June 1972.

8. Stone, J. R.: Interim Prediction Method for Jet Noise, NASA TM X-71618, 1974.

TABLE 1.

JET NOISE DENSITY EXPONENT.

$\text{Log}_{10}\ (V_e/c_\infty)$	ω
-0.4	-0.90
-0.35	-0.76
-0.30	-0.58
-0.25	-0.41
-0.20	-0.22
-0.15	0.0
-0.10	0.22
-0.05	0.50
0.0	0.77
0.05	1.07
0.10	1.39
0.15	1.74
0.20	1.95
0.25	2.0
0.30	2.0
0.35	2.0
0.40	2.0

TABLE 2.

POWER DEVIATION FACTOR.

$\log_{10}(V_e/c_\infty)$	$10\log_{10}(P)$, dB
-0.40	-1.3
-0.35	-1.3
-0.30	-1.3
-0.25	-1.3
-0.20	-1.3
-0.15	-1.2
-0.10	-1.0
-0.05	-0.5
0.0	0.0
0.05	1.0
0.10	2.1
0.15	3.2
0.20	4.1
0.25	4.3
0.30	4.1
0.35	3.1
0.40	1.4

TABLE 3.

COANNULAR JET NOISE POWER REDUCTION FACTOR.

10 $\text{Log}_{10}(Q)$, dB

V_2/V_1	$\text{Log}_{10}(V_e/c_\infty)$						
	0.00	.05	.10	.15	.20	.25	.30
1.0	0.0	0.0	0.0	0.0	0.0	0.0	0.0
1.1	0.0	0.0	0.0	0.0	0.0	0.0	0.0
1.2	0.0	0.0	0.0	1.0	1.0	1.0	.5
1.3	0.0	1.0	1.0	2.0	2.0	1.5	1.0
1.4	0.0	1.0	1.5	3.0	3.0	2.0	1.5
1.5	0.0	1.0	2.0	3.0	3.5	3.0	2.0
1.6	0.0	1.5	2.0	3.0	4.0	3.5	2.5
1.7	0.0	1.0	2.0	3.0	4.0	4.0	3.0
1.8	0.0	1.0	1.5	2.5	4.0	4.0	3.5
1.9	0.0	1.0	1.5	2.5	3.5	4.0	4.0
2.0	0.0	1.0	1.5	2.5	3.0	4.0	4.0
2.1	0.0	1.0	1.5	2.0	2.5	4.0	4.0
2.2	0.0	.5	1.0	1.5	2.5	3.5	4.0
2.3	0.0	.5	1.0	1.5	2.0	3.0	4.0
2.4	0.0	.5	1.0	1.5	2.0	2.5	4.0
2.5	0.0	.5	.5	1.0	2.0	2.5	3.5
2.6	0.0	.5	.5	1.0	1.5	2.0	3.0
2.7	0.0	0.0	.5	1.0	1.5	2.0	2.5
2.8	0.0	0.0	.5	.5	1.0	1.5	2.5
2.9	0.0	0.0	0.0	.5	1.0	1.5	2.0
3.0	0.0	0.0	0.0	.5	1.0	1.5	2.0

TABLE 4.

COANNULAR JET NOISE DIRECTIVITY INDEX,

10 $\text{Log}_{10}(D)$, dB

Directivity angle, θ	$\text{Log}_{10}(V_e/c_\infty)$							
	0.00	.05	.10	.15	.20	.25	.30	.35
0	-8.60	-9.70	-11.55	-12.40	-13.02	-13.44	-13.98	-14.49
10	-8.40	-9.50	-11.35	-12.15	-12.72	-13.14	-13.63	-14.09
20	-8.20	-9.30	-11.10	-11.85	-12.42	-12.84	-13.28	-13.69
30	-8.00	-9.10	-10.85	-11.55	-12.02	-12.44	-12.93	-13.19
40	-7.70	-8.80	-10.55	-11.15	-11.62	-12.04	-12.37	-12.69
50	-7.40	-8.50	-10.25	-10.75	-11.17	-11.54	-11.84	-12.09
60	-7.00	-8.10	-9.85	-10.35	-10.72	-11.02	-11.20	-11.39
70	-6.40	-7.70	-8.98	-9.35	-9.68	-9.88	-10.16	-10.20
80	-5.70	-6.80	-7.60	-7.98	-8.22	-8.43	-8.53	-8.70
90	-4.70	-5.80	-6.41	-6.75	-6.45	-7.06	-7.09	-7.00
100	-3.20	-4.10	-4.71	-5.06	-5.33	-5.47	-5.59	-5.60
110	-1.30	-2.00	-2.46	-2.74	-2.95	-3.08	-3.19	-3.20
120	.90	.50	.14	-.02	-.13	-.16	-.16	-.10
130	3.40	3.20	3.04	3.04	3.03	3.06	3.12	3.20
140	5.20	5.70	5.99	6.26	6.45	6.61	6.68	6.71
150	6.30	7.00	7.49	7.81	7.95	8.02	8.08	8.09
160	6.10	6.30	6.55	6.14	5.97	5.73	5.60	5.50
170	5.10	4.50	3.64	2.96	2.33	1.74	1.18	1.20
180	4.60	3.80	2.94	2.26	1.63	.99	.46	.60

TABLE 5.

JET NOISE FORWARD VELOCITY INDEX.

Directivity Angle, θ	m(θ)
0	3.0
10	1.65
20	1.1
30	0.5
40	0.2
50	0.0
60	0.0
70	0.1
80	0.4
90	1.0
100	1.9
110	3.0
120	4.7
130	7.0
140	8.5
150	8.5
160	8.5
170	8.5
180	8.5

TABLE 6.

LOCATION OF FIRST PEAK STROUHAL NUMBER.

$\text{Log}_{10}(S_1)$

Directivity angle, θ	$\text{Log}_{10}(V_e/c_\infty)$							
	0.00	.05	.10	.15	.20	.25	.30	.35
90	0.00	0.00	0.00	0.00	0.00	0.00	0.00	0.00
100	-.05	-.05	-.05	-.05	-.05	-.05	-.05	-.05
110	-.12	-.12	-.12	-.12	-.12	-.12	-.12	-.12
120	-.22	-.22	-.22	-.22	-.22	-.22	-.23	-.24
130	-.33	-.33	-.33	-.33	-.33	-.35	-.36	-.37
140	-.42	-.42	-.42	-.42	-.42	-.45	-.49	-.53
150	-.50	-.50	-.50	-.50	-.52	-.57	-.62	-.66
160	-.58	-.59	-.61	-.62	-.65	-.77	-.87	-.94
170	-.75	-.77	-.79	-.82	-.88	-1.06	-1.17	-1.25

TABLE 7.

LOCATION OF SECOND PEAK STROUHAL NUMBER.

$\text{Log}_{10}(S_2)$

Directivity angle, θ	$\text{Log}_{10}(V_e/c_\infty)$							
	0.00	.05	.10	.15	.20	.25	.30	.35
110	-.59	-.59	-.59	-.59	-.59	-.59	-.59	-.59
120	-.34	-.35	-.35	-.36	-.37	-.39	-.41	-.45
130	-.24	-.24	-.24	-.24	-.25	-.29	-.39	-.52
140	-.21	-.20	-.18	-.18	-.25	-.38	-.50	-.66
150	-.06	-.12	-.19	-.27	-.36	-.48	-.60	-.89
160	-.06	-.13	-.22	-.31	-.43	-.56	-.87	-1.27
170	-.03	-.13	-.24	-.36	-.52	-.69	-1.04	-1.34

TABLE 8.

FACTOR RELATING RELATIVE HEIGHT OF SECOND SPECTRAL PEAK TO FIRST SPECTRAL PEAK.

$10 \text{ Log}_{10}(\alpha)$

Directivity angle = 110 degrees								
V_2/V_1	$\text{Log}_{10}(V_e/c_\infty)$							
	0.00	.05	.10	.15	.20	.25	.30	.35
1.0	3.70	3.70	3.70	3.70	3.70	3.70	3.70	3.70
1.1	3.70	3.70	3.70	3.70	3.70	3.70	3.70	3.70
1.2	3.70	3.70	3.70	3.70	3.70	3.70	3.70	3.70
1.3	3.70	3.70	3.70	3.70	3.70	3.70	3.70	3.70
1.4	3.70	3.70	3.70	3.70	3.70	3.70	3.70	3.70
1.5	3.70	3.70	3.70	3.70	3.70	3.70	3.70	3.70
1.6	3.70	3.70	3.70	3.70	3.70	3.70	3.70	3.70
1.7	3.70	3.70	3.70	3.70	3.70	3.70	3.70	3.70
1.8	3.70	3.70	3.70	3.70	3.70	3.70	3.70	3.70
1.9	3.70	3.70	3.70	3.70	3.70	3.70	3.70	3.70
2.0	3.70	3.70	3.70	3.70	3.70	3.70	3.70	3.70
2.1	3.70	3.70	3.70	3.70	3.70	3.70	3.70	3.70
2.2	3.70	3.70	3.70	3.70	3.70	3.70	3.70	3.70

Directivity angle = 120 degrees								
V_2/V_1	$\text{Log}_{10}(V_e/c_\infty)$							
	0.00	.05	.10	.15	.20	.25	.30	.35
1.0	3.58	3.58	3.58	3.58	3.58	3.58	3.58	3.58
1.1	3.59	3.59	3.60	3.61	3.62	3.62	3.63	3.63
1.2	3.61	3.63	3.64	3.66	3.68	3.70	3.72	3.72
1.3	3.70	3.70	3.70	3.70	3.70	3.72	3.75	3.90
1.4	3.75	3.75	3.76	3.77	3.78	3.79	3.82	3.90
1.5	3.80	3.82	3.83	3.85	3.88	3.92	3.96	4.05
1.6	3.81	3.86	3.92	3.99	4.02	4.05	4.11	4.20
1.7	3.97	4.01	4.05	4.10	4.14	4.18	4.24	4.32
1.8	4.09	4.13	4.17	4.22	4.25	4.28	4.34	4.40
1.9	4.25	4.28	4.31	4.35	4.36	4.40	4.46	4.55
2.0	4.40	4.44	4.48	4.53	4.55	4.59	4.65	4.71
2.1	4.61	4.64	4.67	4.71	4.73	4.76	4.81	4.87
2.2	4.61	4.64	4.67	4.71	4.73	4.76	4.81	4.87

Table 8. - Continued.

10 $\log_{10}(\alpha)$

Directivity angle = 130 degrees								
V_2/V_1	$\log_{10}(V_e/c_\infty)$							
	0.00	.05	.10	.15	.20	.25	.30	.35
1.0	-6.88	-5.43	-3.70	-1.96	-.10	1.59	2.97	3.80
1.1	-4.14	-3.04	-1.81	-.42	.98	2.37	3.38	4.19
1.2	-2.53	-1.62	-.60	.54	1.75	2.92	3.73	4.46
1.3	-1.20	-.41	.47	1.46	2.23	3.31	4.07	4.82
1.4	-.24	.45	1.23	2.10	2.82	3.61	4.41	5.06
1.5	.78	1.34	1.97	2.68	3.36	4.07	4.76	5.28
1.6	1.68	2.14	2.66	3.24	3.89	4.51	5.09	5.48
1.7	2.48	2.86	3.30	3.78	4.38	4.92	5.40	5.66
1.8	3.16	3.49	3.86	4.28	4.82	5.30	5.69	5.88
1.9	3.68	3.98	4.32	4.71	5.20	5.61	5.95	6.04
2.0	4.02	4.32	4.65	5.03	5.47	5.84	6.11	6.20
2.1	4.15	4.46	4.81	5.21	5.61	5.97	6.21	6.30
2.2	4.15	4.46	4.81	5.21	5.61	5.97	6.21	6.30

Directivity angle = 140 degrees								
V_2/V_1	$\log_{10}(V_e/c_\infty)$							
	0.00	.05	.10	.15	.20	.25	.30	.35
1.0	-13.68	-12.24	-10.64	-8.85	-6.93	-4.94	-3.41	-1.99
1.1	-9.90	-8.75	-7.45	-6.00	-4.37	-2.81	-1.38	-.16
1.2	-6.89	-5.89	-4.76	-3.50	-2.22	-.99	.21	1.36
1.3	-4.54	-3.68	-2.73	-1.64	-.64	.50	1.43	2.45
1.4	-2.52	-1.81	-1.01	-.12	.76	1.66	2.50	3.56
1.5	-.59	-.08	.50	1.15	1.95	2.75	3.51	4.35
1.6	.91	1.37	1.89	2.47	3.05	3.77	4.38	5.04
1.7	2.09	2.51	2.98	3.51	4.01	4.61	5.12	5.63
1.8	2.92	3.31	3.76	4.25	4.76	5.24	5.66	6.12
1.9	3.64	4.00	4.40	4.86	5.27	5.69	6.05	6.44
2.0	4.29	4.60	4.95	5.35	5.72	6.08	6.35	6.72
2.1	4.82	5.12	5.45	5.83	6.32	6.40	6.83	6.90
2.2	4.82	5.12	5.45	5.83	6.32	6.40	6.83	6.90

Table 8. - Concluded.

10 $\mathrm{Log}_{10}(\alpha)$

Directivity angle = 150 degrees								
V_2/V_1	$\mathrm{Log}_{10}(V_e/c_\infty)$							
	0.00	.05	.10	.15	.20	.25	.30	.35
1.0	-22.33	-19.72	-16.79	-13.51	-9.89	-6.53	-4.17	-2.81
1.1	-16.66	-14.61	-12.32	-9.74	-6.87	-4.00	-2.22	-.62
1.2	-13.82	-11.84	-9.63	-7.15	-4.44	-2.20	-.60	.65
1.3	-9.65	-7.92	-5.98	-3.80	-1.77	-.37	.93	2.05
1.4	-4.89	-4.03	-3.08	-2.00	-.54	.63	1.71	2.68
1.5	-3.33	-2.45	-1.46	-.36	.69	1.63	2.48	3.31
1.6	-1.69	-.97	-.16	.74	1.58	2.35	3.02	3.74
1.7	-.20	.41	1.08	1.84	2.54	3.16	3.70	4.32
1.8	.98	1.48	2.04	2.67	3.26	3.78	4.30	4.84
1.9	2.11	2.54	3.03	3.57	4.07	4.54	5.04	5.48
2.0	3.26	3.64	4.06	4.52	4.95	5.35	5.69	6.05
2.1	4.37	4.67	5.00	5.38	5.74	6.03	6.32	6.59
2.2	5.38	5.73	6.12	6.57	6.88	7.13	7.37	7.57

Directivity angle = 160 degrees								
V_2/V_1	$\mathrm{Log}_{10}(V_e/c_\infty)$							
	0.00	.05	.10	.15	.20	.25	.30	.35
1.0	-37.12	-32.31	-26.91	-20.85	-15.03	-6.67	1.69	4.05
1.1	-31.91	-27.77	-23.13	-17.93	-12.48	-4.86	1.99	3.88
1.2	-27.88	-24.12	-19.99	-15.16	-9.99	-3.24	2.21	3.76
1.3	-22.65	-19.60	-16.18	-12.34	-7.59	-1.86	2.33	3.69
1.4	-18.20	-15.73	-12.95	-9.84	-5.65	-.91	2.42	3.64
1.5	-15.67	-13.33	-10.71	-7.76	-4.19	-.14	2.55	3.57
1.6	-13.17	-11.07	-8.72	-6.07	-3.09	.45	2.59	3.54
1.7	-10.94	-9.14	-7.13	-4.87	-2.15	.93	2.64	3.52
1.8	-10.13	-8.27	-6.17	-3.83	-1.39	1.28	2.72	3.47
1.9	-9.38	-7.52	-5.42	-3.06	-.73	1.61	2.75	3.45
2.0	-8.73	-6.87	-4.77	-2.43	-.25	1.80	2.77	3.44
2.1	-8.23	-6.38	-4.31	-1.98	.12	1.93	2.77	3.44
2.2	-7.81	-5.98	-3.93	-1.62	.39	1.90	2.77	3.44

TABLE 9.

NORMALIZED SPECTRAL DISTRIBUTION.

10 Log$_{10}$(G), dB

LOG10 (σ=8)	DIRECTIVITY ANGLE,θ,DEGREES						
	≥110	120	130	140	150	160	170
-1.2	-25.60	-26.72	-31.32	-36.15	-41.30	-50.00	-52.20
-1.1	-23.60	-24.52	-28.42	-32.55	-37.40	-44.60	-47.10
-1.0	-22.00	-22.32	-25.52	-28.95	-33.50	-39.20	-42.00
-.9	-20.20	-20.12	-22.62	-25.35	-29.60	-33.20	-36.90
-.8	-18.40	-18.07	-20.12	-22.25	-25.70	-28.70	-31.60
-.7	-16.60	-16.27	-17.82	-19.40	-22.20	-24.90	-26.80
-.6	-14.80	-14.74	-15.72	-17.00	-19.10	-21.30	-23.10
-.5	-13.24	-13.42	-13.92	-14.75	-16.00	-17.80	-19.80
-.4	-12.44	-12.42	-12.57	-13.10	-13.90	-15.00	-16.60
-.3	-11.74	-11.67	-11.42	-11.55	-11.90	-12.50	-13.50
-.2	-11.24	-11.02	-10.52	-10.25	-10.10	-10.10	-10.50
-.1	-10.86	-10.57	-10.00	-9.41	-8.85	-8.30	-8.60
0.0	-10.74	-10.42	-9.82	-9.15	-8.40	-7.53	-6.51
.1	-10.84	-10.54	-10.01	-9.45	-8.90	-8.40	-7.70
.2	-11.14	-10.96	-10.57	-10.35	-10.00	-9.90	-9.70
.3	-11.64	-11.63	-11.52	-11.40	-11.40	-11.50	-11.80
.4	-12.32	-12.34	-12.57	-12.65	-12.90	-13.30	-13.70
.5	-13.24	-13.22	-13.62	-13.95	-14.40	-15.10	-15.50
.6	-14.20	-14.32	-14.82	-15.15	-15.90	-16.70	-17.50
.7	-15.28	-15.52	-16.12	-16.60	-17.40	-18.40	-19.30
.8	-16.49	-16.92	-17.52	-17.95	-18.90	-20.10	-21.30
.9	-17.74	-18.24	-18.92	-19.55	-20.40	-21.80	-23.00
1.0	-18.99	-19.62	-20.32	-21.05	-21.80	-23.50	-25.00
1.1	-20.29	-20.97	-21.72	-22.65	-23.50	-25.30	-26.90
1.2	-21.56	-22.37	-23.22	-24.15	-25.30	-27.10	-28.80
1.3	-22.71	-23.[illegible]7	-24.57	-25.70	-27.00	-29.00	-30.60
1.4	-24.04	-25.02	-25.97	-27.25	-28.90	-30.80	-32.50
1.5	-25.34	-26.32	-27.37	-28.75	-30.60	-32.50	-34.30

MICROFILMED FROM
BEST AVAILABLE COPY

TABLE 10.

COANNULAR JET FLOW PROPERTIES FOR STATIC DATA CASES.

CASE	MODEL	VE M/S	V2/V1	T1 DEG K	T2 DEG K	W1 KG/S	W2 KG/S	V1 M/S	V2 M/S	P1/PA	P2/PA
1	2	315.1	1.159	380.4	377.6	2.280	1.969	293.5	340.2	1.520	1.780
2	2	450.3	1.178	700.9	394.3	1.658	3.497	401.7	473.4	1.530	3.190
3	2	486.3	2.098	399.6	702.6	2.253	2.715	303.9	637.6	1.530	3.220
4	2	433.2	1.893	403.7	705.0	2.244	2.094	302.7	573.0	1.520	2.480
5	2	364.1	1.581	387.1	705.4	2.297	1.481	296.6	468.8	1.520	1.800
6	2	382.8	1.728	402.1	685.0	2.256	1.319	301.8	521.5	1.520	1.770
7	2	550.5	2.561	413.2	1077.1	2.249	2.233	309.7	793.1	1.530	3.210
8	2	482.3	2.285	413.7	1065.0	2.263	1.725	310.0	708.4	1.540	2.490
9	2	495.9	1.432	695.9	704.3	1.718	2.096	400.8	573.9	1.530	2.500
10	2	589.5	1.794	704.8	901.5	1.679	2.376	402.3	721.8	1.530	3.190
11	2	312.7	1.206	380.6	903.7	2.304	.785	297.2	358.4	1.520	1.290
12	2	456.2	1.344	693.2	906.5	1.694	1.280	397.5	534.0	1.520	1.800
13	2	562.6	1.813	700.9	1093.7	1.711	1.716	399.9	724.8	1.520	2.550
14	2	557.9	1.473	812.6	703.2	1.532	2.637	429.5	632.5	1.520	3.150
15	2	551.2	1.514	808.7	907.1	1.569	1.846	431.3	653.2	1.530	2.500
16	2	475.8	1.244	805.4	897.1	1.625	1.302	429.2	534.0	1.520	1.810
17	2	642.1	1.849	808.7	1097.1	1.589	2.165	431.0	797.1	1.520	3.180
18	2	495.0	1.338	808.7	1089.3	1.612	1.177	433.1	579.7	1.530	1.780
19	2	617.3	1.313	810.4	1085.4	2.084	1.674	541.6	711.4	1.990	2.470
20	2	559.1	1.065	808.7	1087.1	2.142	1.176	546.5	582.2	2.020	1.790
21	2	629.5	1.027	820.9	708.2	2.581	2.062	620.9	637.9	2.500	3.190
22	2	750.3	1.386	829.3	1099.3	2.376	2.784	624.2	865.3	2.500	4.040
23	2	652.0	1.172	812.1	1093.2	2.609	1.684	610.8	715.7	2.450	2.480
24	2	598.3	1.245	1087.1	719.8	1.352	2.674	502.9	646.5	1.530	3.230
25	2	593.3	1.290	1094.3	904.8	1.374	1.862	508.4	655.9	1.540	2.530

Table 10. - Concluded.

CASE	MODEL	VE M/S	V2/V1	T1 DEG K	T2 DEG K	W1 KG/S	W2 KG/S	V1 M/S	V2 M/S	P1/PA	P2/PA
26	2	681,5	1,572	1077.1	1082.6	1.366	2.185	504.1	792.5	1.540	3.190
27	3	586,2	1,464	810.9	701.5	1.123	3.461	434.0	635.5	1.530	3.200
28	3	531,8	1,326	809.3	700.0	1.151	2.703	432.8	573.9	1.530	2.510
29	3	643,9	2,567	448.7	1094.3	1.617	2.963	319.7	820.8	1.520	3.450
30	3	538,8	2,295	419.8	1088.7	1.704	2.165	312.4	716.9	1.540	2.500
31	3	433,4	1,935	397.6	1084.8	1.774	1.516	303.0	586.1	1.530	1.810
32	3	306,4	1,066	389.3	702.1	1.823	1.089	299.0	318.8	1.530	1.300
33	3	748,4	1,945	843.7	1079.8	1.230	3.414	441.7	858.9	1.530	4.060
34	4	347,3	1,529	282.2	543.3	4.739	2.484	293.8	449.3	1.702	2.048
35	4	490,2	1,990	430.0	632.8	3.498	2.400	338.3	673.3	1.642	2.480
36	4	501,0	1,517	670.9	730.0	2.514	2.753	394.4	598.3	1.525	2.040
37	4	612,8	1,983	677.2	1004.0	2.542	3.130	397.2	787.6	1.536	3.552
38	4	670,9	1,991	804.4	1087.2	2.322	3.276	424.6	845.5	1.509	3.677
39	4	386,9	1,460	557.2	551.7	2.372	2.503	313.0	456.9	1.377	2.074
40	4	477,3	1,956	551.1	752.2	2.423	2.607	315.5	616.9	1.389	2.734
41	4	524,6	1,501	557.2	786.1	3.539	2.866	428.5	643.1	1.809	2.861
42	4	628,3	1,984	556.7	1091.7	3.564	3.293	426.9	846.4	1.860	3.864
43	4	430,7	2,030	288.9	648.0	4.717	3.524	299.0	606.9	1.796	3.179
44	4	414,4	1,483	427.2	523.9	3.503	3.190	336.8	499.6	1.641	2.577
45	4	471,8	2,026	426.7	930.0	3.488	2.415	332.2	673.0	1.619	2.604
46	4	464,5	1,517	552.6	573.9	2.813	3.363	362.4	549.9	1.552	2.897
47	4	528,8	2,034	556.7	1097.2	2.843	2.264	363.6	739.4	1.552	2.057
48	4	675,7	1,243	806.7	453.9	3.827	3.110	609.3	757.4	2.461	3.401

TABLE 11.

SPECTRAL COMPARISON PARAMETERS FOR STATIC DATA CASES.

CASE		DIRECTIVITY ANGLE								
		60	75	90	105	120	130	140	150	165
1	CORR COEF	.951	.051	.046	.799	.826	.952	.238	.945	.548
	STD DEV	2.785	6.630	1.806	2.395	2.055	4.174	15.928	3.203	9.693
	DELTA OASPL	1.960	-6.813	.550	.998	2.148	3.680	14.521	3.098	-2.431
2	CORR COEF	.876	.915	.818	.749	.737	.635	.791	.883	.156
	STD DEV	2.845	5.587	2.324	3.153	3.188	5.333	4.462	3.985	6.033
	DELTA OASPL	-2.408	2.042	-1.327	-1.035	-.992	1.826	2.253	2.424	-1.632
3	CORR COEF	.799	.813	.872	.913	.887	.945	.825	.793	.619
	STD DEV	3.357	4.029	1.946	2.878	2.968	2.250	1.714	2.969	5.740
	DELTA OASPL	-.612	-2.503	-.743	-1.387	-.879	-.897	-.233	.492	2.718
4	CORR COEF	.871	.915	.959	.854	.899	.961	.965	.933	.617
	STD DEV	3.360	2.461	1.487	2.972	2.769	2.080	1.302	2.772	6.980
	DELTA OASPL	-.258	-1.373	-.114	-1.563	-1.205	-.613	.842	2.237	2.981
5	CORR COEF	.942	.880	.911	.779	.911	.953	.986	.954	.770
	STD DEV	2.332	3.529	2.146	3.473	2.563	3.069	3.587	5.369	5.164
	DELTA OASPL	.573	1.092	-.170	-.368	-.144	1.492	3.148	4.251	3.479
6	CORR COEF	.937	.867	.905	.776	.914	.964	.991	.966	.808
	STD DEV	1.909	3.937	2.537	4.363	2.961	2.360	2.487	3.551	4.156
	DELTA OASPL	.136	.248	-1.035	-1.266	-1.009	.859	2.309	3.727	3.205
7	CORR COEF	.758	.819	.887	.842	.913	.981	.976	.953	.772
	STD DEV	4.079	3.417	2.942	3.737	3.464	2.172	1.722	3.655	7.550
	DELTA OASPL	1.079	.399	.961	-.325	-1.696	-.835	1.081	2.717	3.720

Table 11. - Continued.

CASE		DIRECTIVITY ANGLE								
		60	75	90	105	120	130	140	150	165
8	CORR COEF	.807	.937	.873	.750	.894	.954	.976	.955	.779
	STD DEV	4.379	2.059	2.334	3.939	3.839	2.792	1.551	3.181	5.405
	DELTA OASPL	1.473	.585	-.590	-1.761	-3.118	-1.768	.867	2.413	2.932
9	CORR COEF	.860	.909	.950	.883	.946	.986	.904	.796	.801
	STD DEV	3.042	2.274	1.396	2.185	1.932	1.465	2.168	2.901	4.773
	DELTA OASPL	-1.286	-1.051	-.177	-.360	-.290	.642	1.410	1.143	1.311
10	CORR COEF	.784	.861	.929	.897	.933	.975	.951	.966	.810
	STD DEV	3.592	2.811	1.377	2.063	2.094	1.402	1.481	2.214	8.786
	DELTA OASPL	.082	-.821	.336	-.046	-1.030	-.873	-.109	-.061	1.847
11	CORR COEF	.979	.968	.936	.884	.708	.921	.983	.979	0.000
	STD DEV	1.797	2.024	1.642	3.286	2.955	4.720	4.716	4.915	0.000
	DELTA OASPL	1.074	1.337	.812	1.161	1.162	3.390	4.699	4.776	0.000
12	CORR COEF	.979	.971	.961	.911	.983	.994	.959	.898	0.000
	STD DEV	2.102	1.931	1.322	3.208	1.762	2.155	3.828	4.149	0.000
	DELTA OASPL	-.280	.240	-.125	.338	.264	1.738	3.352	3.038	0.000
13	CORR COEF	.398	.694	.901	.850	.955	.986	.919	.882	.857
	STD DEV	6.846	2.767	2.380	2.042	2.130	1.268	2.013	2.875	6.901
	DELTA OASPL	-.055	-.265	.246	-.671	-1.727	-.915	.258	.564	1.907
14	CORR COEF	.610	.725	.908	.852	.933	.895	.796	.919	.862
	STD DEV	5.923	4.301	1.480	2.467	4.383	1.672	2.499	1.670	4.504
	DELTA OASPL	-3.371	-3.248	-.430	.166	2.078	.056	-.351	-.320	.424
15	CORR COEF	.830	.927	.943	.893	.967	.982	.927	.917	.947
	STD DEV	4.562	1.402	2.058	2.726	1.816	1.315	1.629	2.422	2.794
	DELTA OASPL	-.621	.167	-.020	-1.765	-1.366	-.538	.149	.134	-.862

MICROFILMED FROM
BEST AVAILABLE COPY

Table 11. - Continued.

CASE		DIRECTIVITY ANGLE								
		60	75	90	105	120	130	140	150	165
16	CORR COEF	.911	.940	.988	.949	.995	.984	.946	.935	.908
	STD DEV	2.713	2.731	1.511	2.349	2.269	2.916	4.307	4.265	2.956
	DELTA OASPL	.026	1.488	.886	.336	.999	1.839	2.506	2.018	.160
17	CORR COEF	0.000	.899	.919	.890	.951	.974	.951	.950	.875
	STD DEV	0.000	2.284	1.903	2.165	2.105	1.436	1.741	2.140	5.650
	DELTA OASPL	0.000	-.048	.592	-.356	-1.123	-.787	-.036	-.322	-.352
18	CORR COEF	0.000	.922	.973	.927	.989	.988	.946	.935	.862
	STD DEV	0.000	4.447	2.957	2.396	1.119	1.342	2.525	2.413	5.254
	DELTA OASPL	0.000	-.197	-1.347	-.979	-.524	.830	1.739	1.064	1.011
19	CORR COEF	.988	.758	.974	.908	.990	.981	.983	.973	.870
	STD DEV	38.490	3.512	2.639	2.942	2.472	2.175	2.171	2.671	2.634
	DELTA OASPL	34.412	1.613	1.921	1.050	1.195	1.302	.427	-.411	.520
20	CORR COEF	.679	.965	.994	.964	.991	.966	.980	.962	.866
	STD DEV	10.039	3.801	3.471	3.469	4.206	4.393	3.538	3.626	3.278
	DELTA OASPL	-5.611	4.072	3.044	2.545	2.627	2.444	.856	-.266	2.226
21	CORR COEF	.290	.928	.968	.971	.991	.968	.958	.970	.916
	STD DEV	12.614	4.744	5.161	4.942	5.199	4.374	3.137	3.321	5.683
	DELTA OASPL	8.921	3.907	4.150	3.608	3.720	2.492	-.215	1.206	2.849
22	CORR COEF	.585	.715	.977	.950	.980	.973	.986	.974	.976
	STD DEV	12.122	4.579	3.875	3.833	4.276	3.046	2.482	3.577	4.593
	DELTA OASPL	-5.596	2.801	3.514	2.293	2.881	1.903	.352	1.728	2.616
23	CORR COEF	.888	.790	.952	.934	.991	.976	.953	.955	.937
	STD DEV	10.167	4.219	3.684	3.650	4.104	3.451	3.323	3.777	4.943
	DELTA OASPL	-7.031	1.002	2.092	1.694	2.523	1.860	-.629	.645	2.019

Table 11. - Continued.

CASE		DIRECTIVITY ANGLE								
		60	75	90	105	120	130	140	150	165
24	CORR COEF	.911	.771	.921	.941	.951	.954	.915	.954	.835
	STD DEV	11.958	3.853	1.679	2.319	2.543	2.405	2.109	2.117	4.997
	DELTA OASPL	-8.829	-1.311	.773	.446	1.216	1.211	.071	-.766	2.477
25	CORR COEF	.859	.255	.980	.920	.986	.923	.928	.969	.822
	STD DEV	6.898	5.213	1.514	2.552	2.016	2.632	2.451	2.309	4.807
	DELTA OASPL	-6.045	-3.508	1.289	-.006	.539	.829	.710	.279	2.446
26	CORR COEF	.836	.572	.963	.931	.974	.946	.919	.961	.979
	STD DEV	5.029	3.928	2.791	2.564	2.616	2.338	2.628	2.390	1.895
	DELTA OASPL	-3.442	.917	2.716	1.166	1.392	1.265	1.025	.593	1.383
27	CORR COEF	.946	.962	.856	.936	.918	.985	.929	.925	.943
	STD DEV	1.573	3.045	3.841	2.985	3.733	2.002	2.110	2.334	4.948
	DELTA OASPL	-1.271	-2.157	-2.027	.159	1.255	1.583	1.631	.712	.817
28	CORR COEF	.946	.960	.942	.949	.940	.976	.916	.910	.920
	STD DEV	2.544	1.302	2.101	2.290	3.156	2.062	2.346	2.484	4.639
	DELTA OASPL	.354	-.344	-.567	.502	1.208	1.782	1.789	.615	1.035
29	CORR COEF	.881	.941	.911	.927	.940	.978	.964	.926	.911
	STD DEV	1.930	2.588	3.059	3.310	3.500	2.046	1.794	2.768	5.242
	DELTA OASPL	-.156	-1.518	-1.531	-1.133	-1.217	-.213	1.615	2.121	1.288
30	CORR COEF	.914	.970	.924	.844	.915	.977	.955	.882	.855
	STD DEV	3.033	1.270	2.617	3.639	3.857	2.173	1.723	3.440	4.942
	DELTA OASPL	1.170	-.607	-1.716	-2.299	-2.390	-.938	1.424	1.976	1.790
31	CORR COEF	.944	.905	.806	.757	.897	.987	.950	.864	.814
	STD DEV	3.162	5.046	6.312	6.133	5.044	2.069	1.715	3.447	3.845
	DELTA OASPL	-2.504	-3.506	-3.965	-3.659	-2.999	-.735	1.588	2.566	2.743

Table 11. - Continued.

CASE		DIRECTIVITY ANGLE								
		60	75	90	105	120	130	140	150	165
32	CORR COEF	.846	.961	.930	.956	.995	.963	.990	.981	.955
	STD DEV	6.119	4.228	5.128	4.654	4.162	4.244	4.488	3.656	5.032
	DELTA OASPL	-1.472	.081	-1.018	.050	1.196	1.787	2.469	2.153	1.034
33	CORR COEF	.857	.867	.944	.905	.962	.960	.954	.975	.846
	STD DEV	4.447	4.115	4.303	4.532	5.893	2.549	2.296	1.905	4.209
	DELTA OASPL	-1.842	1.398	-1.140	-1.018	2.497	1.448	-.136	-.394	-.625

CASE		DIRECTIVITY ANGLE								
		60	90	100	110	120	130	140	150	160
34	CORR COEF	.735	.820	.805	.853	.972	.946	.980	.924	.605
	STD DEV	4.302	4.611	5.086	4.215	2.673	2.312	1.363	2.278	6.602
	DELTA OASPL	-2.602	-2.593	-2.730	-2.636	-2.202	-.862	.355	1.737	1.209
35	CORR COEF	.883	.943	.912	.953	.984	.962	.912	.878	.827
	STD DEV	3.351	3.173	3.952	3.854	3.475	2.907	2.817	2.444	5.947
	DELTA OASPL	-4.023	-2.688	-3.181	-3.213	-3.083	-2.907	-1.051	-.024	-1.279
36	CORR COEF	.973	.961	.964	.972	.969	.945	.874	.854	.887
	STD DEV	2.229	2.869	2.980	3.827	3.564	2.975	2.673	3.256	5.524
	DELTA OASPL	-2.131	-2.331	-1.858	-3.305	-3.429	-2.731	-1.238	-.552	-1.336
37	CORR COEF	.831	.956	.945	.962	.937	.931	.853	.750	.754
	STD DEV	2.885	2.891	3.209	4.033	4.497	4.008	4.070	4.312	5.698
	DELTA OASPL	-2.857	-2.221	-1.767	-3.704	-4.206	-4.365	-2.624	-1.019	-1.954
38	CORR COEF	.582	.927	.947	.955	.942	.936	.826	.695	.550
	STD DEV	4.119	2.516	3.083	3.930	5.034	4.576	4.215	4.449	5.956
	DELTA OASPL	-6.300	-1.820	-1.778	-3.803	-4.504	-4.176	-2.750	-1.874	-2.074

Table 11. - Continued.

CASE		DIRECTIVITY ANGLE								
		80	90	100	110	120	130	140	150	160
39	CORR COEF	.860	.958	.935	.971	.983	.976	.945	.860	.742
	STD DEV	2.774	3.134	3.608	3.181	1.737	1.137	2.130	3.679	4.051
	DELTA OASPL	-.703	-1.564	-.878	-1.629	-1.236	-.279	.936	2.175	2.746
40	CORR COEF	.976	.934	.934	.950	.967	.935	.871	.650	.749
	STD DEV	1.917	2.607	3.193	3.391	3.000	2.719	2.997	3.841	4.705
	DELTA OASPL	-.887	-1.177	-.719	-2.397	-2.891	-2.456	-.909	.002	1.100
41	CORR COEF	.935	.970	.969	.977	.959	.937	.866	.902	.898
	STD DEV	2.685	2.761	3.067	3.563	3.232	2.630	2.642	3.196	6.588
	DELTA OASPL	-2.378	-1.899	-1.304	-2.937	-3.155	-2.188	-1.349	-1.230	-2.348
42	CORR COEF	.843	.951	.957	.965	.959	.920	.823	.721	.644
	STD DEV	3.127	2.704	3.227	3.840	3.873	3.842	3.671	4.484	5.256
	DELTA OASPL	-3.342	-1.842	-2.417	-3.311	-3.489	-3.382	-2.050	-1.570	-1.647
43	CORR COEF	.876	.950	.961	.944	.926	.936	.886	.873	.722
	STD DEV	3.060	2.839	3.142	3.572	3.486	2.122	3.085	4.106	5.427
	DELTA OASPL	-4.300	-2.432	-2.475	-2.967	-3.372	-1.751	-1.648	-.294	.173
44	CORR COEF	.925	.957	.935	.956	.970	.981	.953	.821	.708
	STD DEV	3.027	2.128	2.437	2.823	2.365	1.354	1.892	3.686	6.265
	DELTA OASPL	-3.243	-2.051	-1.755	-2.074	-1.722	.179	.283	1.224	.207
45	CORR COEF	.964	.947	.904	.957	.992	.973	.937	.866	.777
	STD DEV	2.728	3.220	3.957	3.836	2.632	2.096	2.056	3.737	5.023
	DELTA OASPL	-2.203	-2.142	-2.379	-2.481	-2.078	-2.002	.046	1.045	1.393
46	CORR COEF	.969	.957	.930	.922	.916	.918	.905	.861	.886
	STD DEV	1.008	1.582	2.250	2.561	3.172	2.643	3.092	3.645	5.304
	DELTA OASPL	-.053	-.225	-.304	-.840	-1.337	-1.028	.586	1.684	.862

Table 11. - Concluded.

CASE		DIRECTIVITY ANGLE								
		80	90	100	110	120	130	140	150	160
47	CORR COEF	.925	.947	.912	.963	.993	.958	.904	.773	.882
	STD DEV	2.267	3.233	4.325	4.346	3.265	2.978	2.943	4.062	5.462
	DELTA OASPL	-1.666	-2.219	-3.127	-3.845	-3.419	-2.680	-.830	-.101	.070
48	CORR COEF	.889	.960	.964	.955	.884	.775	.914	.920	.714
	STD DEV	3.325	4.049	3.088	3.739	2.786	3.211	2.551	4.261	5.330
	DELTA OASPL	1.037	1.919	.818	.107	.263	-2.188	-1.689	1.217	2.244

MICROFILMED FROM
BEST AVAILABLE COPY

TABLE 12.

COANNULAR JET FLOW PROPERTIES FOR WIND TUNNEL DATA.CASES.

CASE	MODEL	VE M/S	V2/V1	T1 DEG K	T2 DEG K	W1 KG/S	W2 KG/S	V1 M/S	V2 M/S	P1/PA	P2/PA	VA M/S
1	7	406.6	1,568	392.6	388.7	.390	.649	300.2	470.6	1,530	3.207	101.5
2	7	369.4	1,432	397.6	391.5	.390	.494	297.5	426.1	1,508	2.505	101.8
3	7	459.4	1,879	402.6	577.6	.413	.544	306.3	575.5	1,539	3.214	31.1
4	7	454.1	1,941	389.3	590.4	.413	.503	299.3	580.9	1,530	3.199	61.3
5	7	480.6	2,068	402.1	692.6	.417	.490	304.8	630.3	1,533	3.201	31.1
6	7	481.4	2,081	408.2	698.7	.408	.472	304.8	634.3	1,523	3.215	61.9
7	7	424.8	1,908	401.5	701.5	.417	.349	300.5	573.3	1,515	2.511	61.6
8	7	426.1	1,900	394.3	703.7	.417	.352	301.8	573.3	1,533	2.503	30.2
9	7	473.3	2,159	388.7	705.9	.381	.413	295.3	637.6	1,514	3.212	124.5
10	7	419.1	1,914	382.1	691.5	.390	.322	296.6	567.5	1,530	2.495	129.5
11	7	422.5	1,943	386.5	705.4	.395	.331	295.4	573.9	1,517	2.501	103.6
12	8	513.7	2,112	389.3	702.6	.340	.594	300.8	635.5	1,538	3.206	31.1
13	8	507.4	2,118	393.2	698.2	.354	.585	299.0	633.4	1,522	3.203	61.6
14	8	459.1	1,924	395.4	706.7	.331	.454	299.3	575.8	1,519	2.506	61.3
15	8	455.6	1,915	394.3	699.8	.340	.458	298.7	572.1	1,519	2.507	30.8
16	8	491.4	1,913	403.2	589.8	.304	.640	303.6	580.6	1,526	3.200	103.6
17	8	515.6	2,069	407.1	705.4	.295	.508	307.5	636.4	1,536	3.201	130.5
18	8	514.2	2,089	402.1	702.6	.304	.526	304.2	635.5	1,530	3.206	103.6
19	8	453.4	1,902	393.7	707.1	.308	.404	299.9	570.6	1,526	2.466	103.9
20	8	455.4	1,936	388.7	709.3	.299	.390	297.8	576.4	1,525	2.511	129.8
21	8	482.2	1,965	379.3	585.9	.349	.676	294.7	579.1	1,527	3.205	61.3
22	8	488.8	1,954	387.1	595.4	.345	.685	299.0	584.3	1,533	3.215	29.9

TABLE 13.

SPECTRAL COMPARISON PARAMETERS FOR WIND TUNNEL DATA CASES.

CASE		DIRECTIVITY ANGLE								
		70	80	90	100	110	120	130	140	150
1	CORR COEF	.971	.989	.979	.970	.958	.966	.953	.915	.889
	STD DEV	7,112	5,638	6,945	5,034	4,857	5,391	8,291	4,336	9,223
	DELTA OASPL	-3,932	-2,733	-1,263	-,777	-,839	-,337	-,991	-1,325	-,677
2	CORR COEF	.944	.930	.916	.902	.843	.870	.784	.743	.814
	STD DEV	8,589	6,851	7,891	7,102	6,085	6,702	9,147	10,297	10,553
	DELTA OASPL	-3,417	-1,592	,474	,953	,677	,172	-1,114	-1,820	-1,389
3	CORR COEF	.934	.960	.967	.967	.918	.945	.856	.943	.919
	STD DEV	3,155	3,015	2,891	2,168	2,085	1,902	2,589	2,746	4,981
	DELTA OASPL	-3,106	-2,316	-1,194	-,797	-1,257	-1,406	-2,145	,549	2,502
4	CORR COEF	.906	.940	.964	.939	.880	.918	.837	.906	.924
	STD DEV	2,945	2,876	3,042	2,720	2,708	2,475	3,118	2,729	4,749
	DELTA OASPL	-3,901	-2,963	-1,599	-1,231	-1,343	-1,432	-2,506	-,331	2,827
5	CORR COEF	.924	.949	.939	.929	.847	.918	.936	.957	.940
	STD DEV	3,096	2,888	2,706	2,345	2,787	2,543	2,144	2,649	5,140
	DELTA OASPL	-3,478	-2,777	-1,607	-1,590	-2,159	-2,408	-1,739	,077	2,238
6	CORR COEF	.903	.937	.935	.896	.812	.888	.915	.943	.919
	STD DEV	3,008	2,870	3,171	3,008	3,299	3,035	2,678	2,311	5,016
	DELTA OASPL	-3,896	-3,017	-1,661	-1,574	-2,030	-2,453	-2,047	-,317	2,448
7	CORR COEF	.915	.904	.871	.796	.753	.882	.928	.944	.922
	STD DEV	3,275	2,640	2,649	3,162	3,587	3,225	2,601	3,102	5,050
	DELTA OASPL	-1,275	-,370	-,281	-1,458	-2,283	-2,720	-2,198	-,448	2,073

Table 13. - Continued.

CASE		DIRECTIVITY ANGLE								
		70	80	90	100	110	120	130	140	150
8	CORR COEF	.958	.949	.919	.848	.794	.911	.950	.959	.925
	STD DEV	2.741	2.706	2.839	3.001	3.392	2.975	2.287	2.303	4.438
	DELTA OASPL	-1.689	-1.100	-1.092	-2.230	-3.068	-3.197	-2.114	-.069	1.970
9	CORR COEF	.856	.922	.906	.821	.725	.828	.878	.768	.773
	STD DEV	6.316	5.679	7.706	6.358	5.738	6.382	10.747	14.370	14.791
	DELTA OASPL	-5.019	-3.591	-2.253	-2.024	-2.010	-2.749	-3.451	-3.210	-.745
10	CORR COEF	.856	.767	.735	.667	.652	.809	.809	.594	.631
	STD DEV	8.043	7.771	7.317	6.217	6.407	7.312	12.391	15.263	14.162
	DELTA OASPL	-1.890	-.401	.153	-.958	-1.920	-3.185	-5.052	-5.706	-2.687
11	CORR COEF	.897	.845	.805	.711	.684	.835	.906	.923	.879
	STD DEV	4.435	5.092	6.773	4.632	5.078	4.475	8.563	10.055	9.625
	DELTA OASPL	-1.246	-.081	.144	-1.304	-2.053	-3.074	-3.137	-2.034	.383
12	CORR COEF	.878	.920	.966	.975	.922	.956	.992	.967	.954
	STD DEV	3.532	3.041	2.491	1.988	2.494	1.918	1.581	2.874	5.363
	DELTA OASPL	-2.837	-1.997	-1.122	-1.270	-1.083	-1.558	-.803	.597	2.070
13	CORR COEF	.866	.902	.958	.960	.894	.936	.977	.982	.935
	STD DEV	3.008	3.026	2.656	2.374	3.208	2.481	2.961	3.241	5.383
	DELTA OASPL	-3.281	-2.413	-1.229	-1.293	-.908	-1.314	-.863	.571	2.713
14	CORR COEF	.922	.910	.904	.903	.806	.899	.967	.476	.919
	STD DEV	4.060	2.732	2.297	2.469	3.734	2.773	2.037	3.176	5.633
	DELTA OASPL	-3.526	-1.490	-.983	-.445	-.565	-1.847	-1.066	1.272	1.820
15	CORR COEF	.921	.894	.889	.920	.814	.911	.966	.958	.908
	STD DEV	3.552	3.207	2.759	2.635	3.151	2.733	2.035	2.060	4.805
	DELTA OASPL	-4.151	-3.205	-1.909	-2.262	-2.482	-2.817	-1.532	-.197	1.485

Table 13. - Concluded.

CASE		DIRECTIVITY ANGLE								
		70	80	90	100	110	120	130	140	150
16	CORR COEF	.903	.931	.976	.968	.933	.946	.979	.986	.925
	STD DEV	5.456	4.583	5.052	3.654	4.626	4.350	7.030	8.345	9.703
	DELTA OASPL	-2.644	-1.523	-.160	-.042	.536	.648	.475	1.476	3.188
17	CORR COEF	.861	.925	.958	.938	.856	.896	.948	.948	.877
	STD DEV	7.415	7.500	7.115	6.423	5.132	5.303	10.392	11.912	11.011
	DELTA OASPL	-3.676	-2.088	-.918	-1.199	-.740	-.879	-2.062	-.821	1.089
18	CORR COEF	.866	.914	.962	.948	.864	.912	.963	.966	.894
	STD DEV	5.314	3.526	4.990	3.329	4.246	4.214	7.034	6.614	9.963
	DELTA OASPL	-3.410	-2.180	-.976	-1.172	-.768	-1.115	-1.403	.066	2.287
19	CORR COEF	.922	.877	.863	.836	.745	.869	.944	.961	.922
	STD DEV	4.166	4.730	6.292	3.842	4.694	5.160	9.240	10.631	10.783
	DELTA OASPL	-3.742	-1.915	-.479	-.922	-1.180	-1.926	-2.077	-.841	1.396
20	CORR COEF	.908	.890	.818	.794	.728	.851	.651	.484	.887
	STD DEV	8.635	6.942	7.839	7.231	5.671	6.311	13.183	14.893	12.402
	DELTA OASPL	-4.355	-2.338	-1.165	-1.286	-.996	-1.803	-4.092	-3.768	.244
21	CORR COEF	.907	.940	.971	.959	.926	.953	.986	.974	.914
	STD DEV	3.367	2.989	2.887	2.432	3.147	2.371	1.892	1.691	4.138
	DELTA OASPL	-3.166	-2.279	-.907	-1.155	-.545	-.638	-.237	.654	2.598
22	CORR COEF	.914	.945	.971	.958	.939	.966	.992	.974	.927
	STD DEV	3.691	3.013	2.612	1.930	2.219	1.669	1.519	2.910	5.321
	DELTA OASPL	-3.383	-2.420	-1.114	-1.366	-.960	-1.055	-.261	.900	2.175

MICROFILMED FROM
BEST AVAILABLE COPY

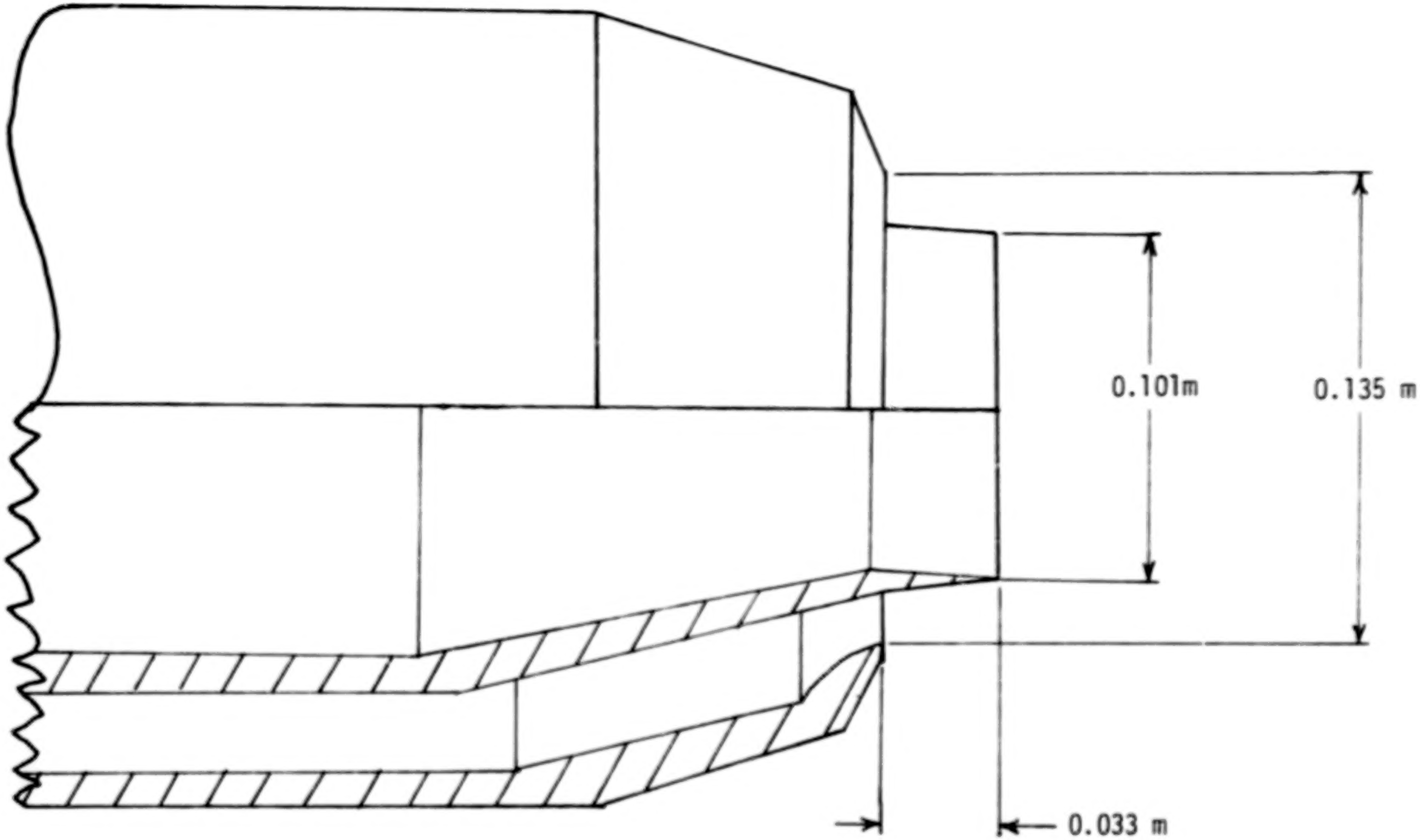
0.101m
0.135 m
0.033 m

Figure 1. —0.75 Area ratio static test coannular nozzle - model 2.

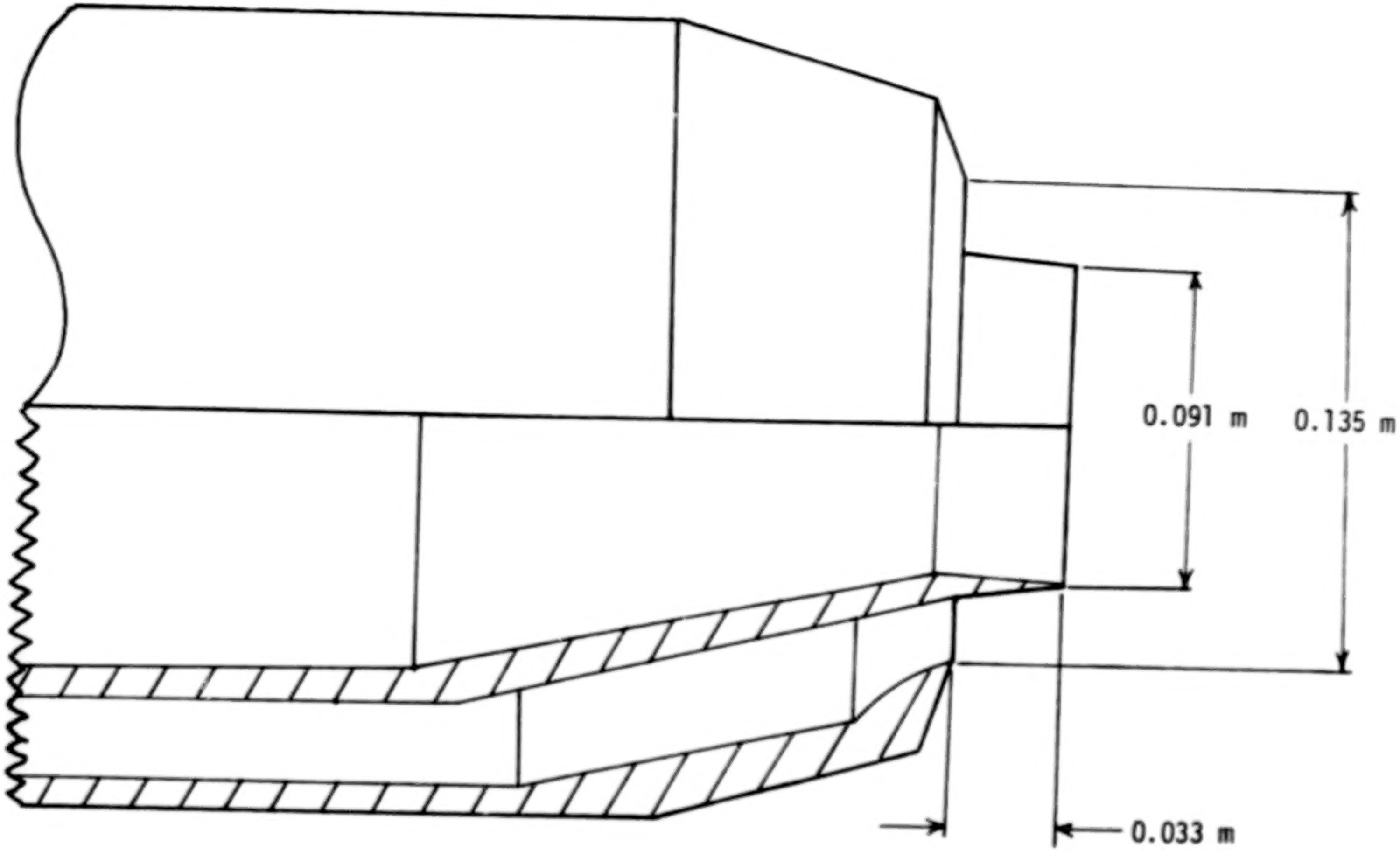
0.091 m
0.135 m
0.033 m

Figure 2. -1.2 Area ratio static test coannular nozzle - model 3.

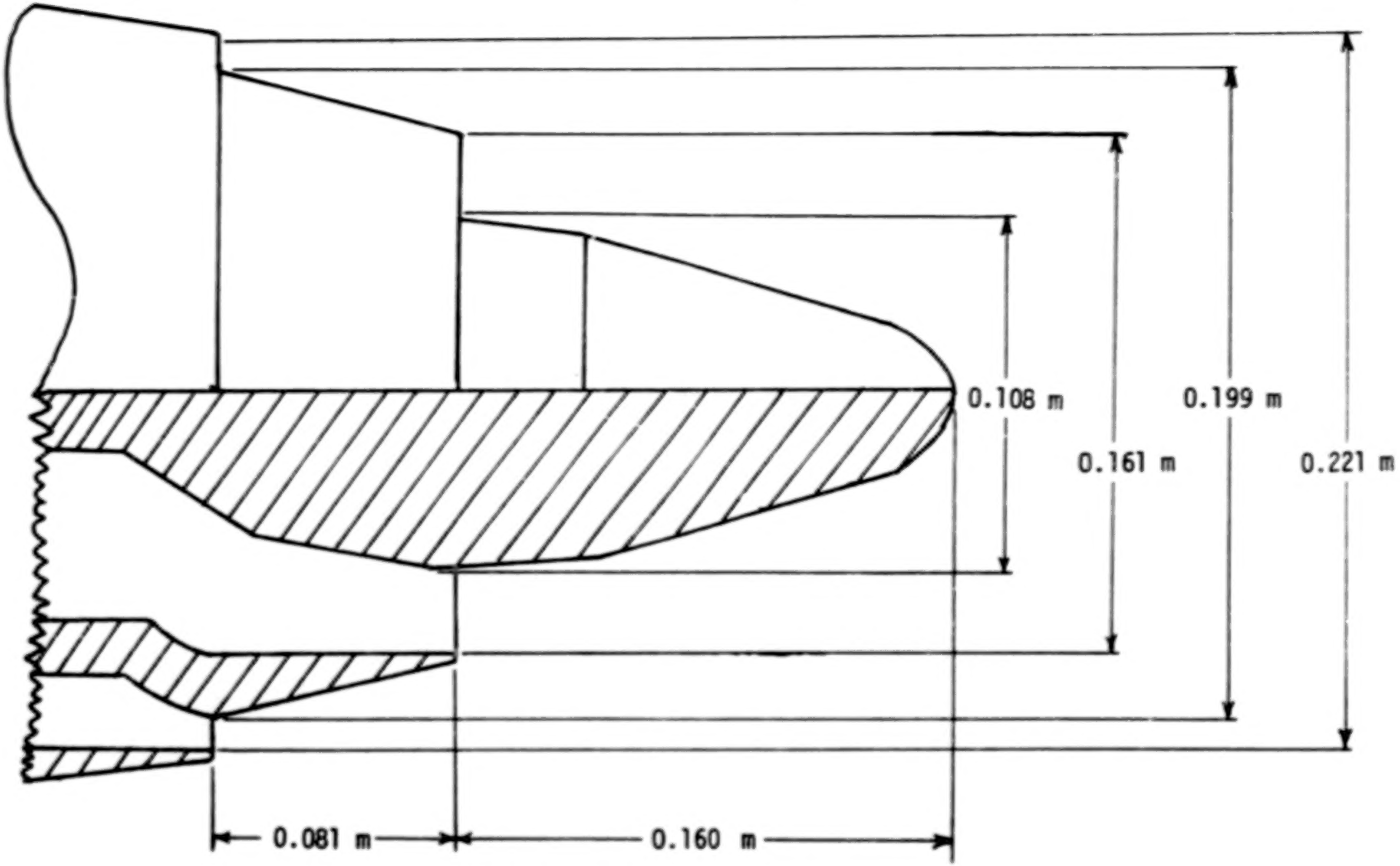
0.108 m
0.199 m
0.161 m
0.221 m
0.081 m
0.160 m

Figure 3. - 0.647 Area ratio static test coannular plug nozzle - model 4.

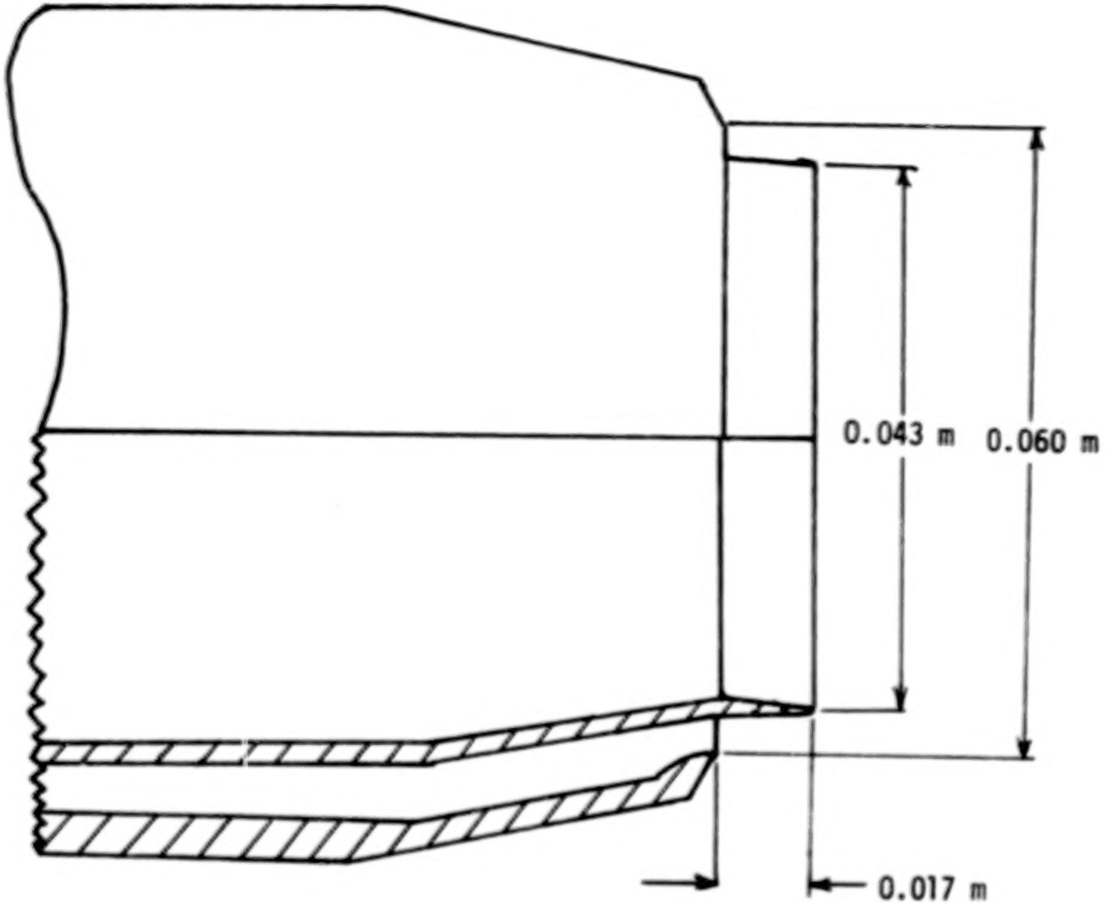
0.043 m
0.060 m
0.017 m

Figure 4. — 0.75 Area ratio wind tunnel test coannular nozzle - model 7.

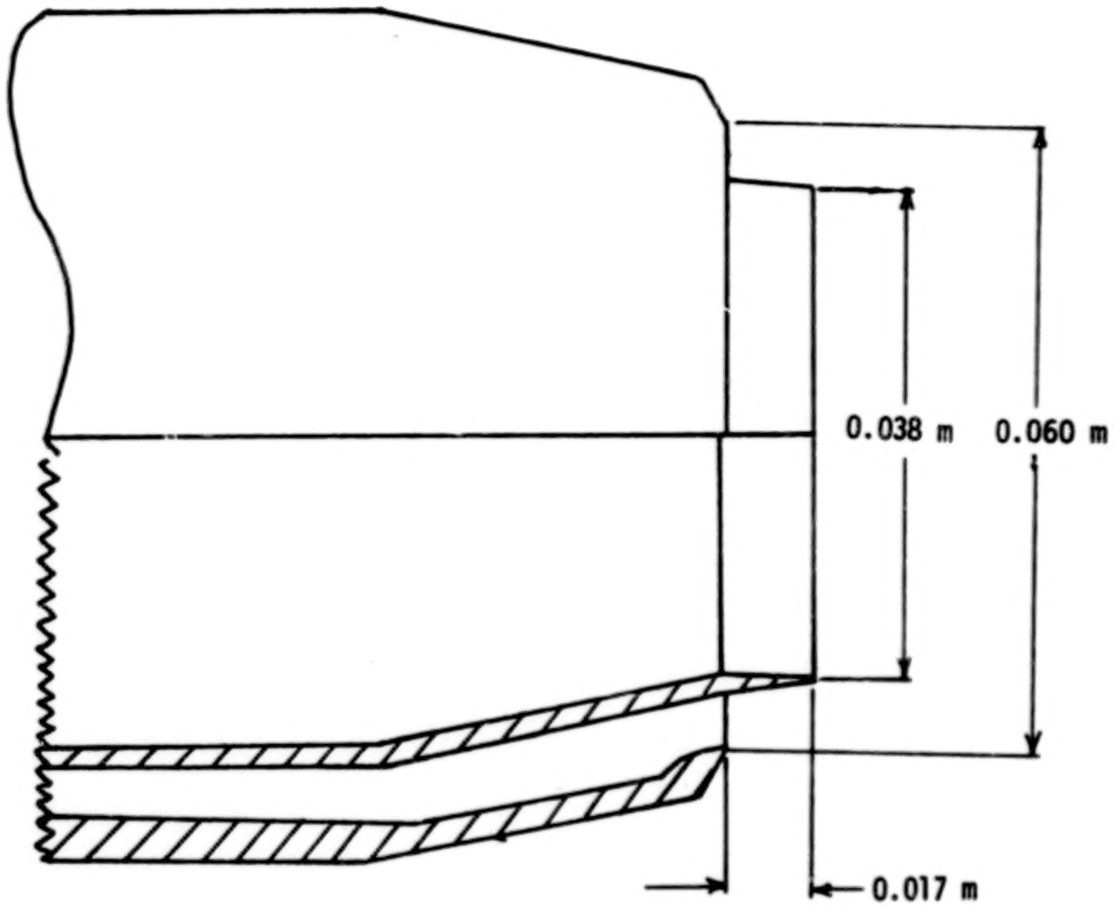
0.038 m
0.060 m
0.017 m

Figure 5. – 1.2 Area ratio wind tunnel test coannular nozzle - model 8.

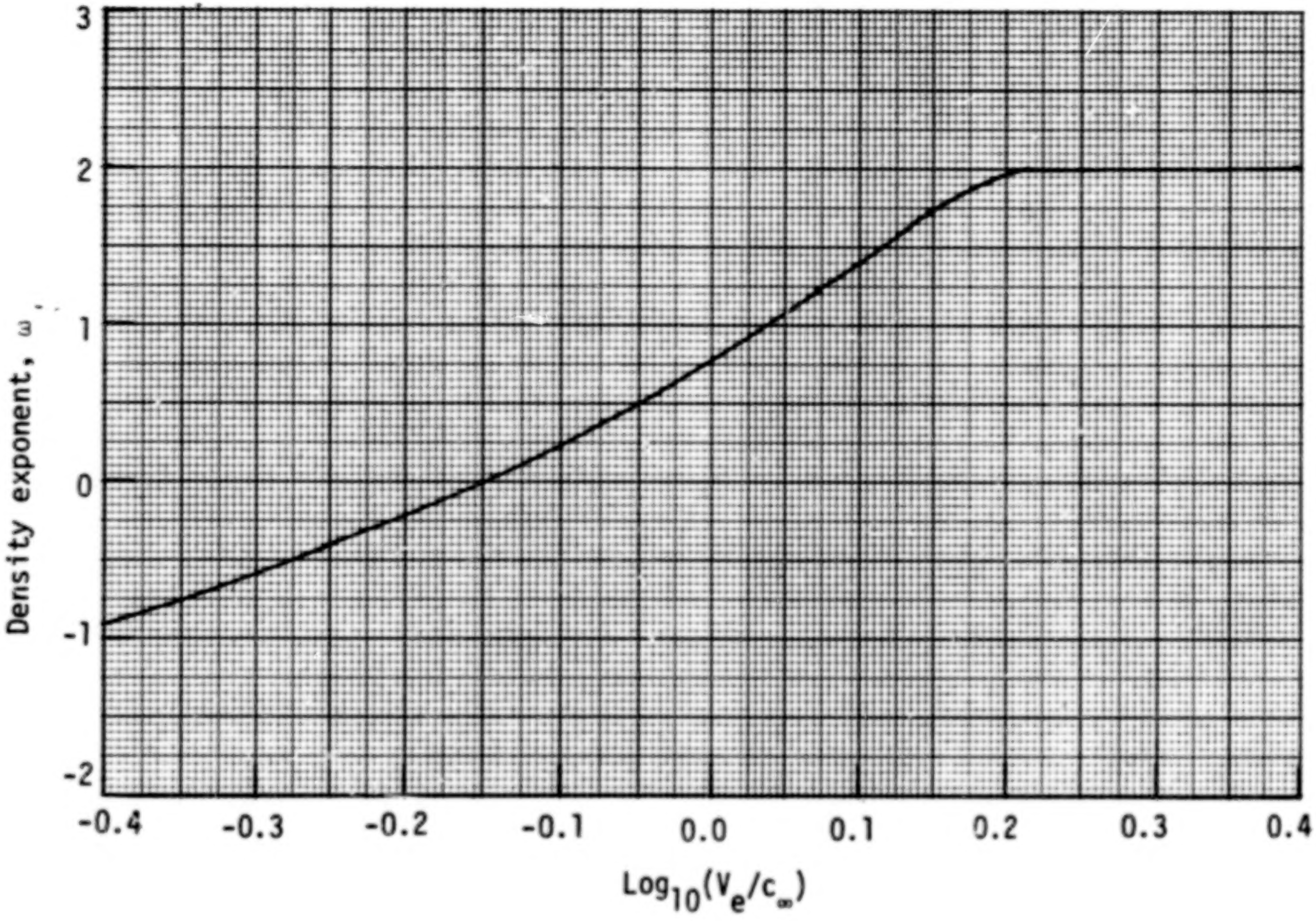

Figure 6. – Jet noise density exponent.

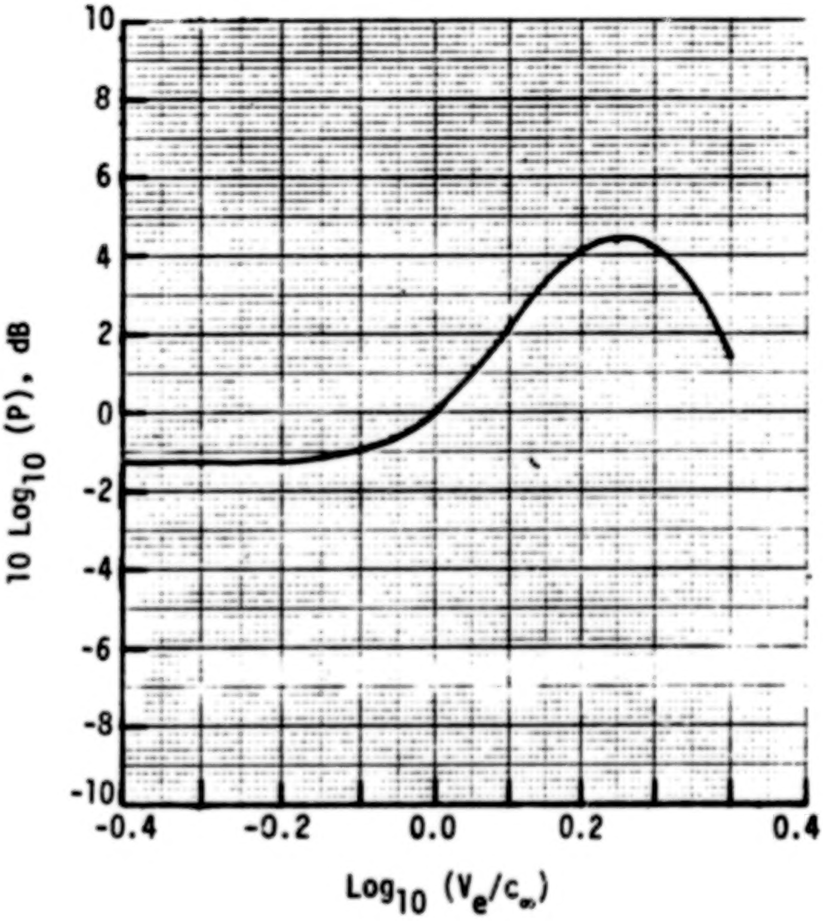

Figure 7. - Jet noise power deviation factor, P.

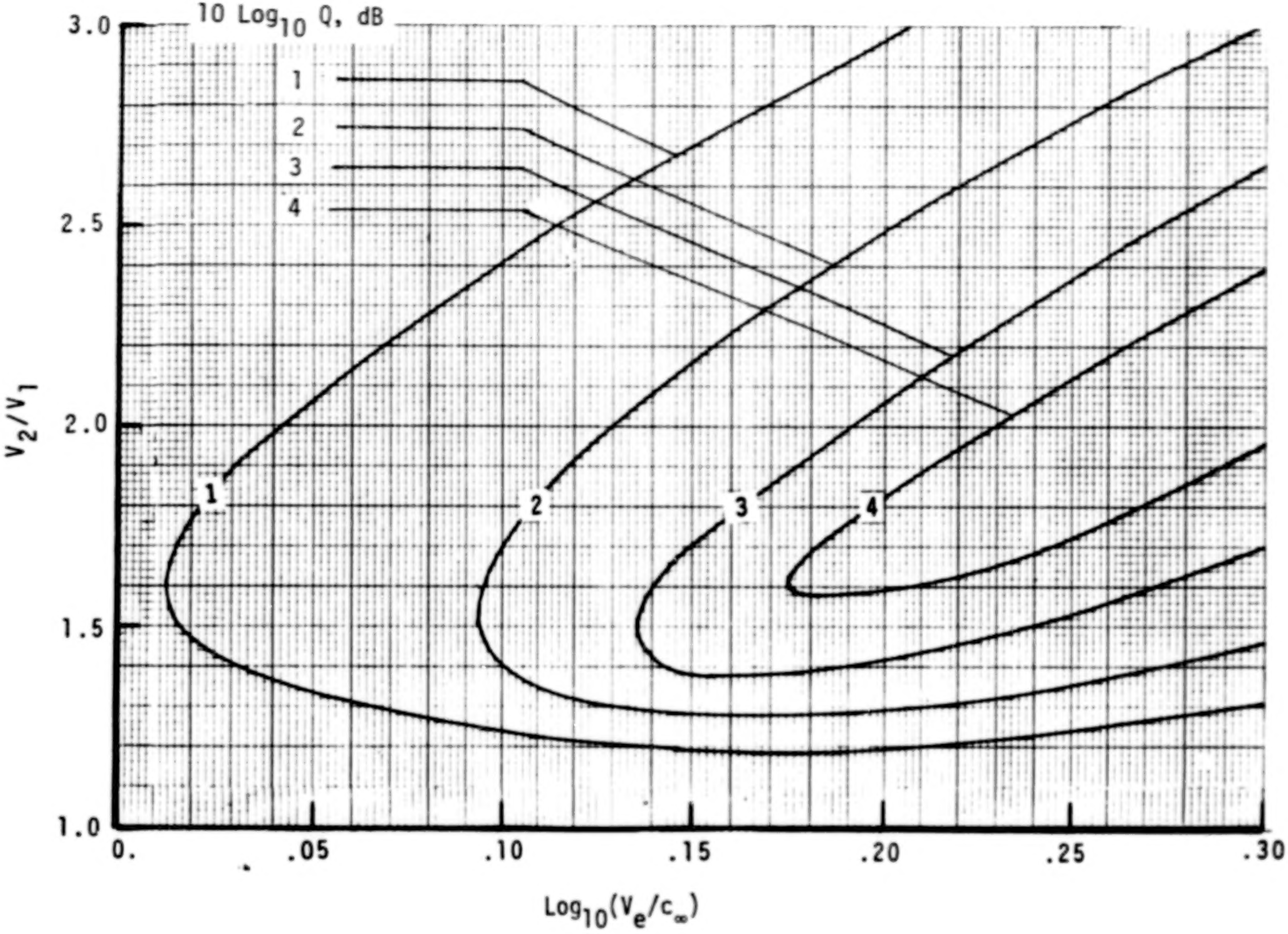

Figure 8. - Coannular jet power reduction factor, Q.

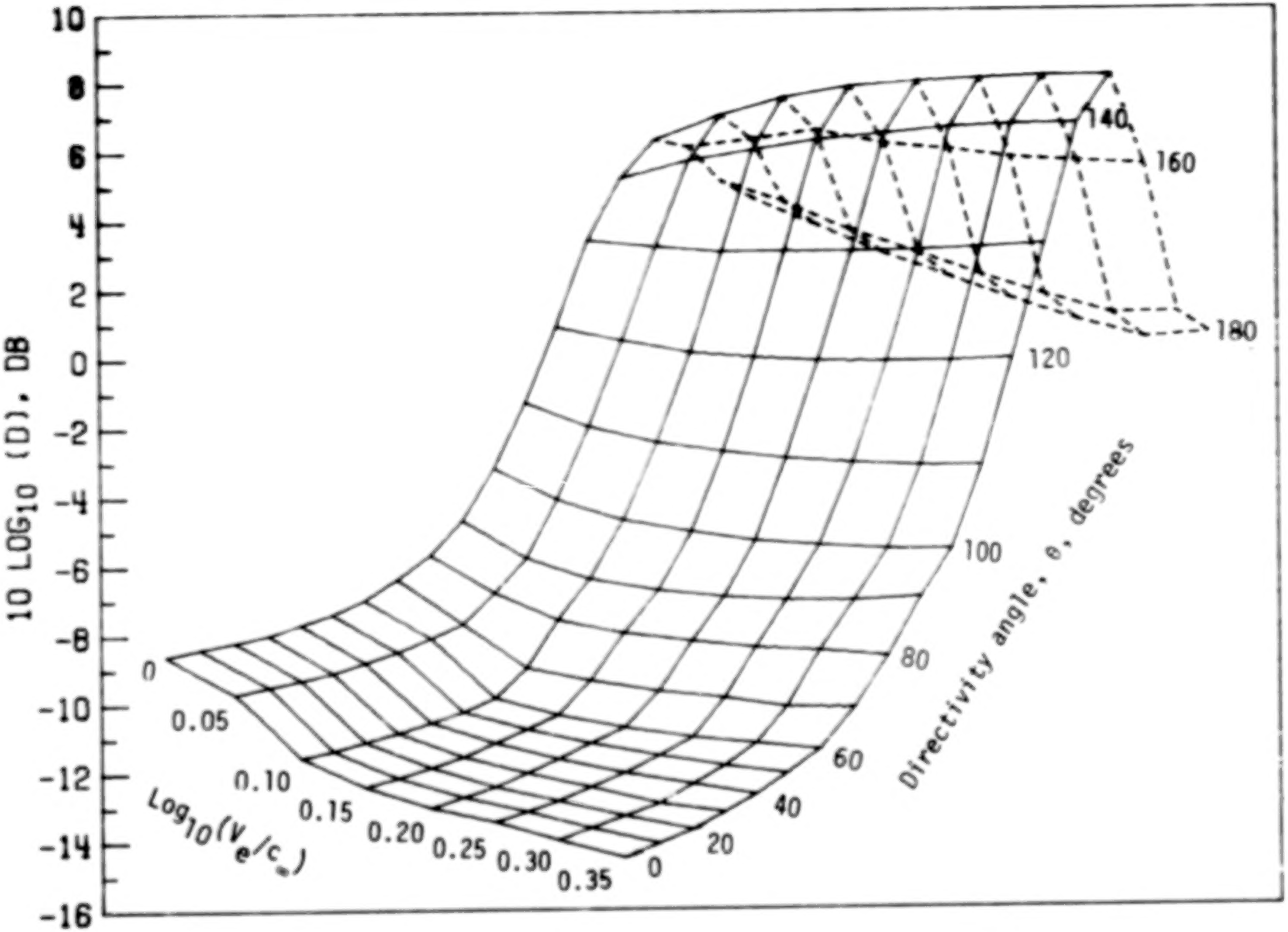

Figure 9. - Coannular jet noise directivity index, D.

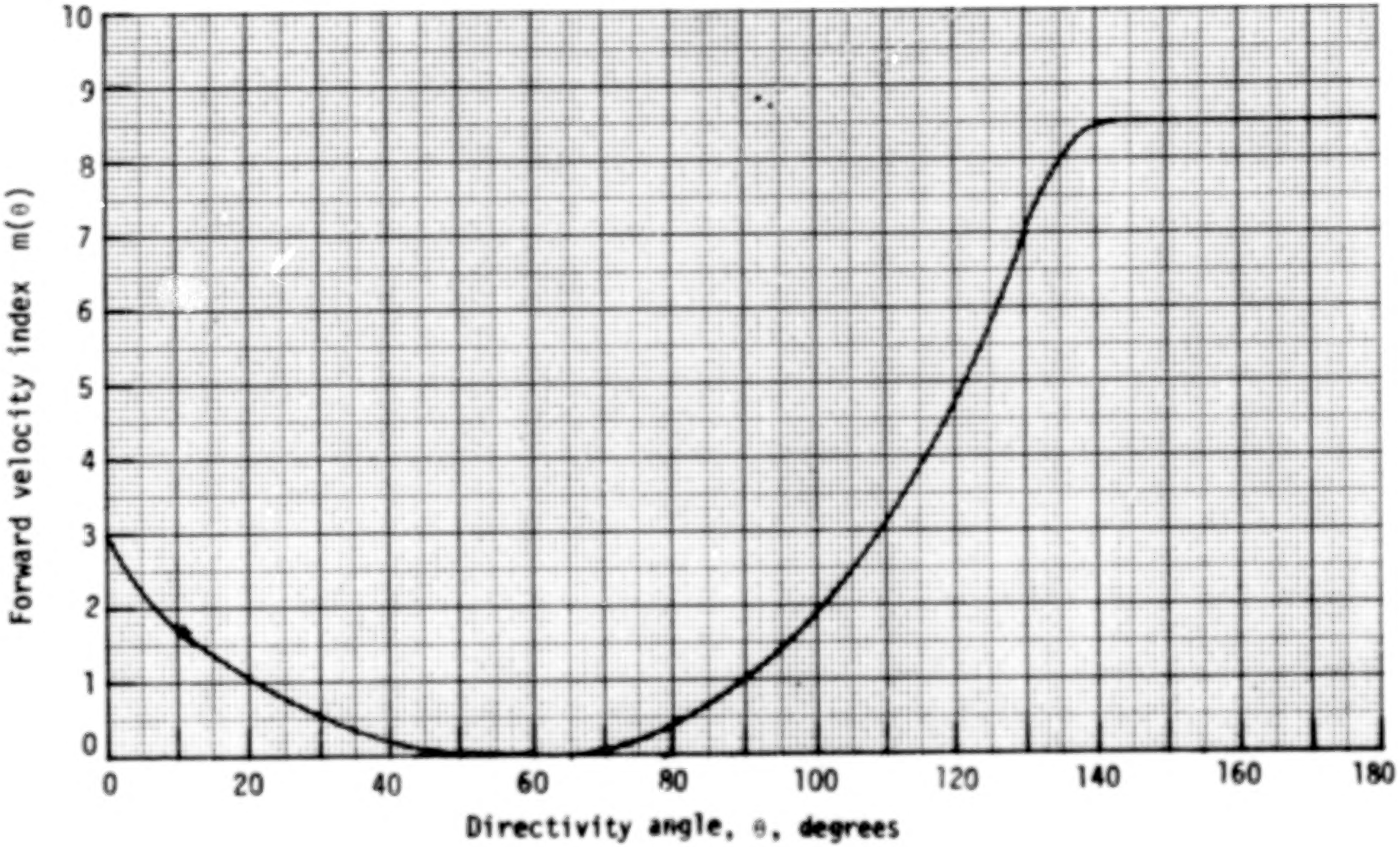

Figure 10. - Jet noise forward velocity index.

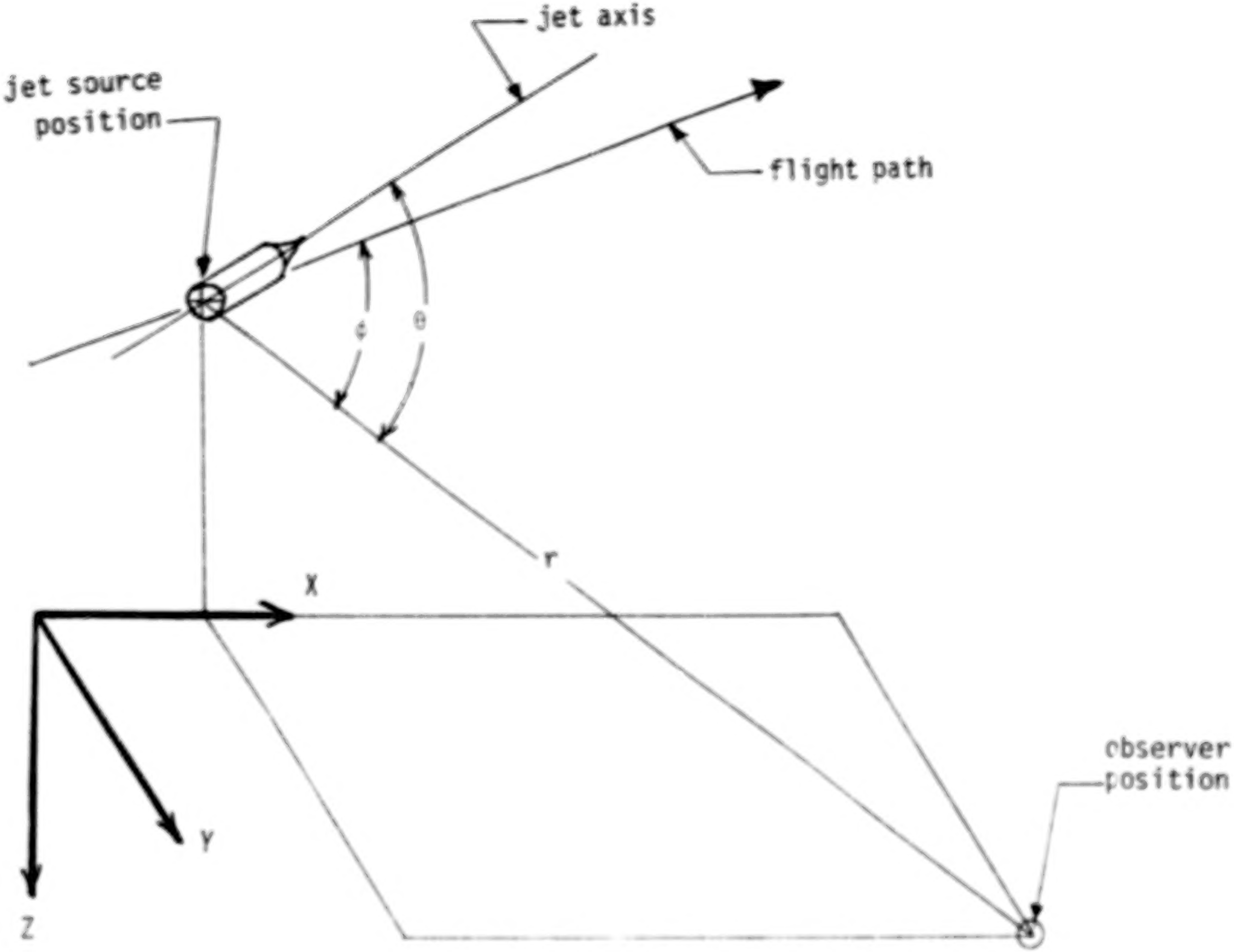
jet axis
jet source position
flight path
φ
θ
r
X
Y
Z
observer position

Figure 11. - Source to observer jet noise geometric characteristics.

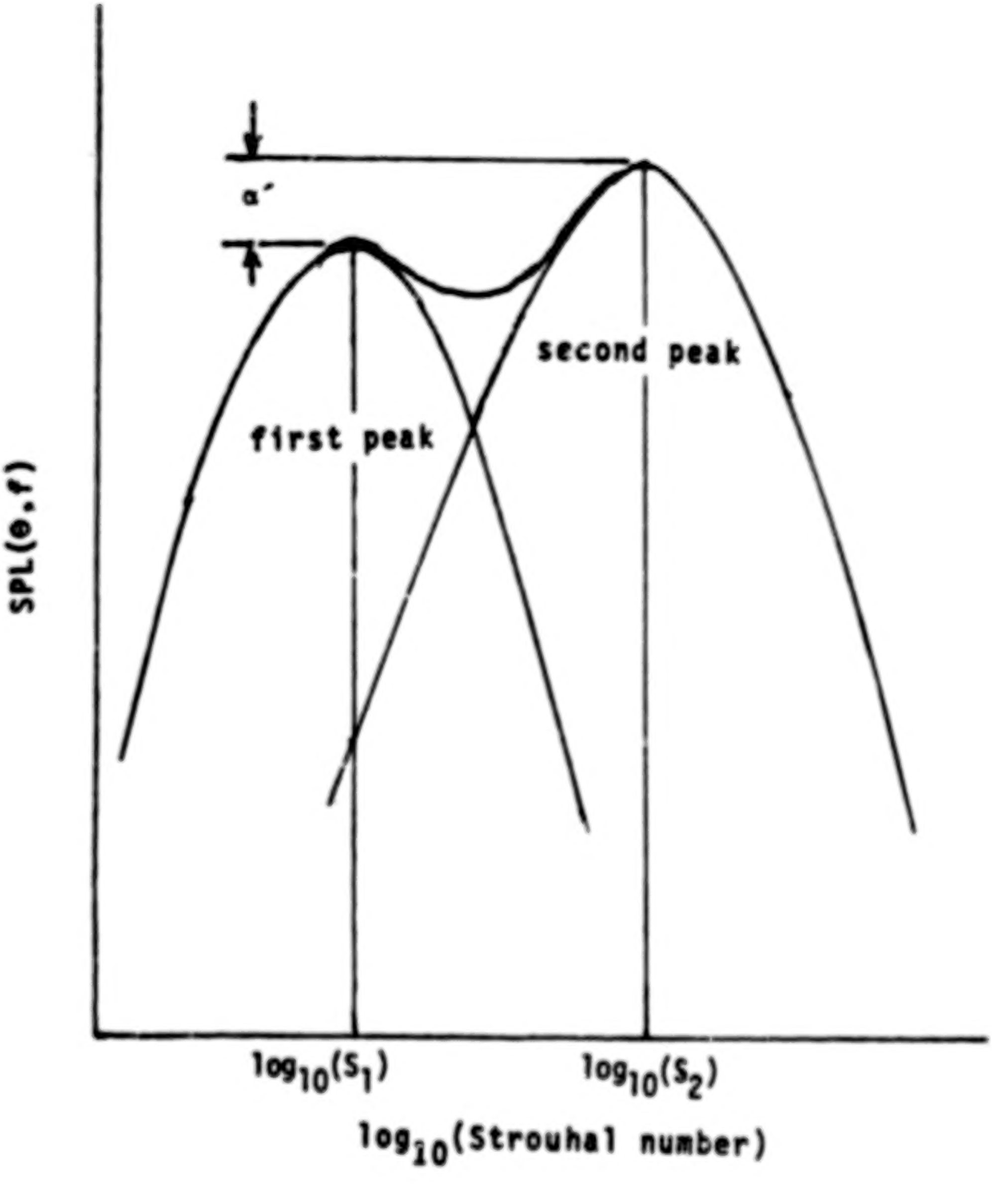
α′
second peak
first peak
SPL(θ,f)
$\log_{10}(S_1)$
$\log_{10}(S_2)$
$\log_{10}$(Strouhal number)

Figure 12. - Coannular jet two component spectrum.

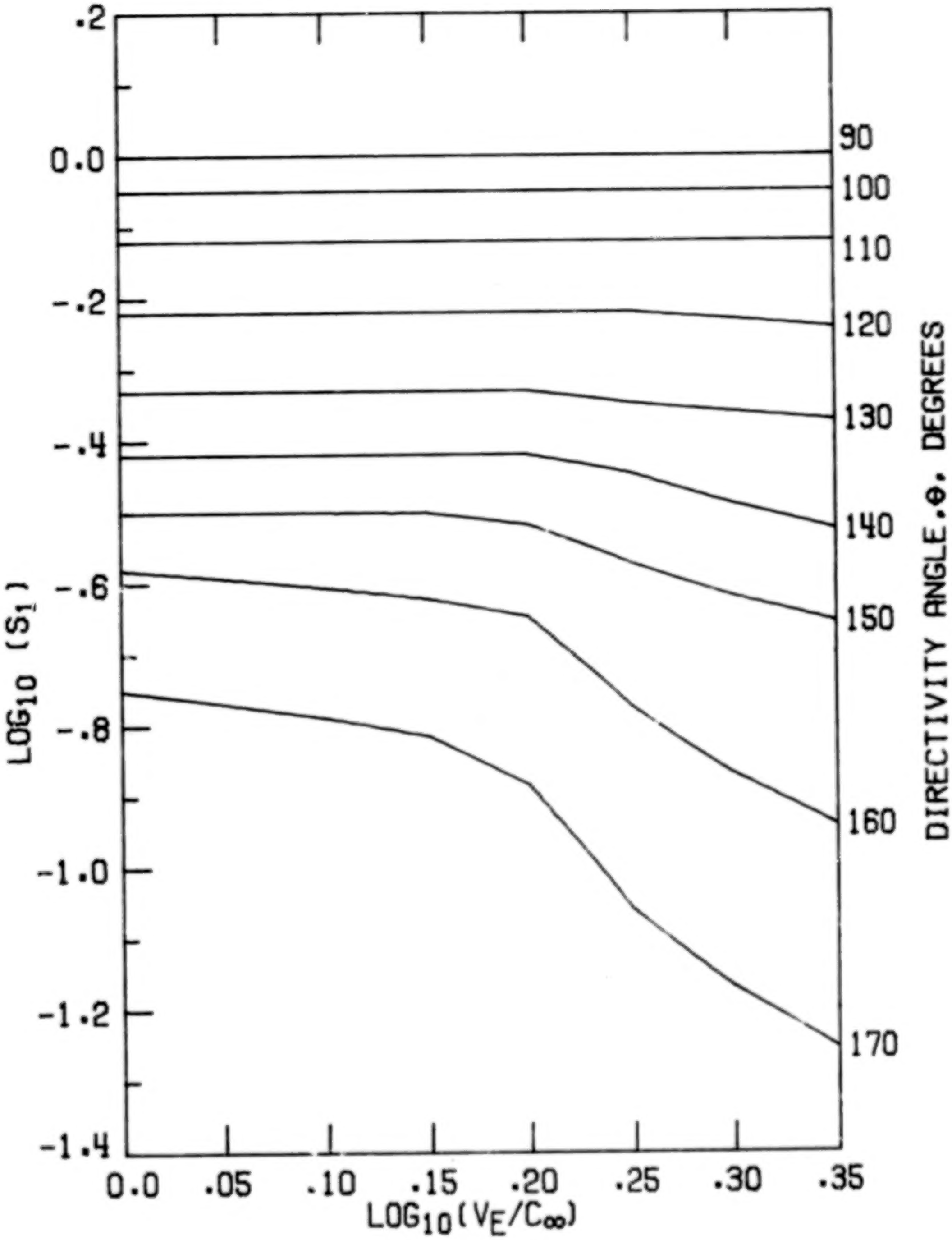

Figure 13. - Location of first peak Strouhal number, S_1.

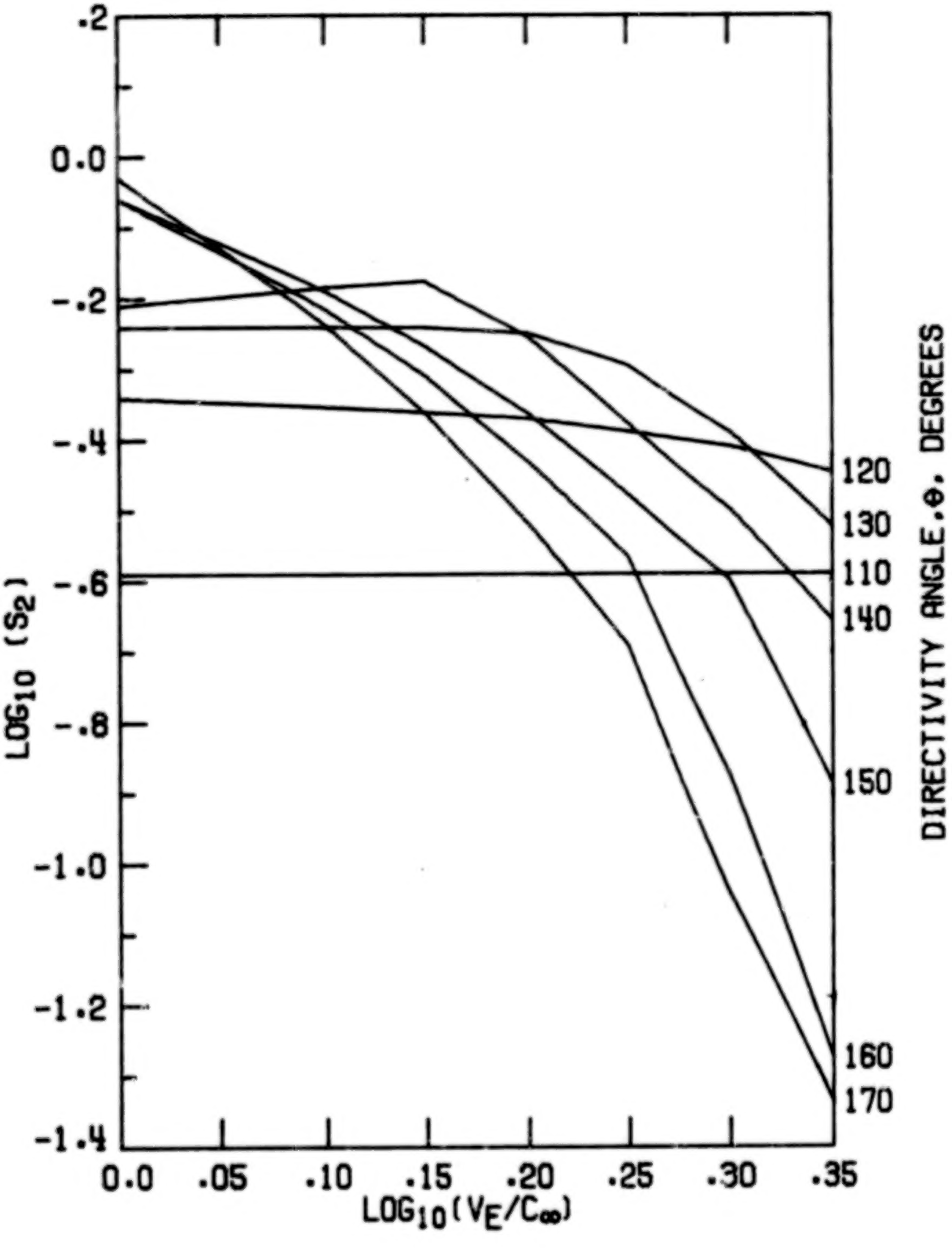

Figure 14. - Location of second peak Strouhal number, S_2.

58

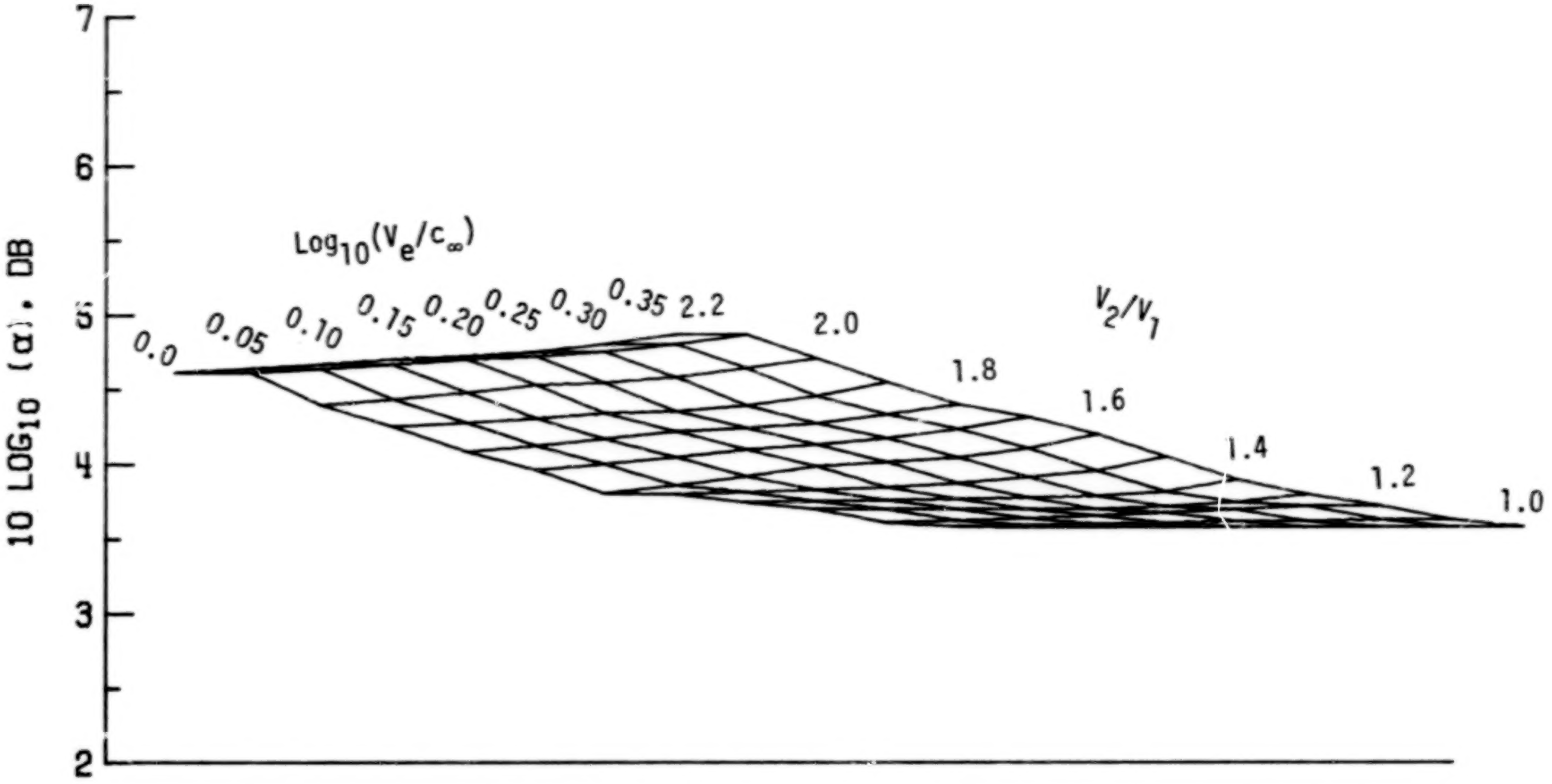

(a) Directivity angle, 120 degrees.

Figure 15. - Factor relating height of second spectral peak to first spectral spectral peak, α.

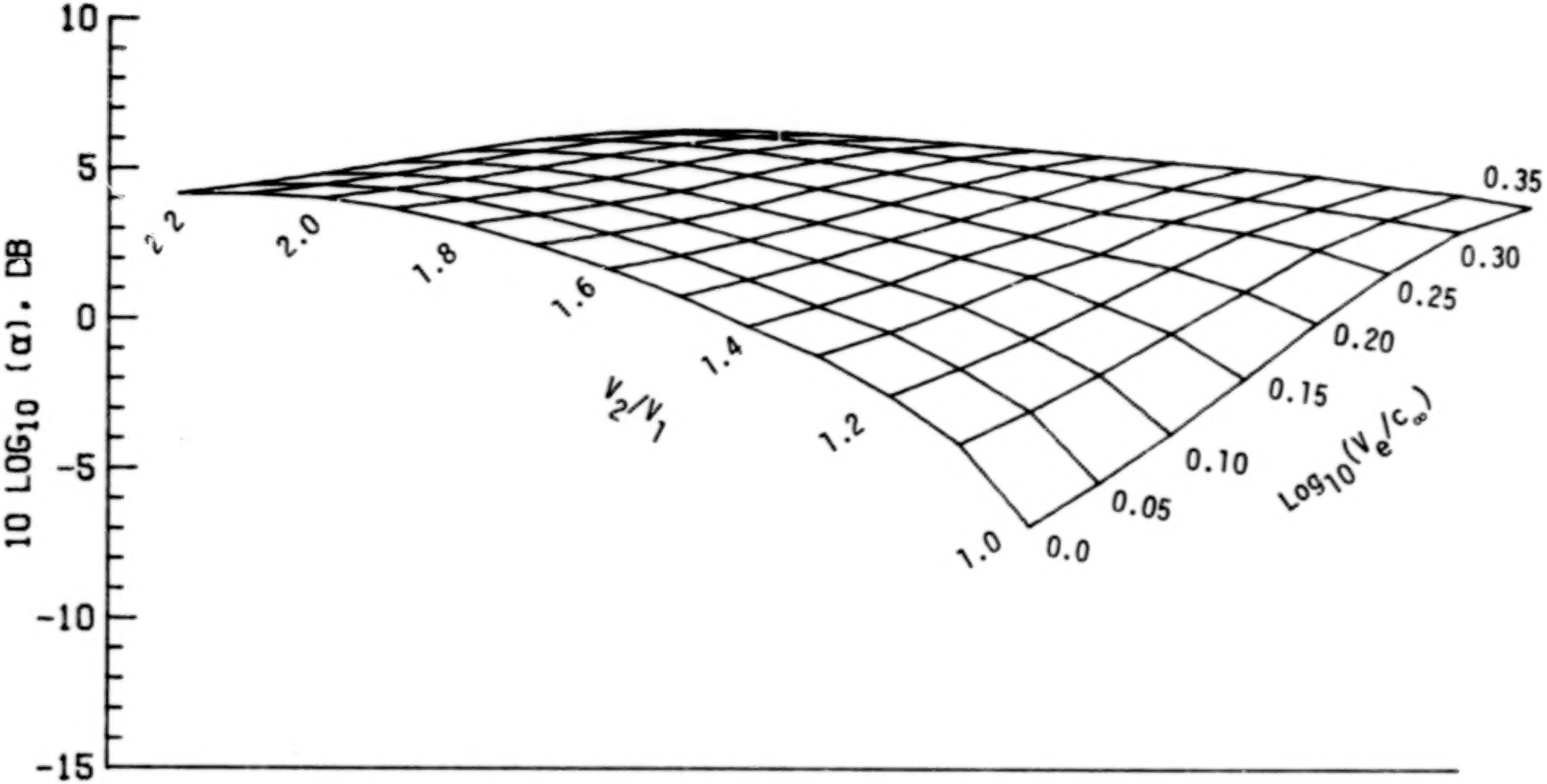

(b) Directivity angle, 130 degrees.

Figure 15. - Continued.

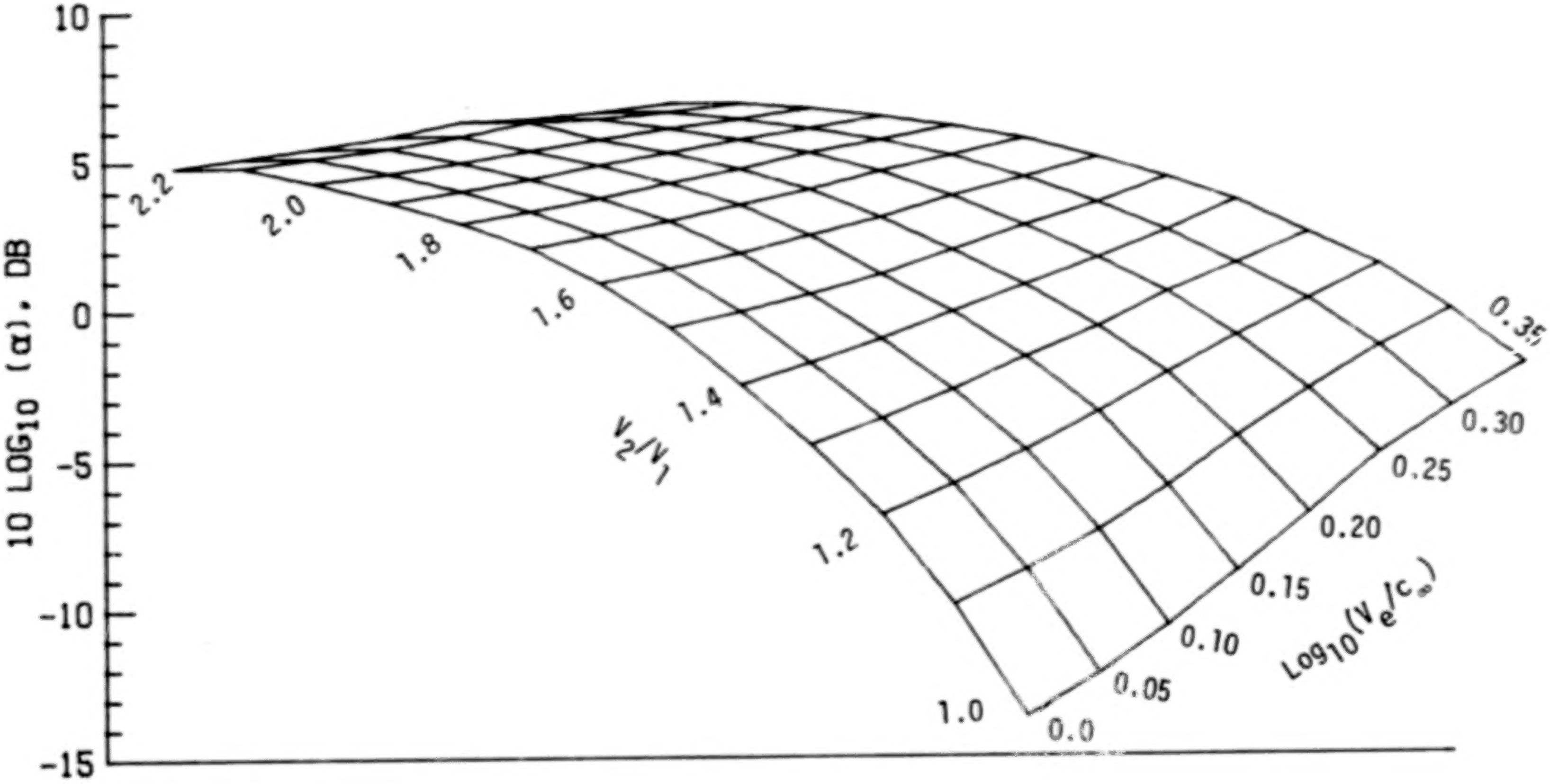

(c) Directivity angle, 140 degrees.

Figure 15. - Continued.

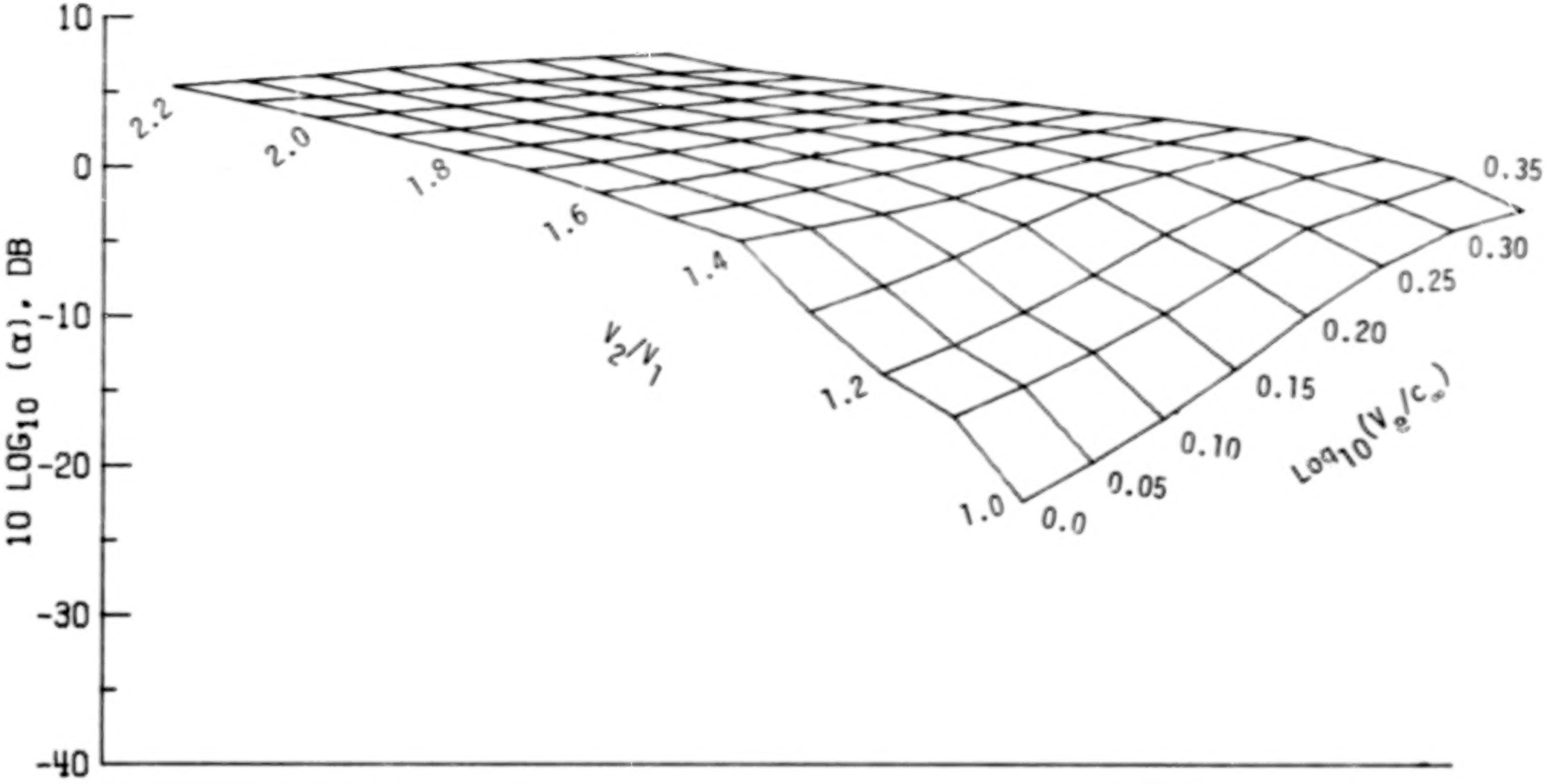

(d) Directivity angle, 150 degrees.

Figure 15. - Continued.

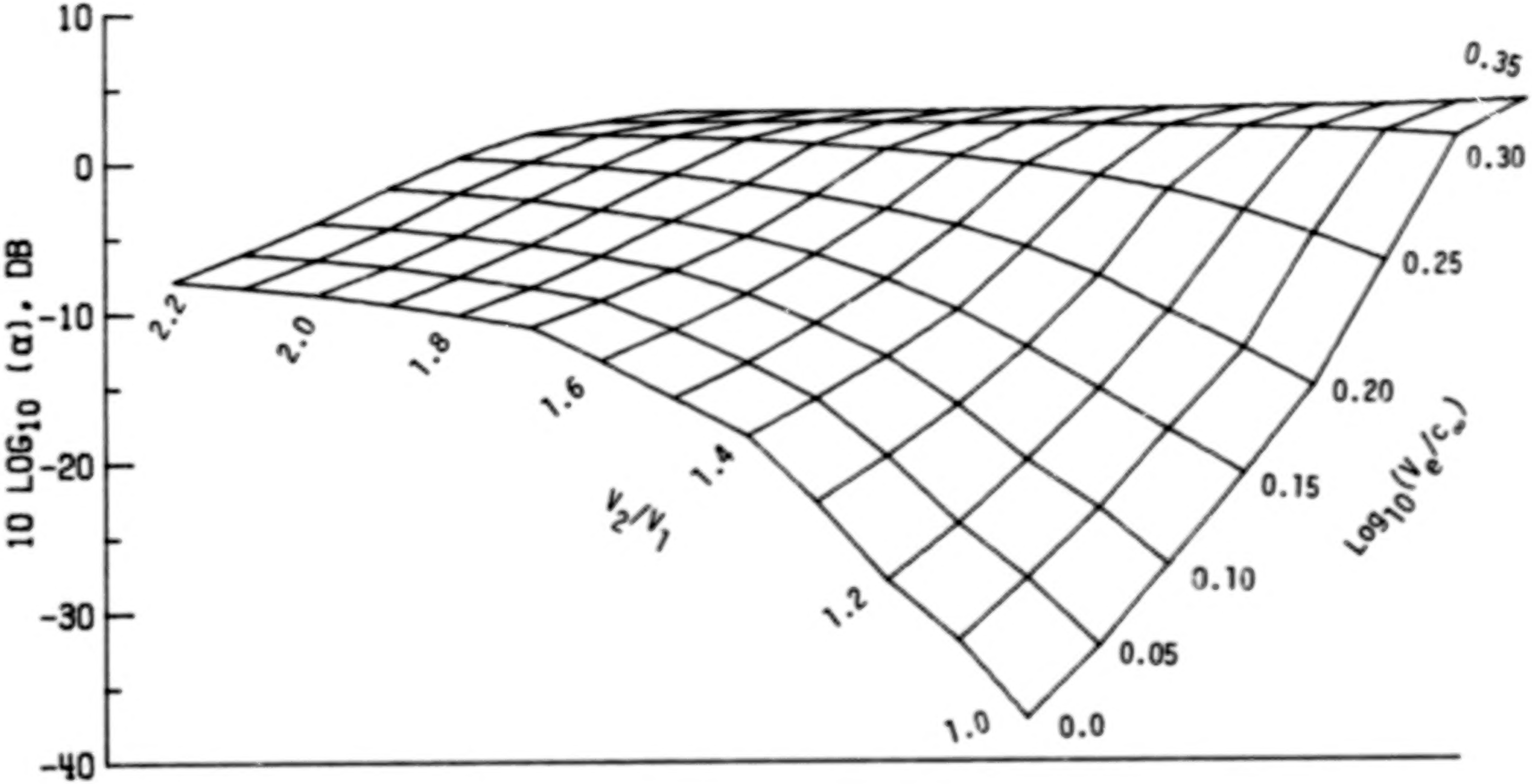

(e) Directivity angle, 165 degrees.

Figure 15. - Concluded.

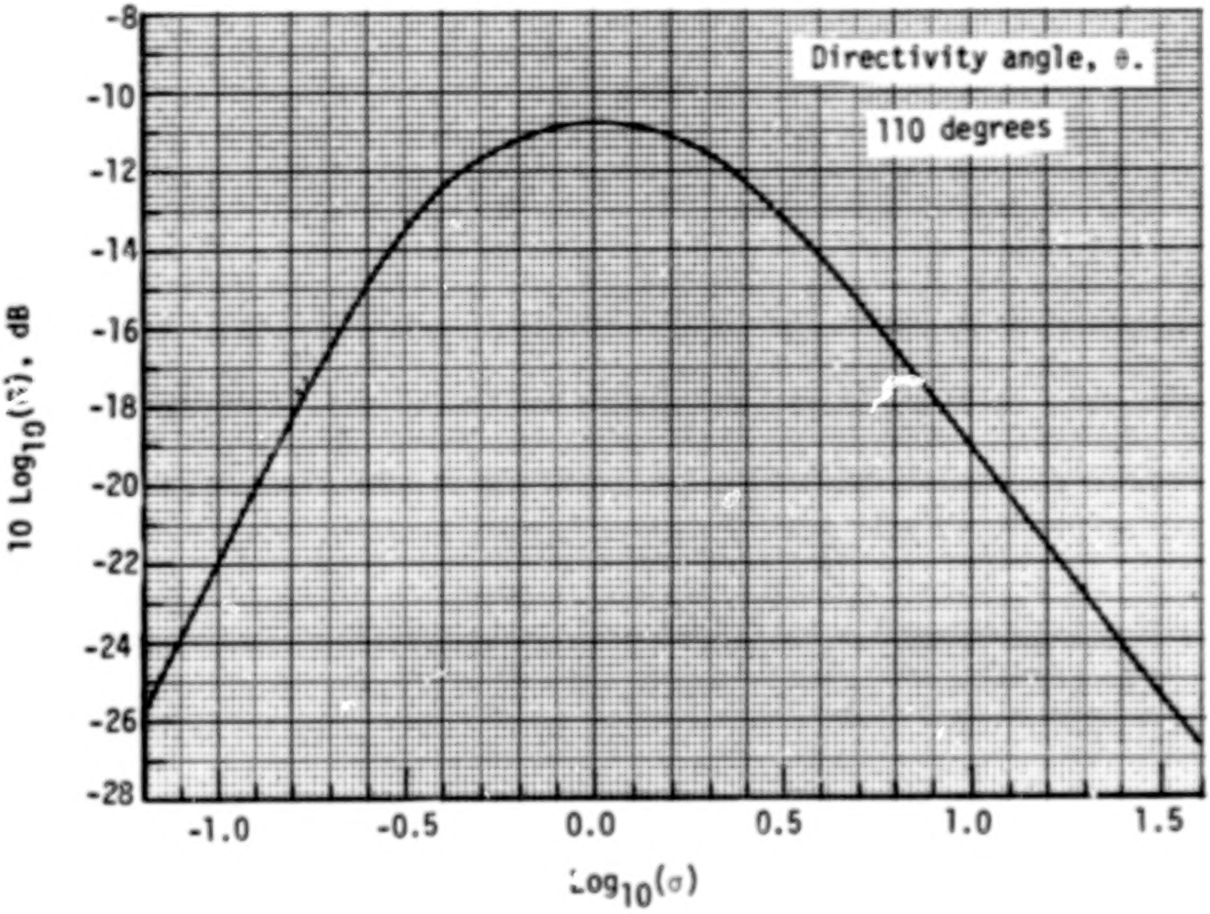

Figure 16. - Normalized spectral distribution, G.

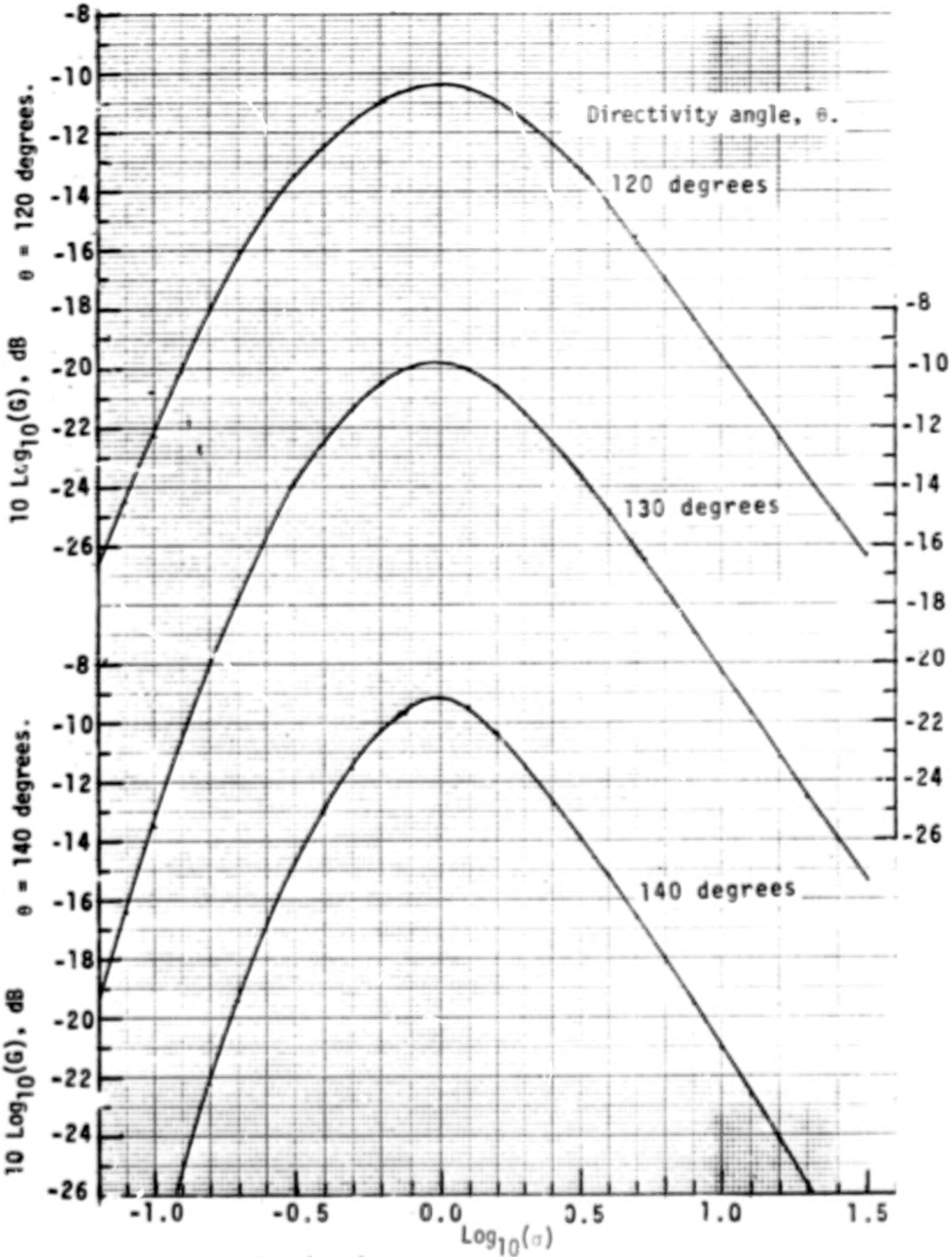

Figure 16. -Continued.

TABLE OF CONTENTS

SUMMARY	1	1/A6
INTRODUCTION	2	1/A7
LIST OF SYMBOLS	3	1/A8
DESCRIPTION OF DATA BASE	6	1/A11
PREDICTION PROCEDURE	8	1/A13
Equivalent Jet	9	1/A14
Acoustic Power	10	1/B1
Directivity and Overall Mean Square Pressure	11	1/B2
Spectral Distribution	12	1/B3
DATA COMPARISONS	13	1/B4
Static Case Data	14	1/B5
Wind Tunnel Case Data	16	1/B7
CONCLUSIONS	18	1/B9
REFERENCES	20	1/B11
TABLES	21	1/B12
FIGURES	44	1/E7
APPENDIX A Typical Static Case Spectral Distributions	79	2/B2
APPENDIX B Typical Wind Tunnel Case Spectral Distributions	128	2/E9

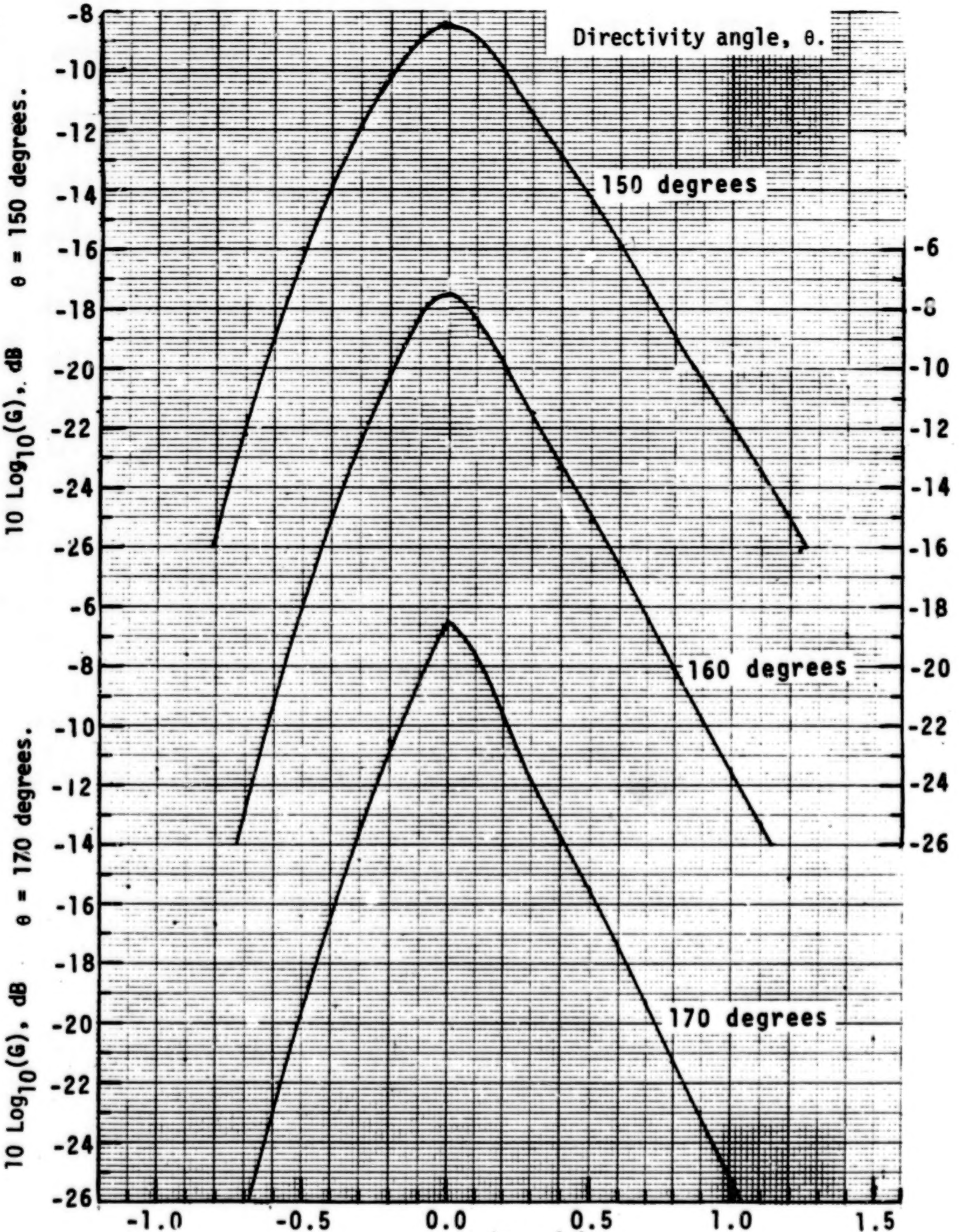

Figure 16. -Concluded.

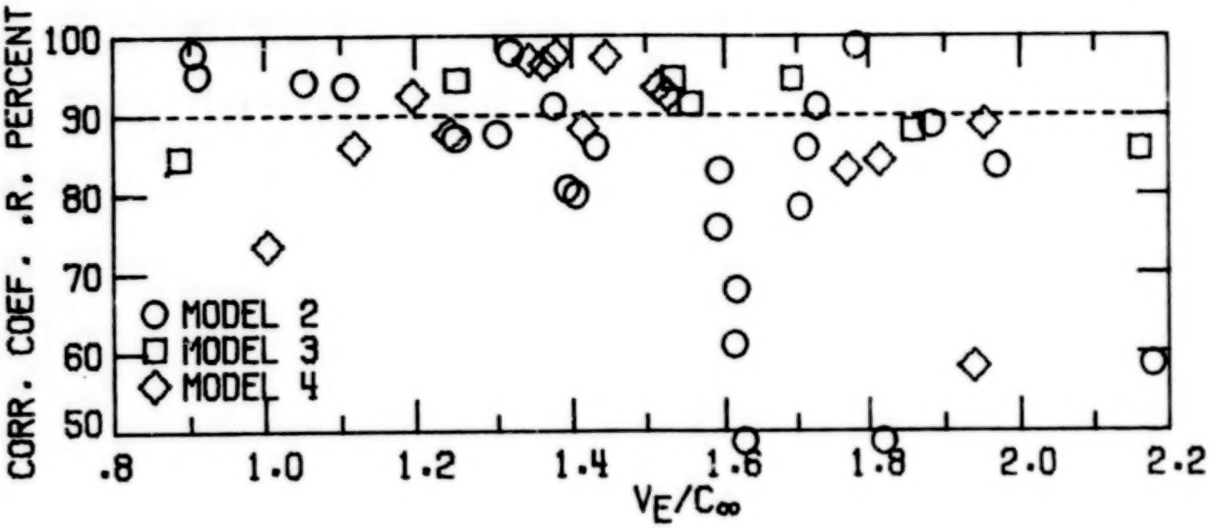

(a) Directivity angle, 60 degrees.

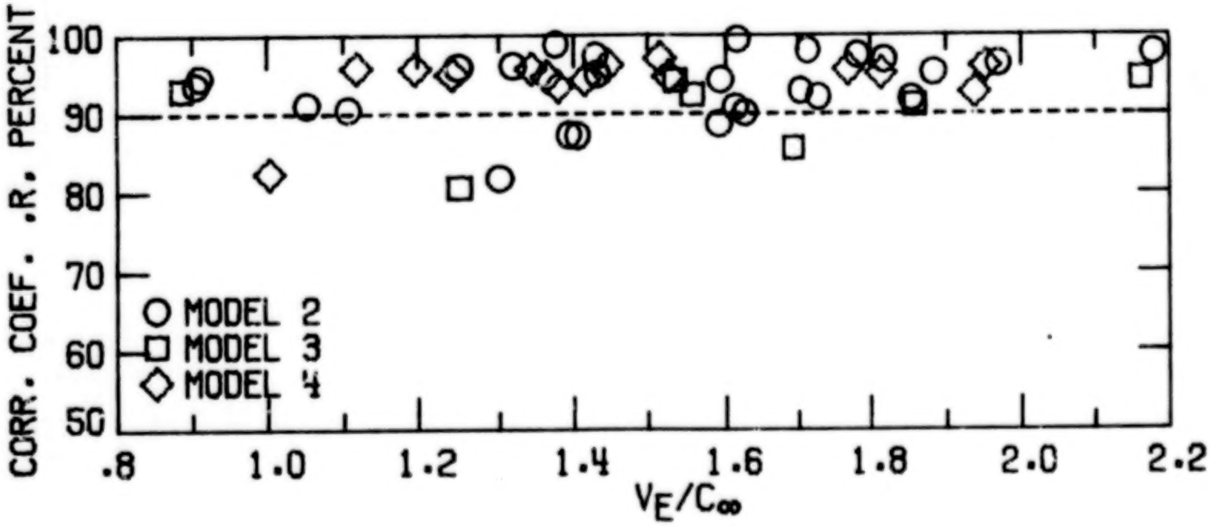

(b) Directivity angle, 90 degrees.

Figure 17. - Spectral mean square pressure correlation coefficients for static data cases.

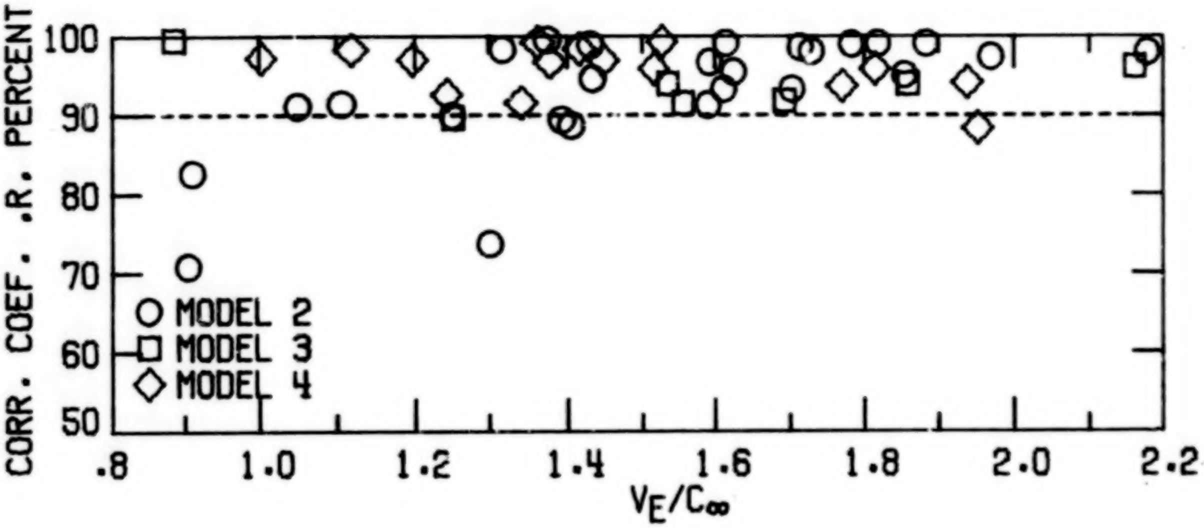

(c) Directivity angle, 120 degrees.

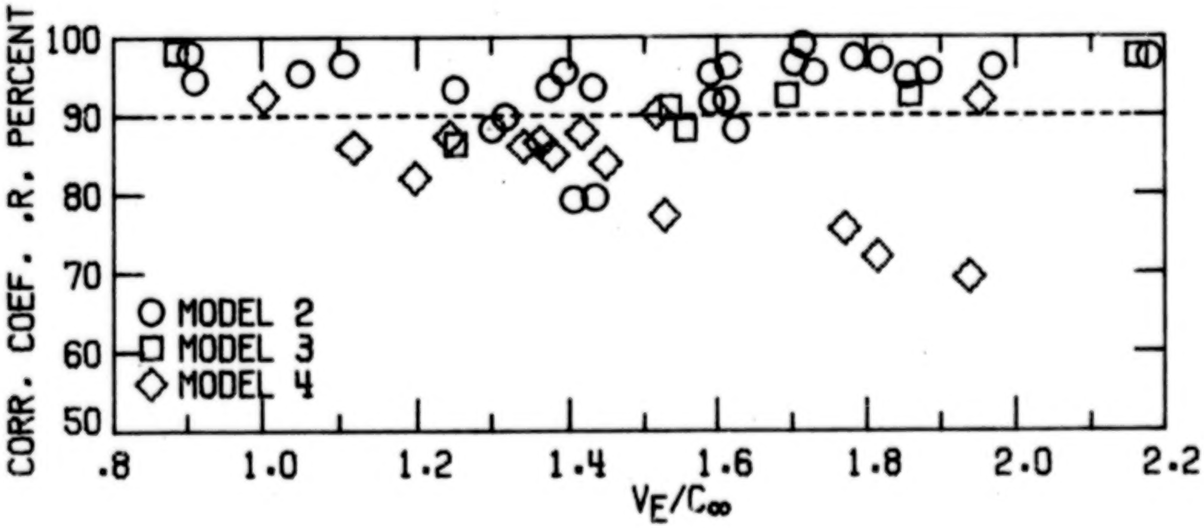

(d) Directivity angle, 150 degrees.

Figure 17. - Concluded.

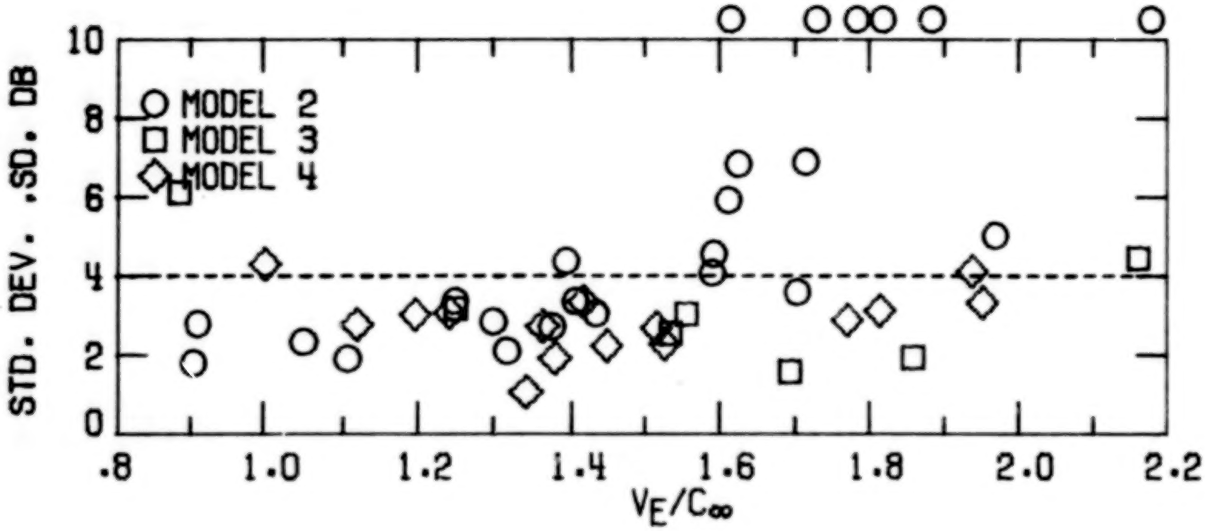

(a) Directivity angle, 60 degrees.

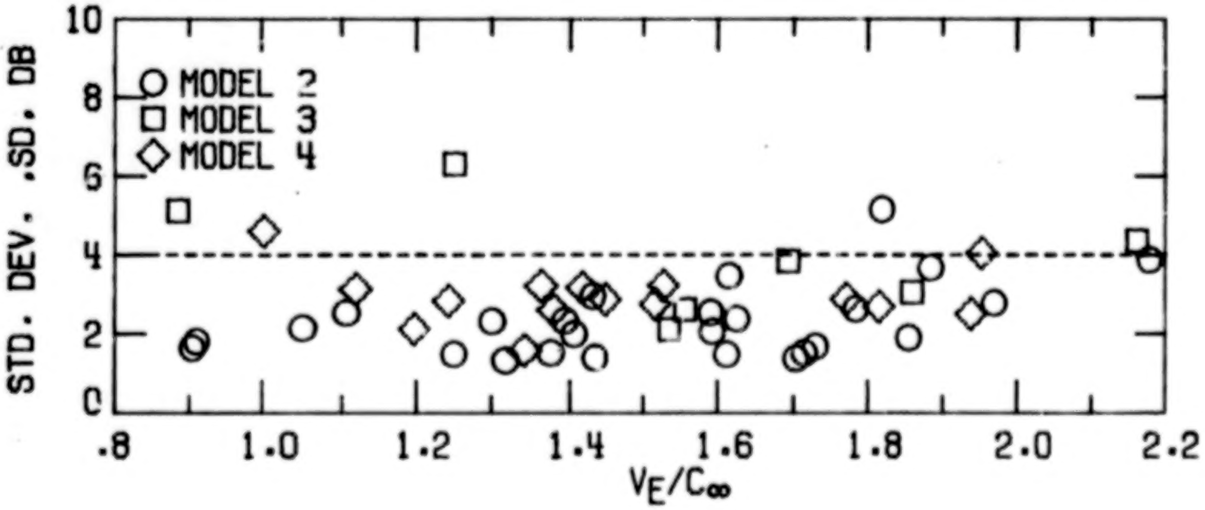

(b) Directivity angle, 90 degrees.

Figure 18. - Spectral sound pressure level standard deviations for static data cases.

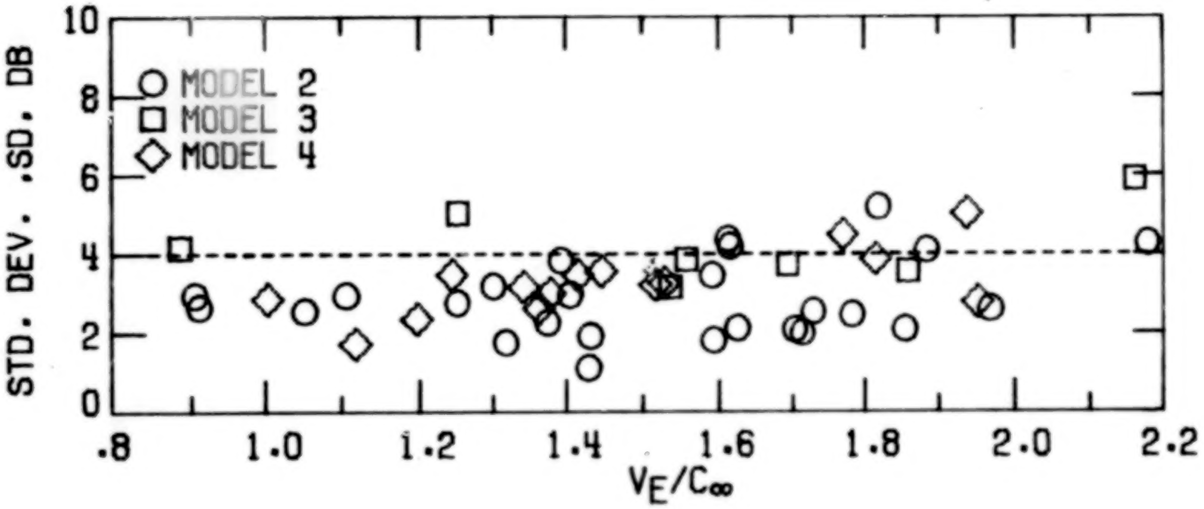

(c) Directivity angle, 120 degrees.

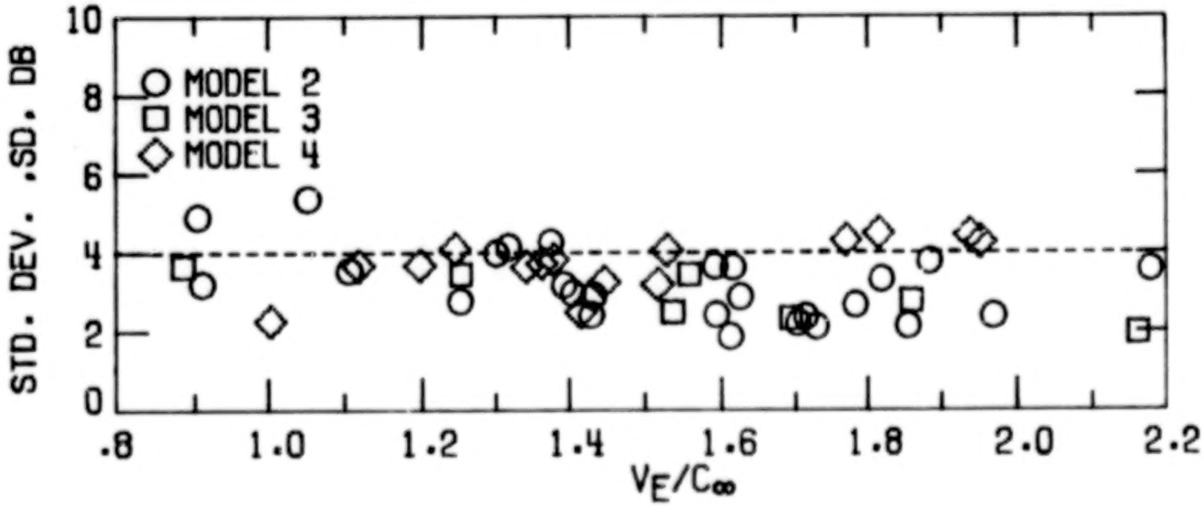

(d) Directivity angle, 150 degrees.

Figure 18. - Concluded.

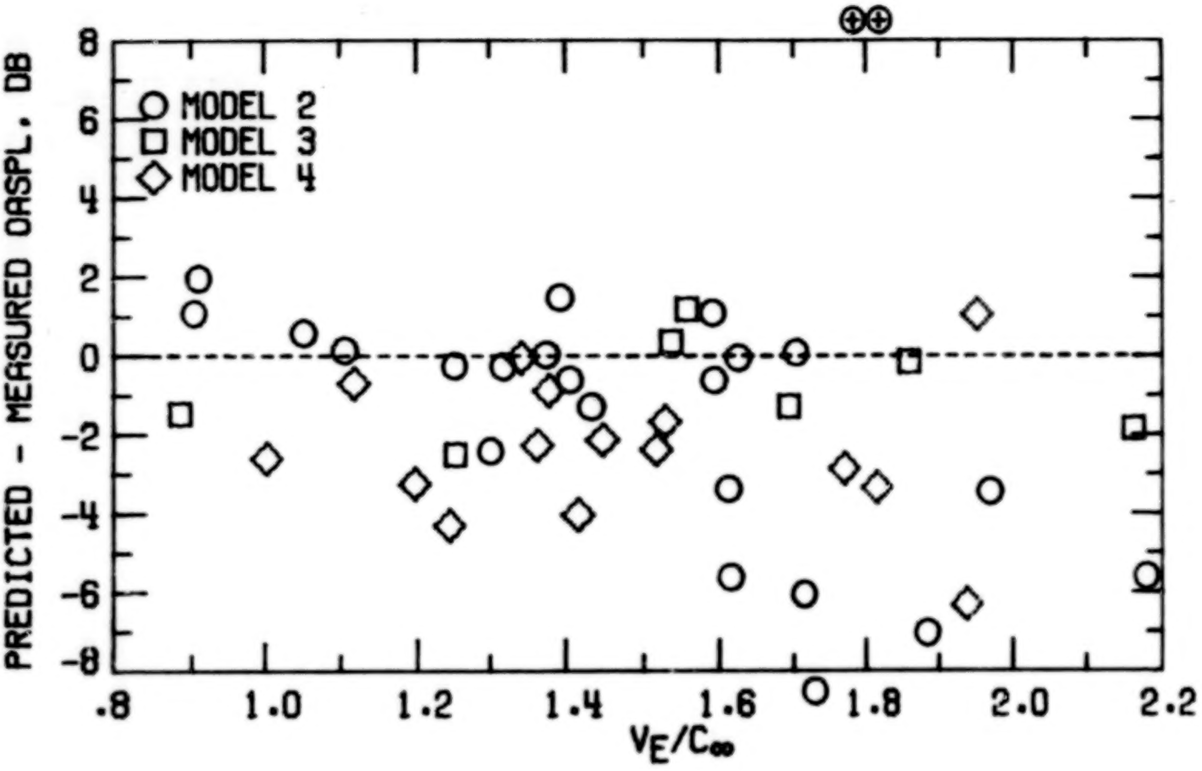

(a) Directivity angle, 60 degrees.

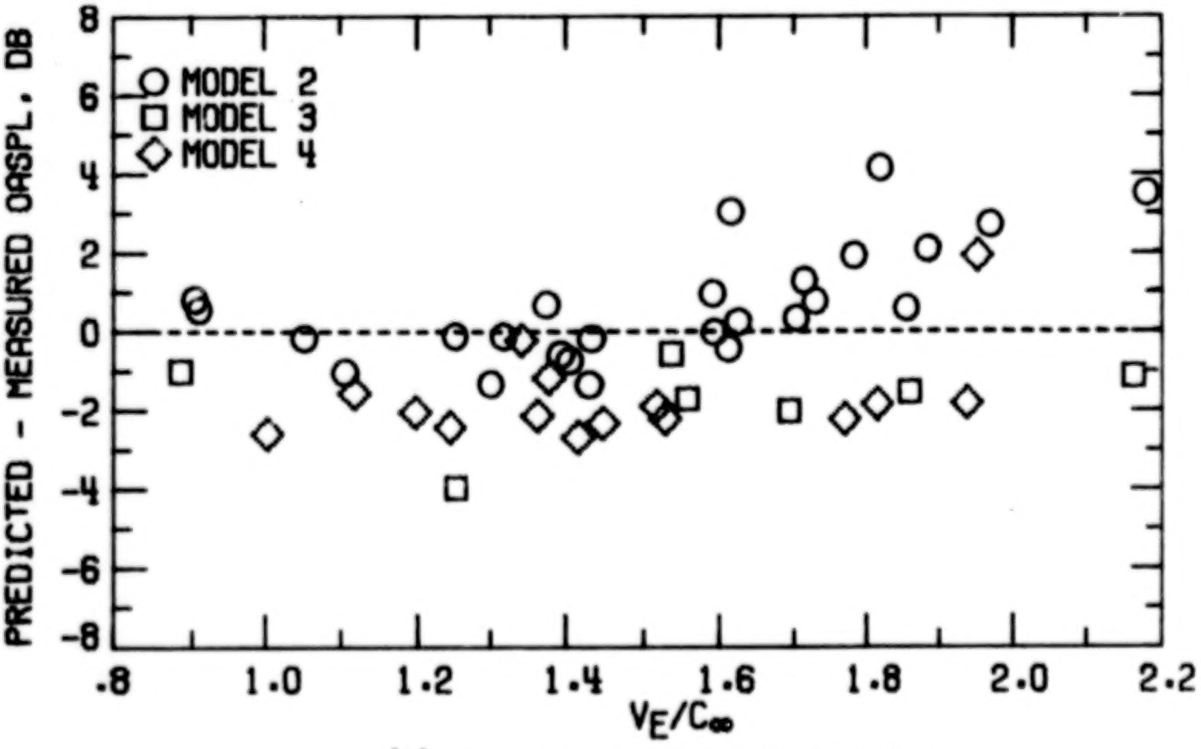

(b) Directivity angle, 90 degrees.

Figure 19. - OASPL comparisons for static data cases.

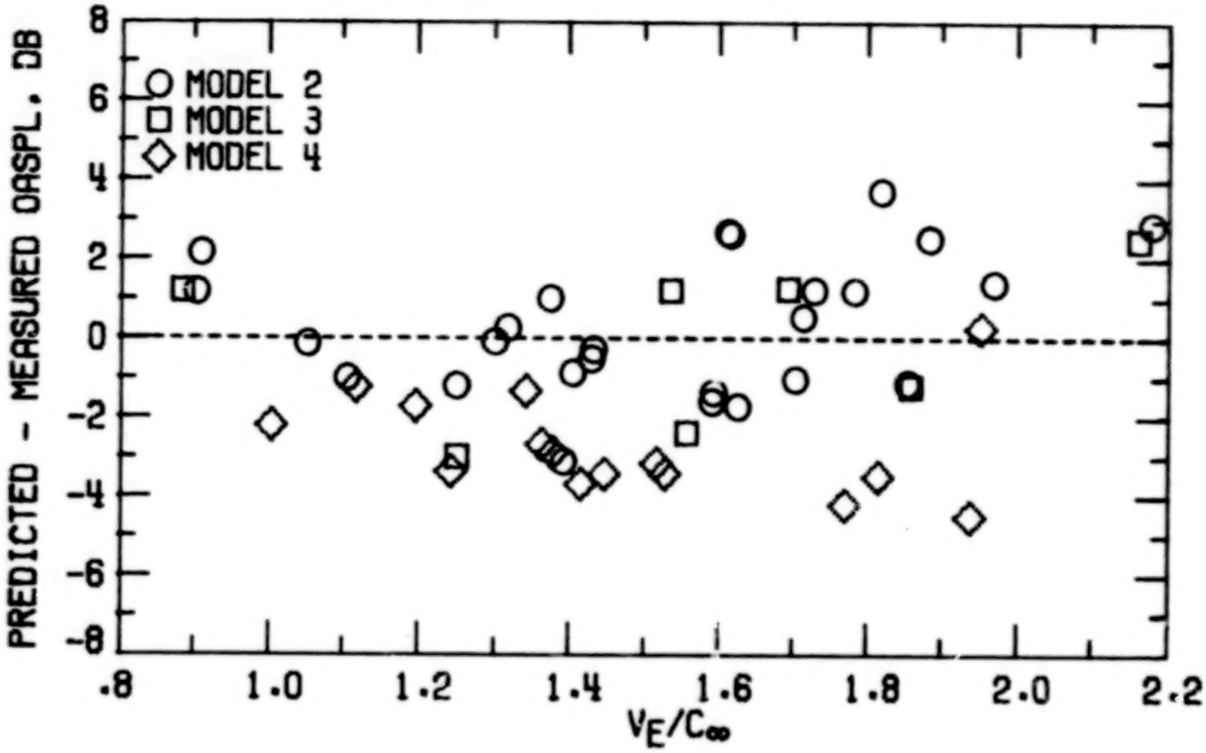

(c) Directivity angle, 120 degrees.

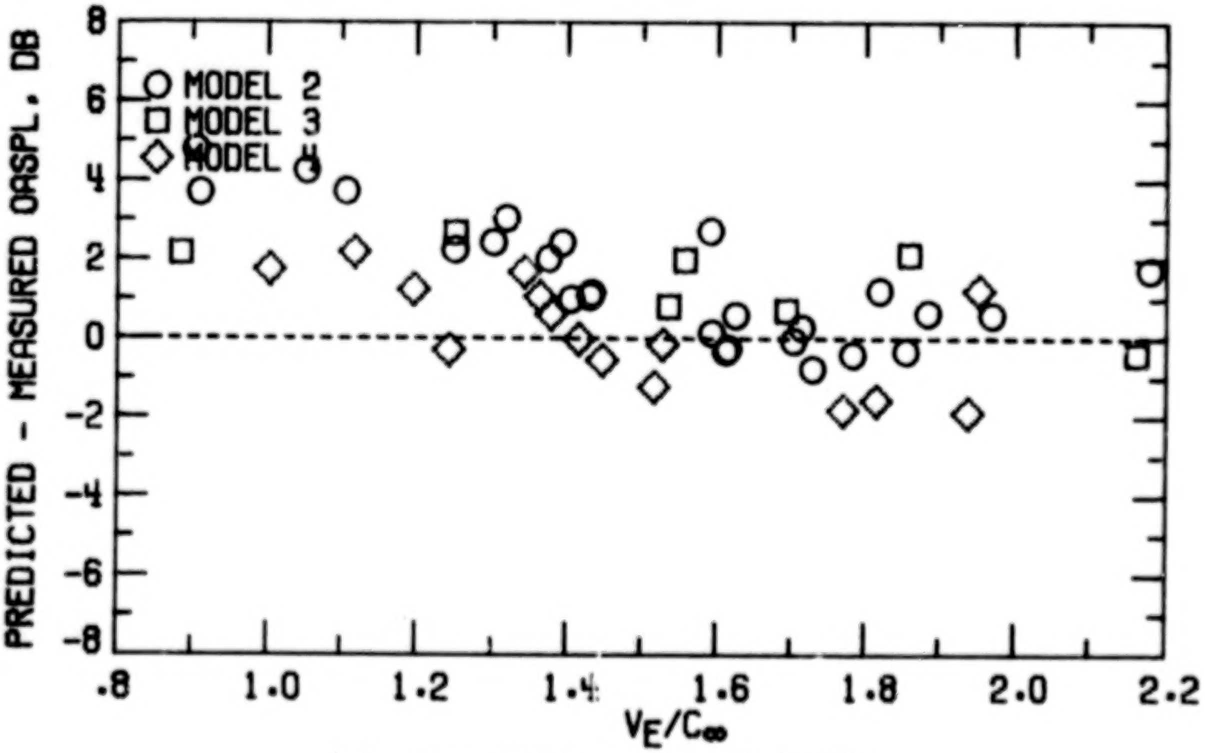

(d) Directivity angle, 150 degrees.

Figure 19. - Concluded.

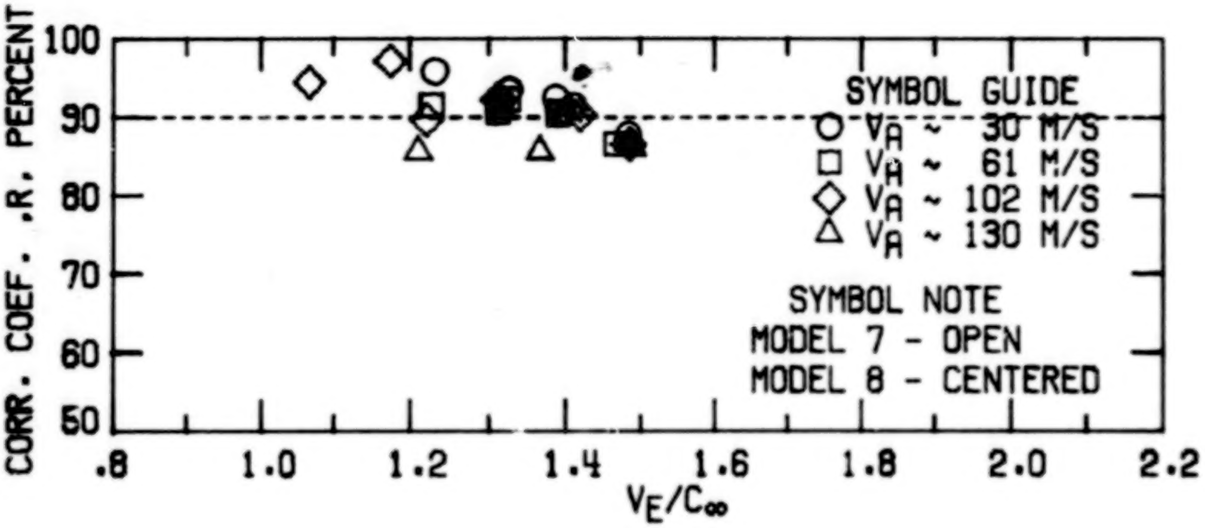

(a) Directivity angle, 60 degrees.

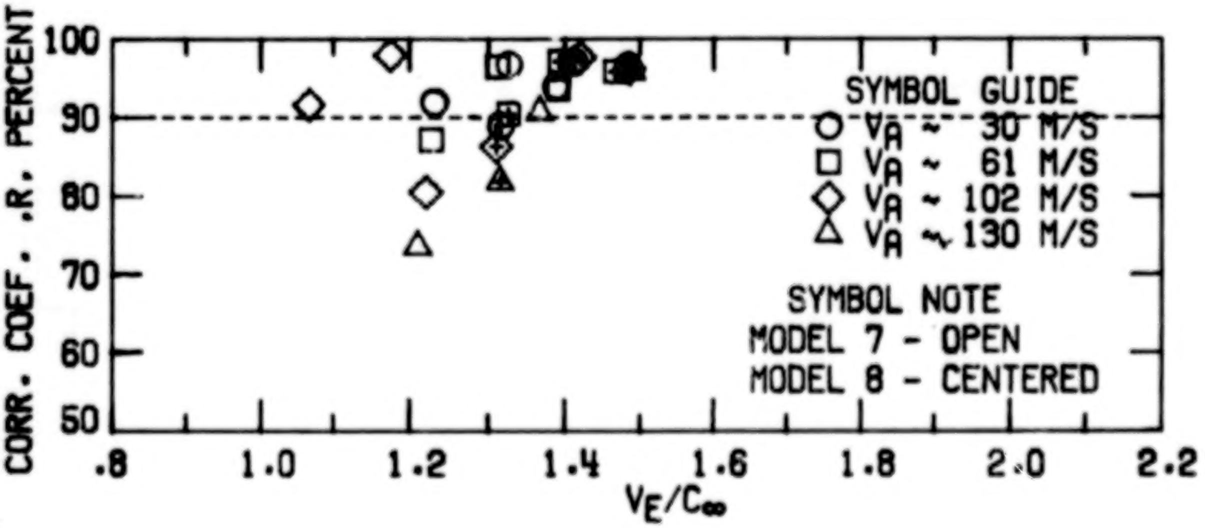

(b) Directivity angle, 90 degrees.

Figure 20. - Spectral mean square pressure correlation coefficients for wind tunnel data cases.

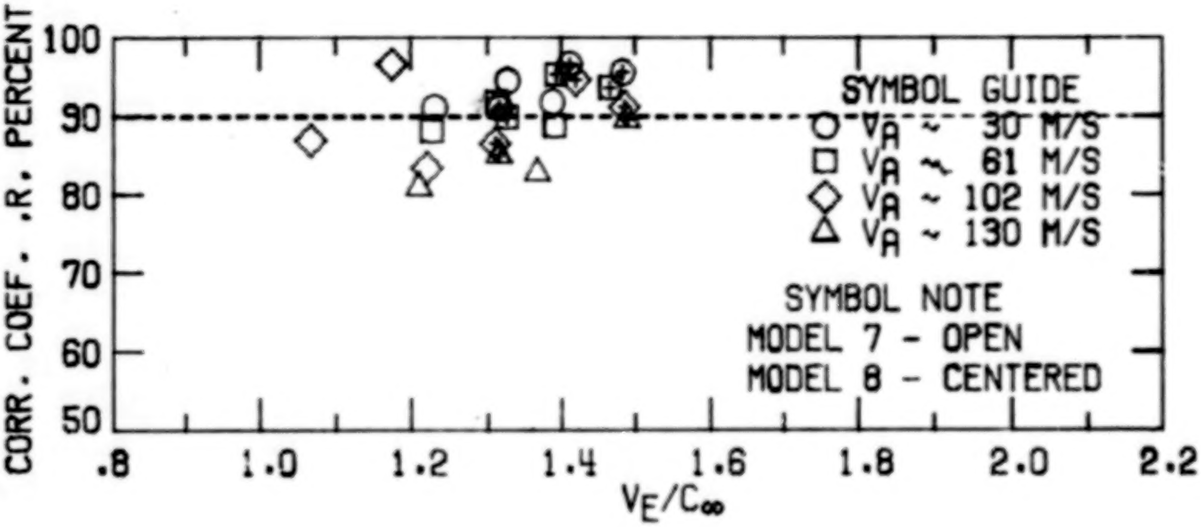

(c) Directivity angle, 120 degrees.

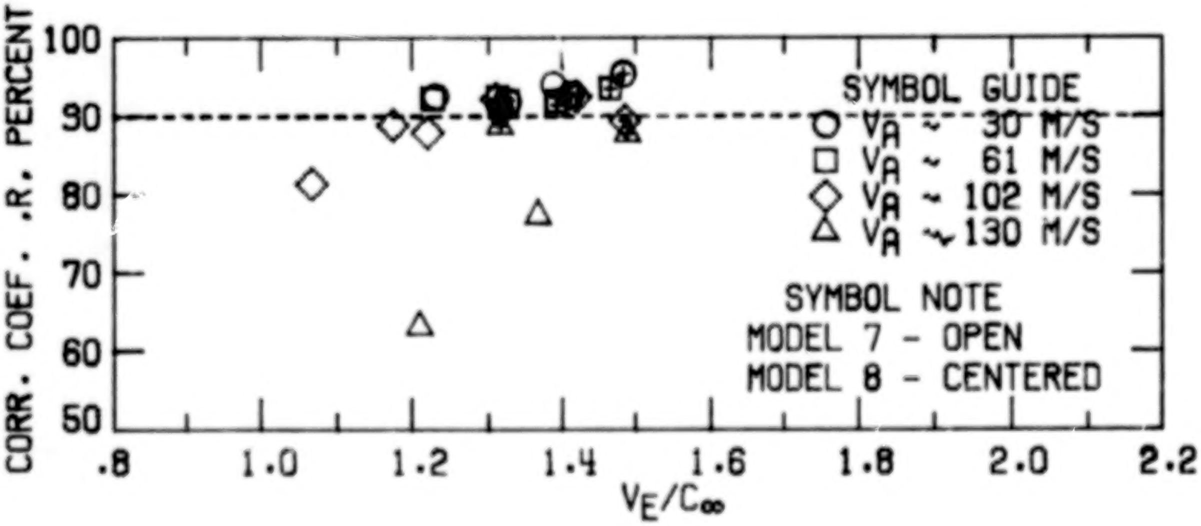

(d) Directivity angle, 150 degrees.

Figure 20. - Concluded.

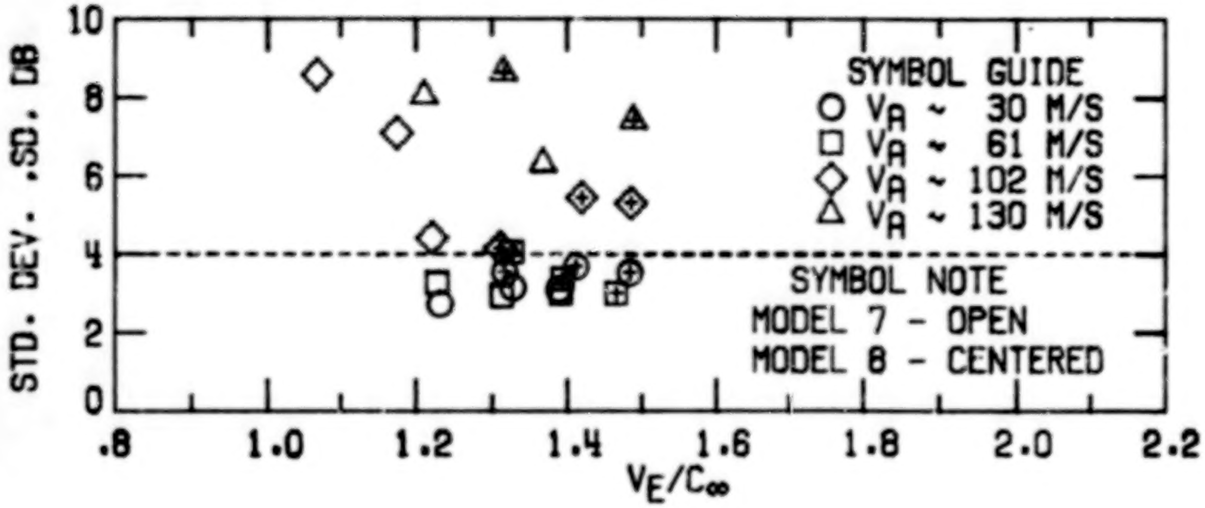

(a) Directivity angle, 60 degrees.

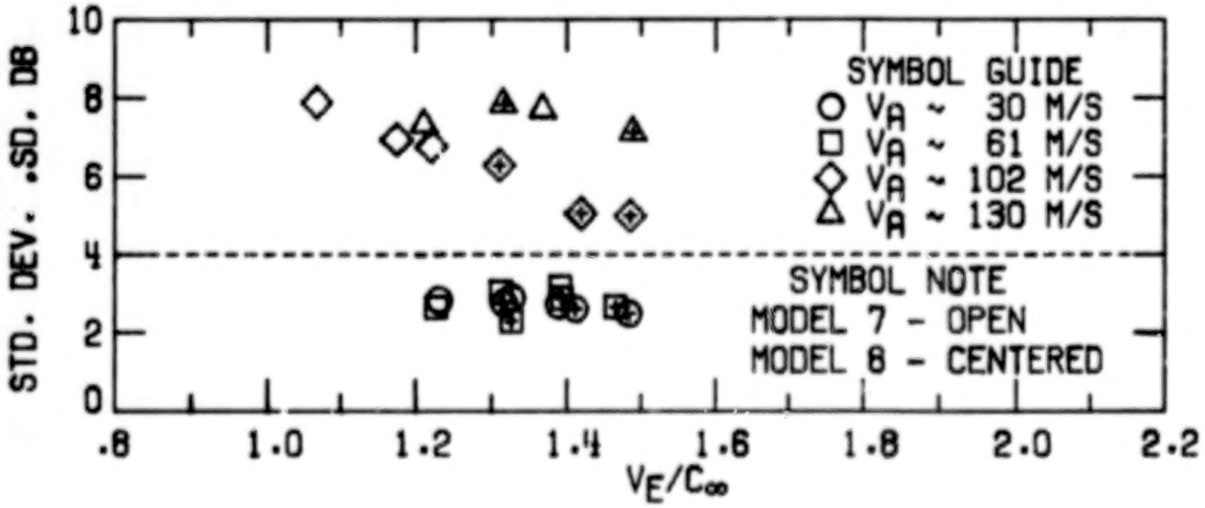

(b) Directivity angle, 90 degrees.

Figure 21. - Spectral sound pressure level standard deviations for wind tunnel data cases.

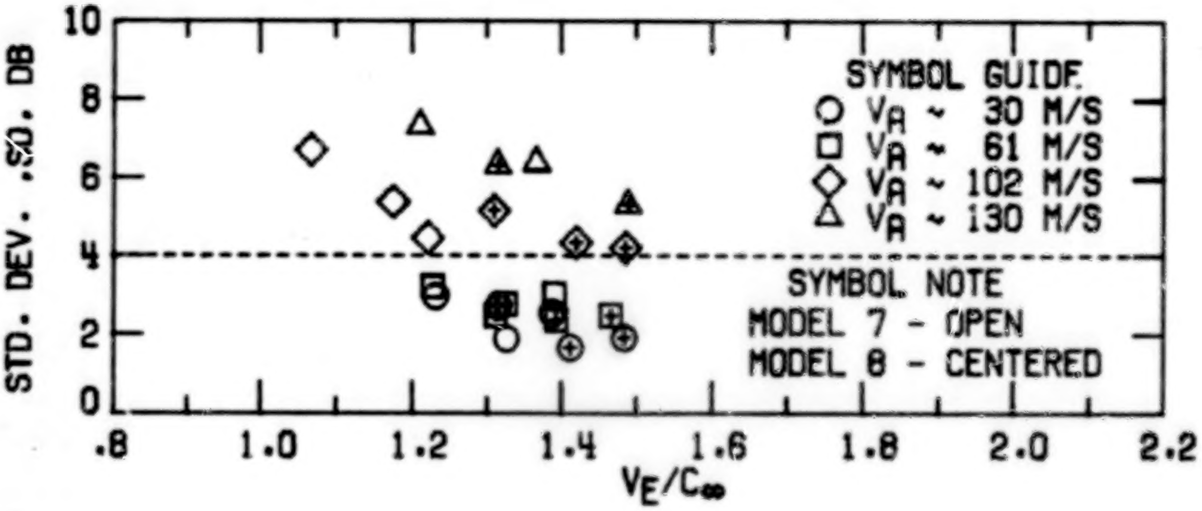

(c) Directivity angle, 120 degrees.

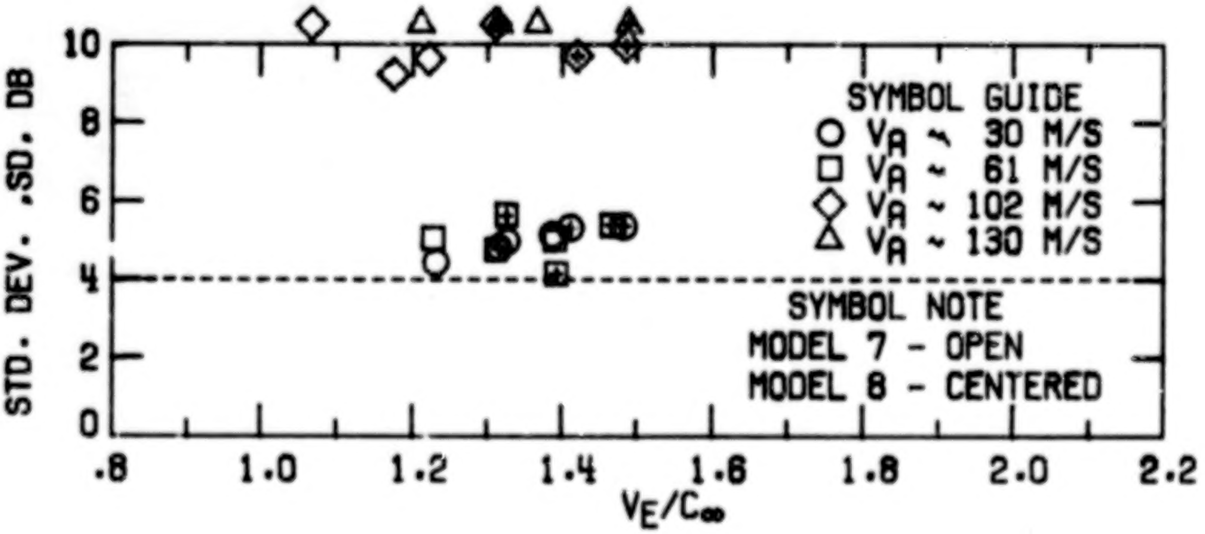

(d) Directivity angle, 150 degrees.

Figure 21. - Concluded.

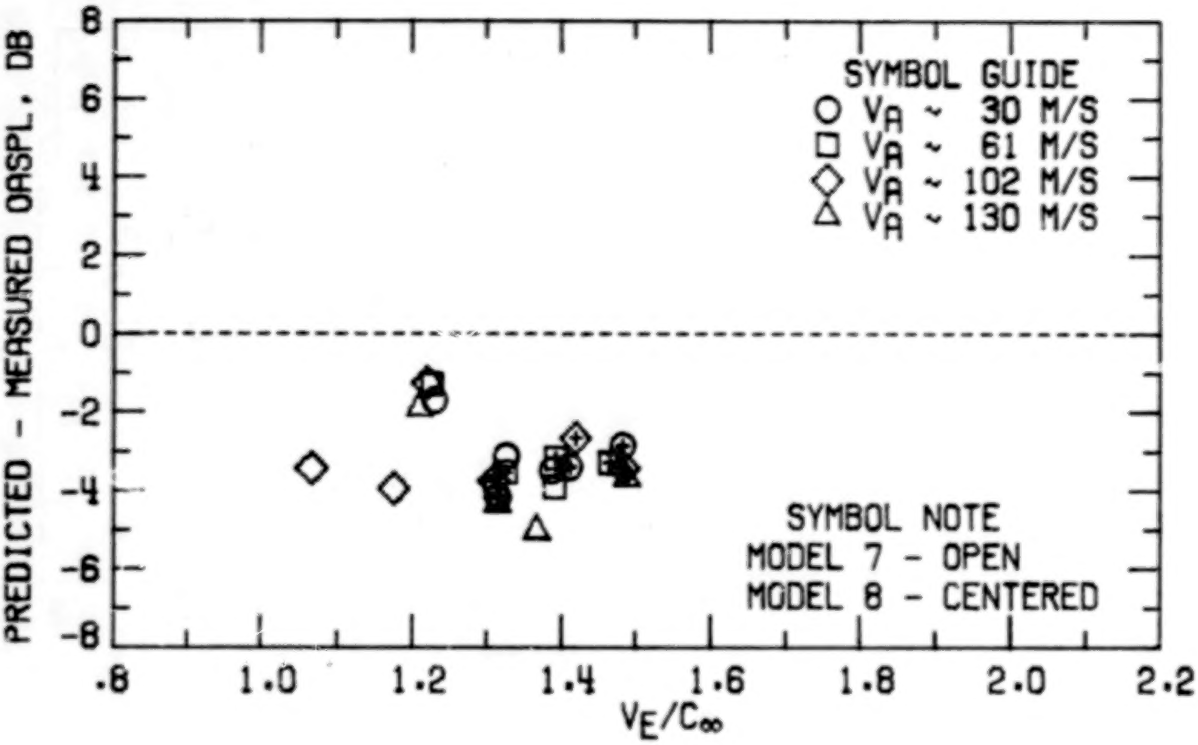

(a) Directivity angle, 60 degrees.

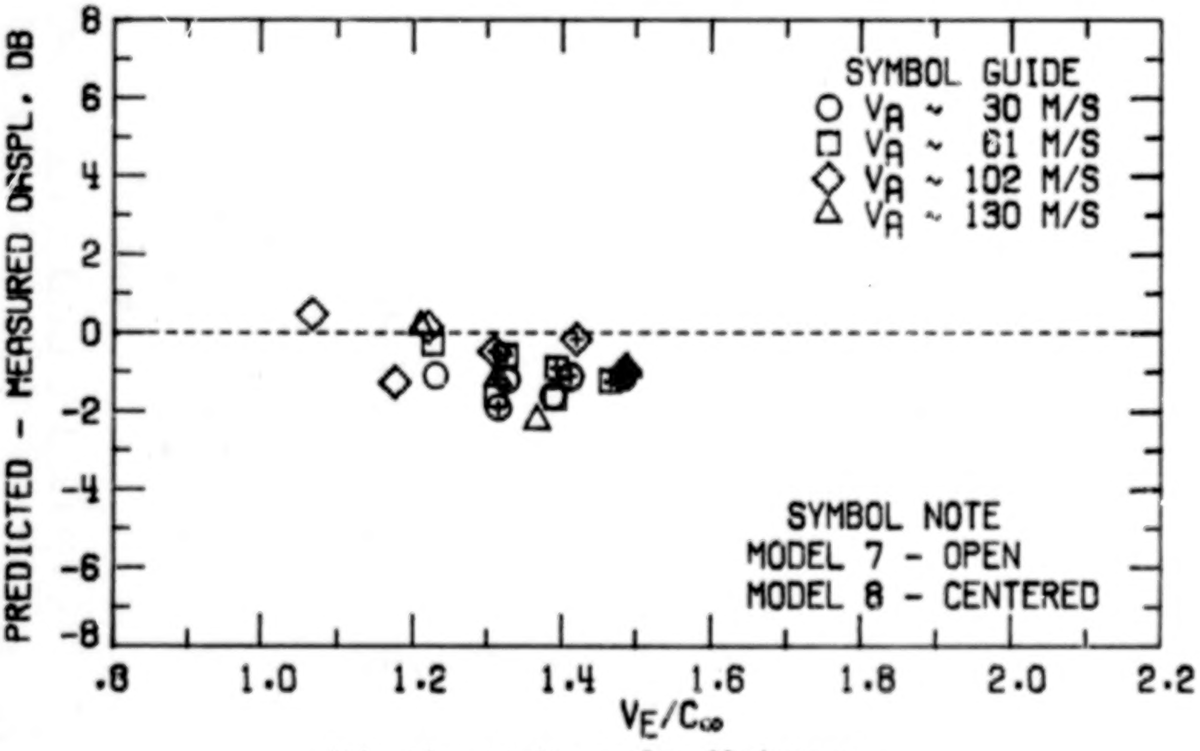

(b) Directivity angle, 90 degrees.

Figure 22. - OASPL comparisons for wind tunnel data cases.

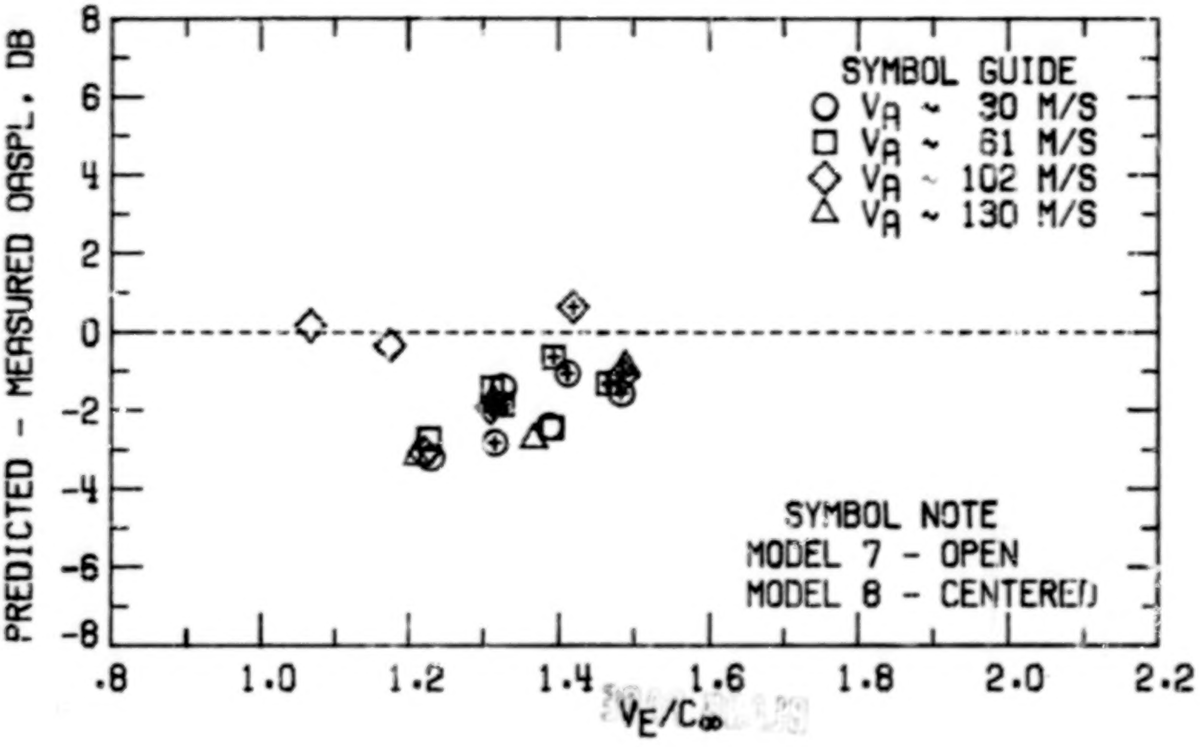

(c) Directivity angle, 120 degrees.

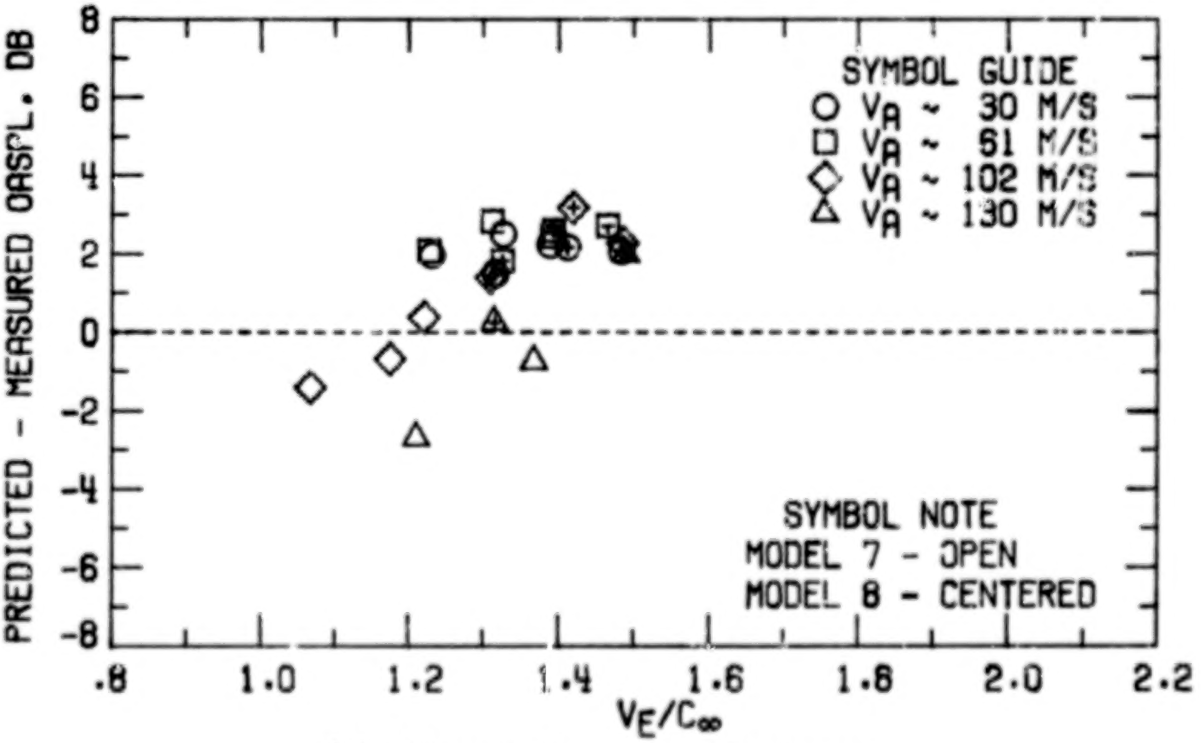

(d) Directivity angle, 150 degrees.

Figure 22. - Concluded.

BLANK PAGE

APPENDIX A

Typical Static Case

Spectral Distributions

FLOW PROPERTIES FOR CASE 1
NOZZLE MODEL 2

FORWARD FLIGHT VELOCITY, V_A = 0.0 M/S

	TEMPERATURE T_T, DEG K	VELOCITY V, M/S	MASS FLOW W, KG/S	P_T/P_A
PRIMARY	380.9	293.5	2.2797	1.5200
SECONDARY	377.6	340.1	1.9690	1.7800
EQUIVALENT	379.3	315.1	4.2488	

REFERENCE RADIUS = 45.7 M

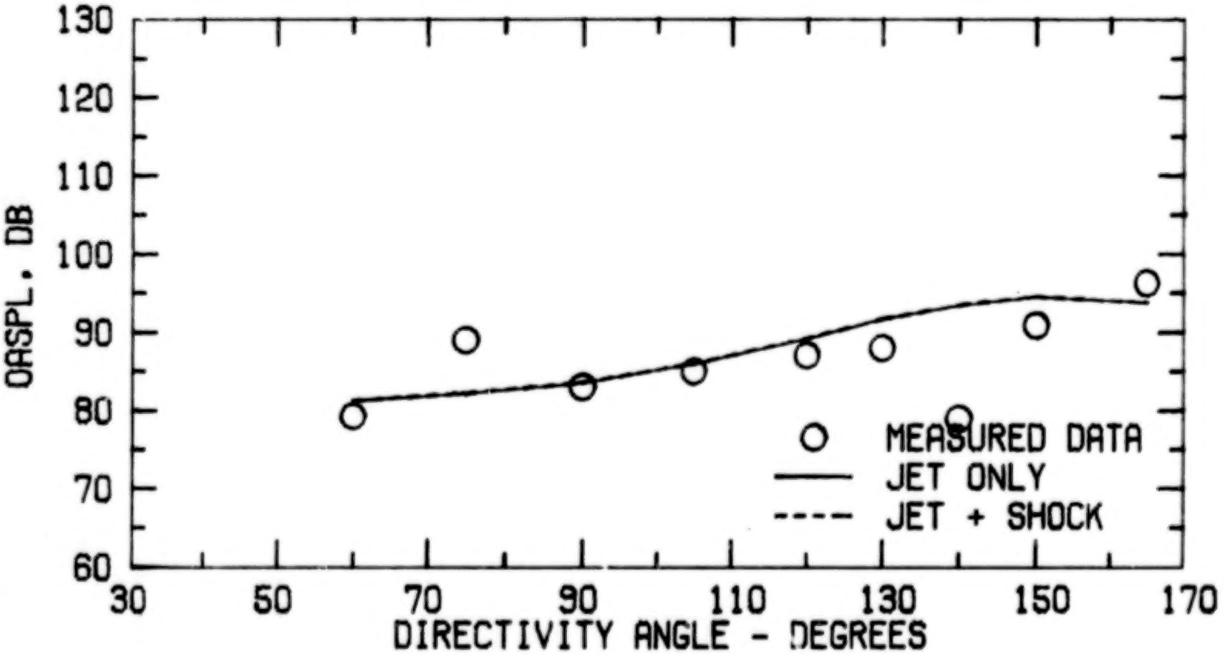

FIGURE A1 . SPECTRA COMPARISON FOR CASE 1
(A) FLOW PROPERTIES AND DIRECTIVITY PLOT

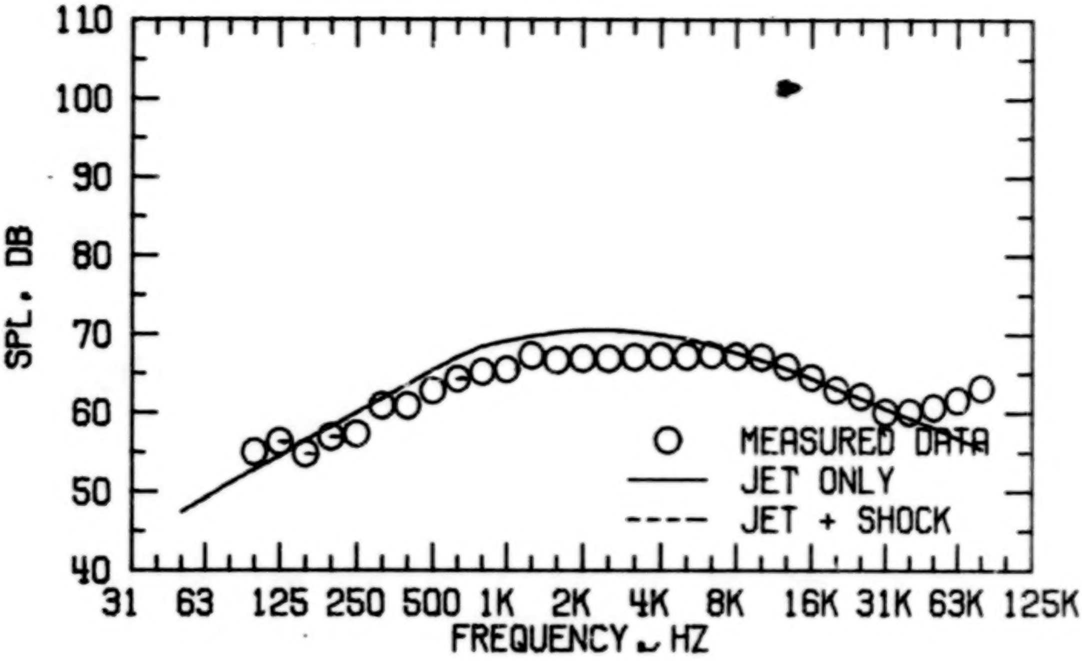

FIGURE A1 . SPECTRA COMPARISON FOR CASE 1
(B) DIRECTIVITY ANGLE = 60 DEGREES

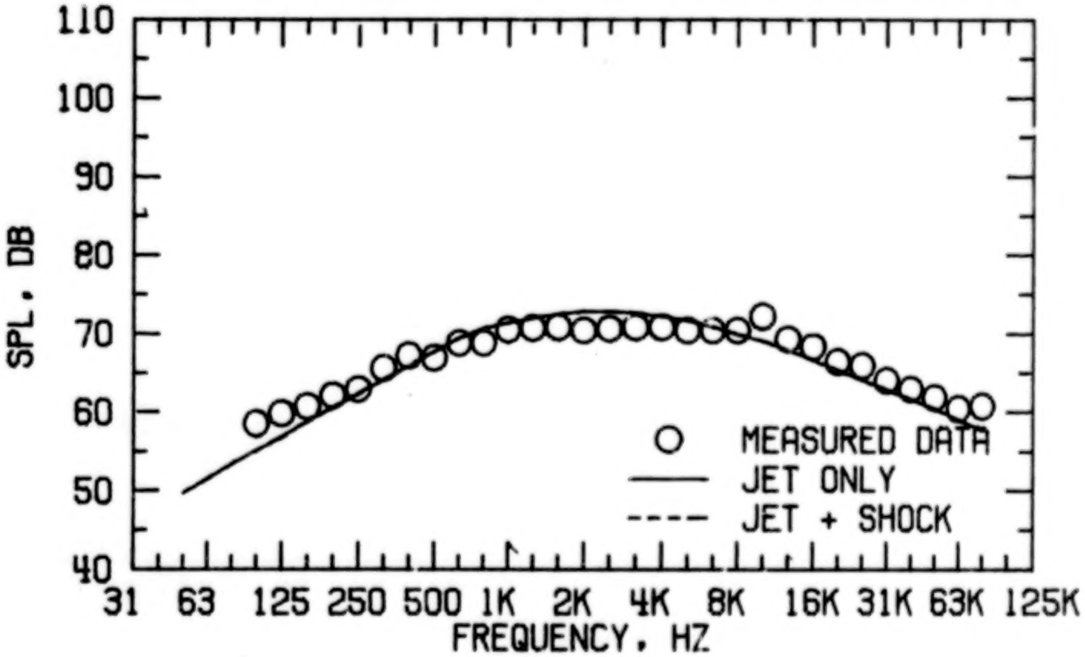

FIGURE A1 . SPECTRA COMPARISON FOR CASE 1
(C) DIRECTIVITY ANGLE = 90 DEGREES

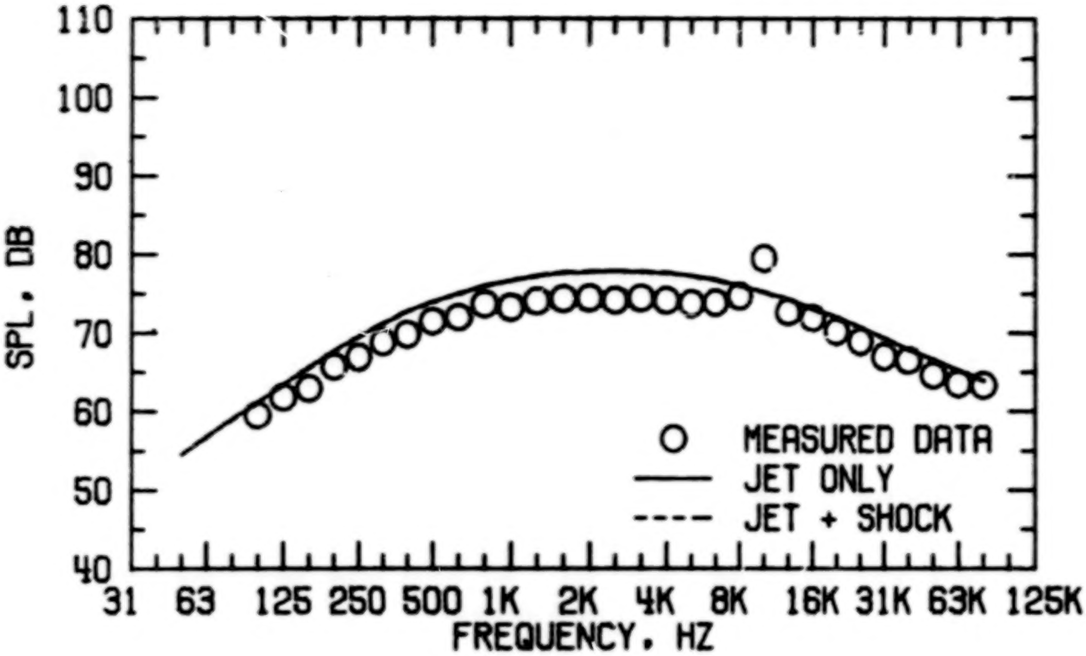

FIGURE A1 . SPECTRA COMPARISON FOR CASE 1
(D) DIRECTIVITY ANGLE = 120 DEGREES

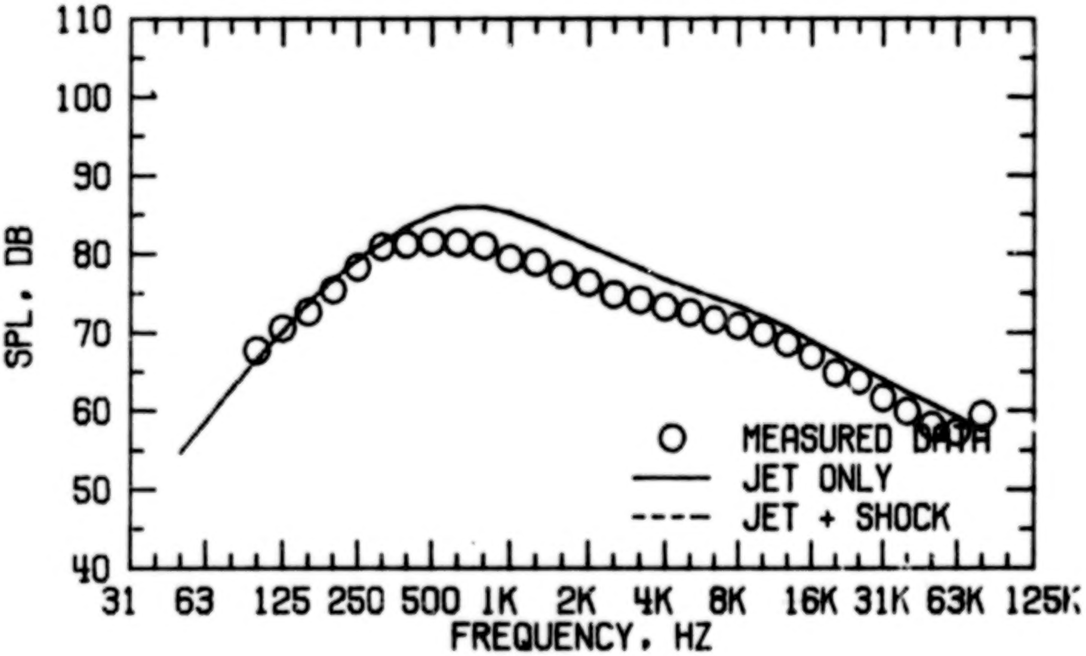

FIGURE A1 . SPECTRA COMPARISON FOR CASE 1
(E) DIRECTIVITY ANGLE = 150 DEGREES

FLOW PROPERTIES FOR CASE 3
NOZZLE MODEL 2

FORWARD FLIGHT VELOCITY, V_A = 0.0 M/S

	TEMPERATURE T_T, DEG K	VELOCITY V, M/S	MASS FLOW W, KG/S	P_T/P_A
PRIMARY	399.6	303.8	2.2529	1.5300
SECONDARY	702.6	637.6	2.7147	3.2200
EQUIVALENT	565.2	486.2	4.9677	

REFERENCE RADIUS = 45.7 M

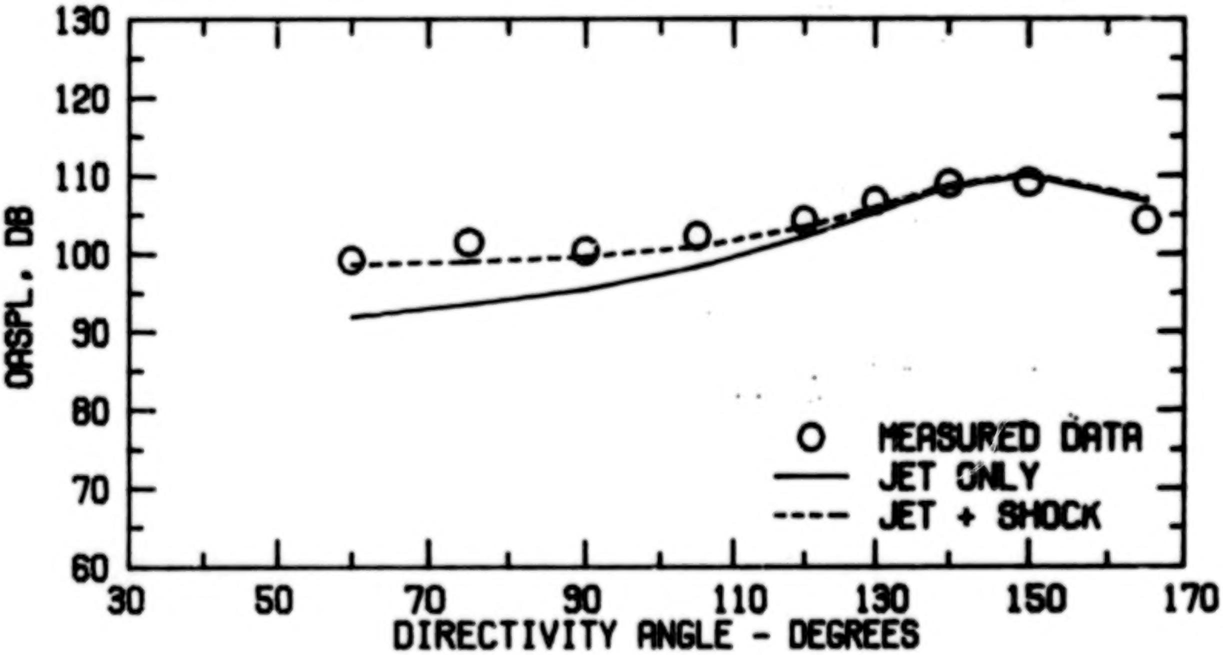

FIGURE A2 . SPECTRA COMPARISON FOR CASE 3
(A) FLOW PROPERTIES AND DIRECTIVITY PLOT

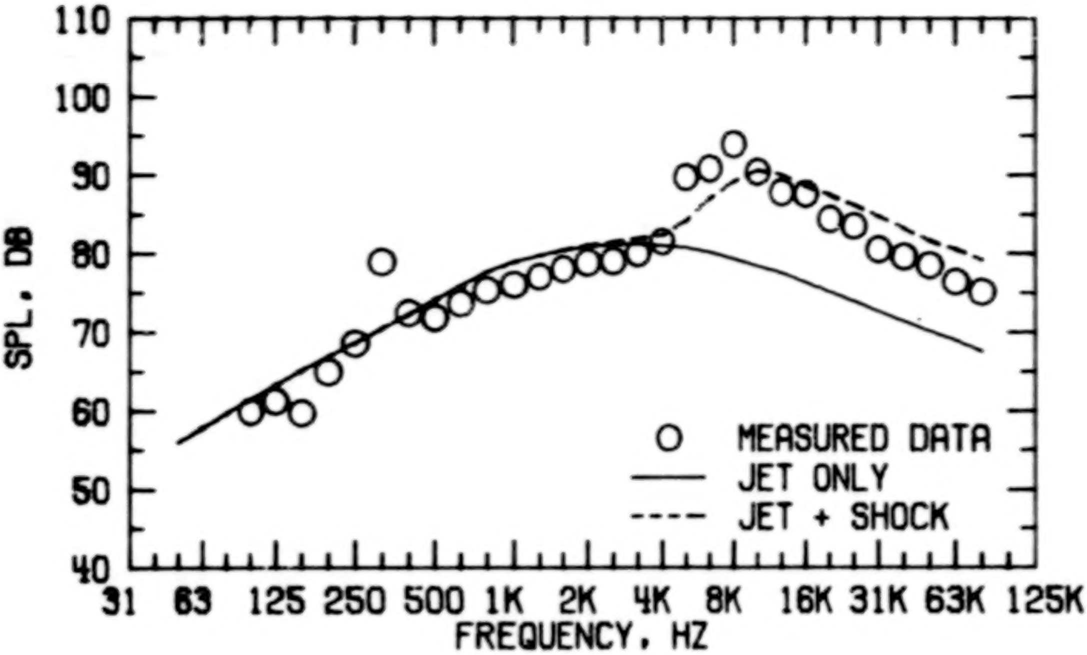

FIGURE A2 . SPECTRA COMPARISON FOR CASE 3
(B) DIRECTIVITY ANGLE = 60 DEGREES

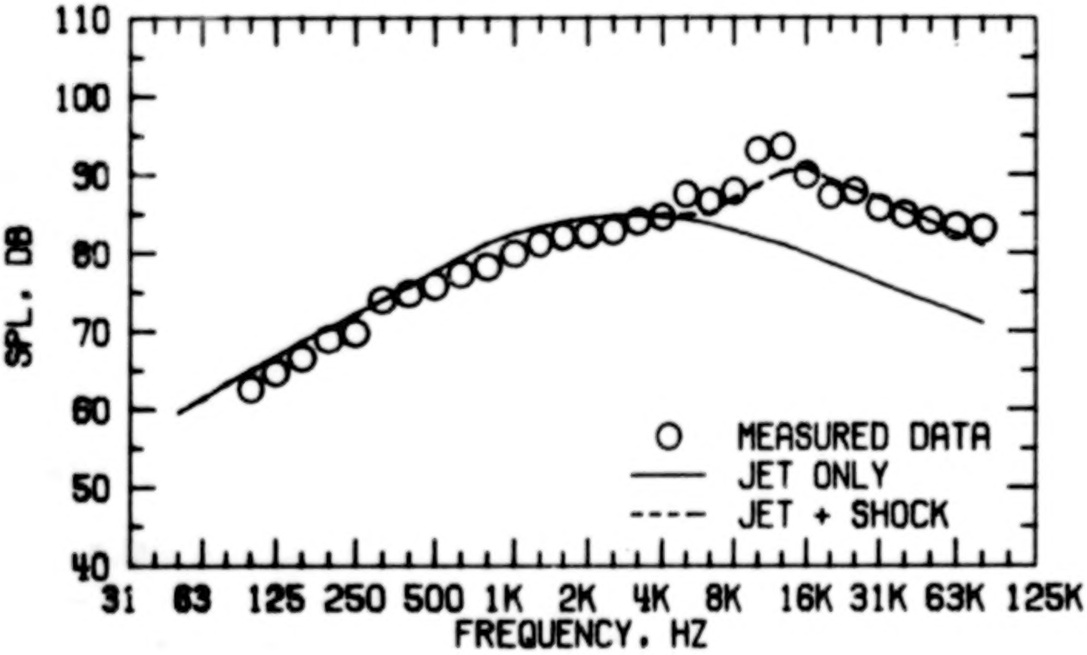

FIGURE A2 . SPECTRA COMPARISON FOR CASE 3
(C) DIRECTIVITY ANGLE = 90 DEGREES

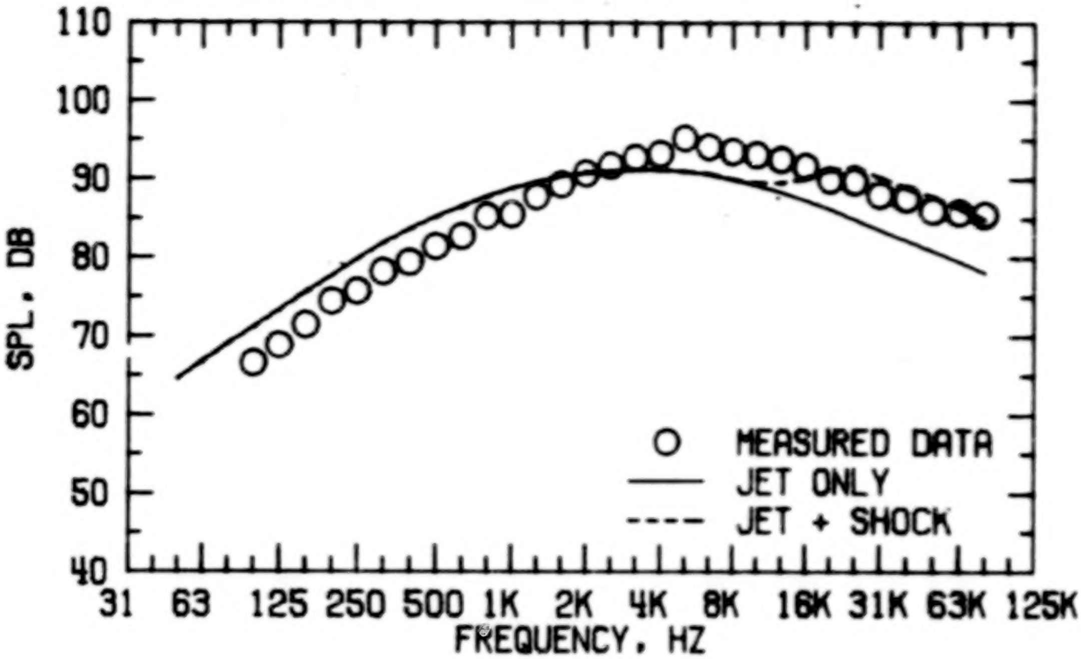

FIGURE A2 . SPECTRA COMPARISON FOR CASE 3
(D) DIRECTIVITY ANGLE = 120 DEGREES

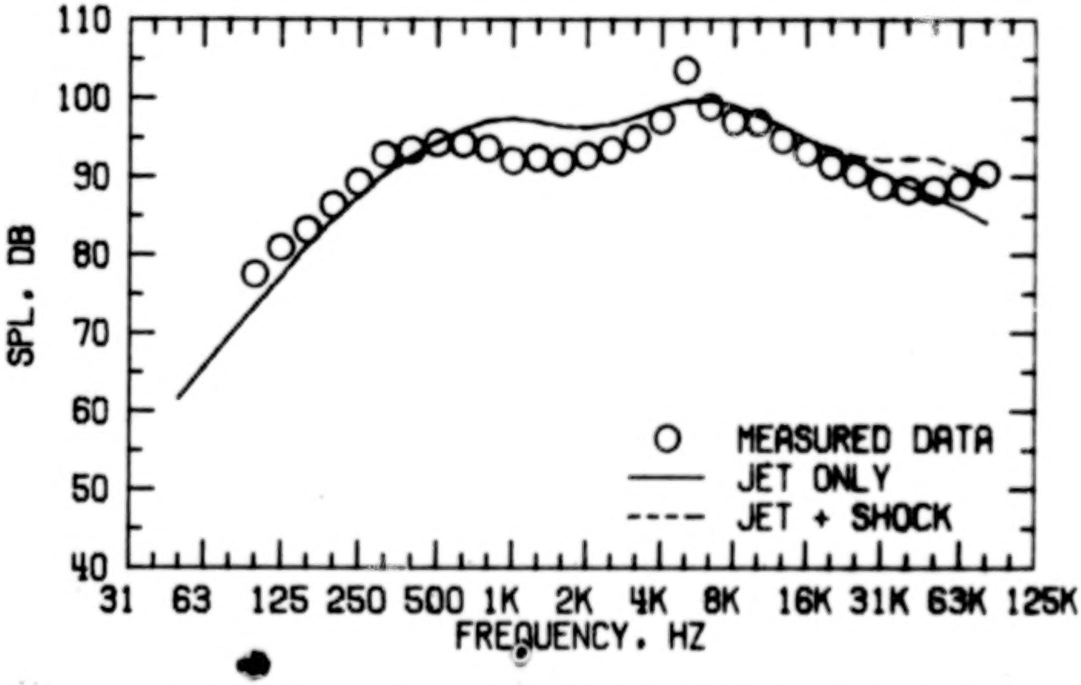

FIGURE A2 . SPECTRA COMPARISON FOR CASE 3
(E) DIRECTIVITY ANGLE = 150 DEGREES

FLOW PROPERTIES FOR CASE 5
NOZZLE MODEL 2

FORWARD FLIGHT VELOCITY, V_A = 0.0 M/S

	TEMPERATURE T_T, DEG K	VELOCITY V, M/S	MASS FLOW W, KG/S	P_T/P_A
PRIMARY	387.0	296.5	2.2974	1.5200
SECONDARY	705.3	468.7	1.4809	1.8000
EQUIVALENT	511.8	364.0	3.7784	

REFERENCE RADIUS = 45.7 M

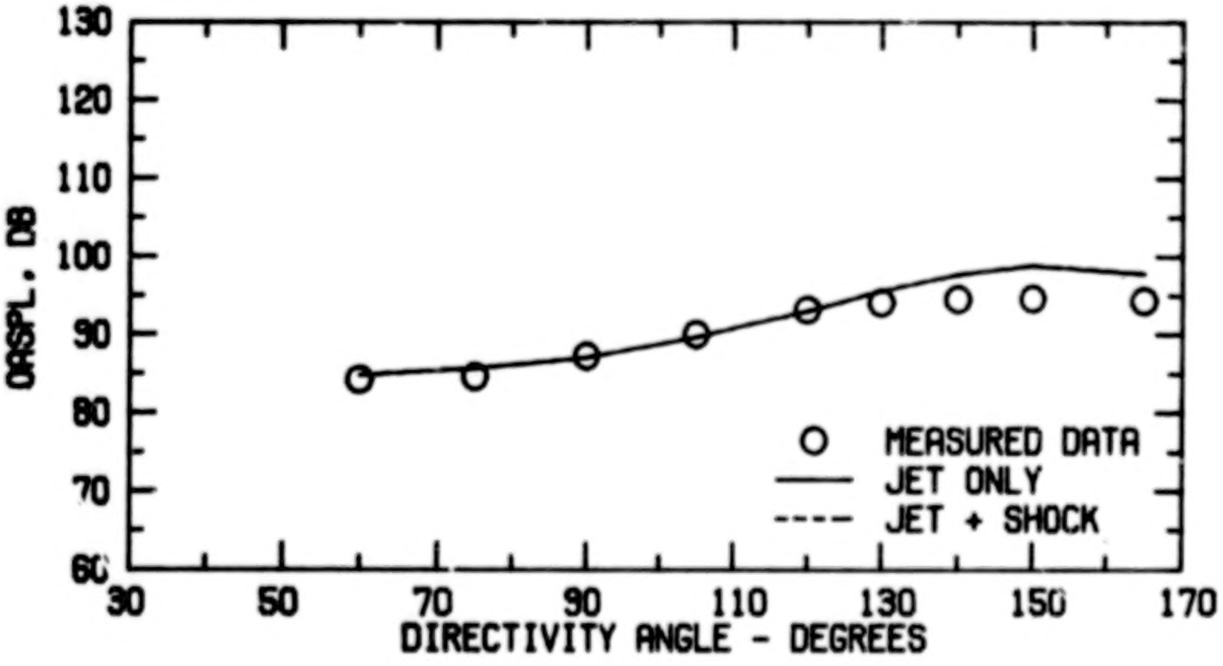

FIGURE A3 . SPECTRA COMPARISON FOR CASE 5
(A) FLOW PROPERTIES AND DIRECTIVITY PLOT

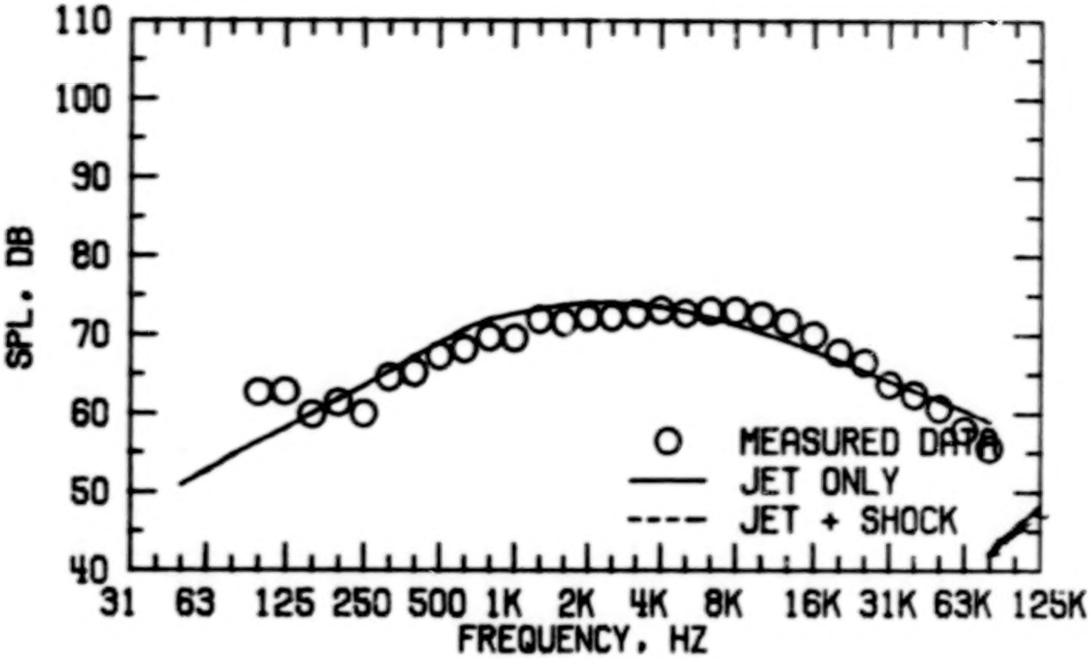

FIGURE A3 . SPECTRA COMPARISON FOR CASE 5
(B) DIRECTIVITY ANGLE = 60 DEGREES

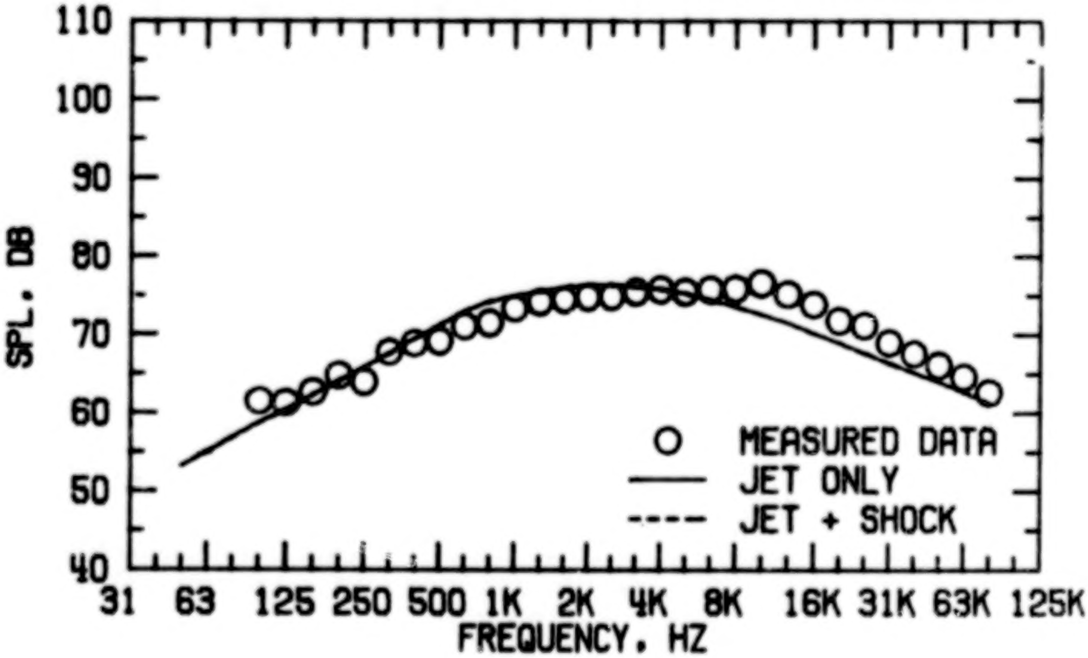

FIGURE A3 . SPECTRA COMPARISON FOR CASE 5
(C) DIRECTIVITY ANGLE = 90 DEGREES

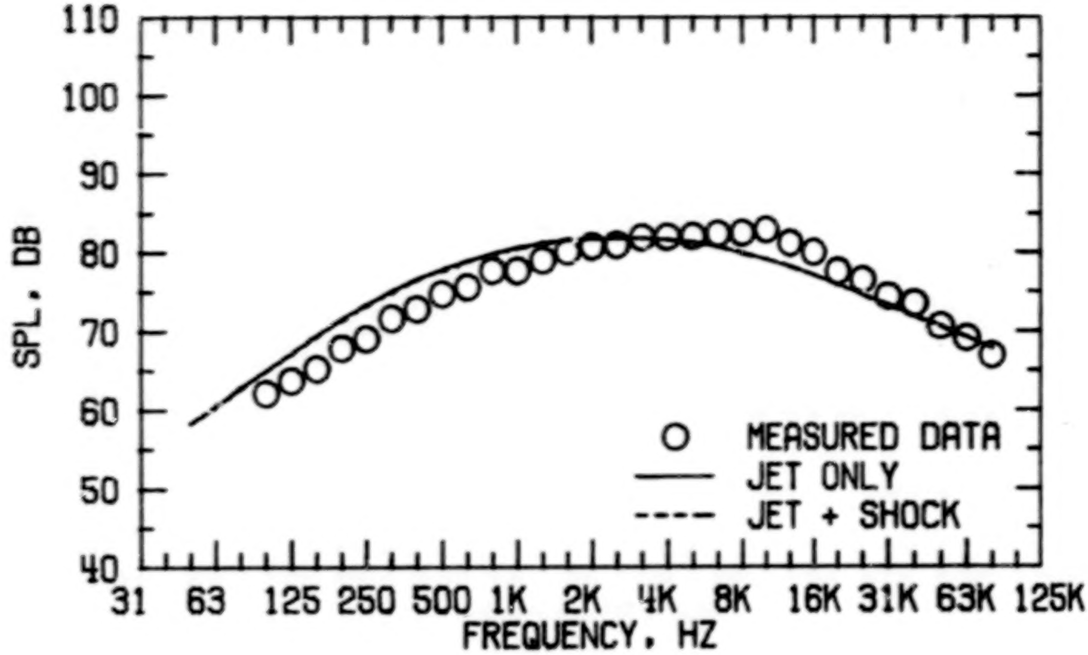

FIGURE A3 . SPECTRA COMPARISON FOR CASE 5
(D) DIRECTIVITY ANGLE = 120 DEGREES

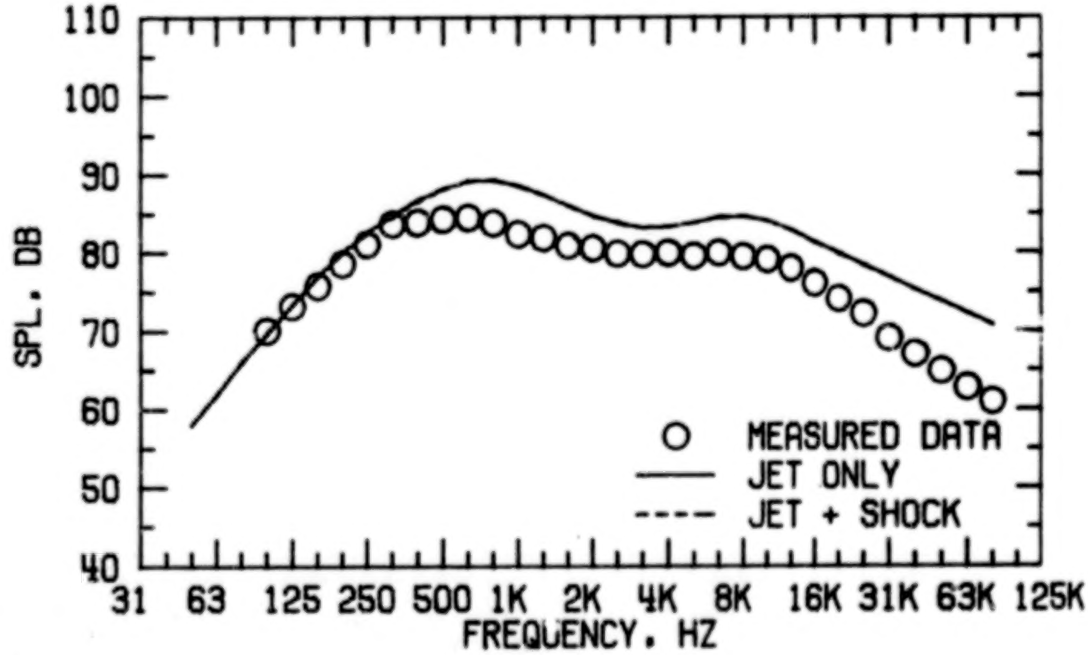

FIGURE A3 . SPECTRA COMPARISON FOR CASE 5
(E) DIRECTIVITY ANGLE = 150 DEGREES

FLOW PROPERTIES FOR CASE 7
NOZZLE MODEL 2

FORWARD FLIGHT VELOCITY, V_A = 0.0 M/S

	TEMPERATURE T_T, DEG K	VELOCITY V, M/S	MASS FLOW W, KG/S	P_T/P_A
PRIMARY	413.1	309.6	2.2493	1.5300
SECONDARY	1077.0	793.0	2.2334	3.2100
EQUIVALENT	743.9	550.5	4.4828	

REFERENCE RADIUS = 45.7 M

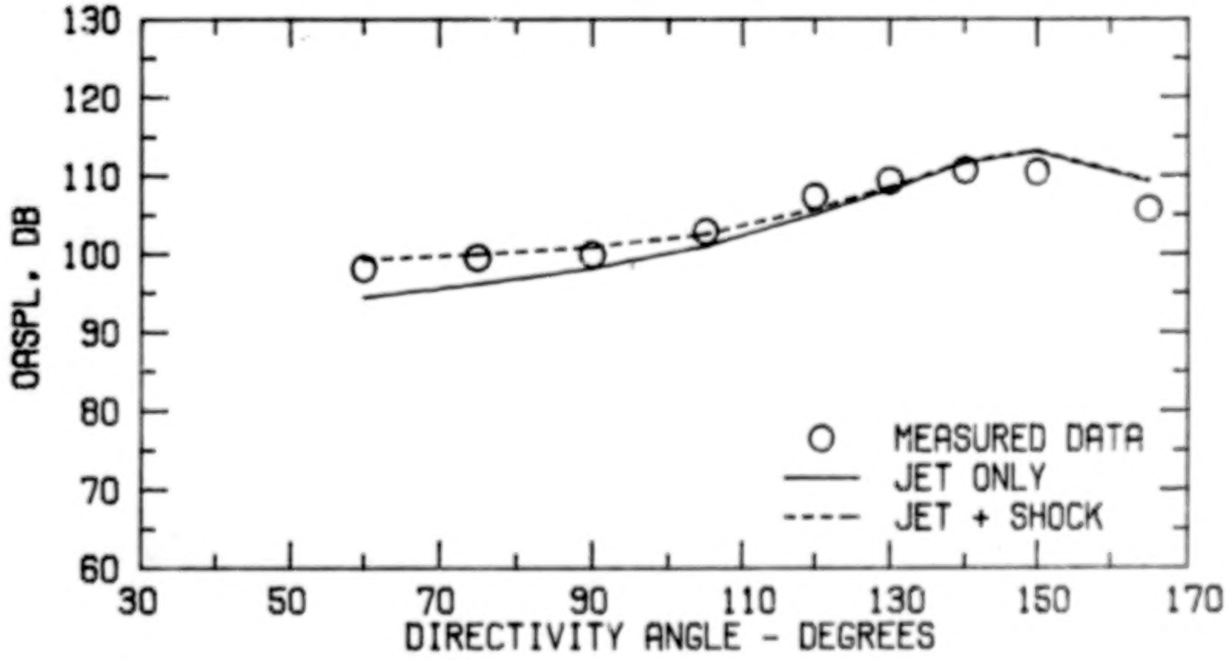

FIGURE A4 . SPECTRA COMPARISON FOR CASE 7
(A) FLOW PROPERTIES AND DIRECTIVITY PLOT

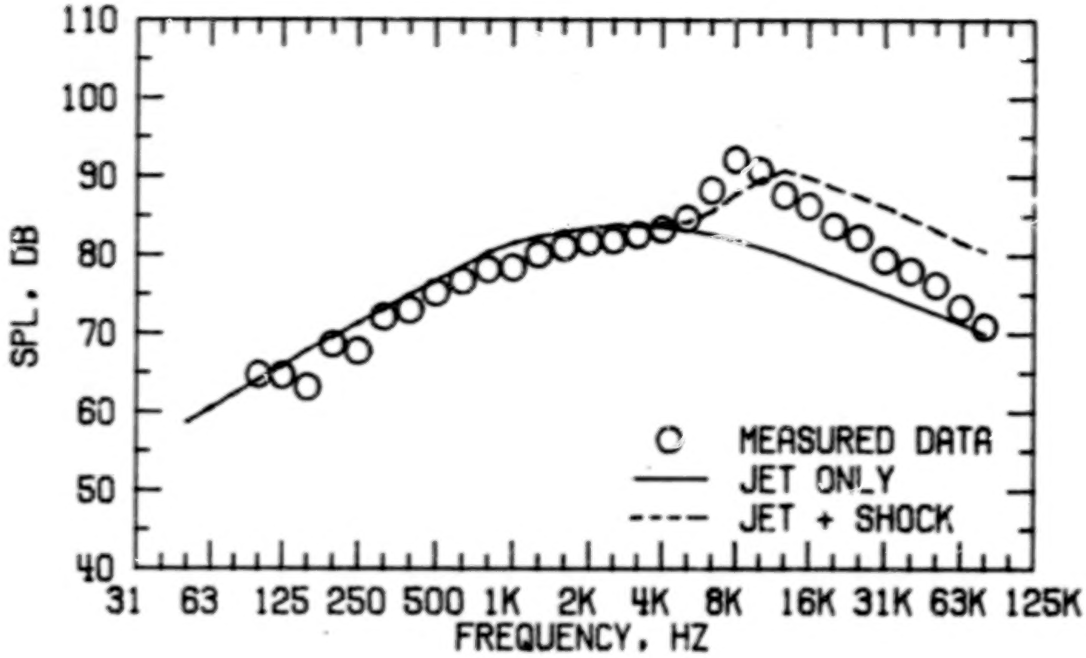

FIGURE A4 . SPECTRA COMPARISON FOR CASE 7
(B) DIRECTIVITY ANGLE = 60 DEGREES

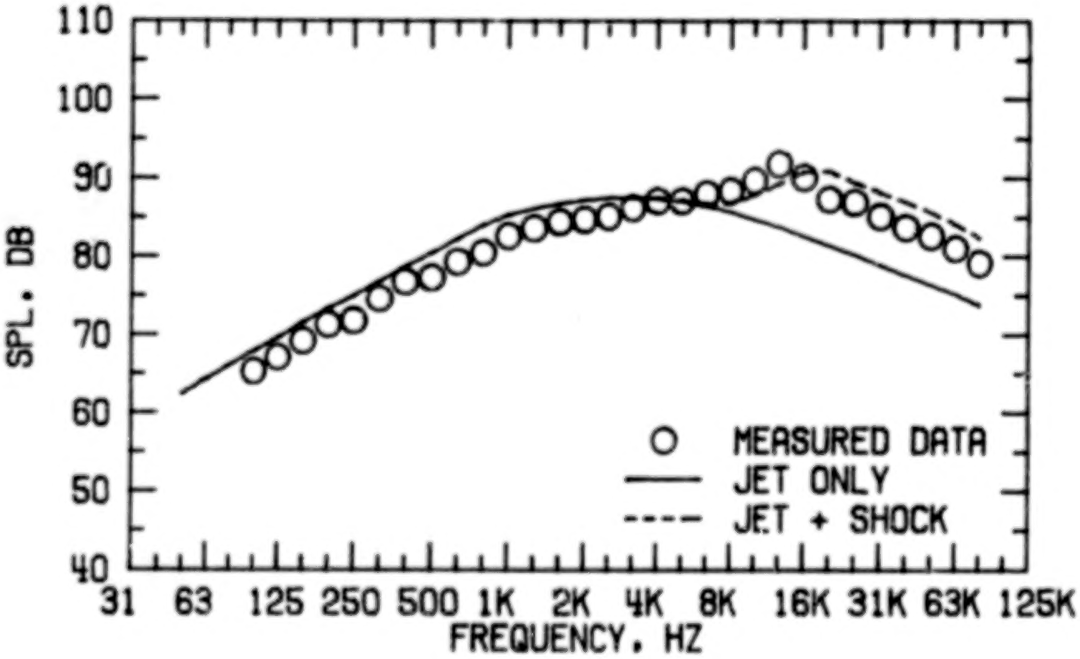

FIGURE A4 . SPECTRA COMPARISON FOR CASE 7
(C) DIRECTIVITY ANGLE = 90 DEGREES

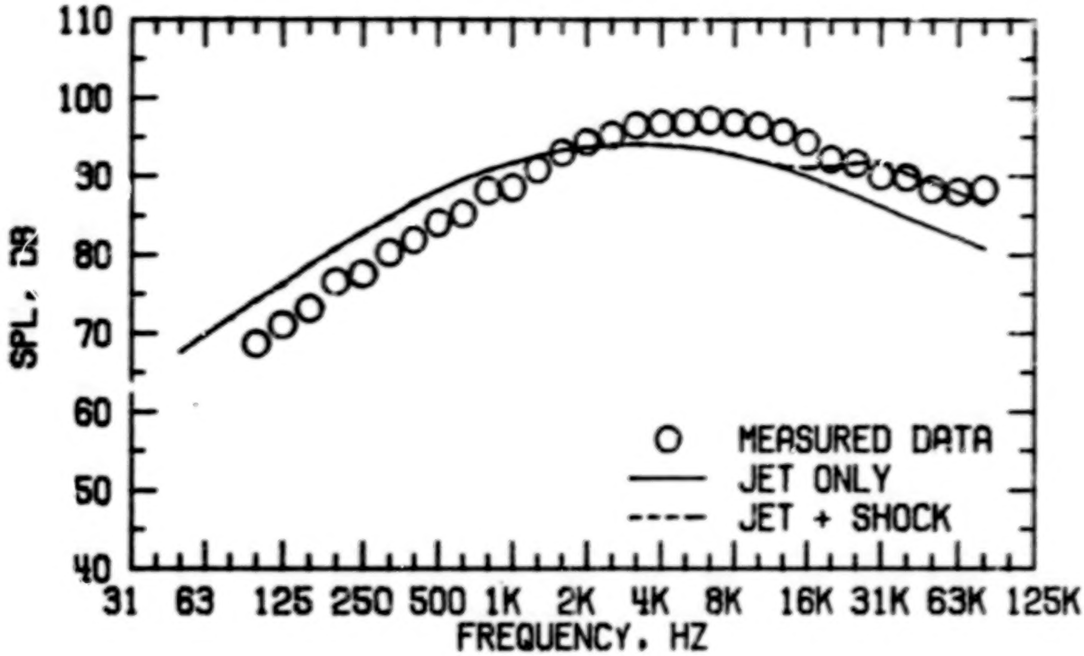

FIGURE A4 . SPECTRA COMPARISON FOR CASE 7
(D) DIRECTIVITY ANGLE = 120 DEGREES

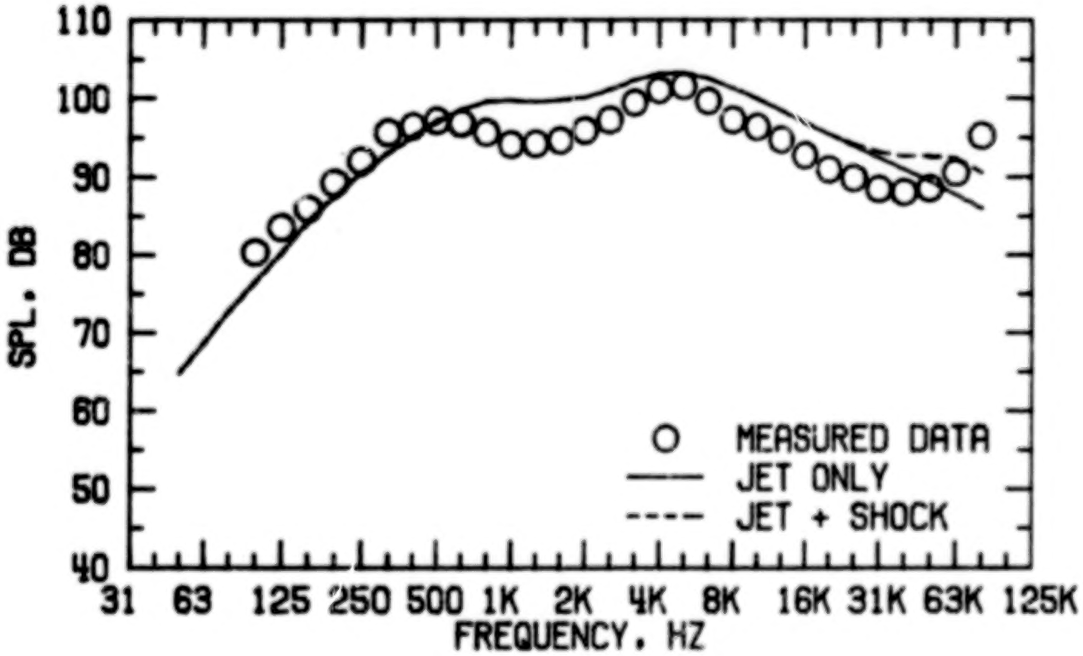

FIGURE A4 . SPECTRA COMPARISON FOR CASE 7
(E) DIRECTIVITY ANGLE = 150 DEGREES

FLOW PROPERTIES FOR CASE 8

NOZZLE MODEL 2

FORWARD FLIGHT VELOCITY, V_A = 0.0 M/S

	TEMPERATURE T_T, DEG K	VELOCITY V, M/S	MASS FLOW W, KG/S	P_T/P_A
PRIMARY	413.7	309.9	2.2634	1.5400
SECONDARY	1065.9	708.3	1.7245	2.4900
EQUIVALENT	695.7	482.2	3.9879	

REFERENCE RADIUS = 45.7 M

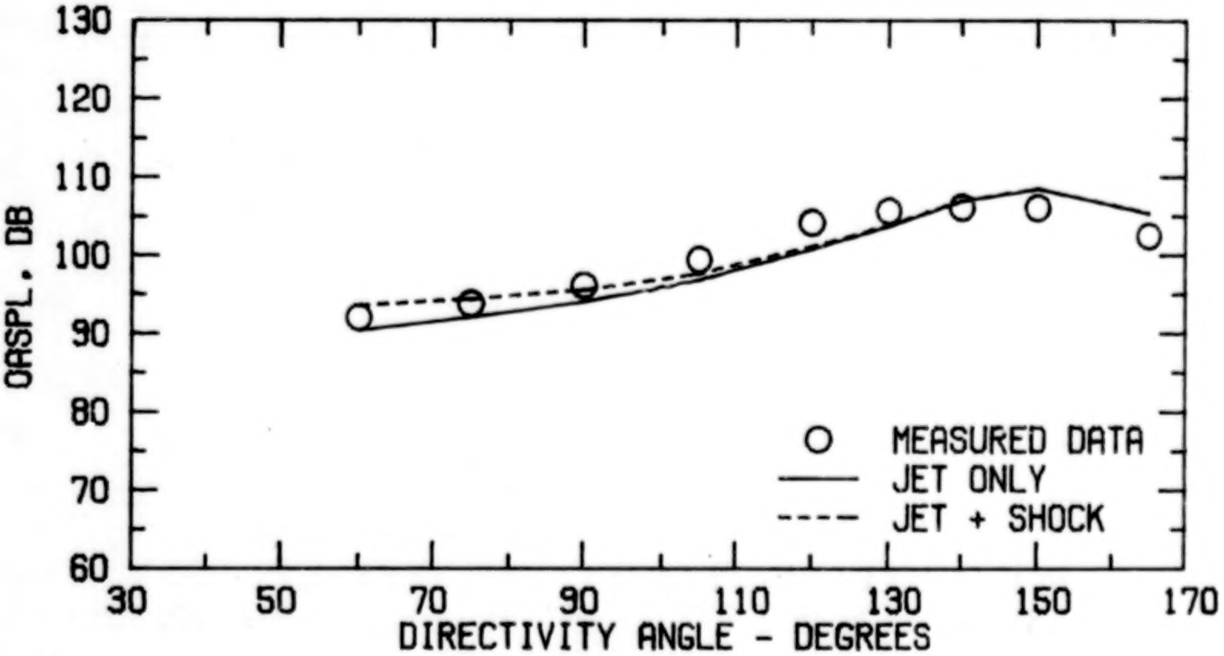

FIGURE A5 . SPECTRA COMPARISON FOR CASE 8
(A) FLOW PROPERTIES AND DIRECTIVITY PLOT

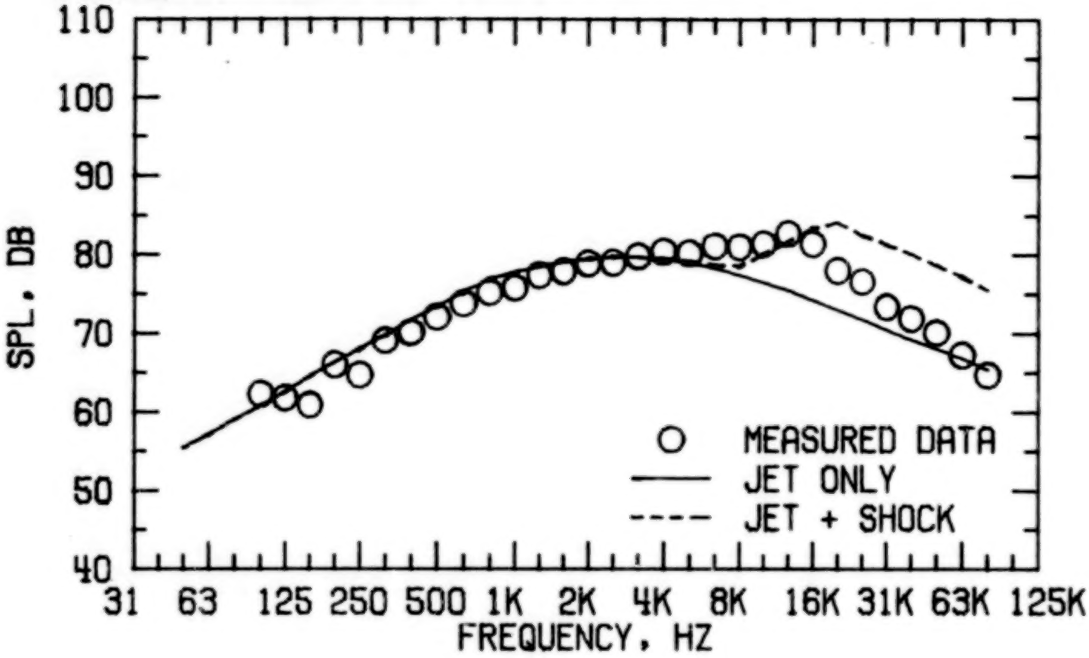

FIGURE A5 . SPECTRA COMPARISON FOR CASE 8
(B) DIRECTIVITY ANGLE = 60 DEGREES

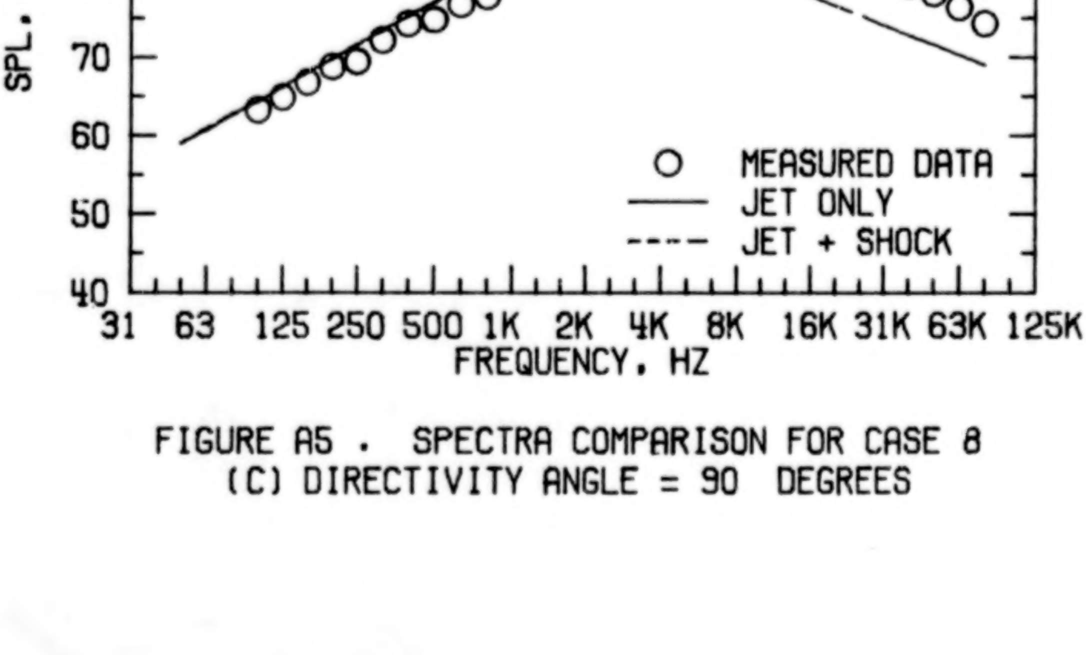

FIGURE A5 . SPECTRA COMPARISON FOR CASE 8
(C) DIRECTIVITY ANGLE = 90 DEGREES

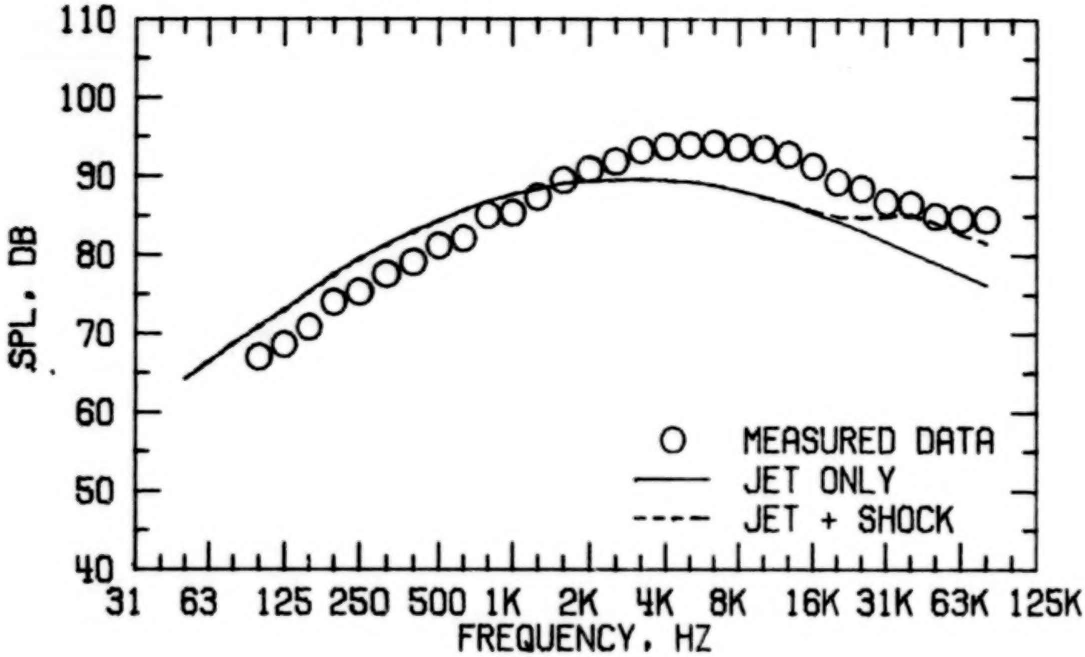

FIGURE A5 . SPECTRA COMPARISON FOR CASE 8
(D) DIRECTIVITY ANGLE = 120 DEGREES

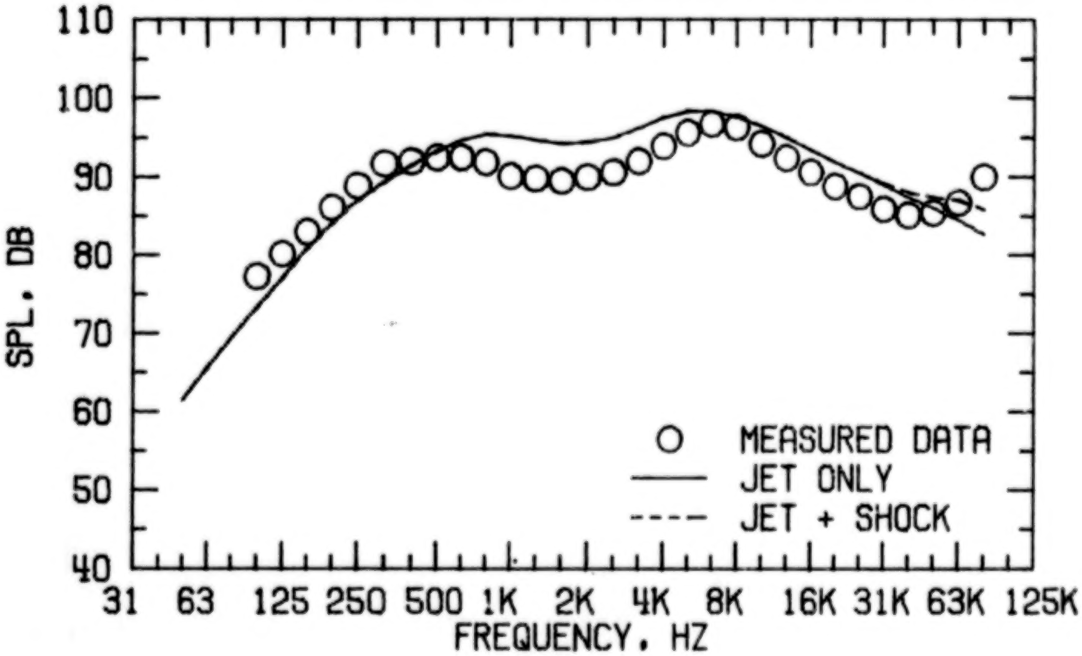

FIGURE A5 . SPECTRA COMPARISON FOR CASE 8
(E) DIRECTIVITY ANGLE = 150 DEGREES

FLOW PROPERTIES FOR CASE 15
NOZZLE MODEL 2

FORWARD FLIGHT VELOCITY, V_A = 0.0 M/S

	TEMPERATURE T_T, DEG K	VELOCITY V, M/S	MASS FLOW W, KG/S	P_T/P_A
PRIMARY	808.7	431.2	1.5685	1.5300
SECONDARY	907.0	653.1	1.8456	2.5000
EQUIVALENT	861.8	551.2	3.4141	

REFERENCE RADIUS = 45.7 M

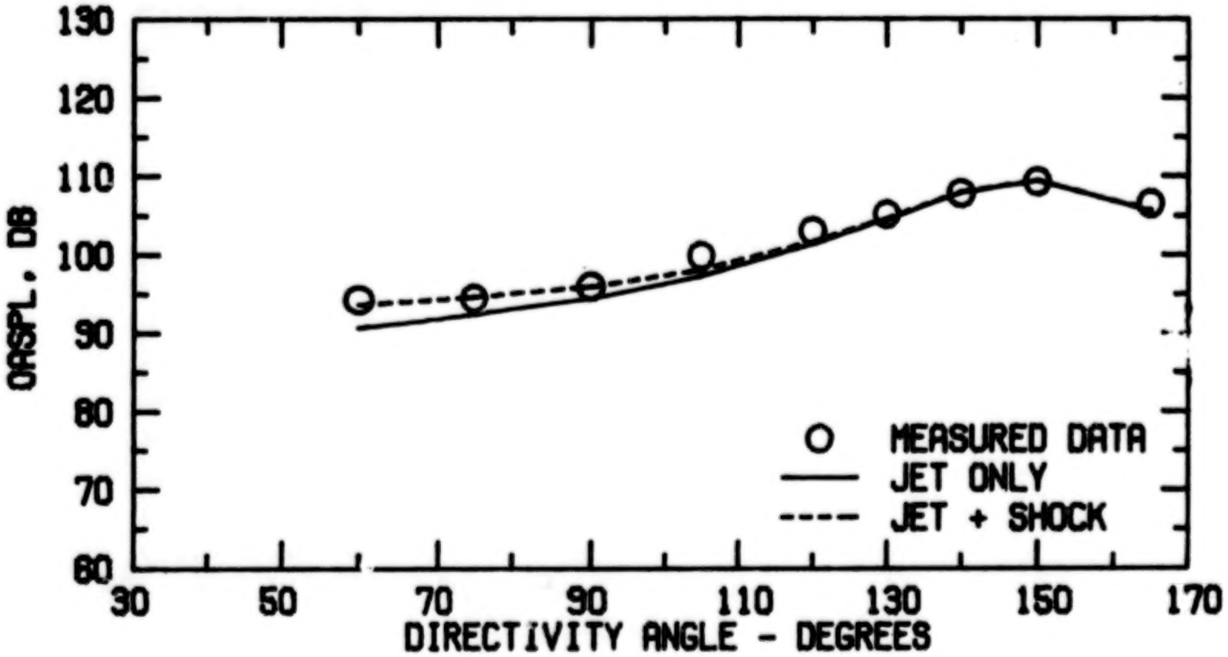

FIGURE A6 . SPECTRA COMPARISON FOR CASE 15
(A) FLOW PROPERTIES AND DIRECTIVITY PLOT

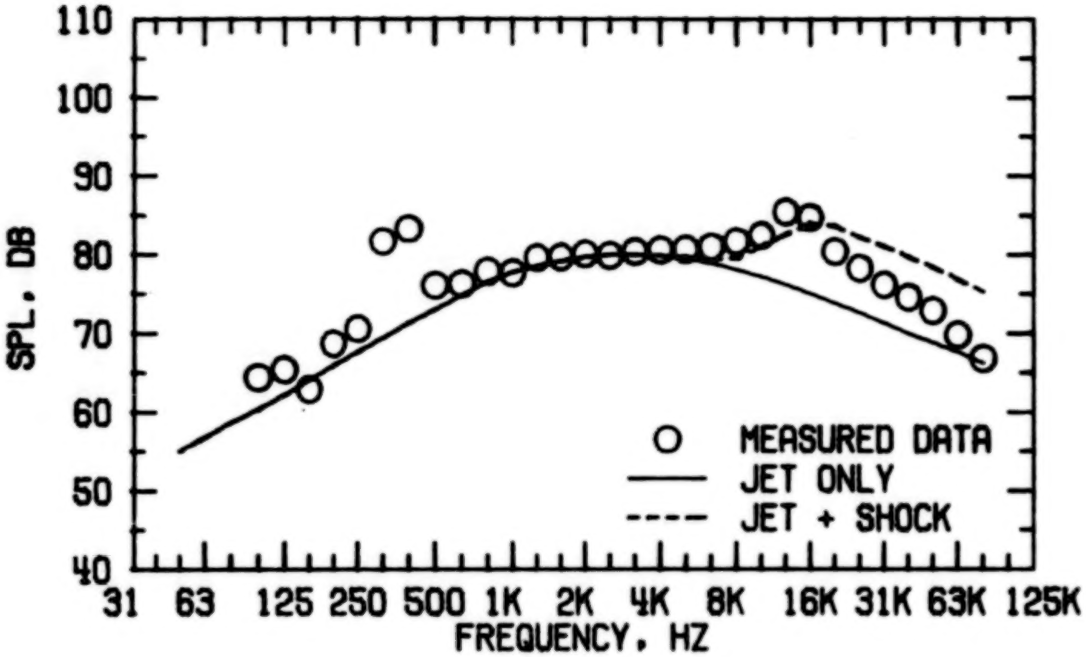

FIGURE A6 . SPECTRA COMPARISON FOR CASE 15
(B) DIRECTIVITY ANGLE = 60 DEGREES

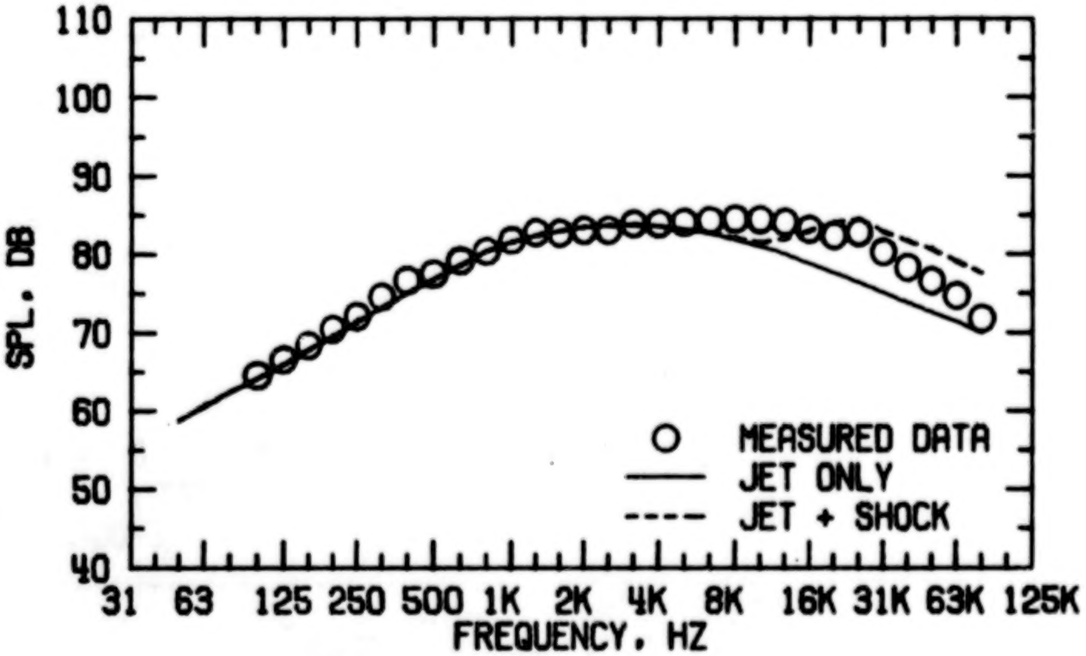

FIGURE A6 . SPECTRA COMPARISON FOR CASE 15
(C) DIRECTIVITY ANGLE = 90 DEGREES

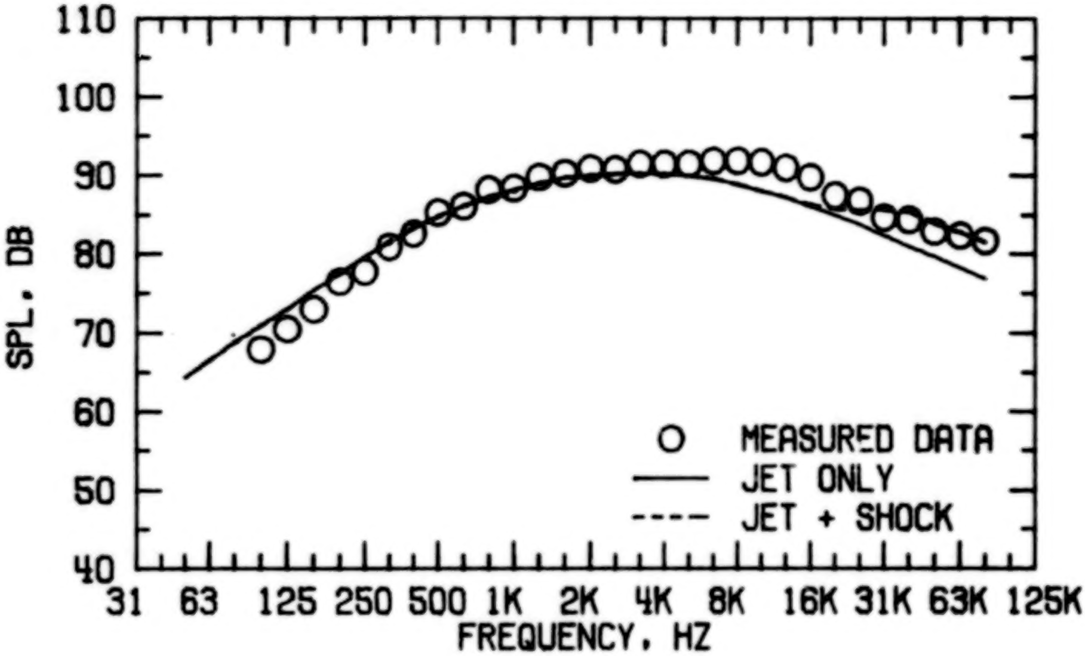

FIGURE A6 . SPECTRA COMPARISON FOR CASE 15
(D) DIRECTIVITY ANGLE = 120 DEGREES

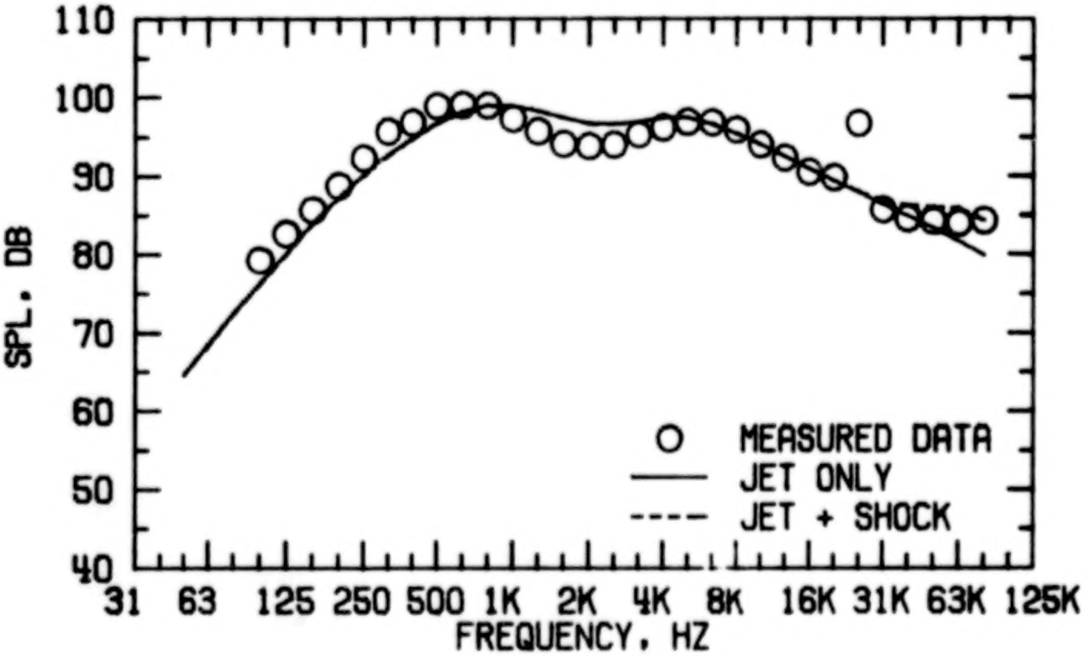

FIGURE A6 . SPECTRA COMPARISON FOR CASE 15
(E) DIRECTIVITY ANGLE = 150 DEGREES

FLOW PROPERTIES FOR CASE 21
NOZZLE MODEL 2

FORWARD FLIGHT VELOCITY, V_A = 0.0 M/S

	TEMPERATURE T_T, DEG K	VELOCITY V, M/S	MASS FLOW W, KG/S	P_T/P_A
PRIMARY	820.9	620.8	2.5809	2.5000
SECONDARY	708.1	637.9	2.6616	3.1900
EQUIVALENT	763.6	629.5	5.2426	

REFERENCE RADIUS = 45.7 M

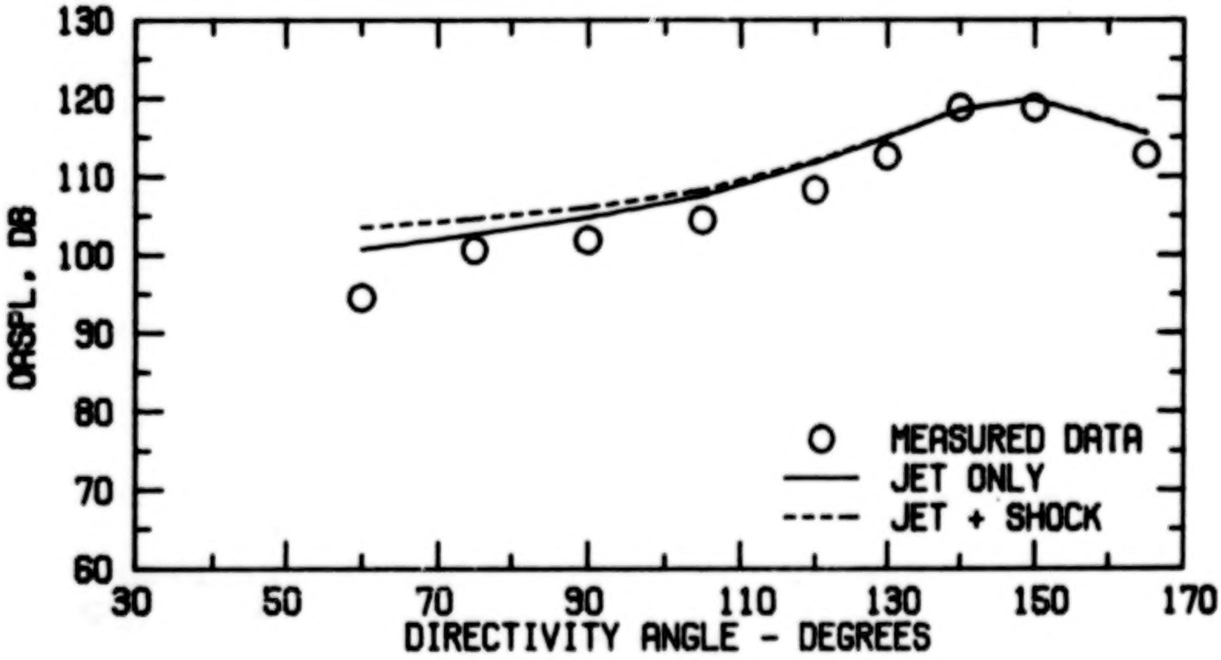

FIGURE A7 . SPECTRA COMPARISON FOR CASE 21
(A) FLOW PROPERTIES AND DIRECTIVITY PLOT

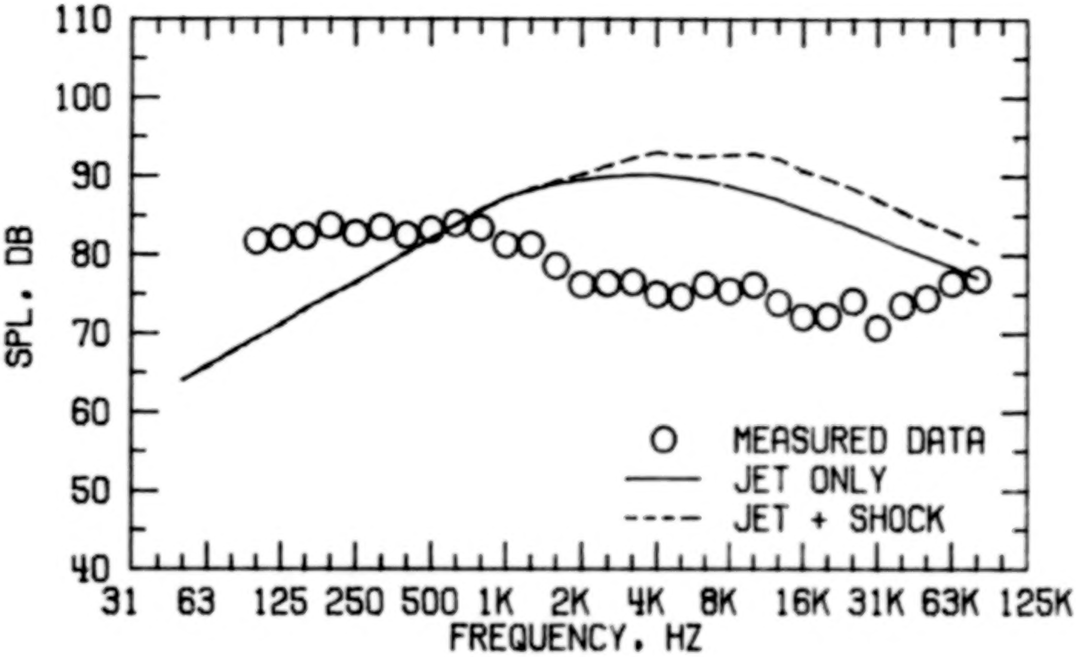

FIGURE A7 . SPECTRA COMPARISON FOR CASE 21
(B) DIRECTIVITY ANGLE = 60 DEGREES

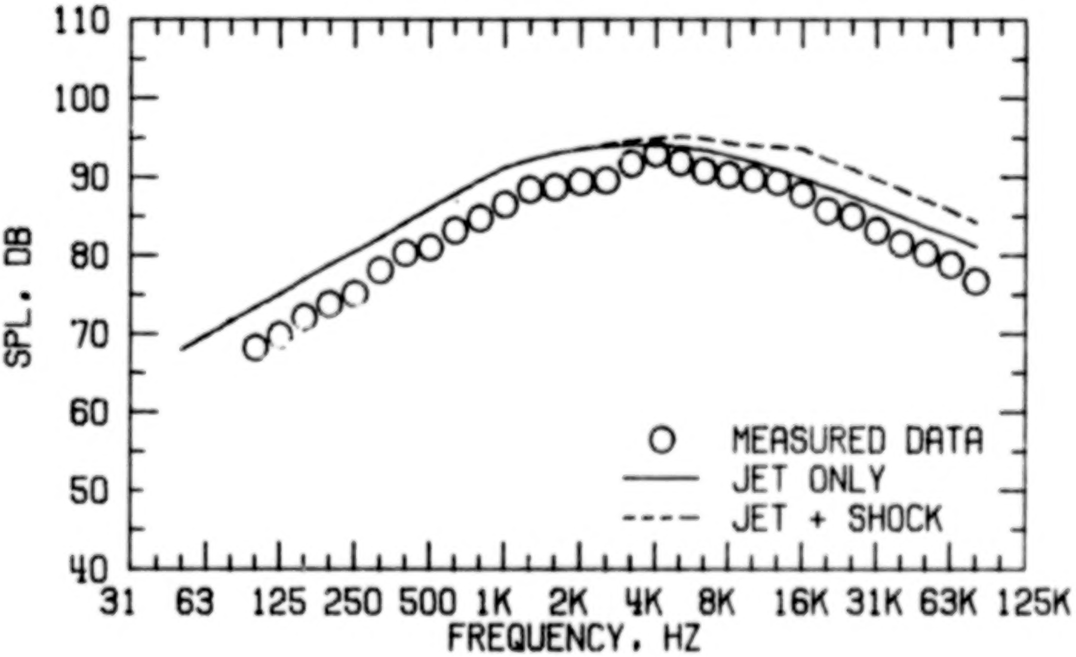

FIGURE A7 . SPECTRA COMPARISON FOR CASE 21
(C) DIRECTIVITY ANGLE = 90 DEGREES

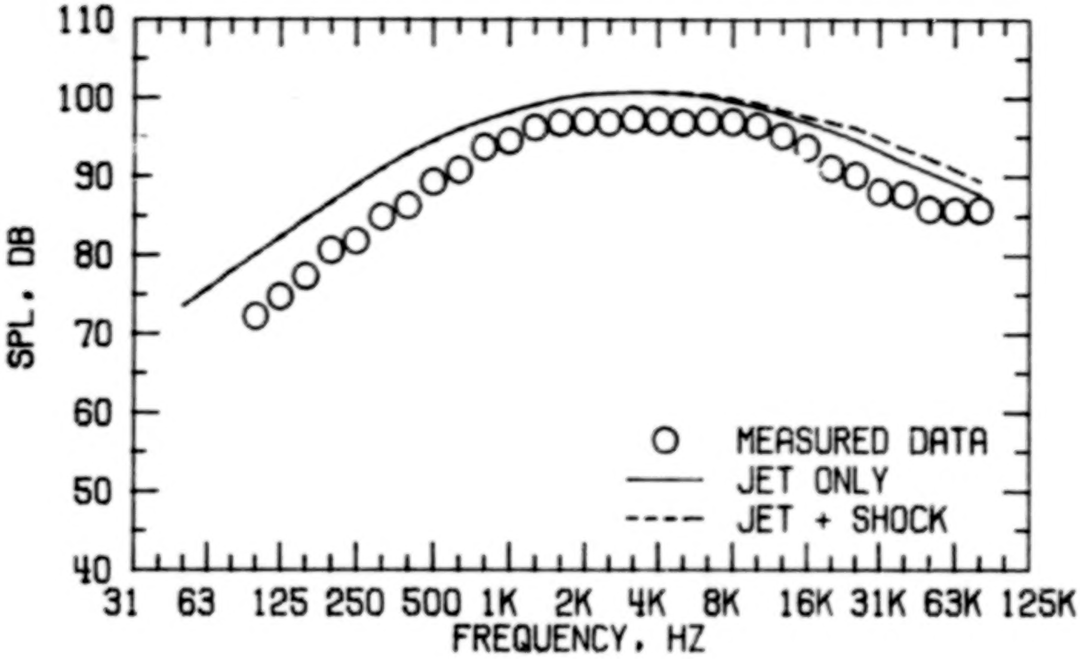

FIGURE A7 . SPECTRA COMPARISON FOR CASE 21
(D) DIRECTIVITY ANGLE = 120 DEGREES

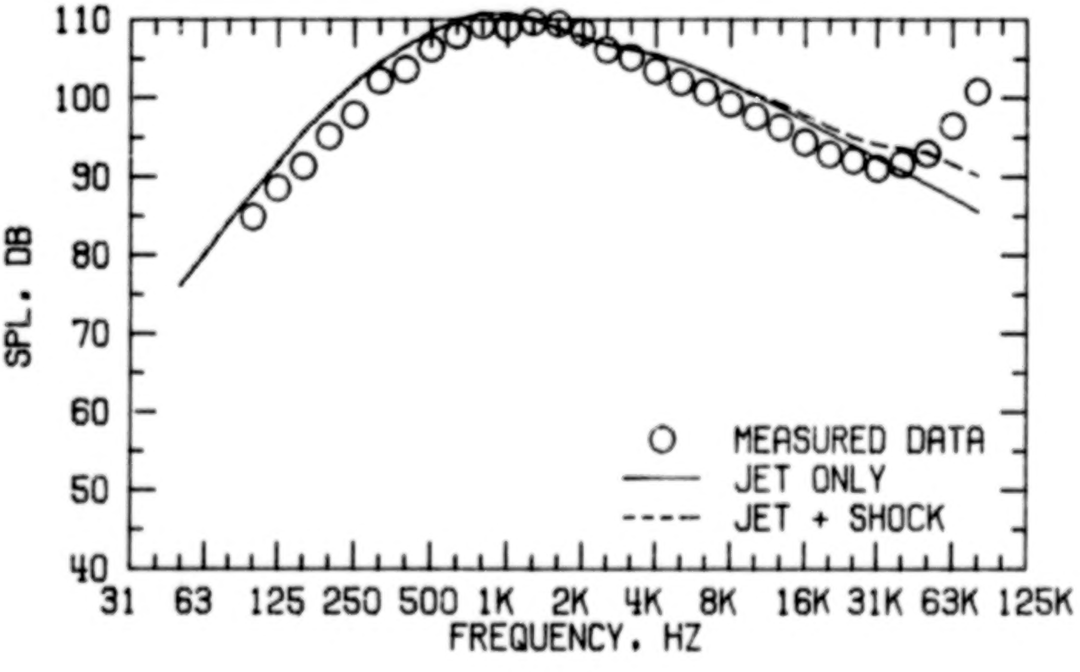

FIGURE A7 . SPECTRA COMPARISON FOR CASE 21
(E) DIRECTIVITY ANGLE = 150 DEGREES

FLOW PROPERTIES FOR CASE 22
NOZZLE MODEL 2

FORWARD FLIGHT VELOCITY, V_A = 0.0 M/S

	TEMPERATURE T_T, DEG K	VELOCITY V, M/S	MASS FLOW W, KG/S	P_T/P_A
PRIMARY	829.2	624.2	2.3763	2.5000
SECONDARY	1099.2	865.3	2.7836	4.0400
EQUIVALENT	974.9	754.2	5.1600	

REFERENCE RADIUS = 45.7 M

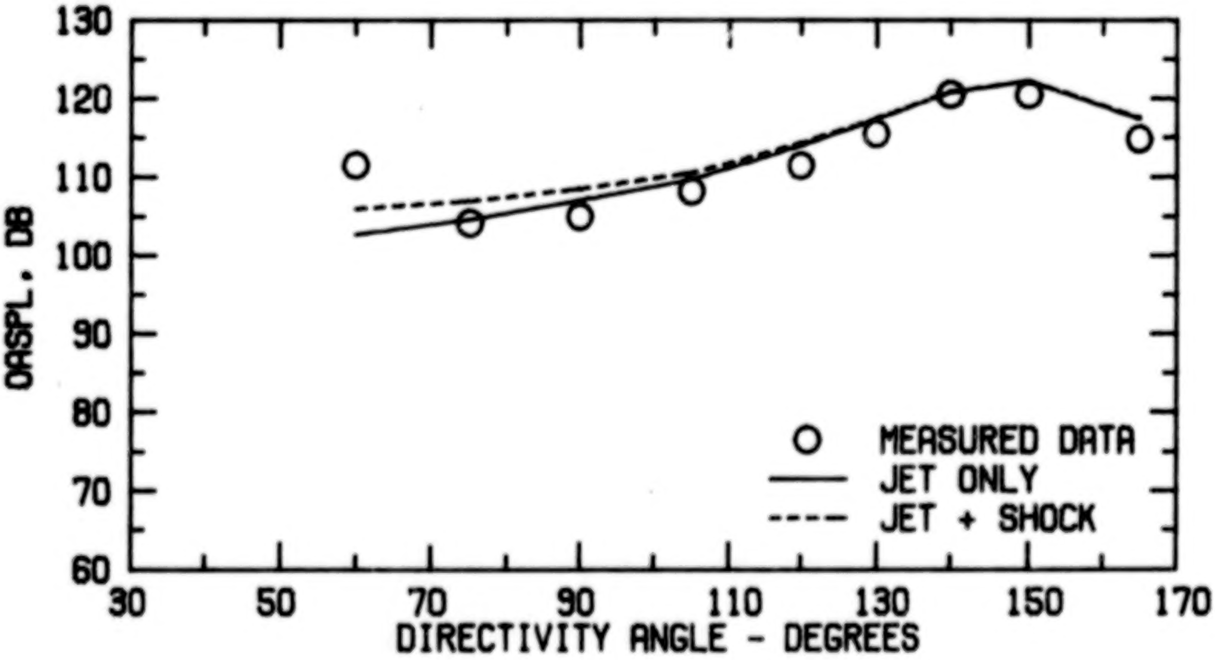

FIGURE A8 . SPECTRA COMPARISON FOR CASE 22
(A) FLOW PROPERTIES AND DIRECTIVITY PLOT

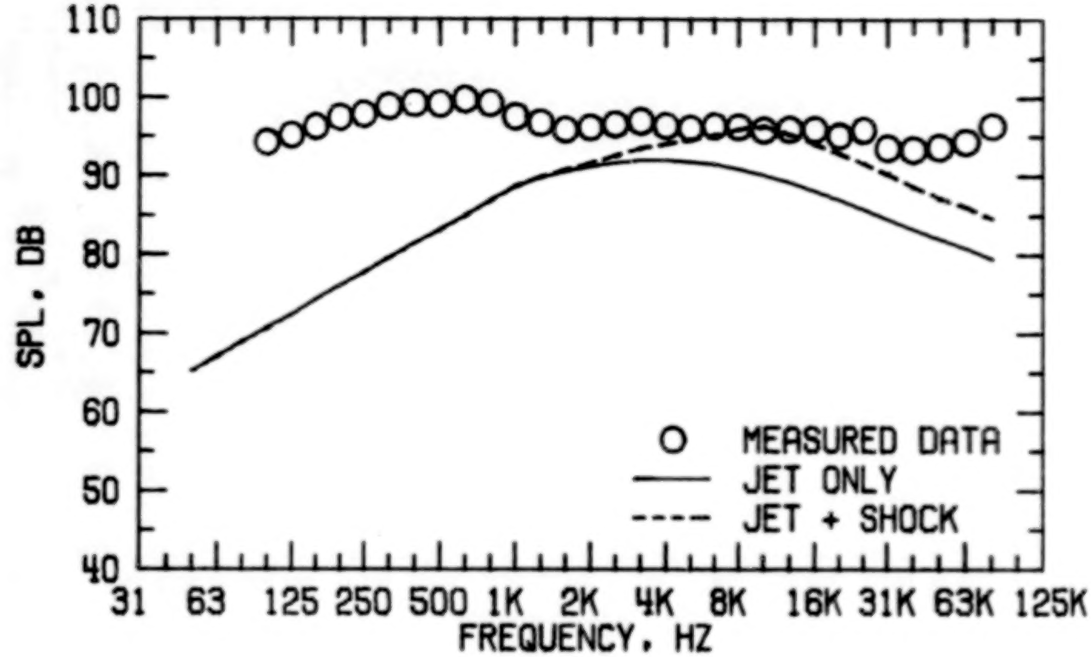

FIGURE A8 . SPECTRA COMPARISON FOR CASE 22
(B) DIRECTIVITY ANGLE = 60 DEGREES

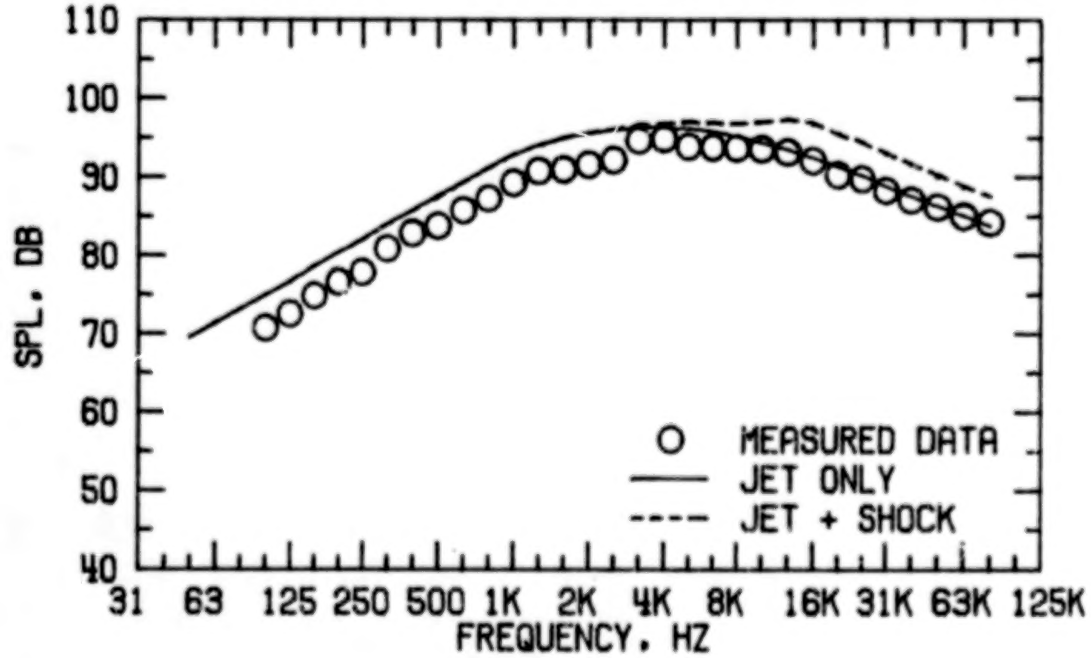

FIGURE A8 . SPECTRA COMPARISON FOR CASE 22
(C) DIRECTIVITY ANGLE = 90 DEGREES

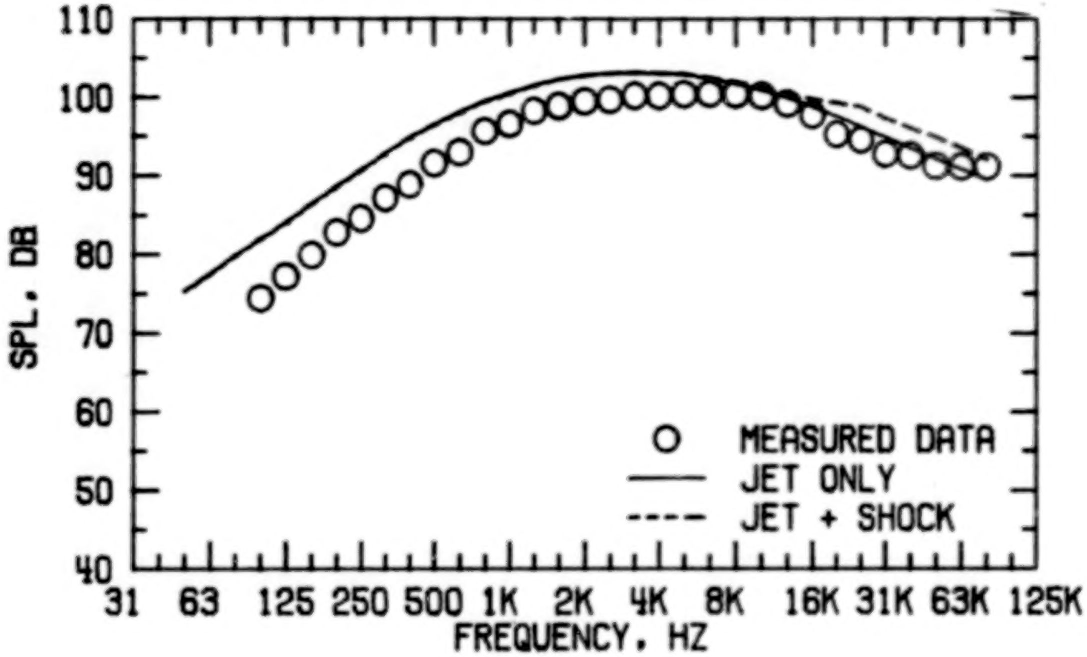

FIGURE A8 . SPECTRA COMPARISON FOR CASE 22
(D) DIRECTIVITY ANGLE = 120 DEGREES

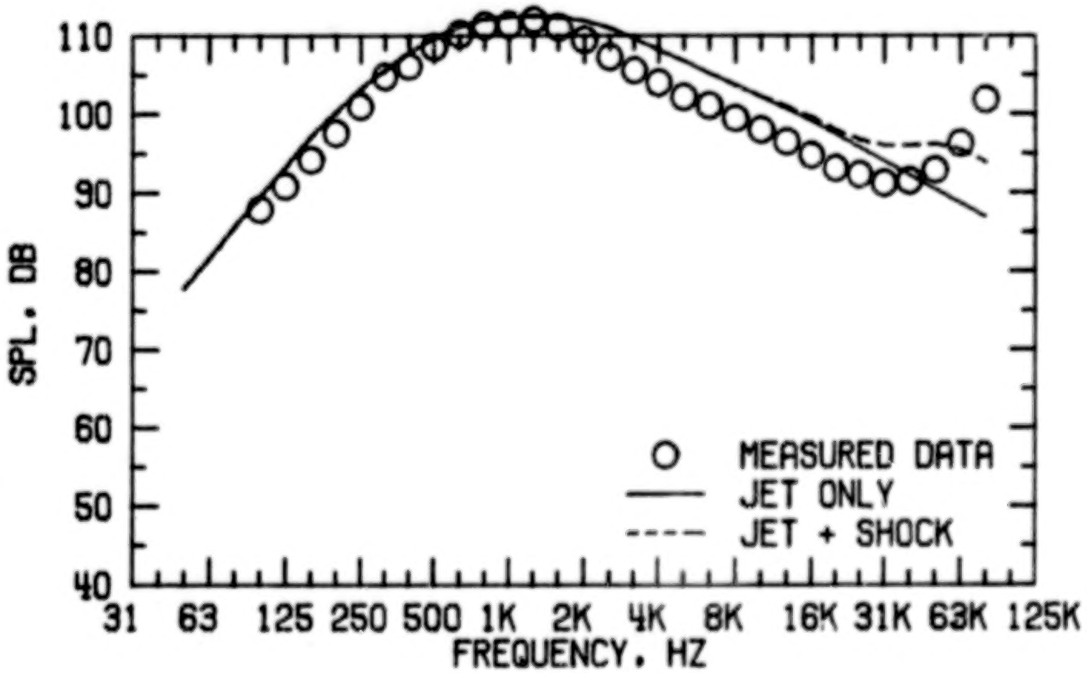

FIGURE A8 . SPECTRA COMPARISON FOR CASE 22
(E) DIRECTIVITY ANGLE = 150 DEGREES

FLOW PROPERTIES FOR CASE 23
NOZZLE MODEL 2

FORWARD FLIGHT VELOCITY, V_A = 0.0 M/S

	TEMPERATURE T_T, DEG K	VELOCITY V, M/S	MASS FLOW W, KG/S	P_T/P_A
PRIMARY	812.0	610.8	2.6086	2.4500
SECONDARY	1093.1	715.6	1.6841	2.4800
EQUIVALENT	922.3	651.9	4.2927	

REFERENCE RADIUS = 45.7 M

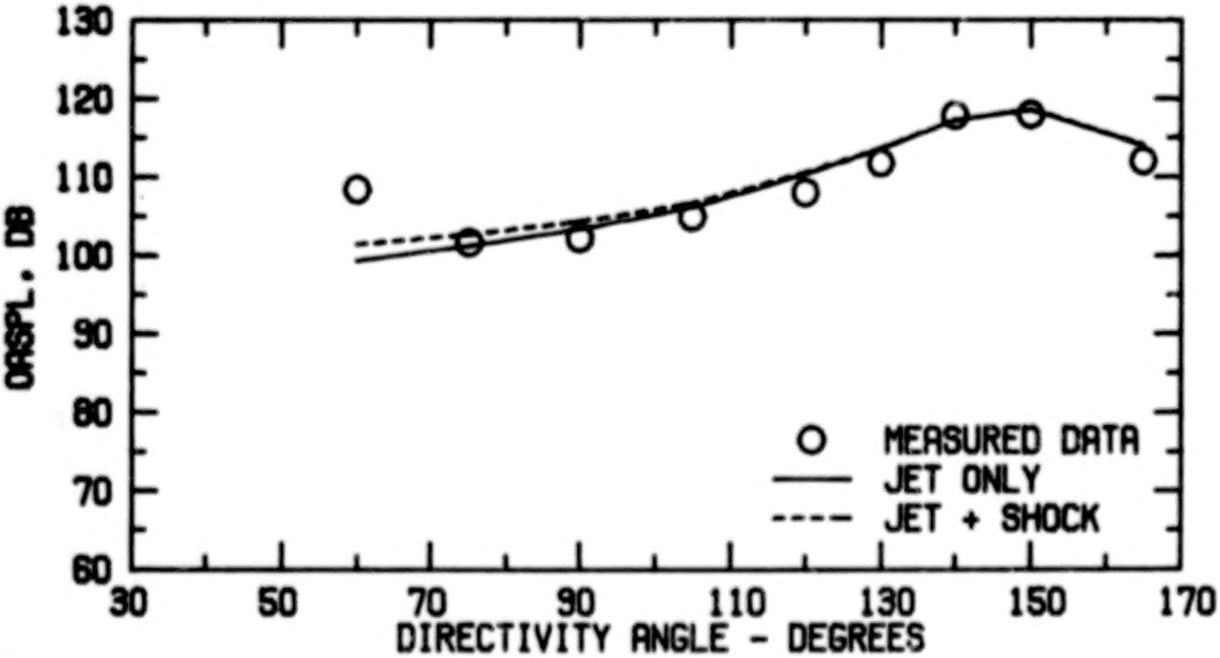

FIGURE A9 . SPECTRA COMPARISON FOR CASE 23
(A) FLOW PROPERTIES AND DIRECTIVITY PLOT

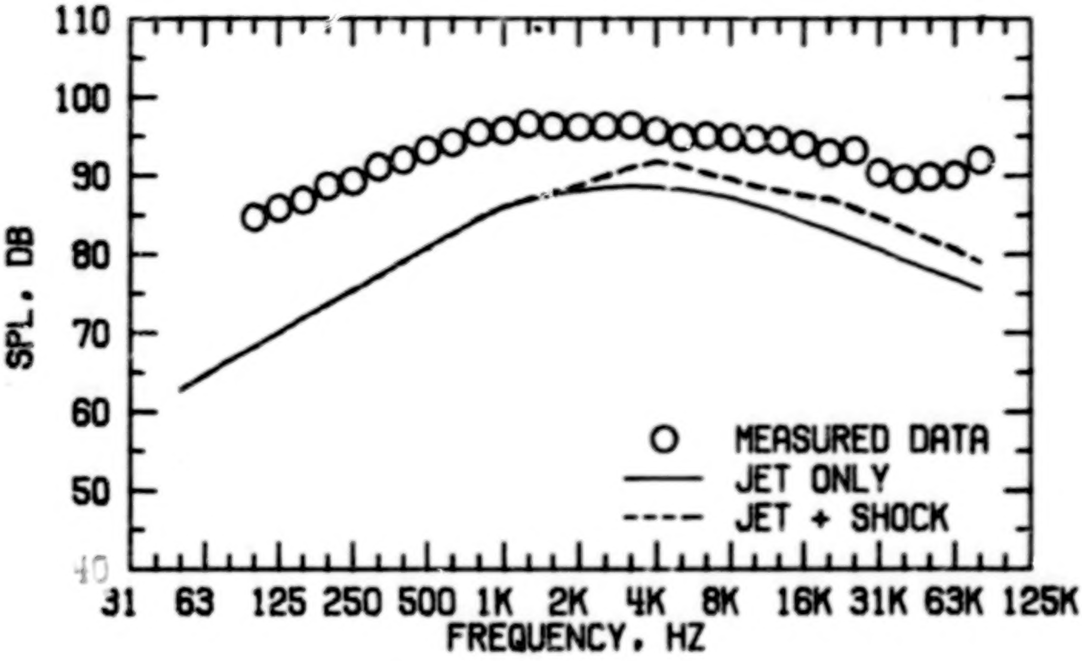

FIGURE A9 . SPECTRA COMPARISON FOR CASE 23
(B) DIRECTIVITY ANGLE = 60 DEGREES

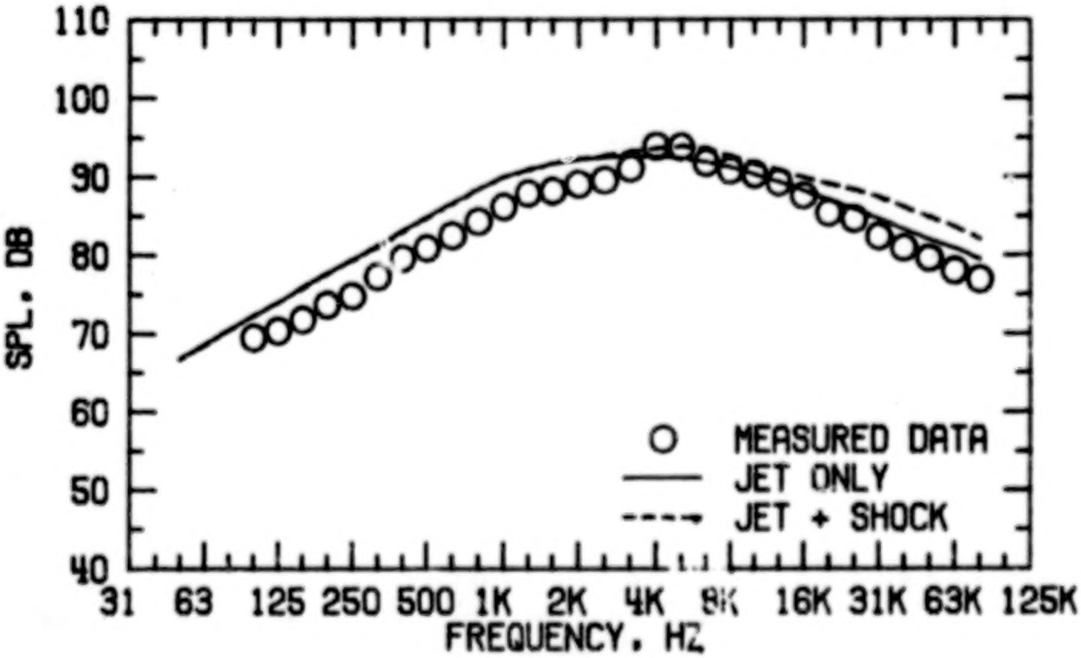

FIGURE A9 . SPECTRA COMPARISON FOR CASE 23
(C) DIRECTIVITY ANGLE = 90 DEGREES

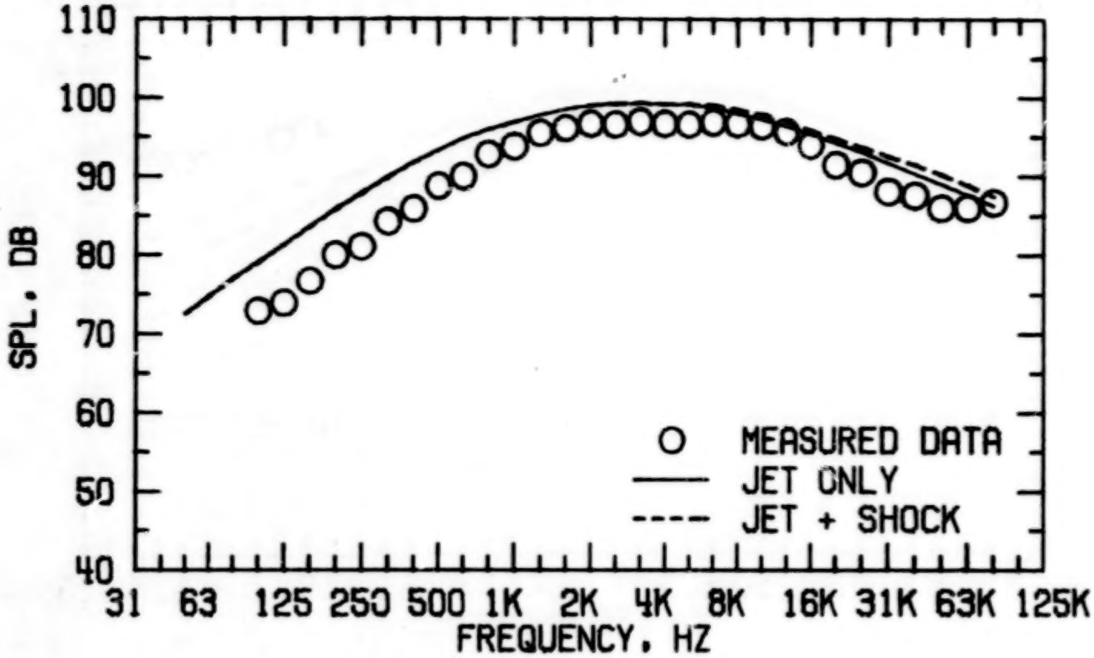

FIGURE A9 . SPECTRA COMPARISON FOR CASE 23
(D) DIRECTIVITY ANGLE = 120 DEGREES

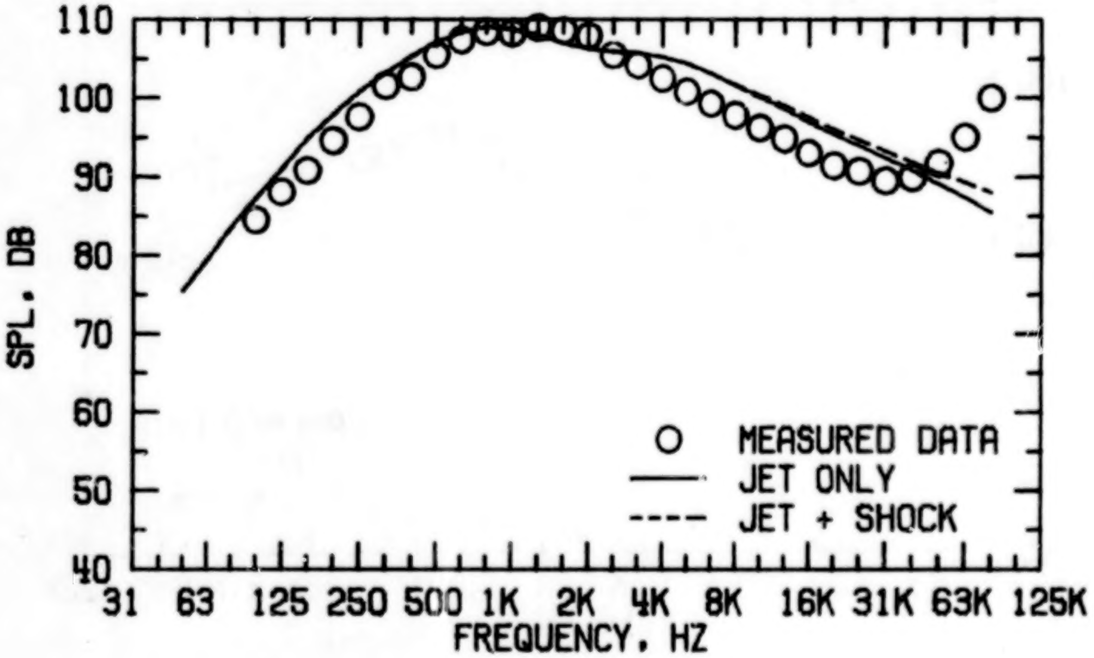

FIGURE A9 . SPECTRA COMPARISON FOR CASE 23
(E) DIRECTIVITY ANGLE = 150 DEGREES

FLOW PROPERTIES FOR CASE 26
NOZZLE MODEL 2

FORWARD FLIGHT VELOCITY, V_A = 0.0 M/S

	TEMPERATURE T_T, DEG K	VELOCITY V, M/S	MASS FLOW W, KG/S	P_T/P_A
PRIMARY	1077.0	504.1	1.3662	1.5400
SECONDARY	1082.6	792.4	2.1849	3.1900
EQUIVALENT	1080.4	681.5	3.5511	

REFERENCE RADIUS = 45.7 M

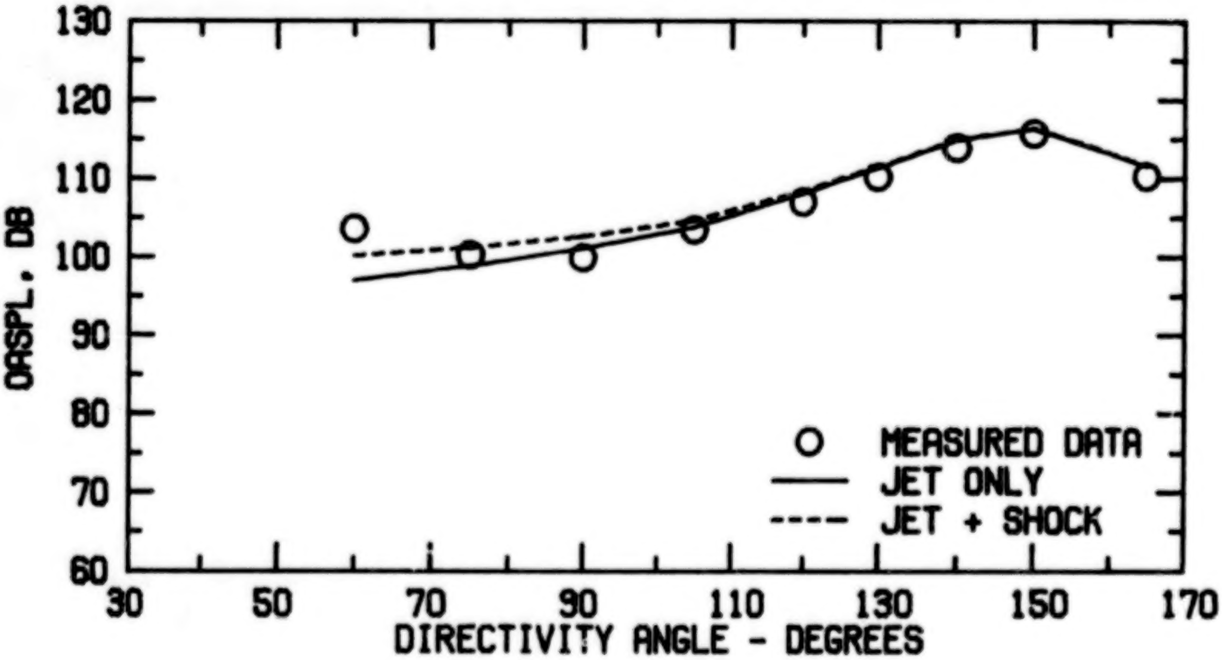

FIGURE A10. SPECTRA COMPARISON FOR CASE 26
(A) FLOW PROPERTIES AND DIRECTIVITY PLOT

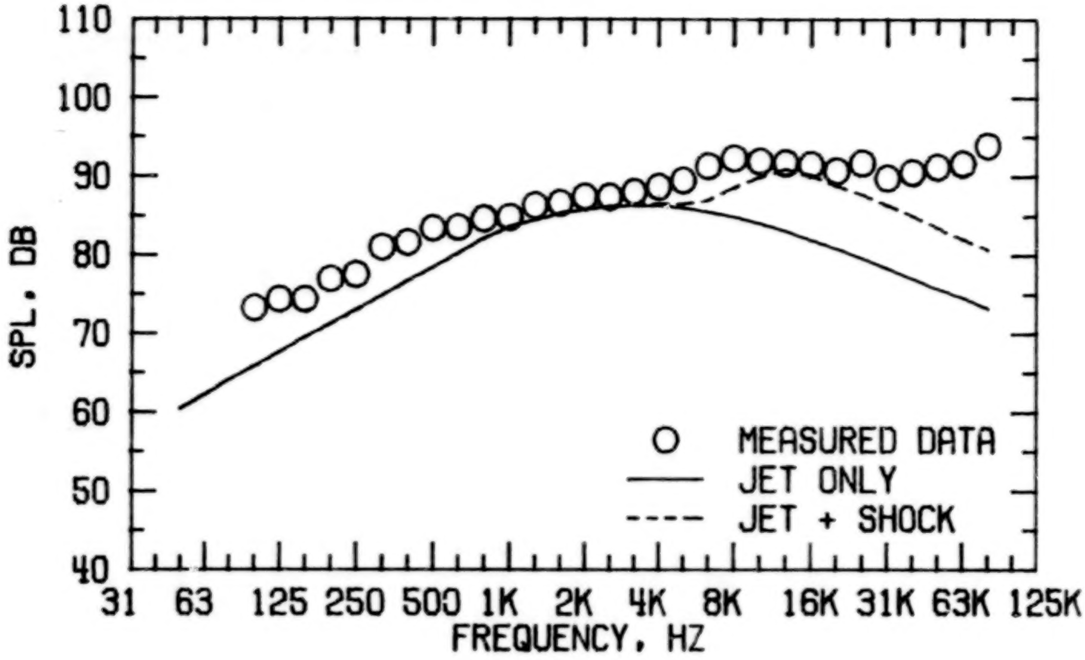

FIGURE A10. SPECTRA COMPARISON FOR CASE 26
(B) DIRECTIVITY ANGLE = 60 DEGREES

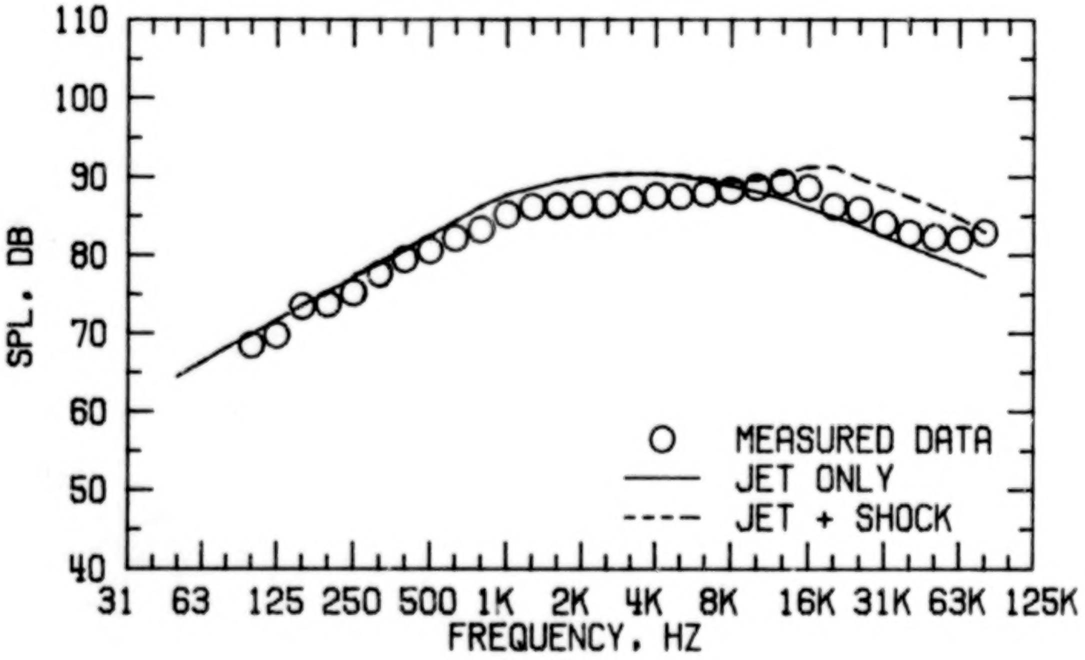

FIGURE A10. SPECTRA COMPARISON FOR CASE 26
(C) DIRECTIVITY ANGLE = 90 DEGREES

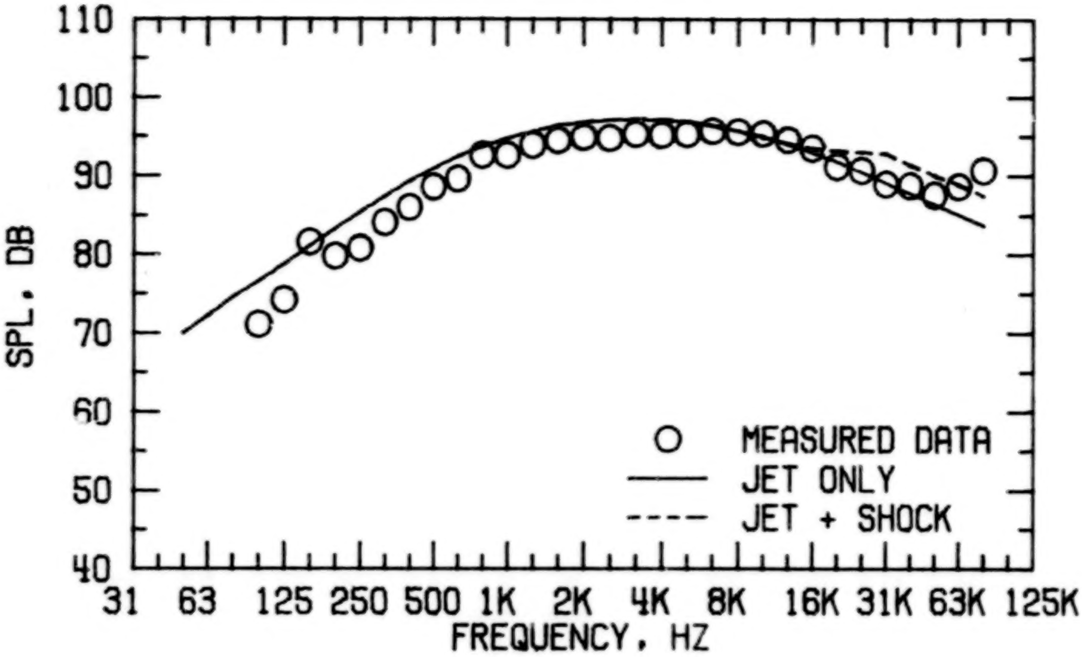

FIGURE A10. SPECTRA COMPARISON FOR CASE 26
(D) DIRECTIVITY ANGLE = 120 DEGREES

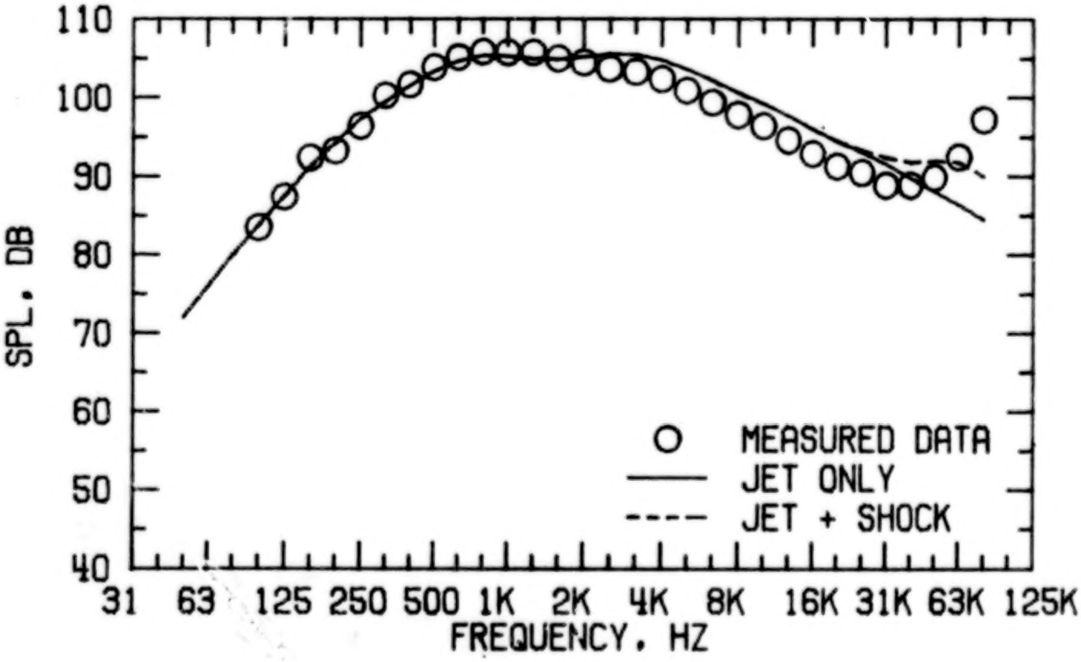

FIGURE A10. SPECTRA COMPARISON FOR CASE 26
(E) DIRECTIVITY ANGLE = 150 DEGREES

FLOW PROPERTIES FOR CASE 32
NOZZLE MODEL 3

FORWARD FLIGHT VELOCITY, V_A = 0.0 M/S

	TEMPERATURE T_T, DEG K	VELOCITY V, M/S	MASS FLOW W, KG/S	P_T/P_A
PRIMARY	389.2	299.0	1.8225	1.5300
SECONDARY	702.0	318.8	1.0890	1.3000
EQUIVALENT	506.2	306.4	2.9116	

REFERENCE RADIUS = 45.7 M

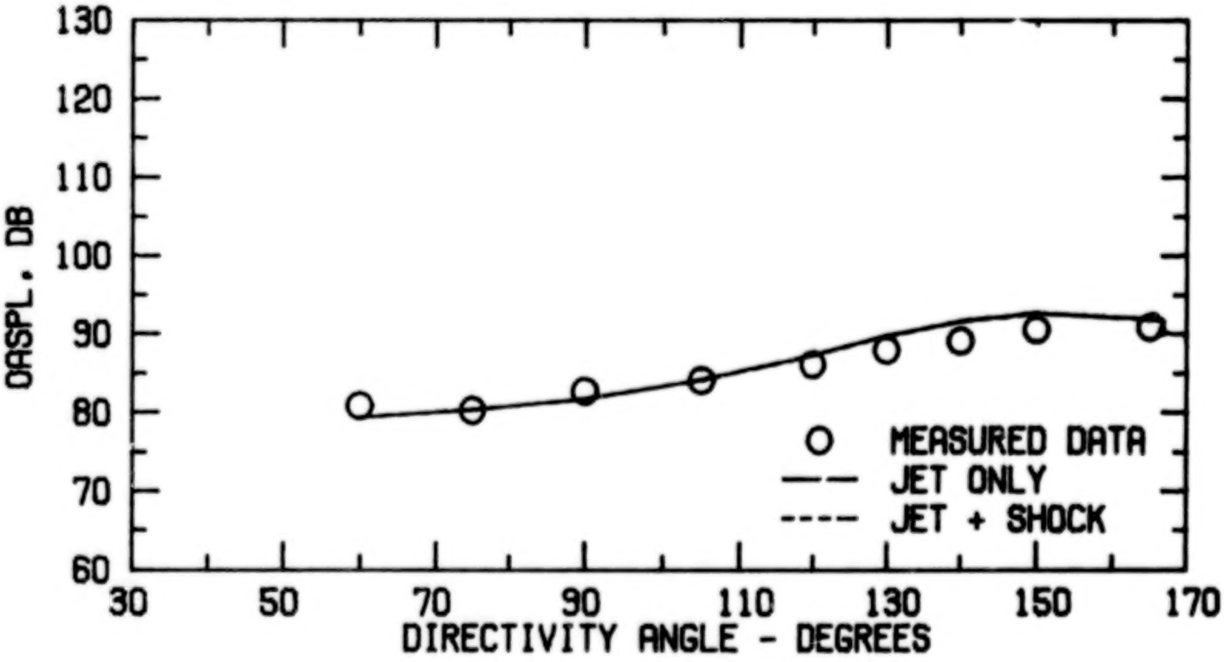

FIGURE A11. SPECTRA COMPARISON FOR CASE 32
(A) FLOW PROPERTIES AND DIRECTIVITY PLOT

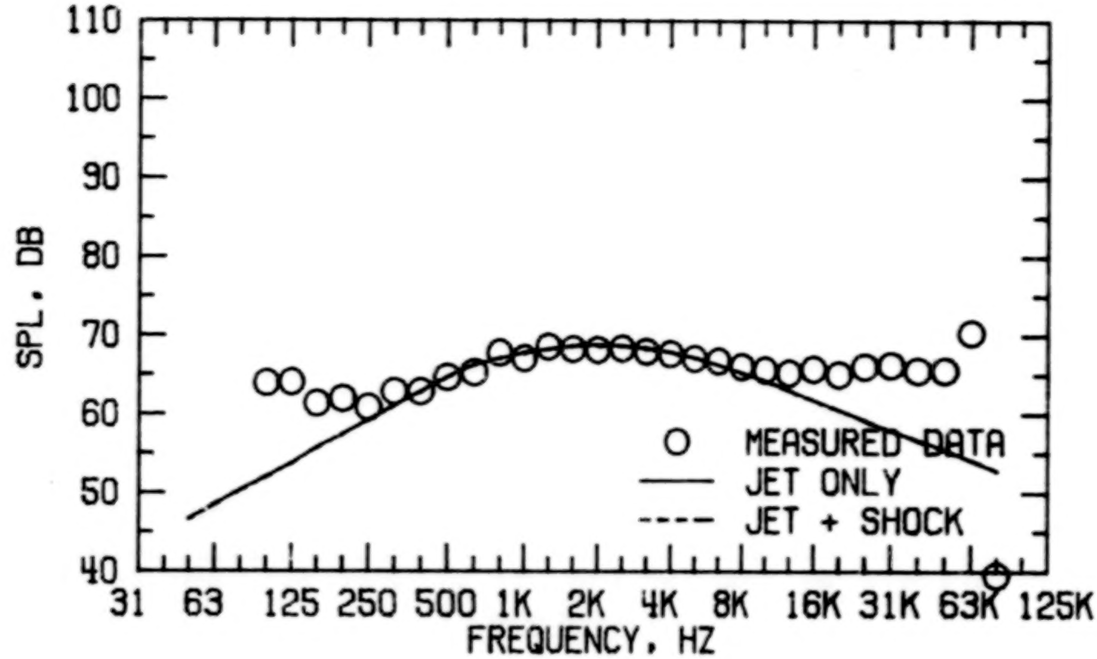

FIGURE A11. SPECTRA COMPARISON FOR CASE 32
(B) DIRECTIVITY ANGLE = 60 DEGREES

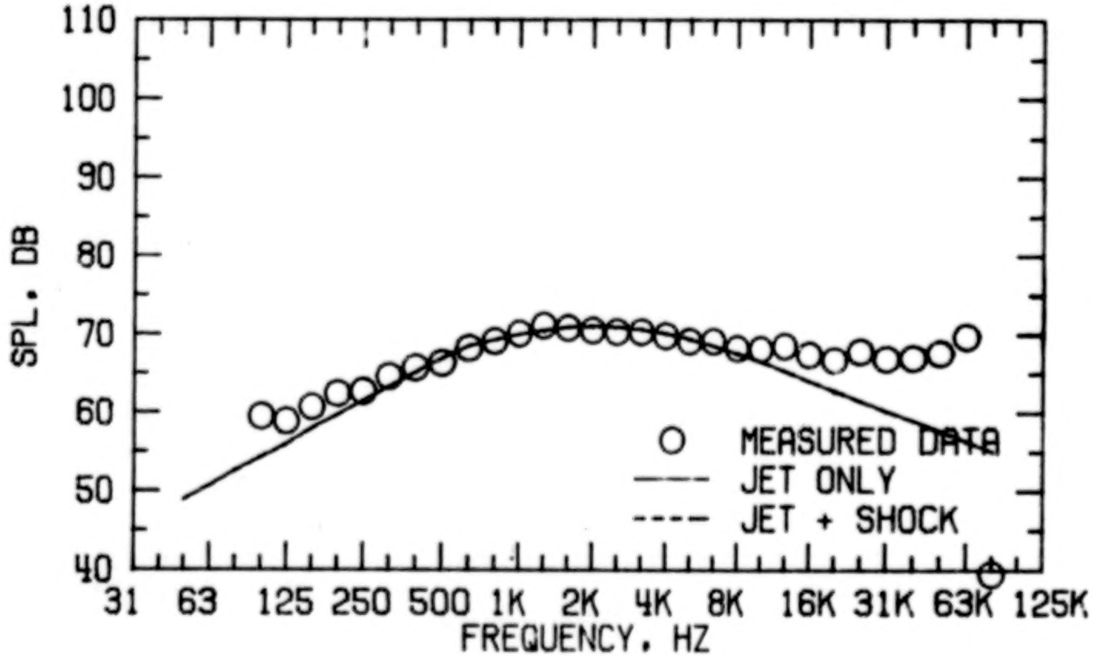

FIGURE A11. SPECTRA COMPARISON FOR CASE 32
(C) DIRECTIVITY ANGLE = 90 DEGREES

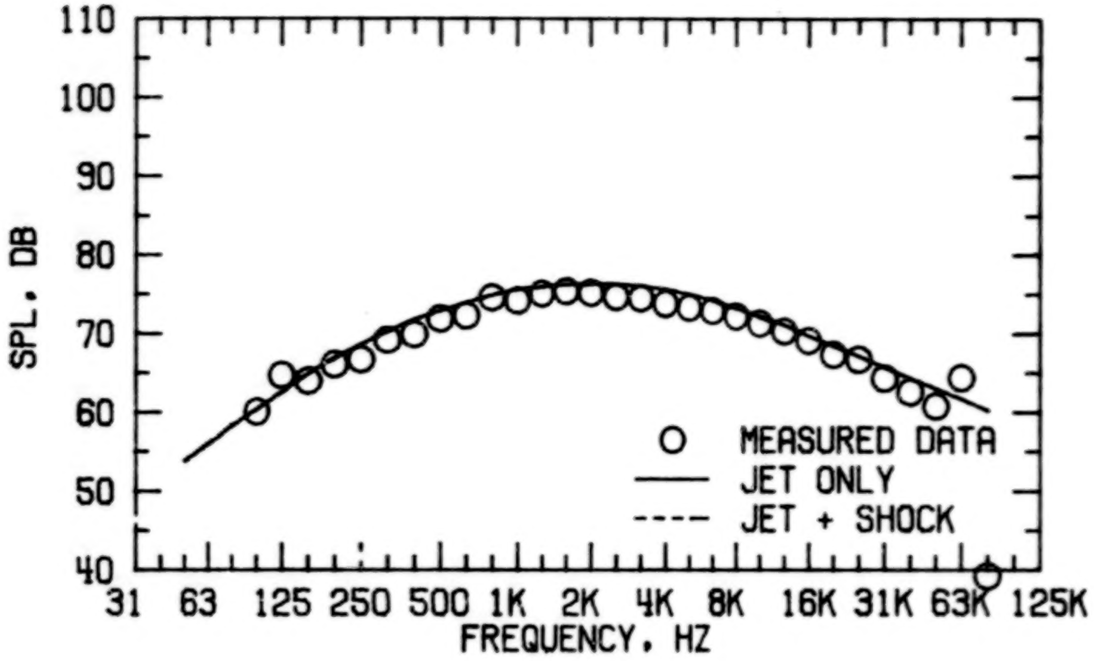

FIGURE A11. SPECTRA COMPARISON FOR CASE 32
(D) DIRECTIVITY ANGLE = 120 DEGREES

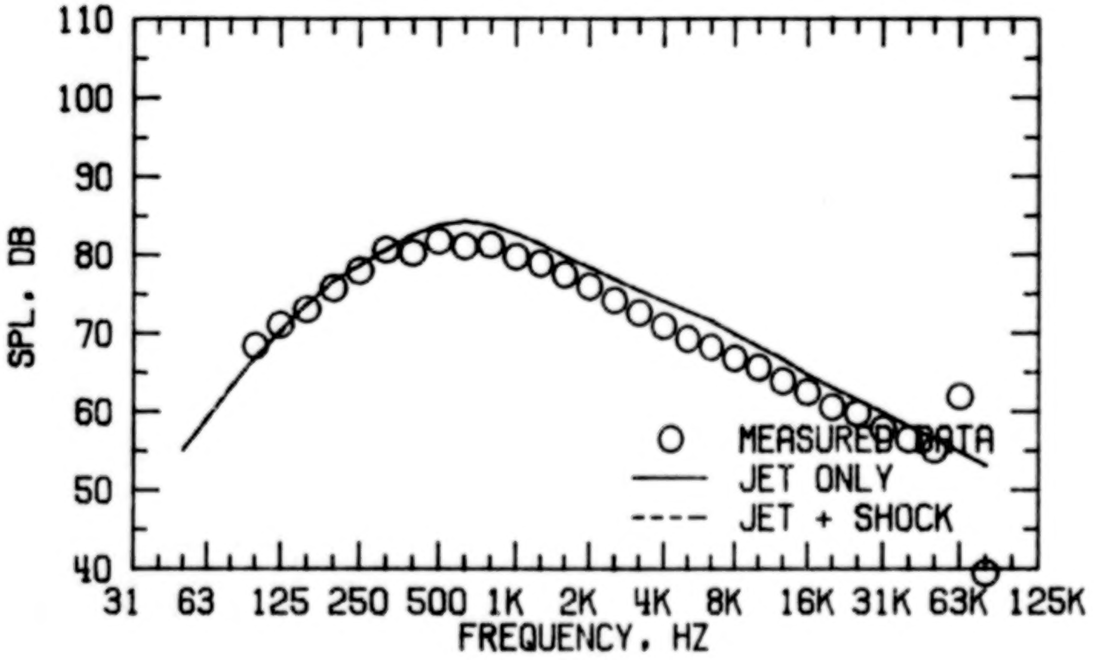

FIGURE A11. SPECTRA COMPARISON FOR CASE 32
(E) DIRECTIVITY ANGLE = 150 DEGREES

FLOW PROPERTIES FOR CASE 33
NOZZLE MODEL 3

FORWARD FLIGHT VELOCITY, V_A = 0.0 M/S

	TEMPERATURE T_T, DEG K	VELOCITY V, M/S	MASS FLOW W, KG/S	P_T/P_A
PRIMARY	843.7	441.6	1.2296	1.5300
SECONDARY	1079.8	858.9	3.4141	4.0600
EQUIVALENT	1017.3	748.4	4.6438	

REFERENCE RADIUS = 45.7 M

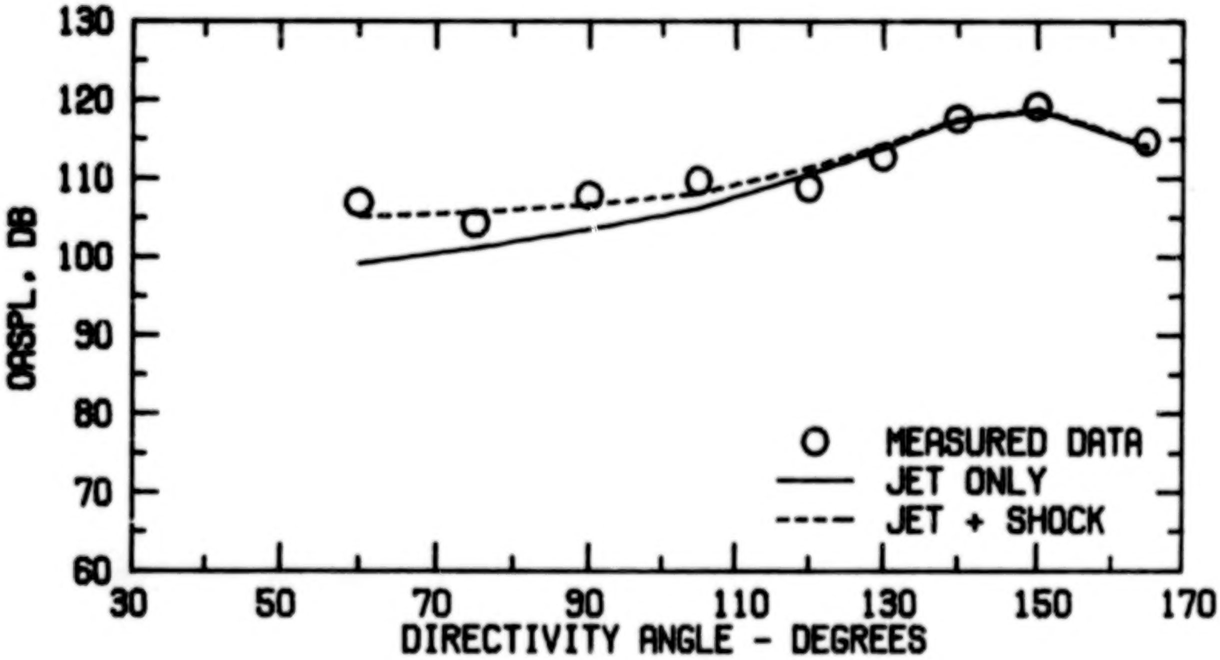

FIGURE A12. SPECTRA COMPARISON FOR CASE 33
(A) FLOW PROPERTIES AND DIRECTIVITY PLOT

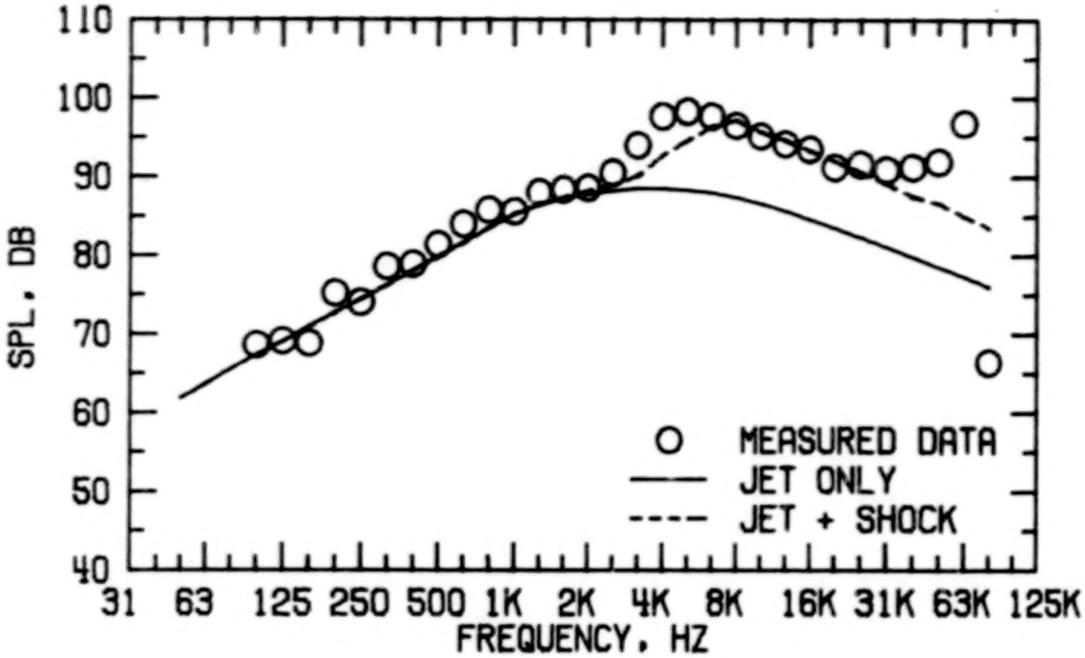

FIGURE A12. SPECTRA COMPARISON FOR CASE 33
(B) DIRECTIVITY ANGLE = 60 DEGREES

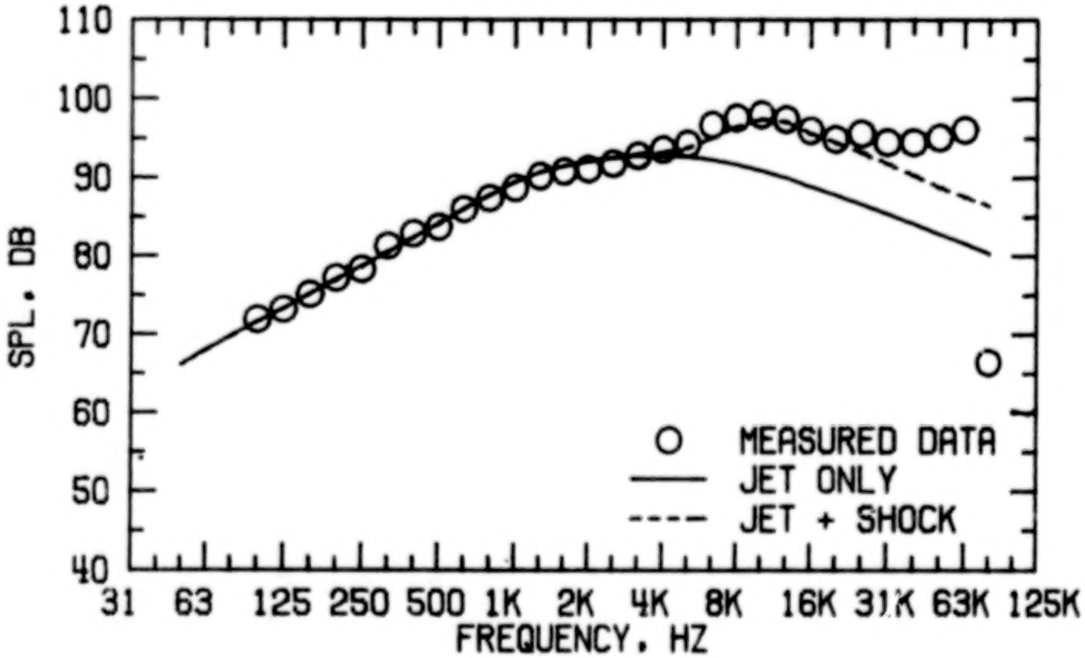

FIGURE A12. SPECTRA COMPARISON FOR CASE 33
(C) DIRECTIVITY ANGLE = 90 DEGREES

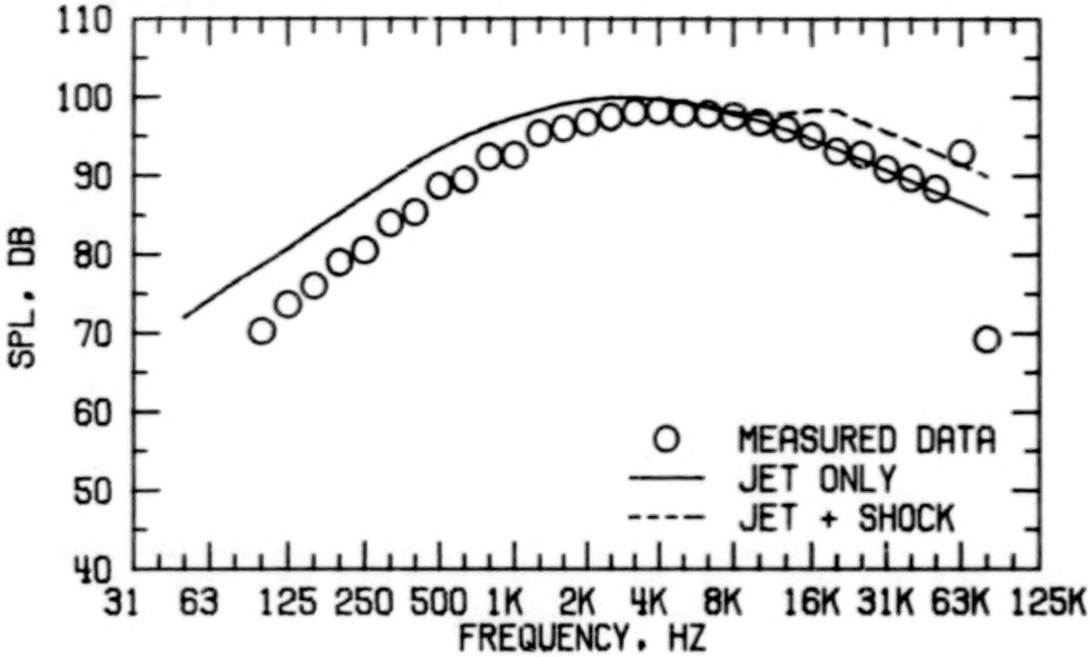

FIGURE A12. SPECTRA COMPARISON FOR CASE 33
(D) DIRECTIVITY ANGLE = 120 DEGREES

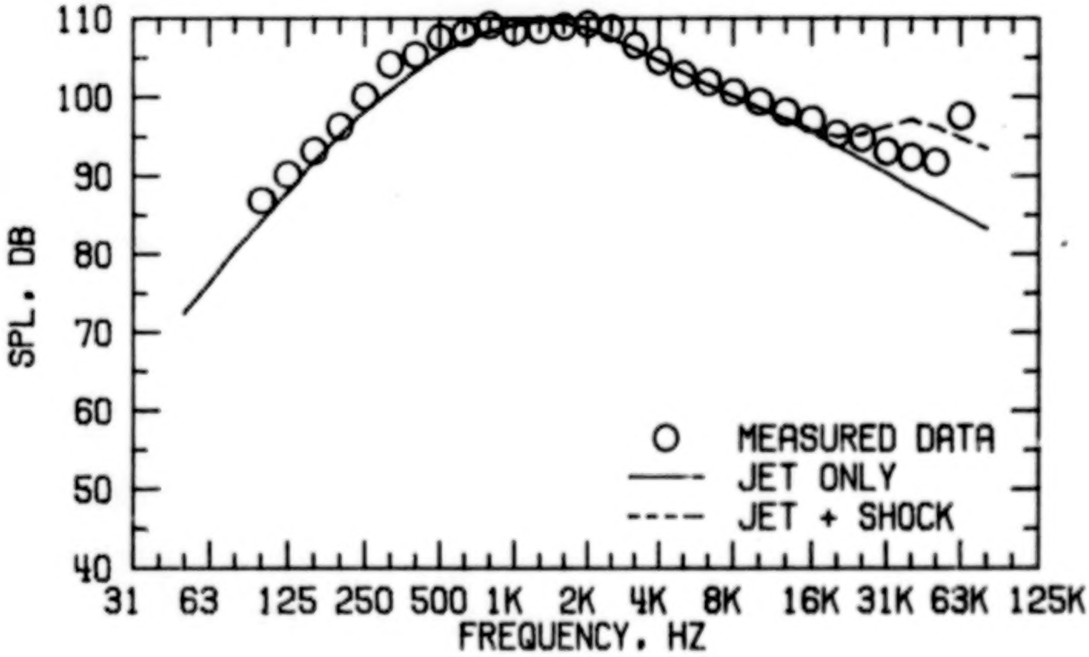

FIGURE A12. SPECTRA COMPARISON FOR CASE 33
(E) DIRECTIVITY ANGLE = 150 DEGREES

FLOW PROPERTIES FOR CASE 34
NOZZLE MODEL 4

FORWARD FLIGHT VELOCITY, V_A = 0.0 M/S

	TEMPERATURE T_T, DEG K	VELOCITY V, M/S	MASS FLOW W, KG/S	P_T/P_A
PRIMARY	282.2	293.8	4.7391	1.7820
SECONDARY	543.3	449.2	2.4838	2.0480
EQUIVALENT	372.0	347.2	7.2230	

REFERENCE RADIUS = 45.7 M

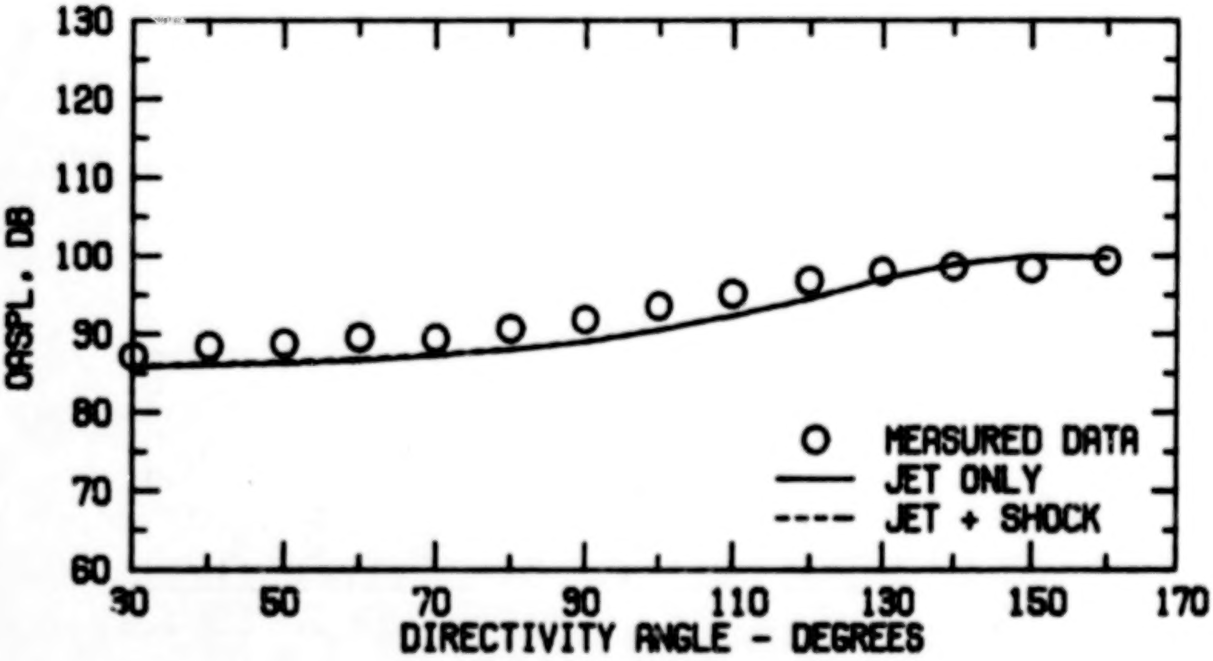

FIGURE A13. SPECTRA COMPARISON FOR CASE 34
(A) FLOW PROPERTIES AND DIRECTIVITY PLOT

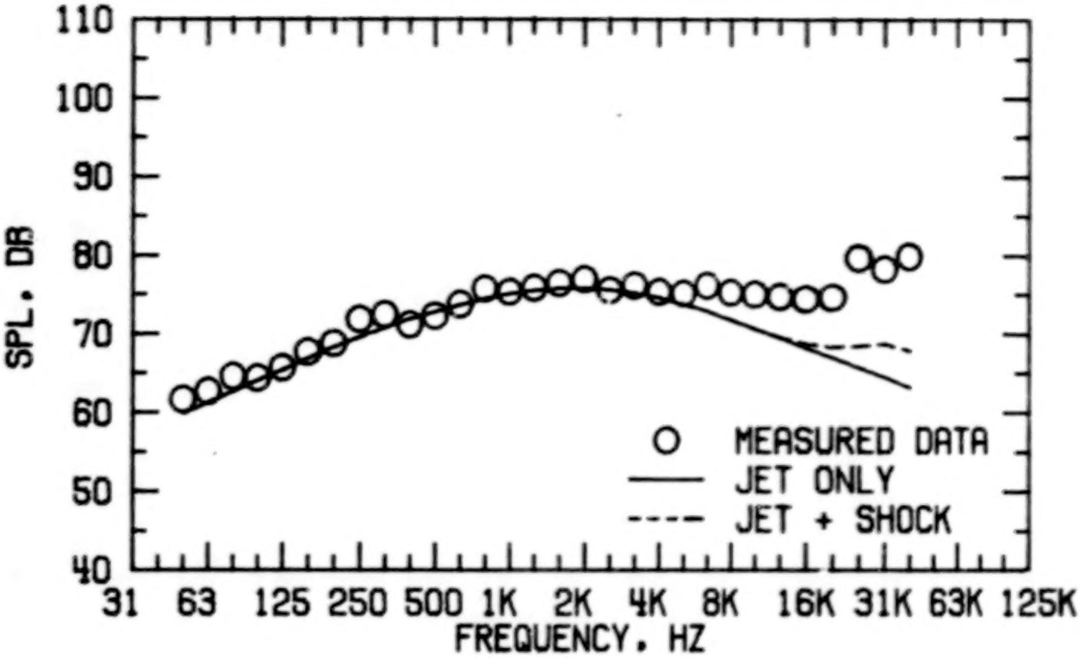

FIGURE A13: SPECTRA COMPARISON FOR CASE 34
(B) DIRECTIVITY ANGLE = 60 DEGREES

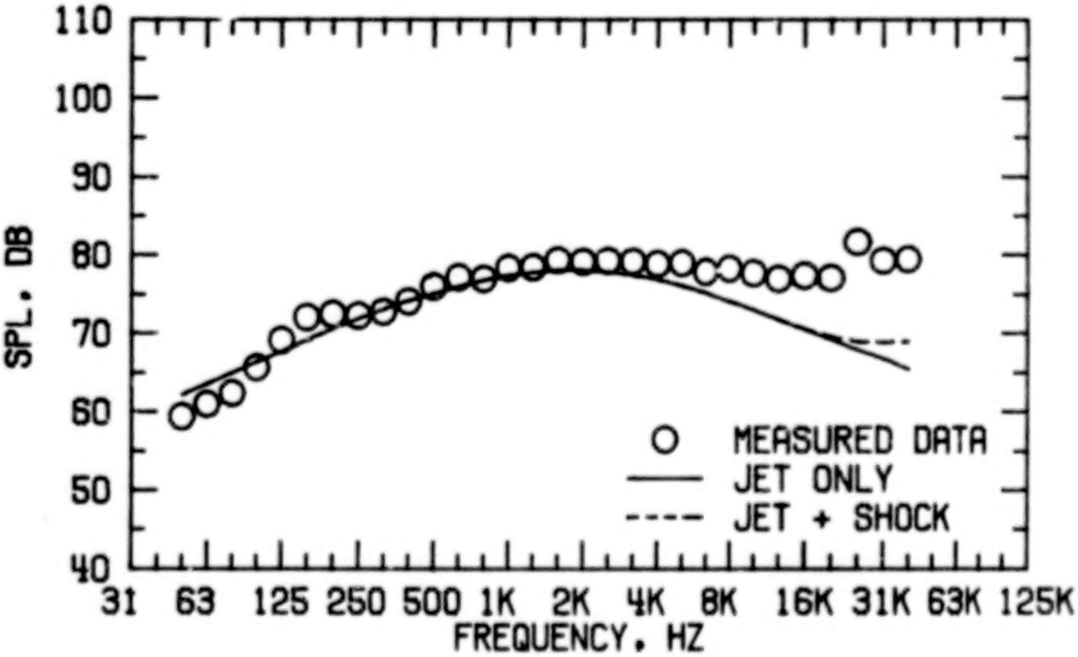

FIGURE A13. SPECTRA COMPARISON FOR CASE 34
(C) DIRECTIVITY ANGLE = 90 DEGREES

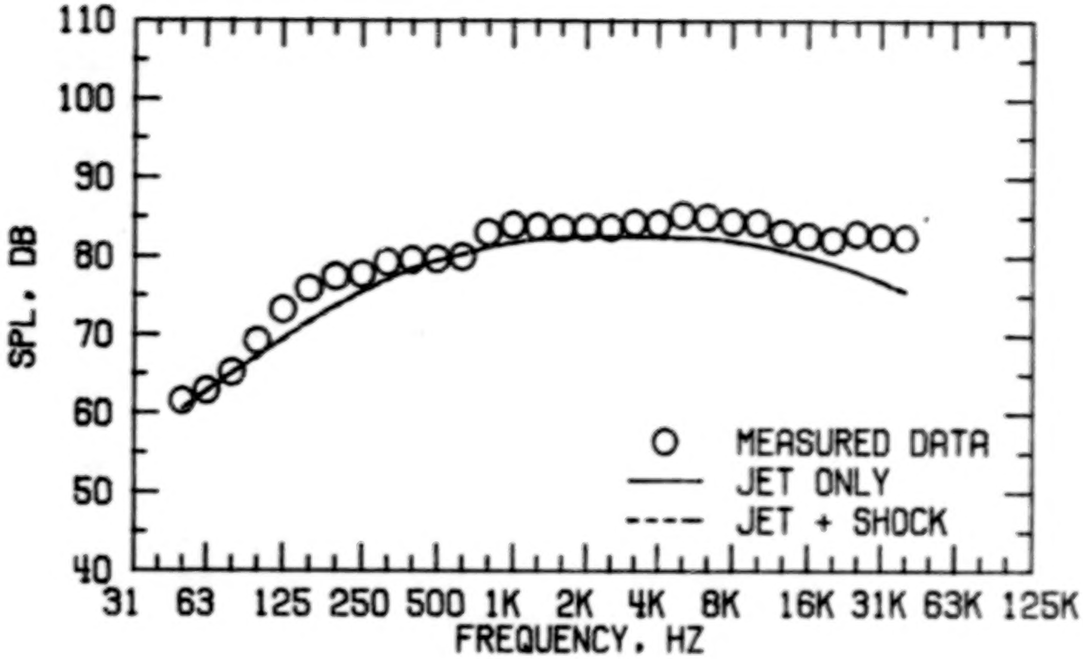

FIGURE A13. SPECTRA COMPARISON FOR CASE 34
(D) DIRECTIVITY ANGLE = 120 DEGREES

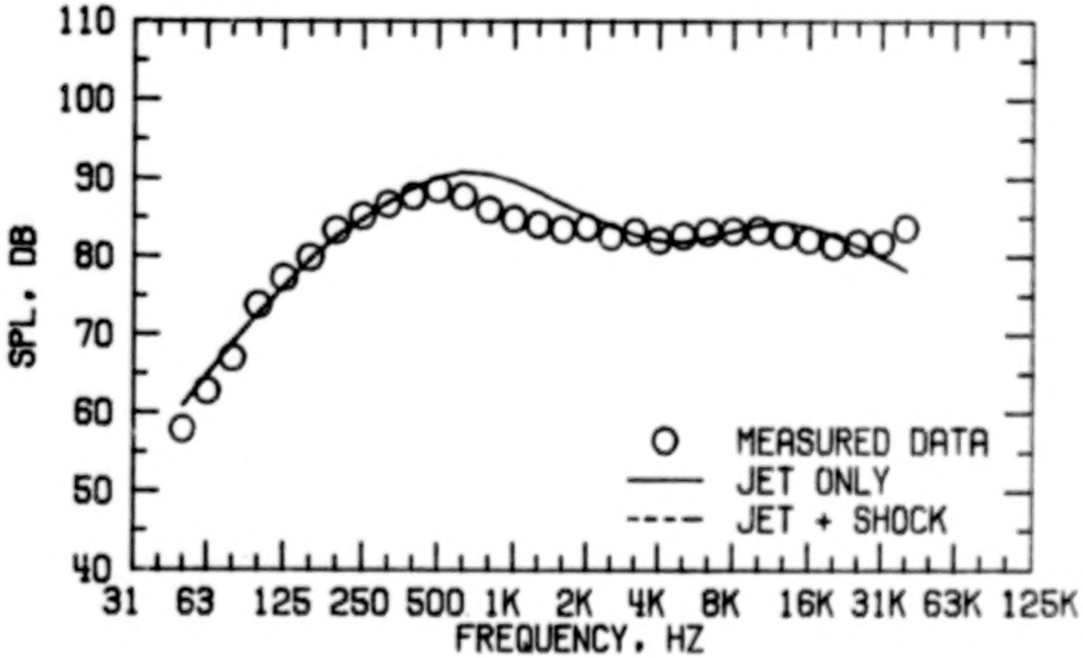

FIGURE A13. SPECTRA COMPARISON FOR CASE 34
(E) DIRECTIVITY ANGLE = 150 DEGREES

FLOW PROPERTIES FOR CASE 38
NOZZLE MODEL 4

FORWARD FLIGHT VELOCITY, V_A = 0.0 M/S

	TEMPERATURE T_T, DEG K	VELOCITY V, M/S	MASS FLOW W, KG/S	P_T/P_A
PRIMARY	804.4	424.5	2.3219	1.5090
SECONDARY	1087.2	845.5	3.2758	3.8770
EQUIVALENT	969.9	670.9	5.5977	

REFERENCE RADIUS = 45.7 M

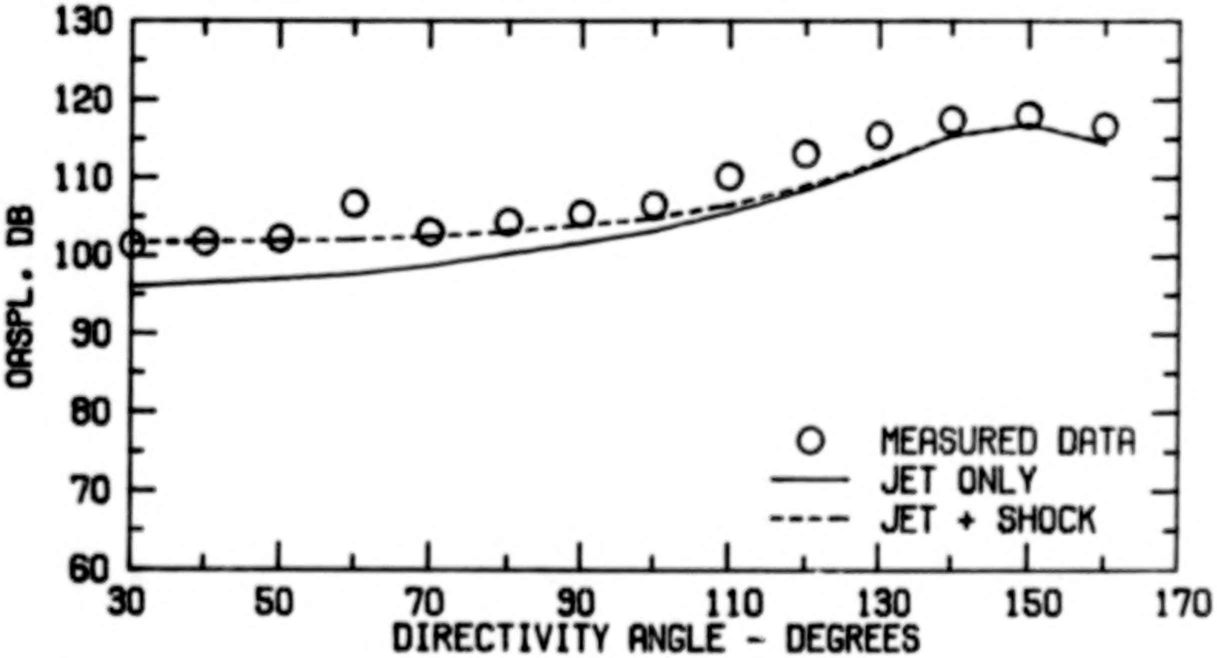

FIGURE A14. SPECTRA COMPARISON FOR CASE 38
(A) FLOW PROPERTIES AND DIRECTIVITY PLOT

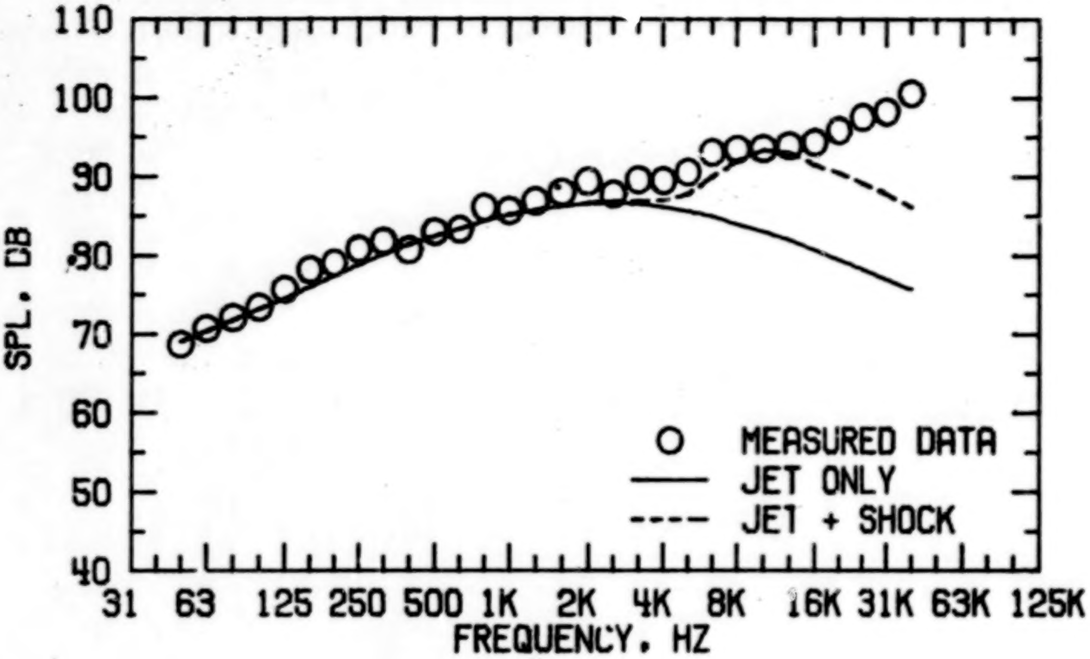

FIGURE A14. SPECTRA COMPARISON FOR CASE 38
(B) DIRECTIVITY ANGLE = 60 DEGREES

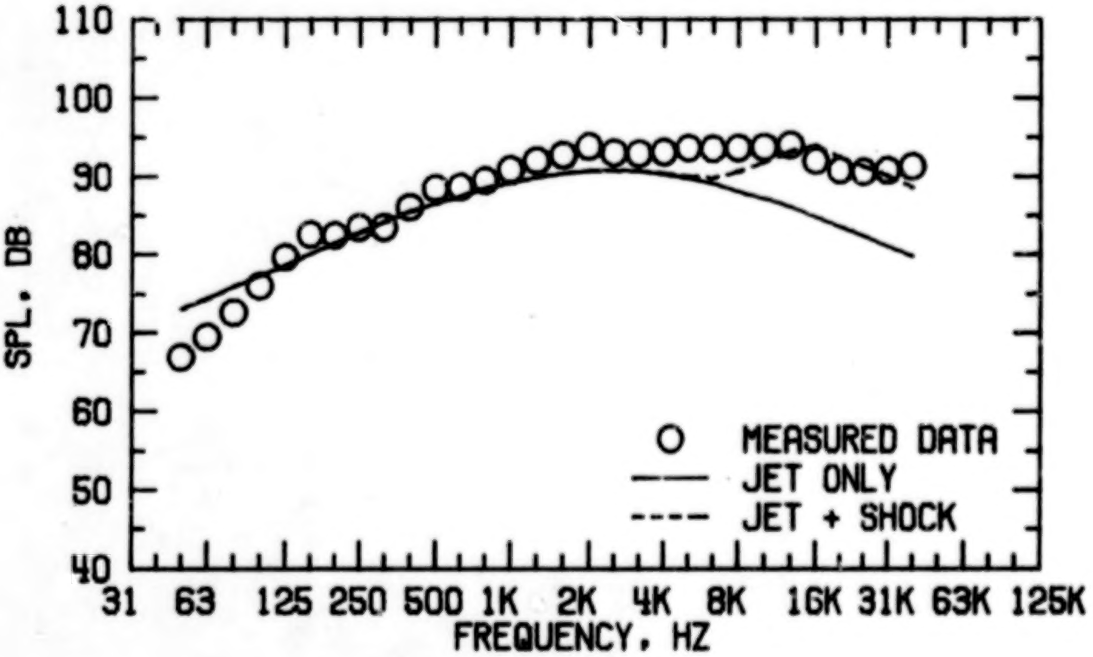

FIGURE A14. SPECTRA COMPARISON FOR CASE 38
(C) DIRECTIVITY ANGLE = 90 DEGREES

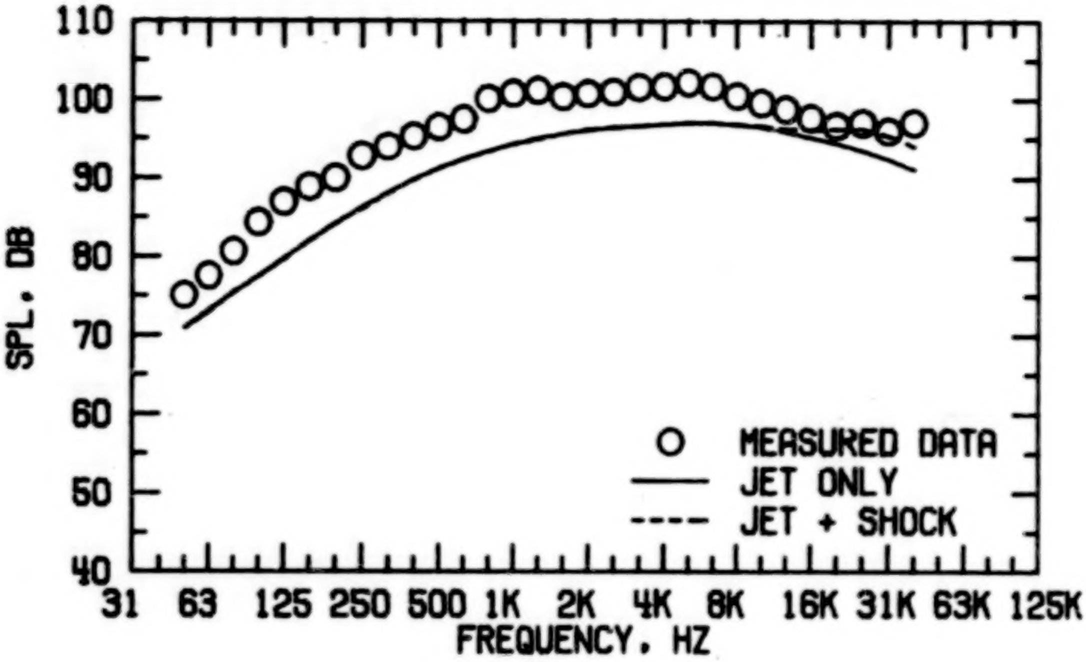

FIGURE A14. SPECTRA COMPARISON FOR CASE 38
(D) DIRECTIVITY ANGLE = 120 DEGREES

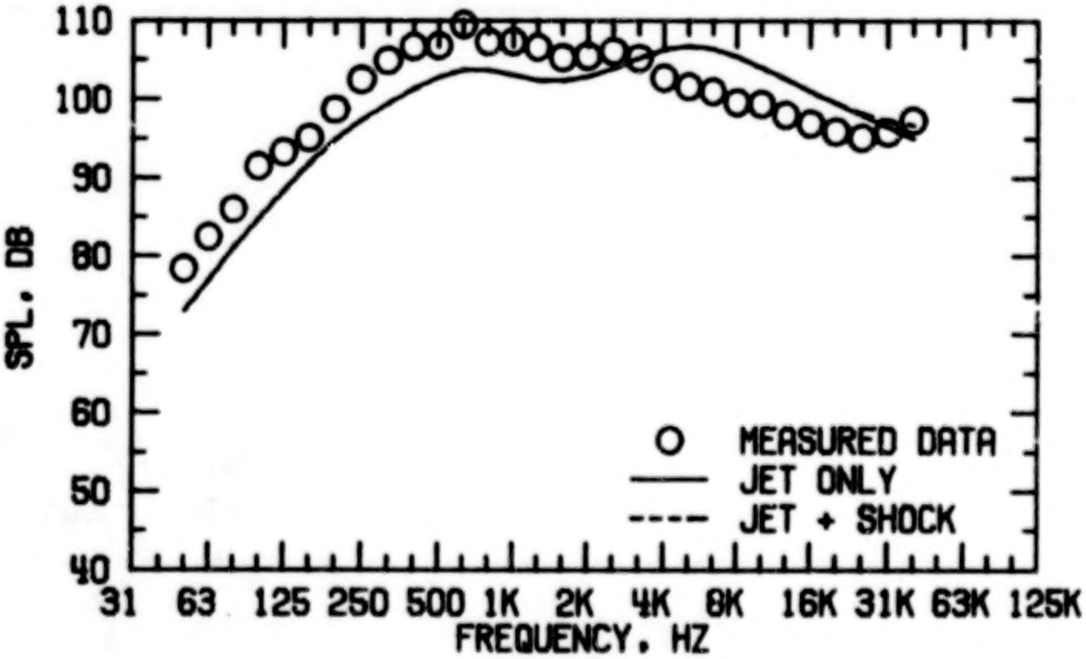

FIGURE A14. SPECTRA COMPARISON FOR CASE 38
(E) DIRECTIVITY ANGLE = 150 DEGREES

FLOW PROPERTIES FOR CASE 43
NOZZLE MODEL 4

FORWARD FLIGHT VELOCITY, V_A = 0.0 M/S

	TEMPERATURE T_T, DEG K	VELOCITY V, M/S	MASS FLOW W, KG/S	P_T/P_A
PRIMARY	288.8	299.0	4.7169	1.7960
SECONDARY	648.8	606.8	3.5239	3.1790
EQUIVALENT	442.8	430.6	8.2408	

REFERENCE RADIUS = 45.7 M

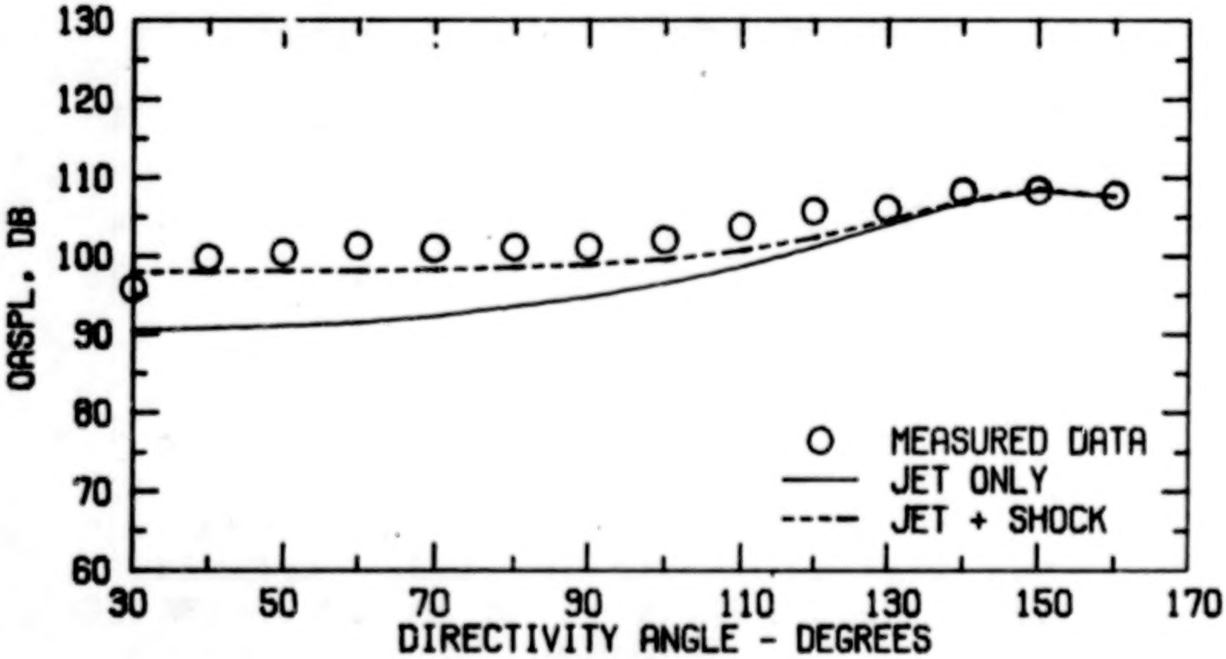

FIGURE A15. SPECTRA COMPARISON FOR CASE 43
(A) FLOW PROPERTIES AND DIRECTIVITY PLOT

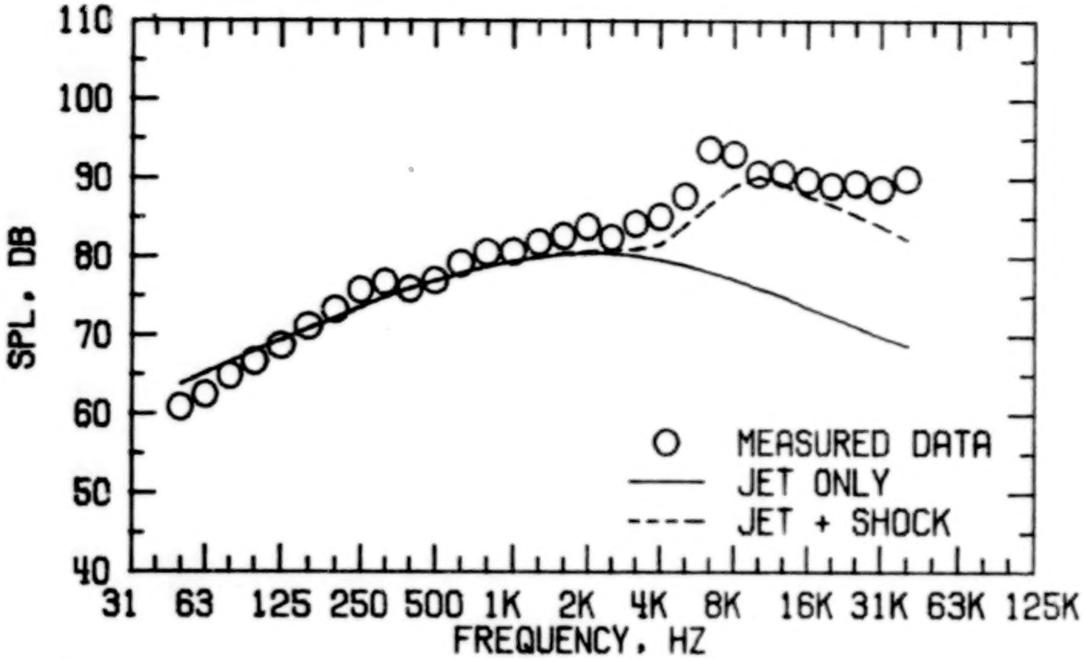

FIGURE A15. SPECTRA COMPARISON FOR CASE 43
(B) DIRECTIVITY ANGLE = 60 DEGREES

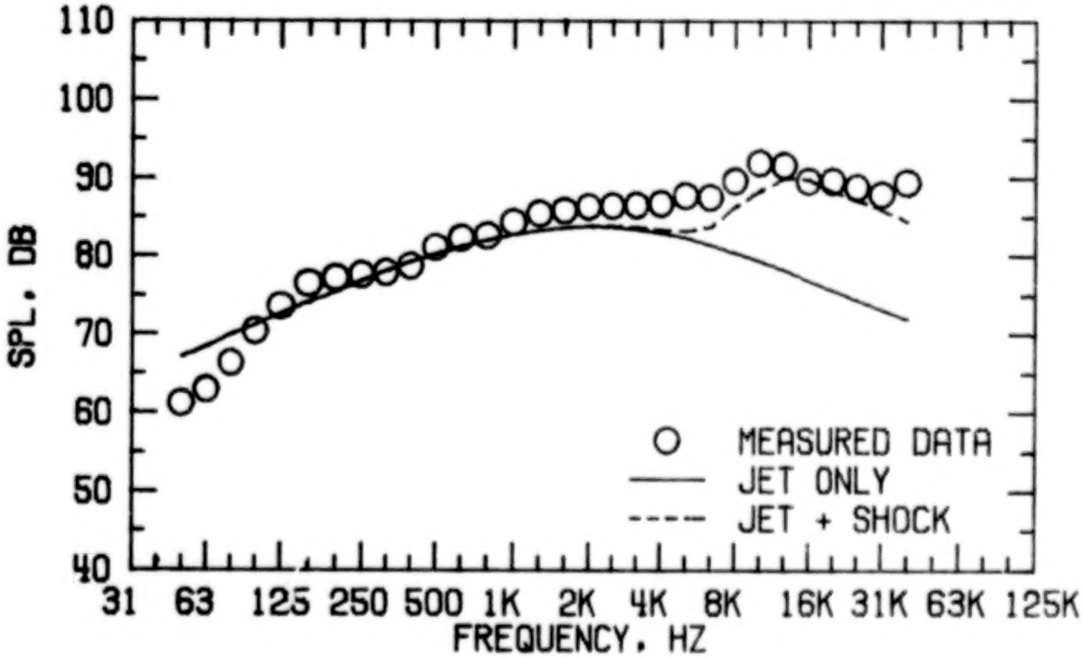

FIGURE A15. SPECTRA COMPARISON FOR CASE 43
(C) DIRECTIVITY ANGLE = 90 DEGREES

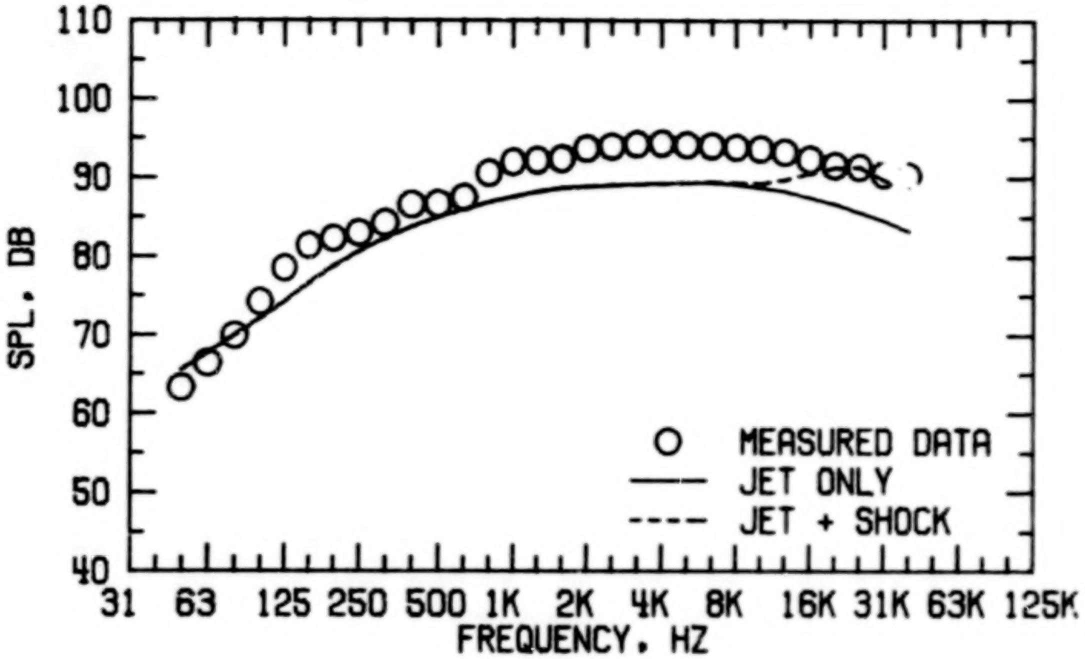

FIGURE A15. SPECTRA COMPARISON FOR CASE 43
(D) DIRECTIVITY ANGLE = 120 DEGREES

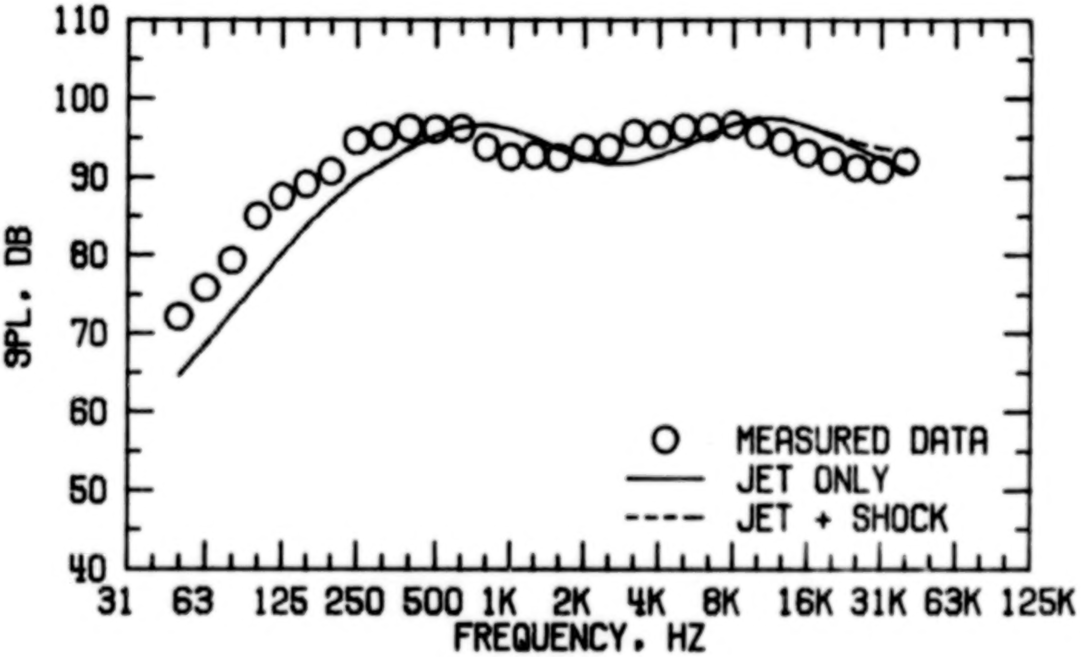

FIGURE A15. SPECTRA COMPARISON FOR CASE 43
(E) DIRECTIVITY ANGLE = 150 DEGREES

FLOW PROPERTIES FOR CASE 48

NOZZLE MODEL 4

FORWARD FLIGHT VELOCITY, V_A = 0.0 M/S

	TEMPERATURE T_T, DEG K	VELOCITY V, M/S	MASS FLOW W, KG/S	P_T/P_A
PRIMARY	806.6	609.2	3.8269	2.4610
SECONDARY	953.8	757.4	3.1098	3.4010
EQUIVALENT	872.6	675.7	6.9367	

REFERENCE RADIUS = 45.7 M

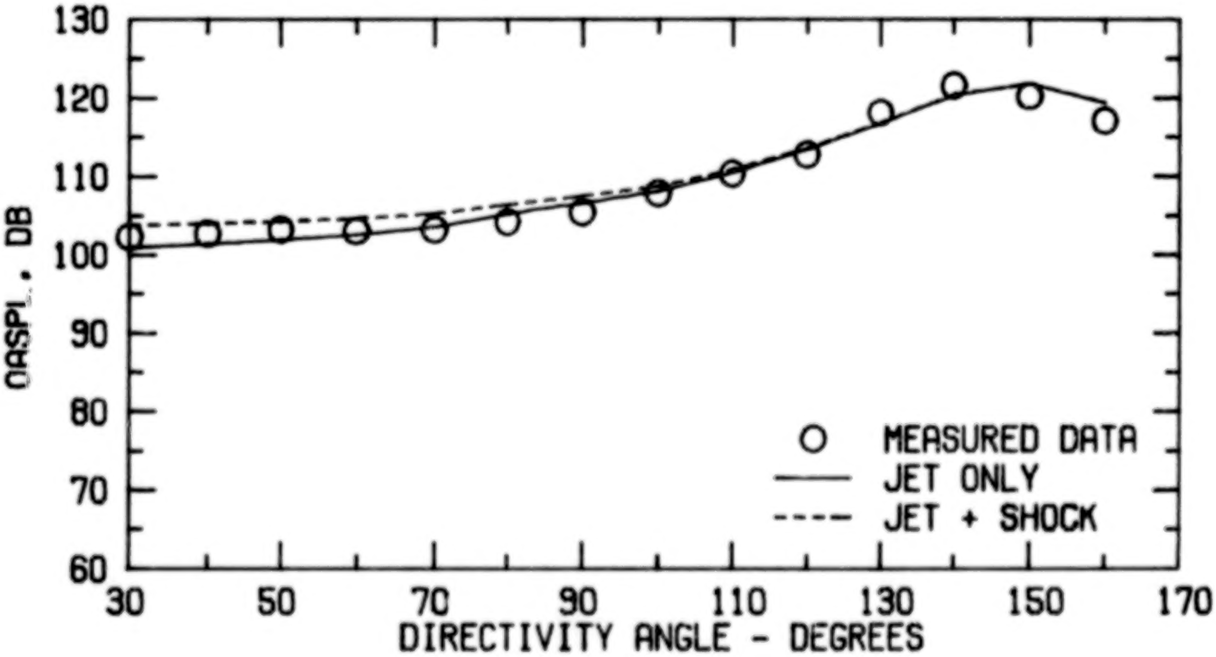

FIGURE A16. SPECTRA COMPARISON FOR CASE 48
(A) FLOW PROPERTIES AND DIRECTIVITY PLOT

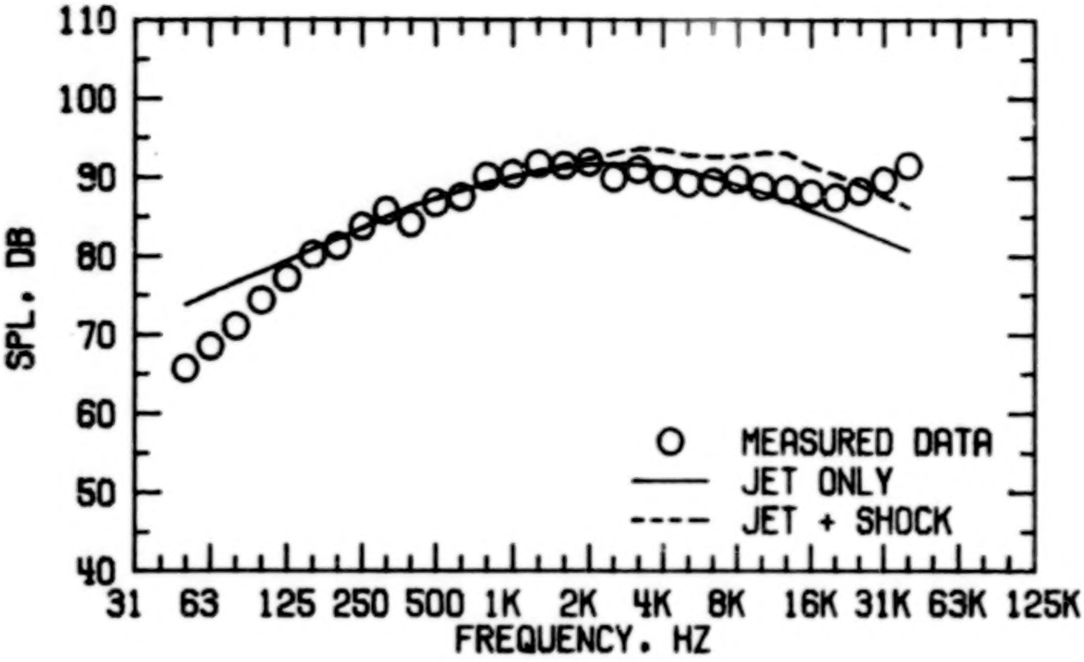

FIGURE A16. SPECTRA COMPARISON FOR CASE 48
(B) DIRECTIVITY ANGLE = 60 DEGREES

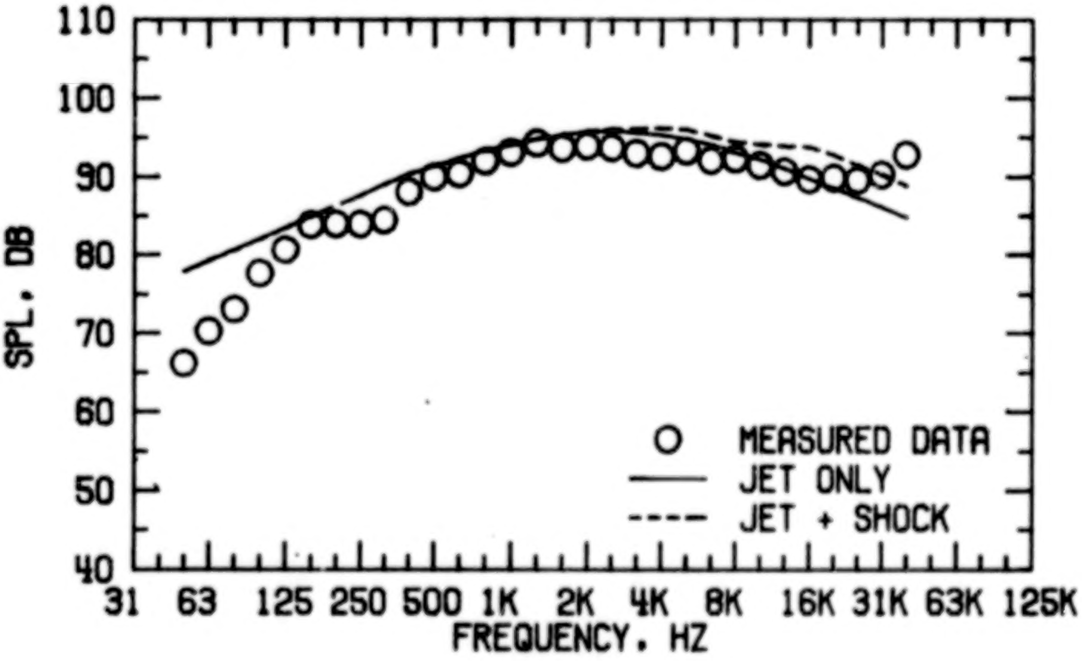

FIGURE A16. SPECTRA COMPARISON FOR CASE 48
(C) DIRECTIVITY ANGLE = 90 DEGREES

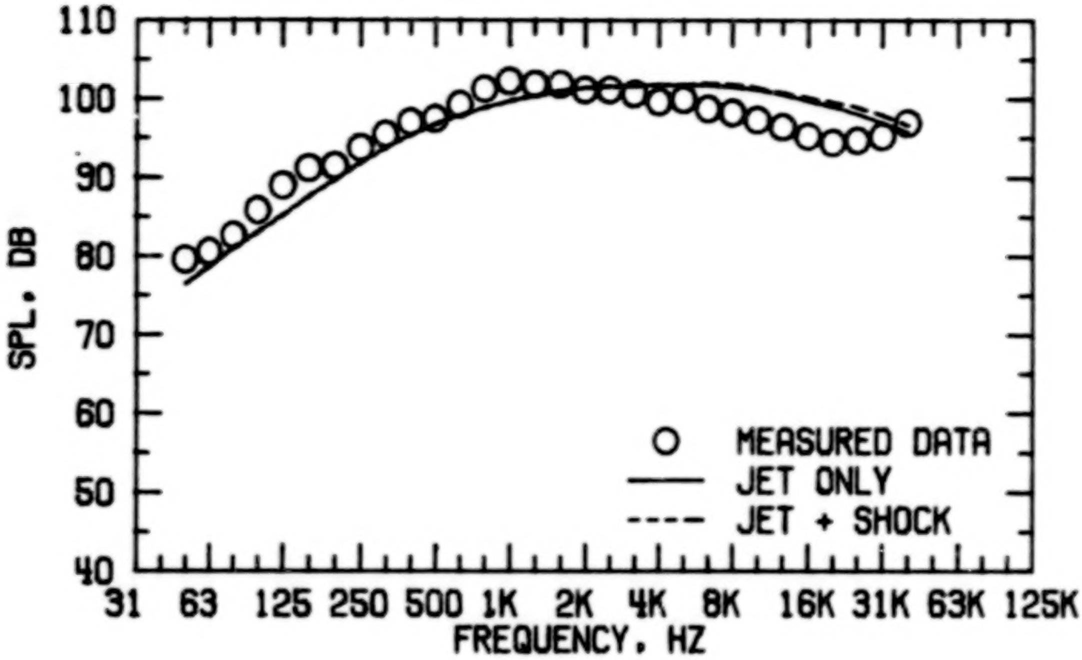

FIGURE A16. SPECTRA COMPARISON FOR CASE 48
(D) DIRECTIVITY ANGLE = 120 DEGREES

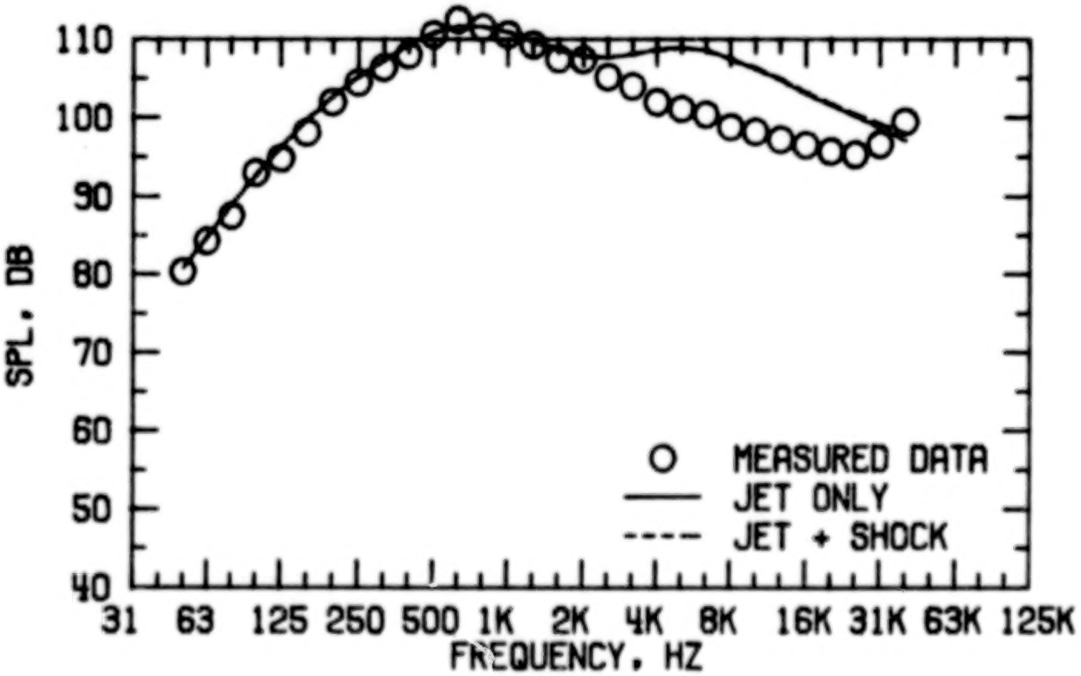

FIGURE A16. SPECTRA COMPARISON FOR CASE 48
(E) DIRECTIVITY ANGLE = 150 DEGREES

APPENDIX B

Typical Wind Tunnel Case

Spectral Distributions

FLOW PROPERTIES FOR CASE 1
NOZZLE MODEL 2

FORWARD FLIGHT VELOCITY, V_A = 101.4 M/S

	TEMPERATURE T_T, DEG K	VELOCITY V, M/S	MASS FLOW W, KG/S	P_T/P_A
PRIMARY	392.6	300.2	.3900	1.5300
SECONDARY	388.7	470.6	.6486	3.2070
EQUIVALENT	390.1	406.6	1.0387	

REFERENCE RADIUS = 45.7 M

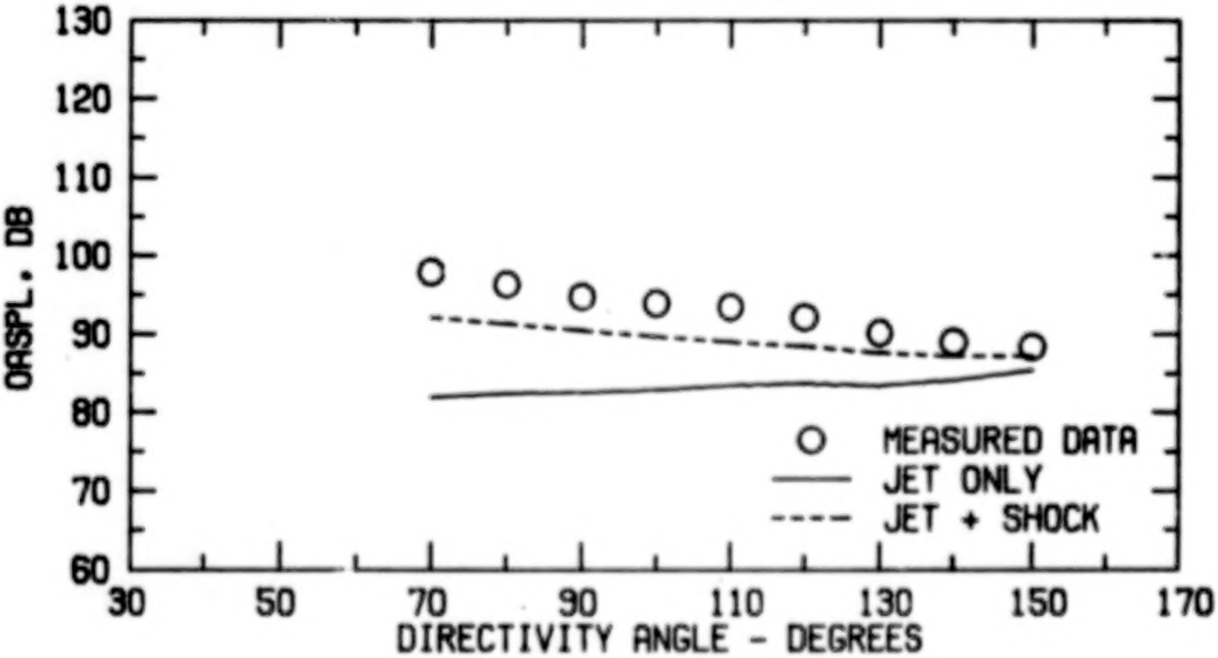

FIGURE B1 . SPECTRA COMPARISON FOR CASE 1
(A) FLOW PROPERTIES AND DIRECTIVITY PLOT

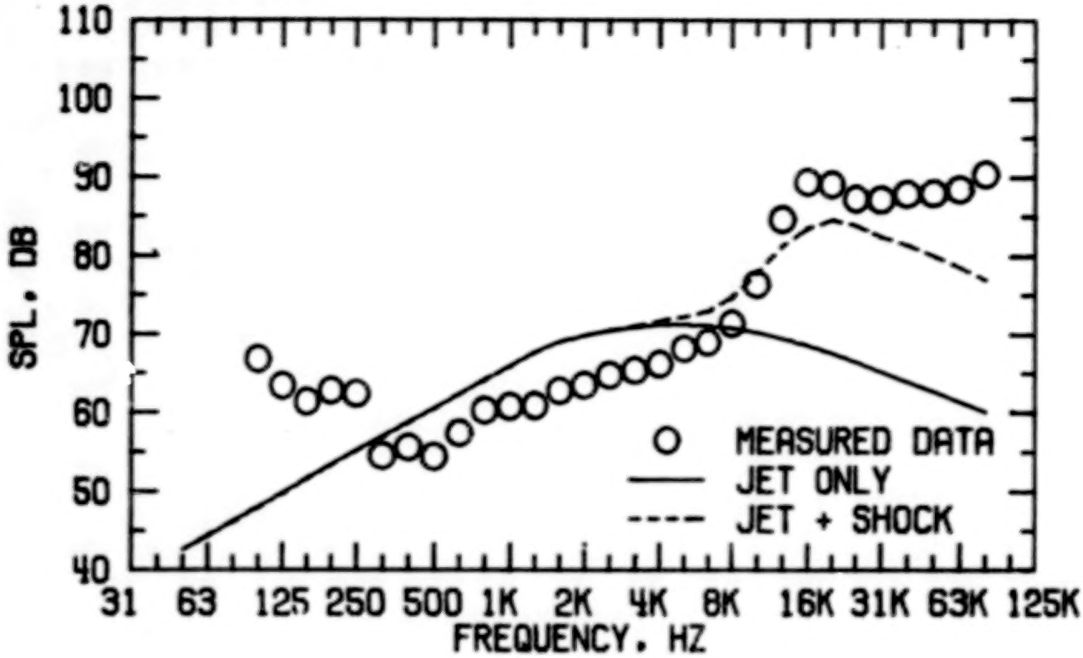

FIGURE B1 . SPECTRA COMPARISON FOR CASE 1
(B) DIRECTIVITY ANGLE = 70 DEGREES

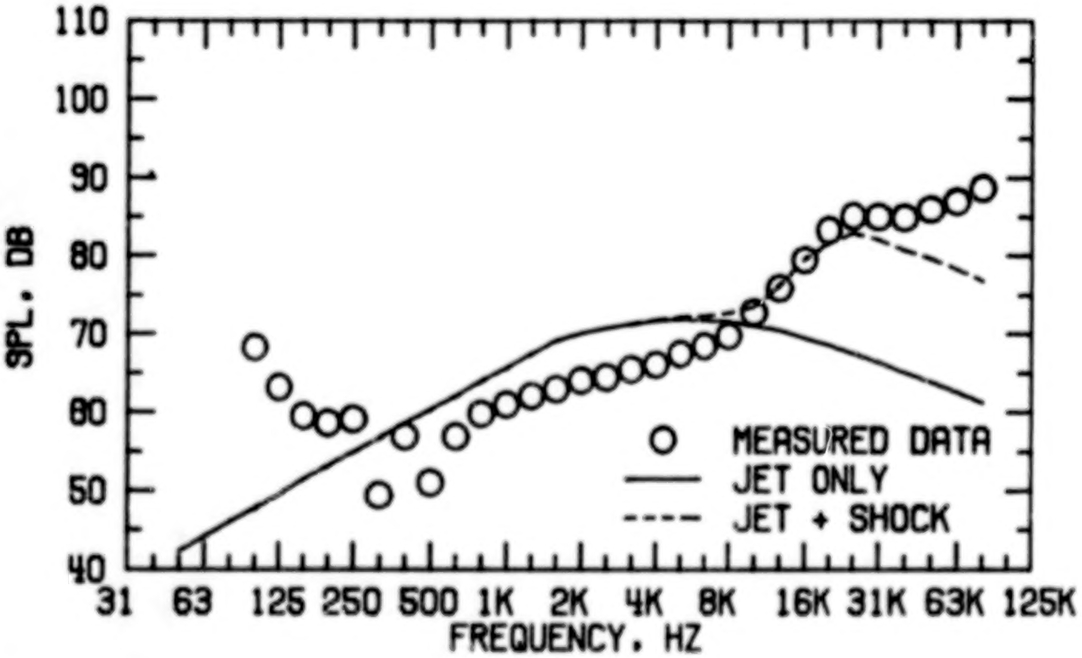

FIGURE B1 . SPECTRA COMPARISON FOR CASE 1
(C) DIRECTIVITY ANGLE = 90 DEGREES

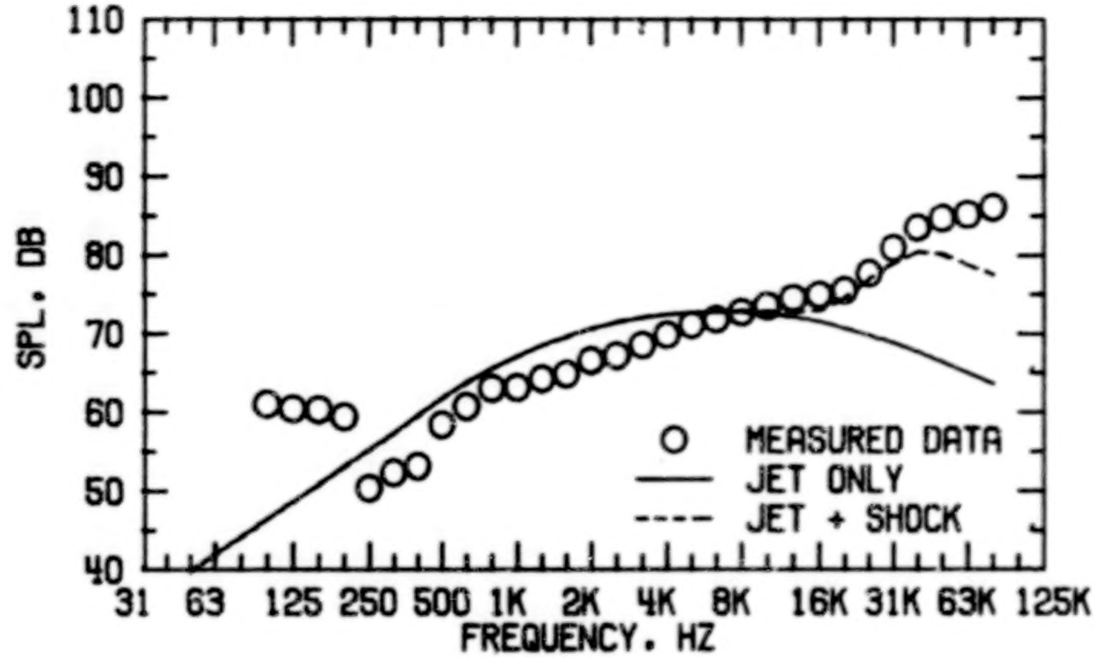

FIGURE B1 . SPECTRA COMPARISON FOR CASE 1
(D) DIRECTIVITY ANGLE = 120 DEGREES

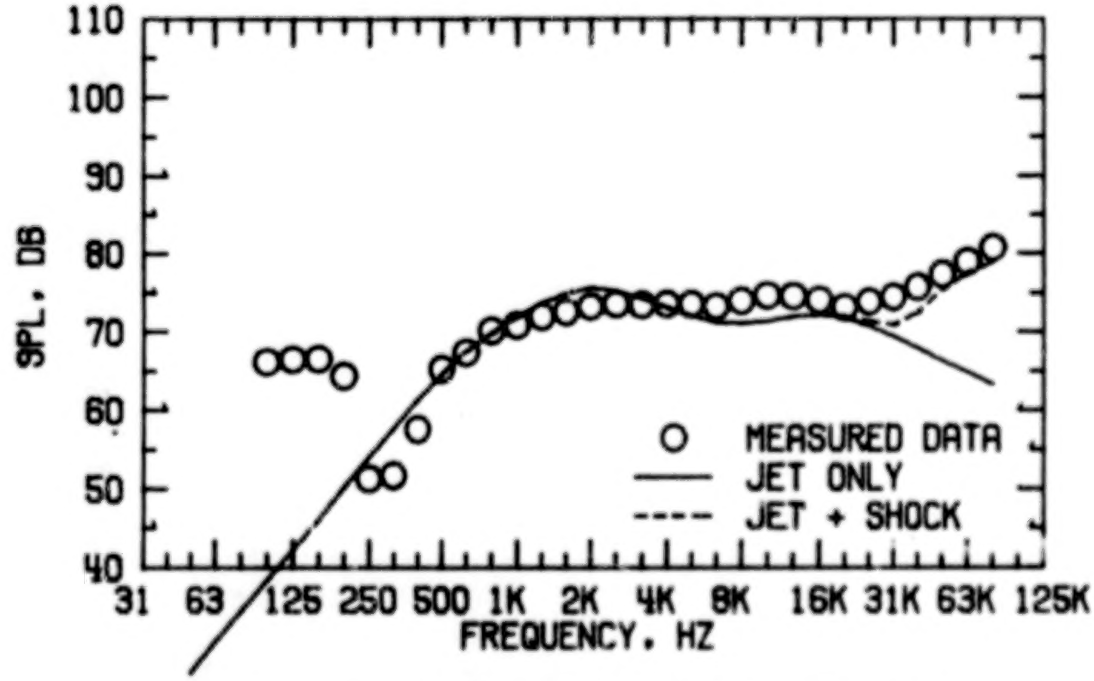

FIGURE B1 . SPECTRA COMPARISON FOR CASE 1
(E) DIRECTIVITY ANGLE = 150 DEGREES

FLOW PROPERTIES FOR CASE 5
NOZZLE MODEL 2

FORWARD FLIGHT VELOCITY, V_A = 31.0 M/S

	TEMPERATURE T_T, DEG K	VELOCITY V, M/S	MASS FLOW W, KG/S	P_T/P_A
PRIMARY	402.0	304.8	.4173	1.5330
SECONDARY	692.6	630.3	.4898	3.2010
EQUIVALENT	558.9	480.5	.9071	

REFERENCE RADIUS = 45.7 M

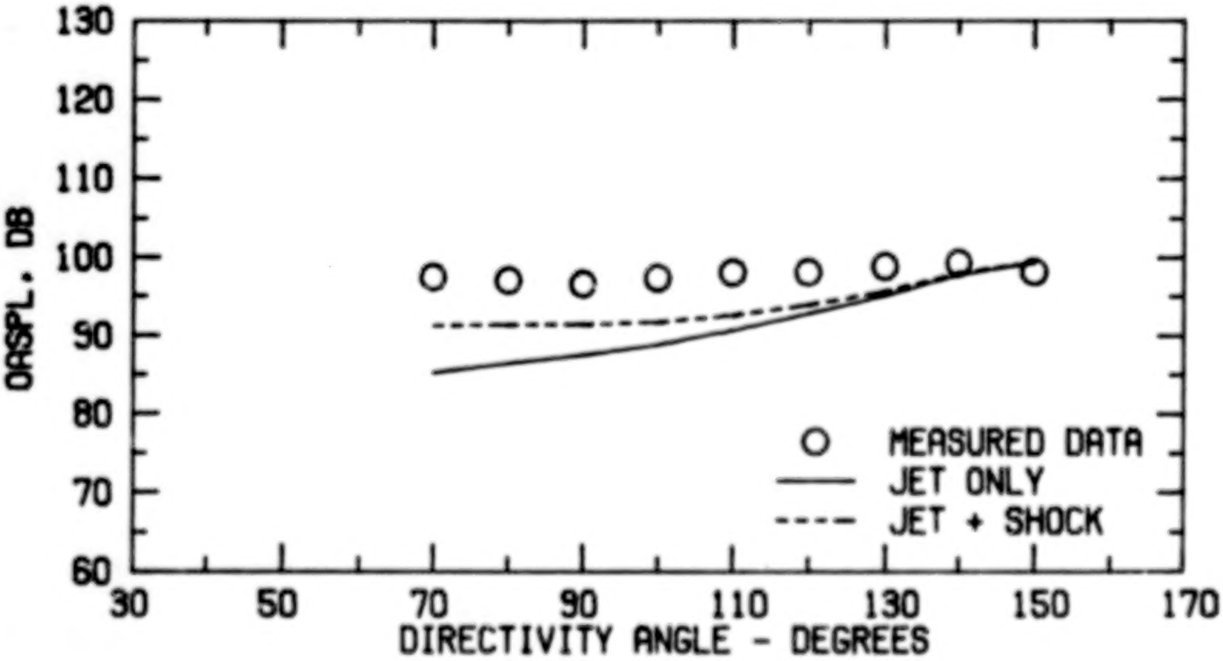

FIGURE B2 . SPECTRA COMPARISON FOR CASE 5
(A) FLOW PROPERTIES AND DIRECTIVITY PLOT

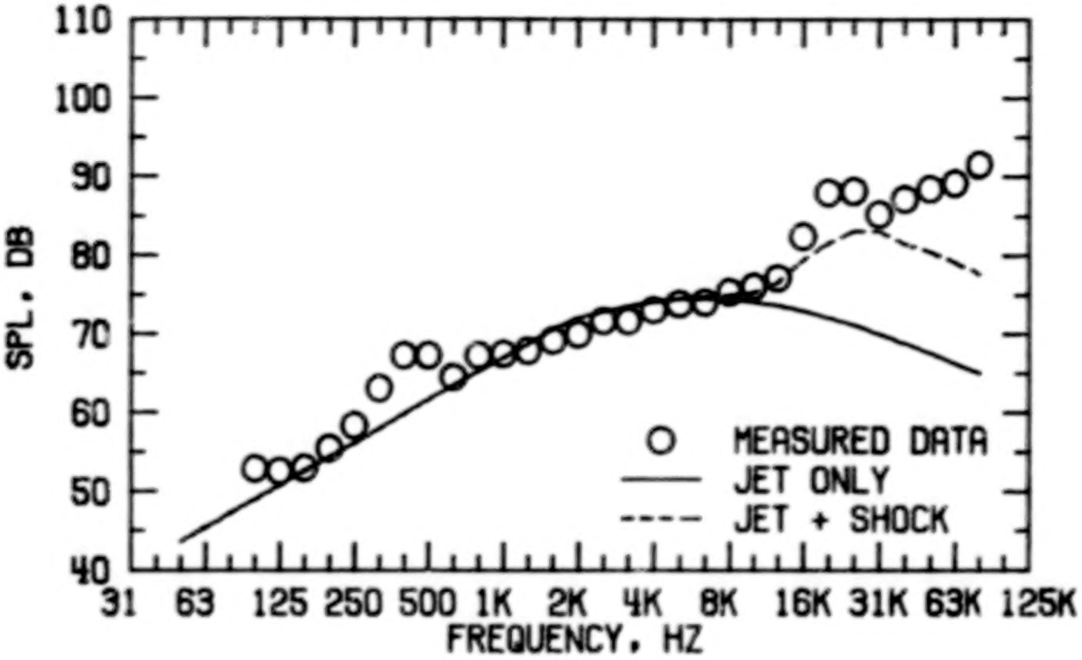

FIGURE B2 . SPECTRA COMPARISON FOR CASE 5
(B) DIRECTIVITY ANGLE = 70 DEGREES

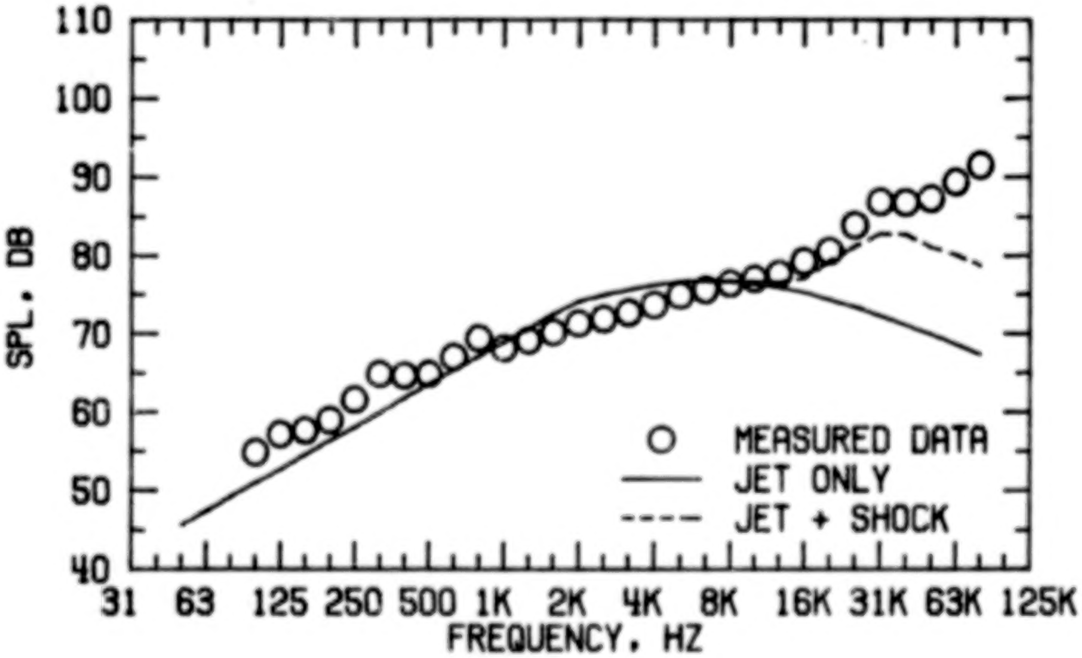

FIGURE B2 . SPECTRA COMPARISON FOR CASE 5
(C) DIRECTIVITY ANGLE = 90 DEGREES

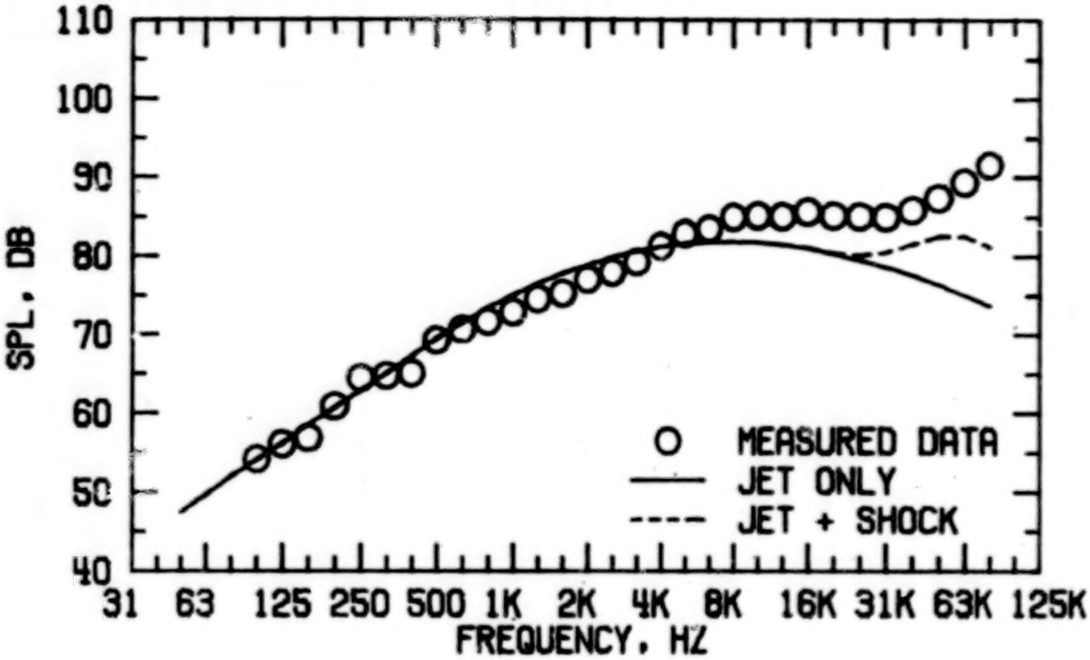

FIGURE B2 . SPECTRA COMPARISON FOR CASE 5
(D) DIRECTIVITY ANGLE = 120 DEGREES

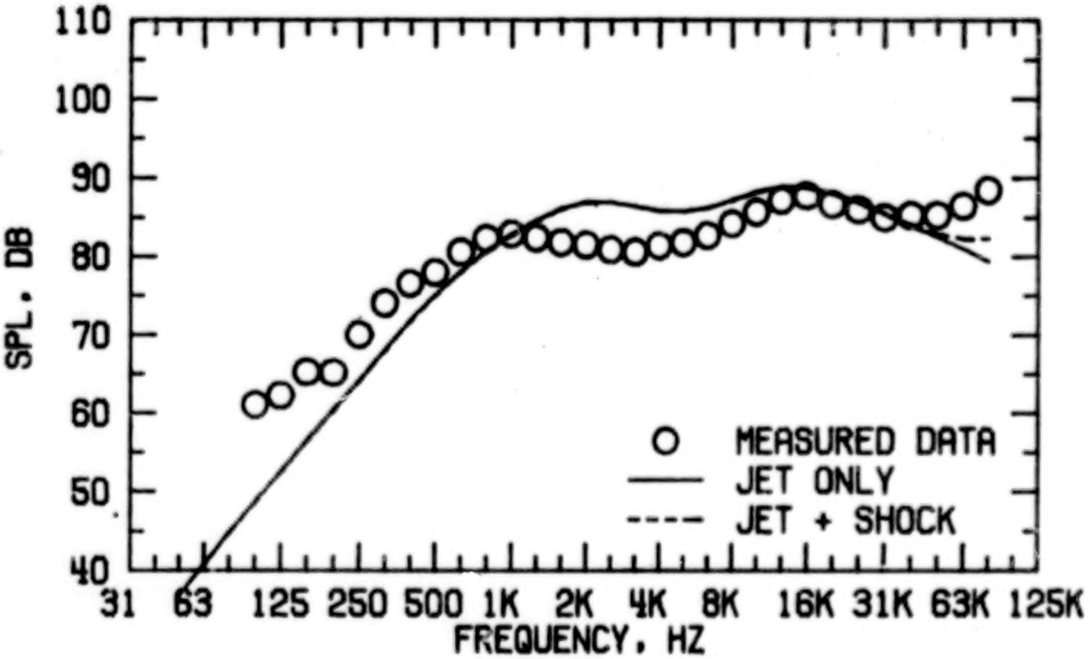

FIGURE B2 . SPECTRA COMPARISON FOR CASE 5
(E) DIRECTIVITY ANGLE = 150 DEGREES

FLOW PROPERTIES FOR CASE 8
NOZZLE MODEL 2

FORWARD FLIGHT VELOCITY, V_A = 30.1 M/S

	TEMPERATURE T_T, DEG K	VELOCITY V, M/S	MASS FLOW W, KG/S	P_T/P_A
PRIMARY	394.2	301.7	.4173	1.5330
SECONDARY	703.7	573.3	.3524	2.5030
EQUIVALENT	535.9	426.0	.7697	

REFERENCE RADIUS = 45.7 M

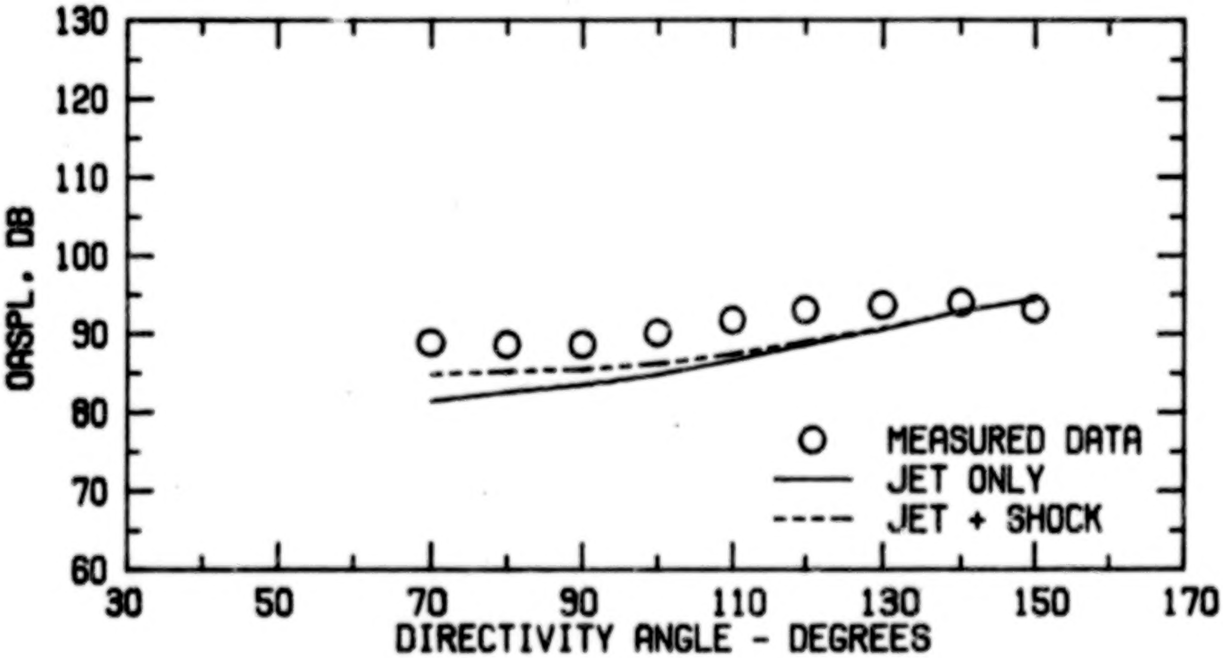

FIGURE B3 . SPECTRA COMPARISON FOR CASE 8
(A) FLOW PROPERTIES AND DIRECTIVITY PLOT

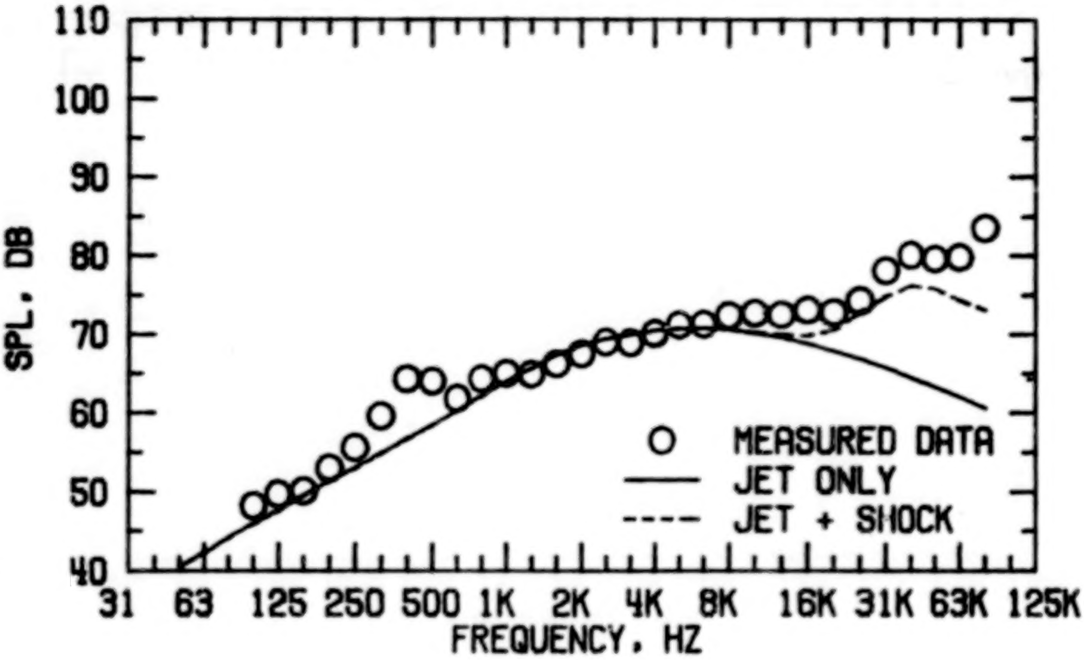

FIGURE B3 . SPECTRA COMPARISON FOR CASE 8
(B) DIRECTIVITY ANGLE = 70 DEGREES

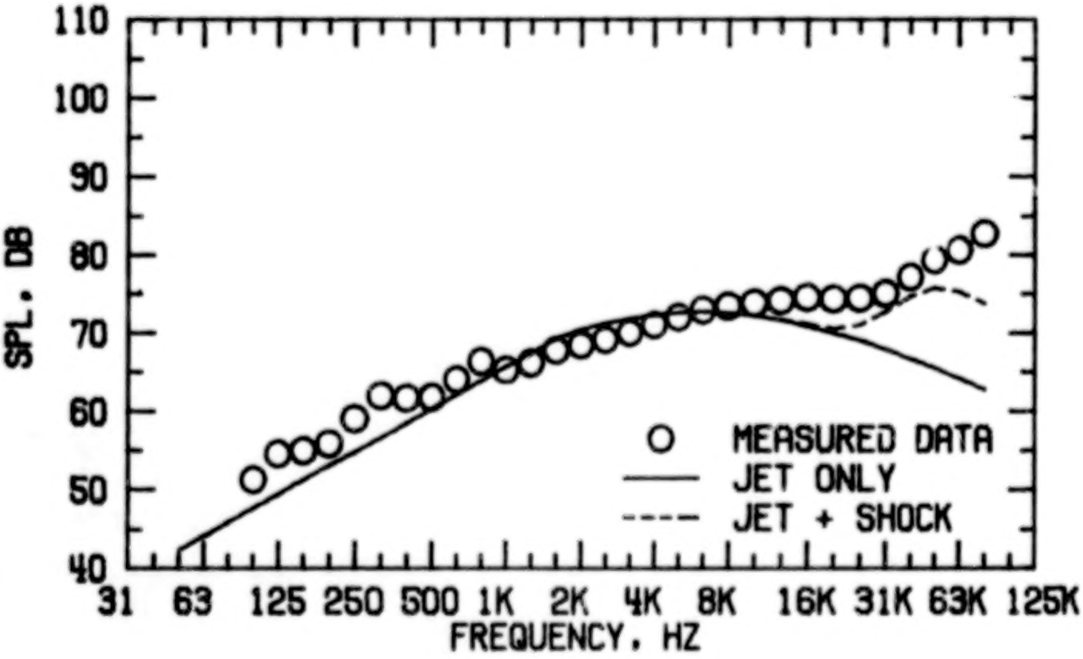

FIGURE B3 . SPECTRA COMPARISON FOR CASE 8
(C) DIRECTIVITY ANGLE = 90 DEGREES

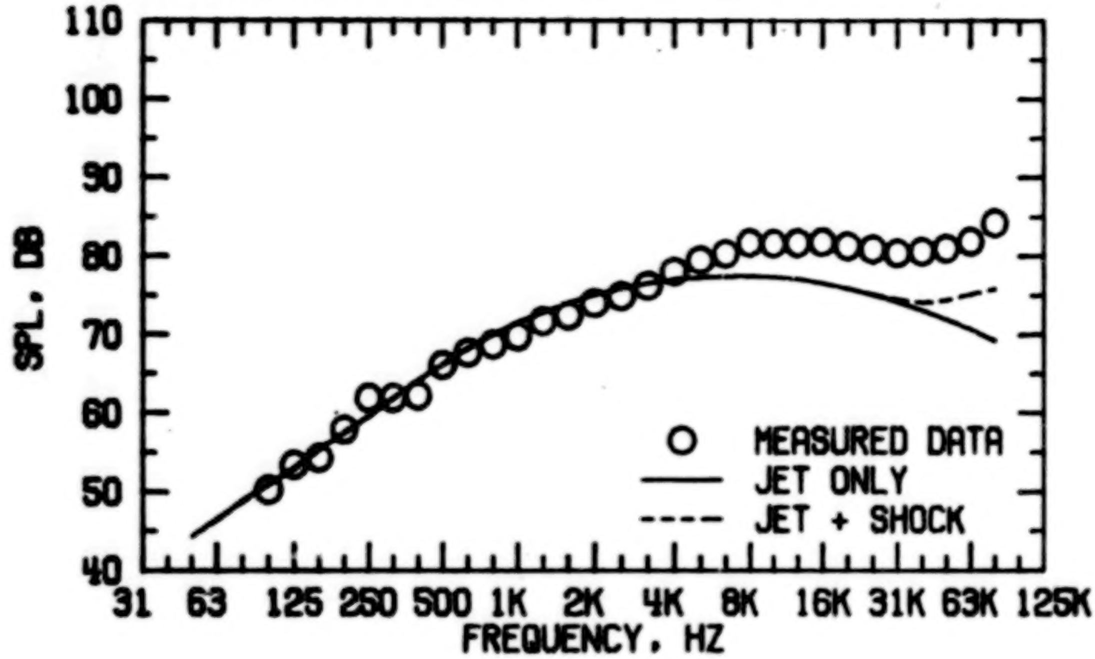

FIGURE B3 . SPECTRA COMPARISON FOR CASE 8
(D) DIRECTIVITY ANGLE = 120 DEGREES

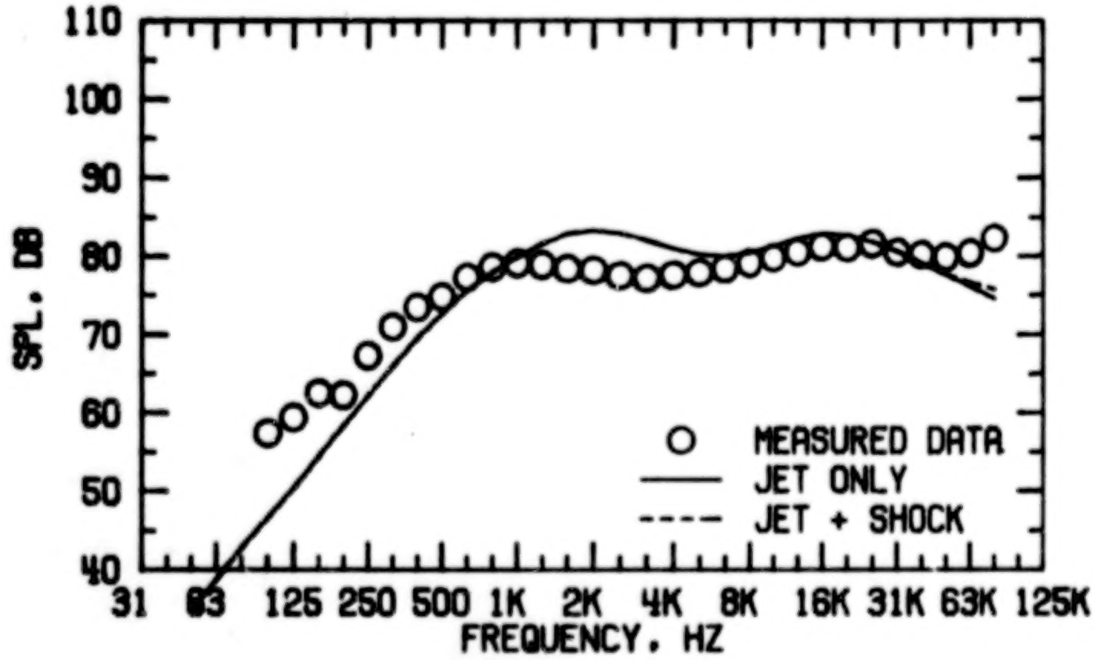

FIGURE B3 . SPECTRA COMPARISON FOR CASE 8
(E) DIRECTIVITY ANGLE = 150 DEGREES

FLOW PROPERTIES FOR CASE 9
NOZZLE MODEL 2

FORWARD FLIGHT VELOCITY, V_A = 129.5 M/S

	TEMPERATURE T_T, DEG K	VELOCITY V, M/S	MASS FLOW W, KG/S	P_T/P_A
PRIMARY	388.7	295.3	.3810	1.5140
SECONDARY	705.9	637.6	.4127	3.2120
EQUIVALENT	553.6	473.3	.7937	

REFERENCE RADIUS = 45.7 M

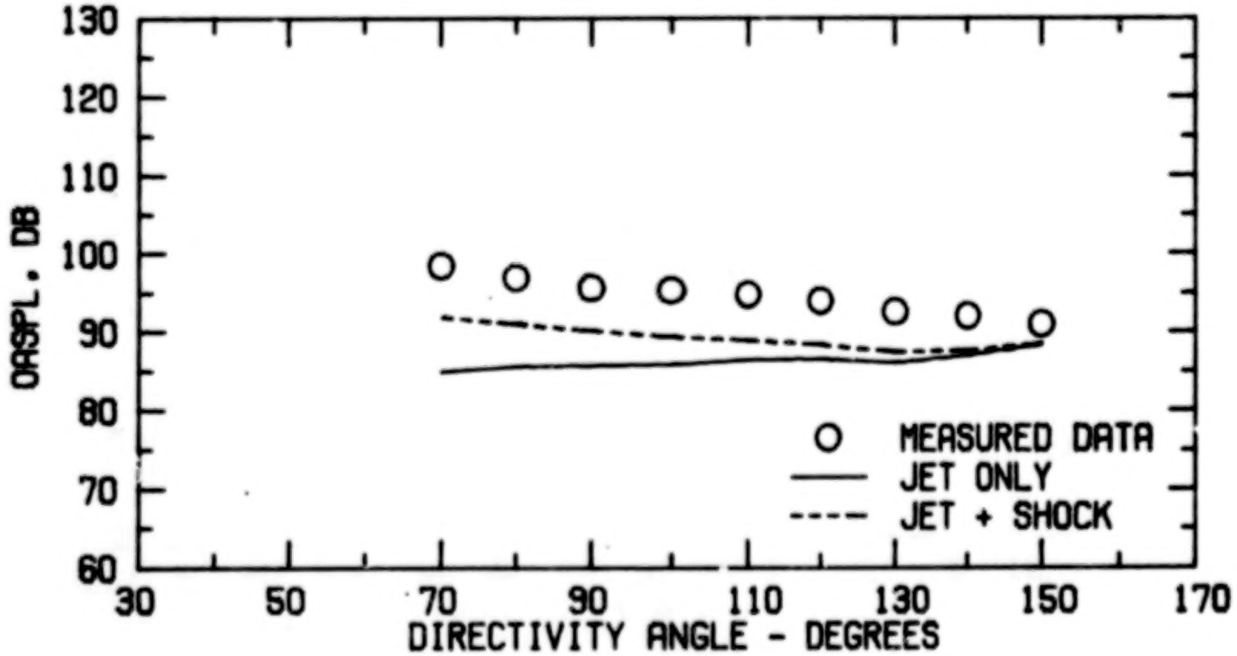

FIGURE B4 . SPECTRA COMPARISON FOR CASE 9
(A) FLOW PROPERTIES AND DIRECTIVITY PLOT

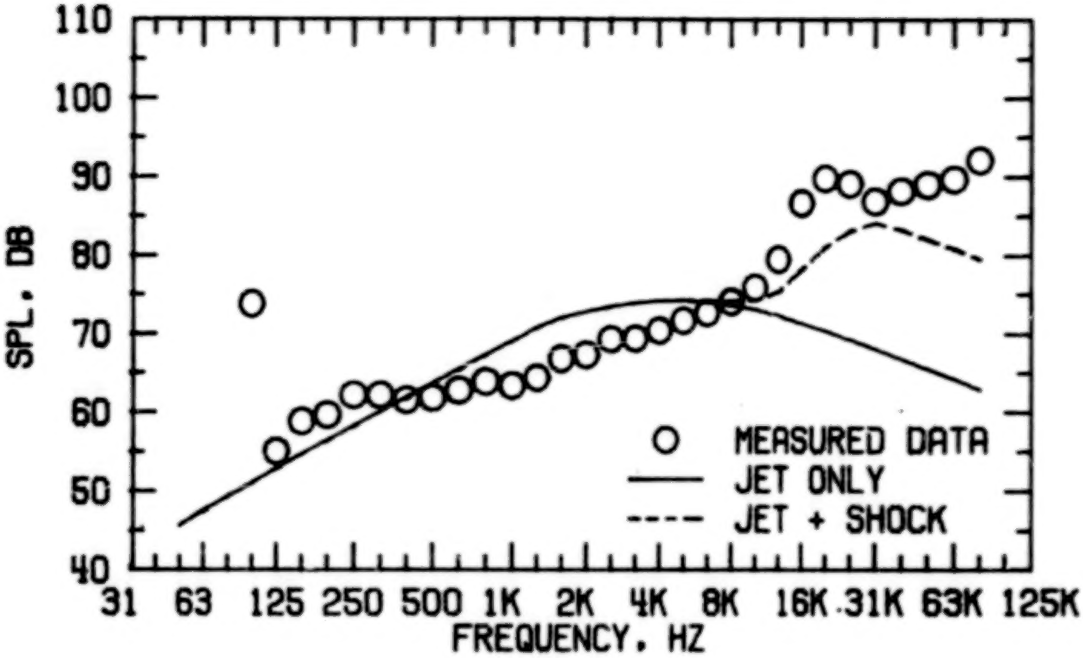

FIGURE B4 . SPECTRA COMPARISON FOR CASE 9
(B) DIRECTIVITY ANGLE = 70 DEGREES

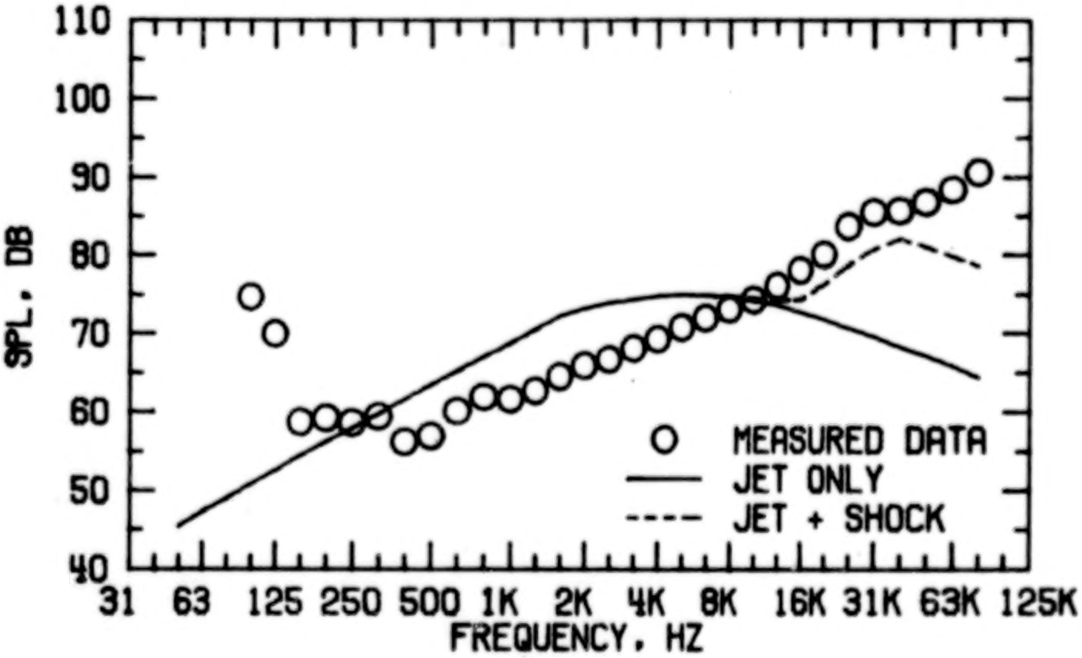

FIGURE B4 . SPECTRA COMPARISON FOR CASE 9
(C) DIRECTIVITY ANGLE = 90 DEGREES

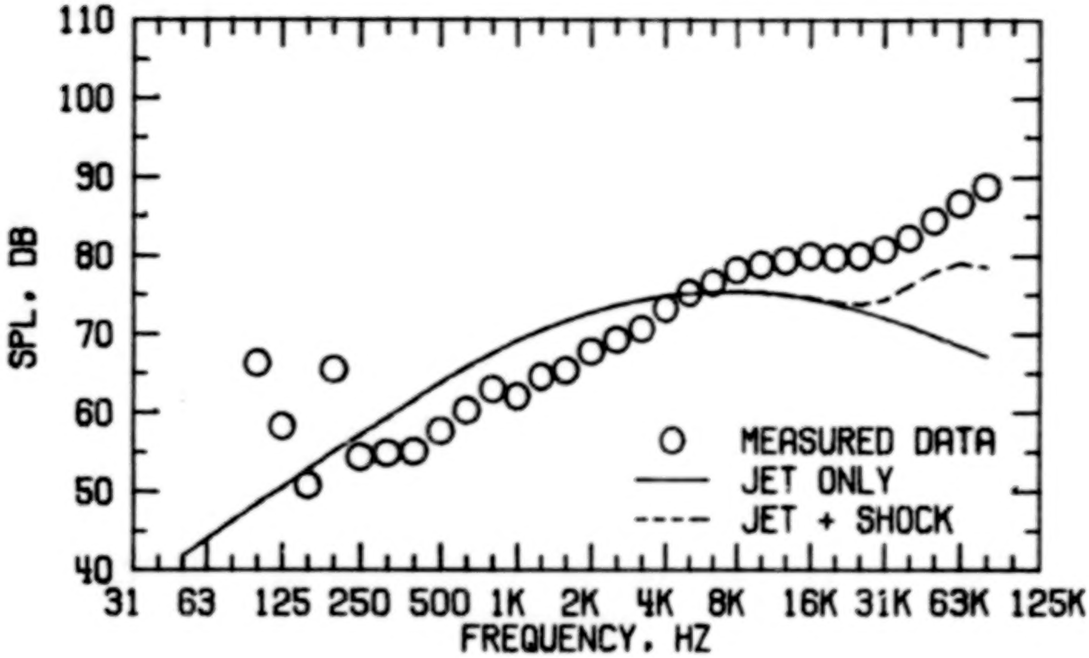

FIGURE B4 . SPECTRA COMPARISON FOR CASE 9
(D) DIRECTIVITY ANGLE = 120 DEGREES

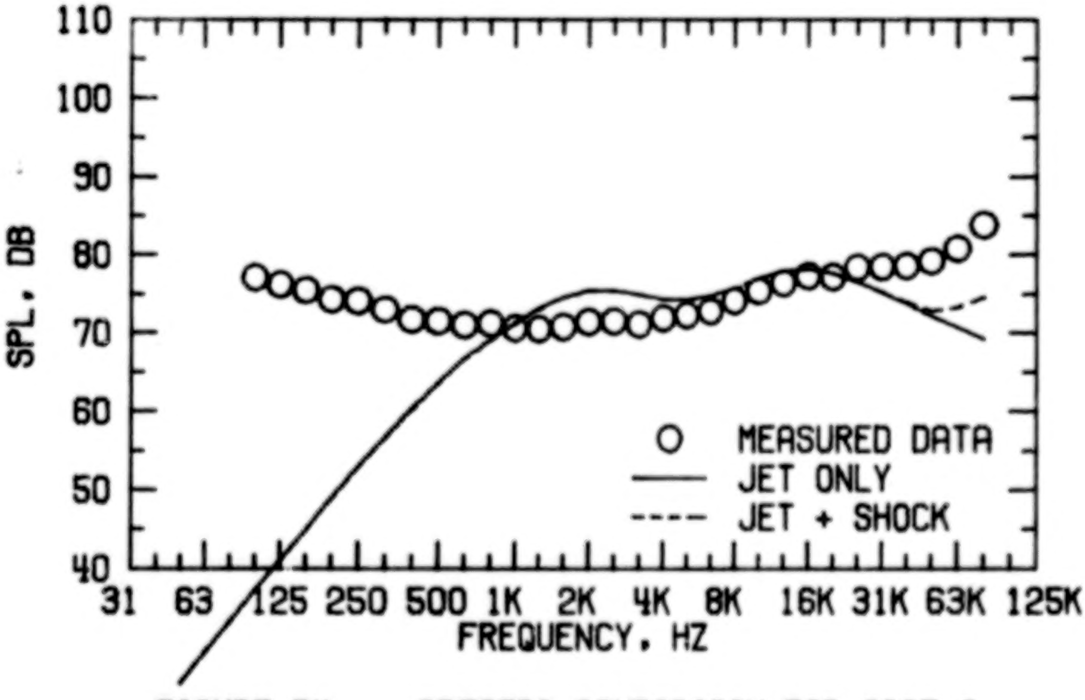

FIGURE B4 . SPECTRA COMPARISON FOR CASE 9
(E) DIRECTIVITY ANGLE = 150 DEGREES

FLOW PROPERTIES FOR CASE 13
NOZZLE MODEL 4

FORWARD FLIGHT VELOCITY, V_A = 61.5 M/S

	TEMPERATURE T_T, DEG K	VELOCITY V, M/S	MASS FLOW W, KG/S	P_T/P_A
PRIMARY	393.1	299.0	.3538	1.5220
SECONDARY	698.1	633.3	.5851	3.2030
EQUIVALENT	583.2	507.3	.9389	

REFERENCE RADIUS = 45.7 M

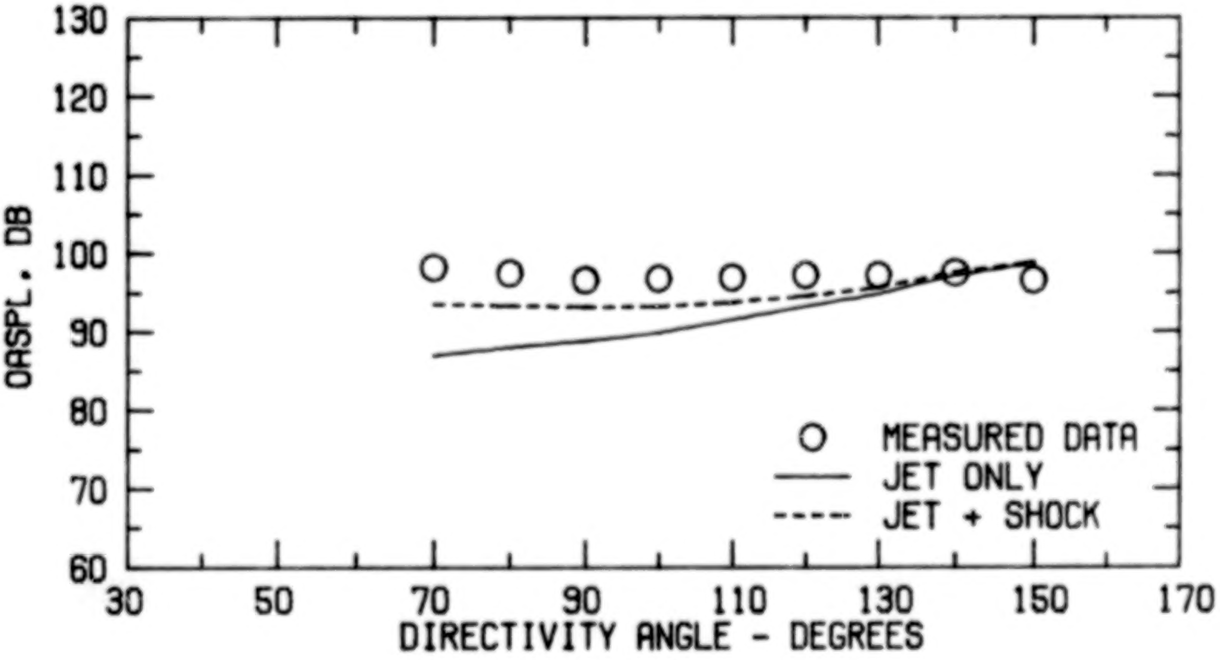

FIGURE B5 . SPECTRA COMPARISON FOR CASE 13
(A) FLOW PROPERTIES AND DIRECTIVITY PLOT

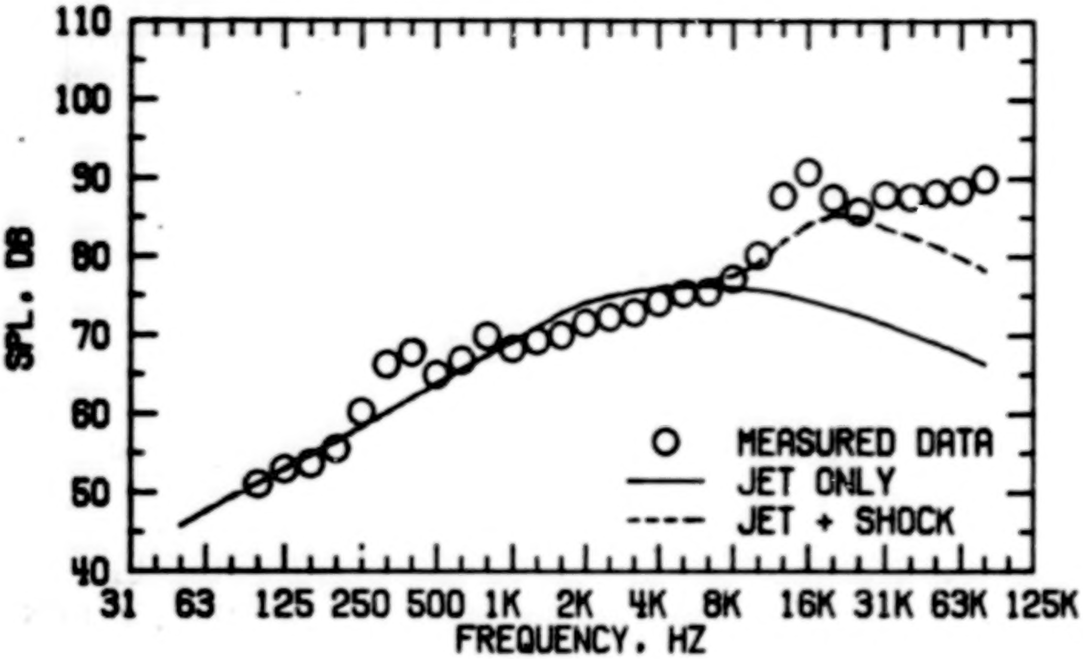

FIGURE B5 . SPECTRA COMPARISON FOR CASE 13
(B) DIRECTIVITY ANGLE = 70 DEGREES

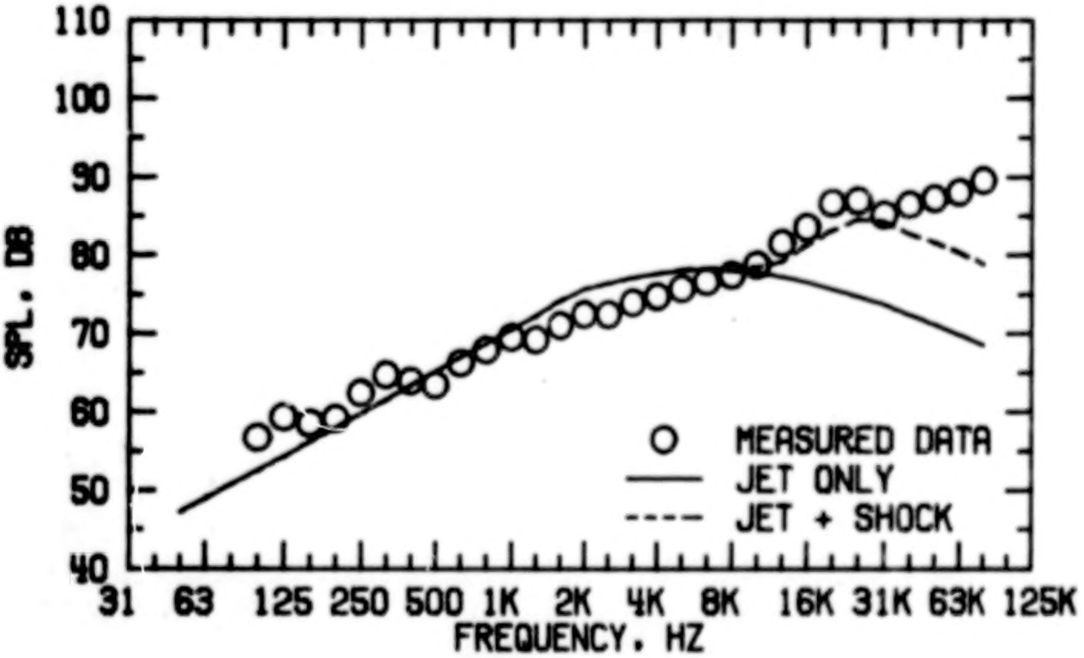

FIGURE B5 . SPECTRA COMPARISON FOR CASE 13
(C) DIRECTIVITY ANGLE = 90 DEGREES

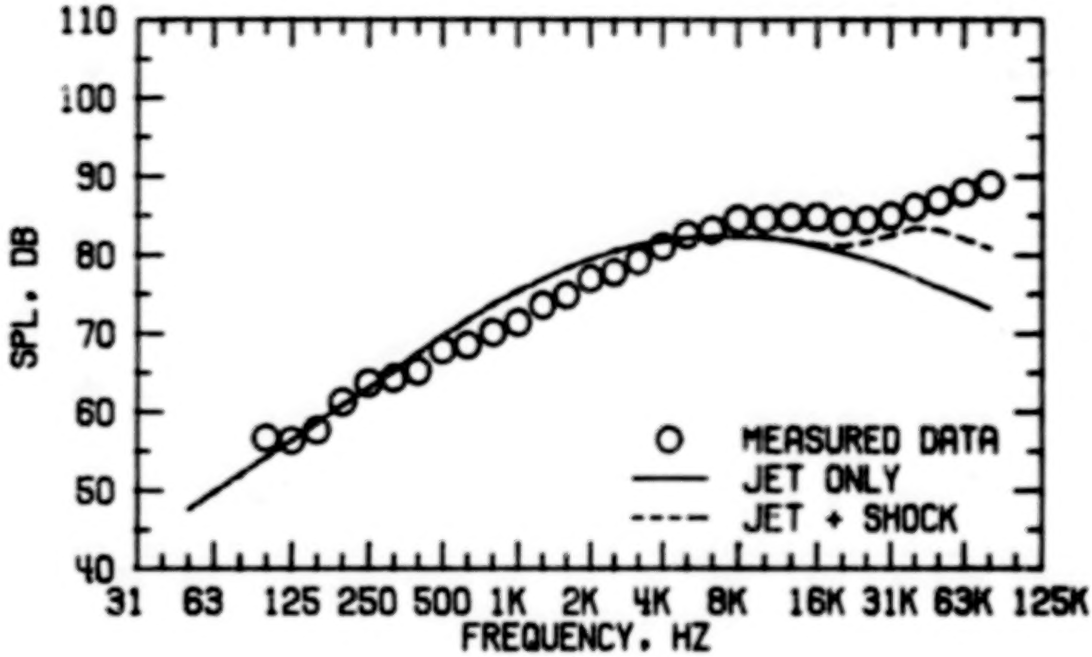

FIGURE B5 . SPECTRA COMPARISON FOR CASE 13
(D) DIRECTIVITY ANGLE = 120 DEGREES

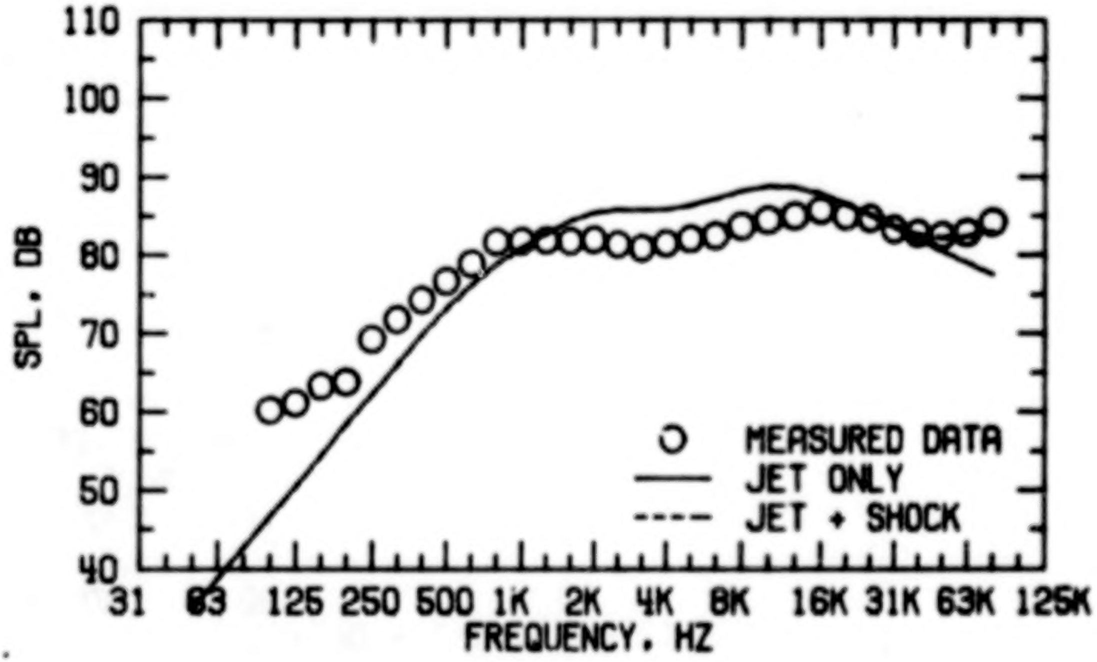

FIGURE B5 . SPECTRA COMPARISON FOR CASE 13
(E) DIRECTIVITY ANGLE = 150 DEGREES

FLOW PROPERTIES FOR CASE 14
NOZZLE MODEL 4

FORWARD FLIGHT VELOCITY, V_A = 61.2 M/S

	TEMPERATURE T_T, DEG K	VELOCITY V, M/S	MASS FLOW W, KG/S	P_T/P_A
PRIMARY	395.3	299.3	.3311	1.5190
SECONDARY	708.7	575.7	.4535	2.5060
EQUIVALENT	576.5	459.1	.7847	

REFERENCE RADIUS = 45.7 M

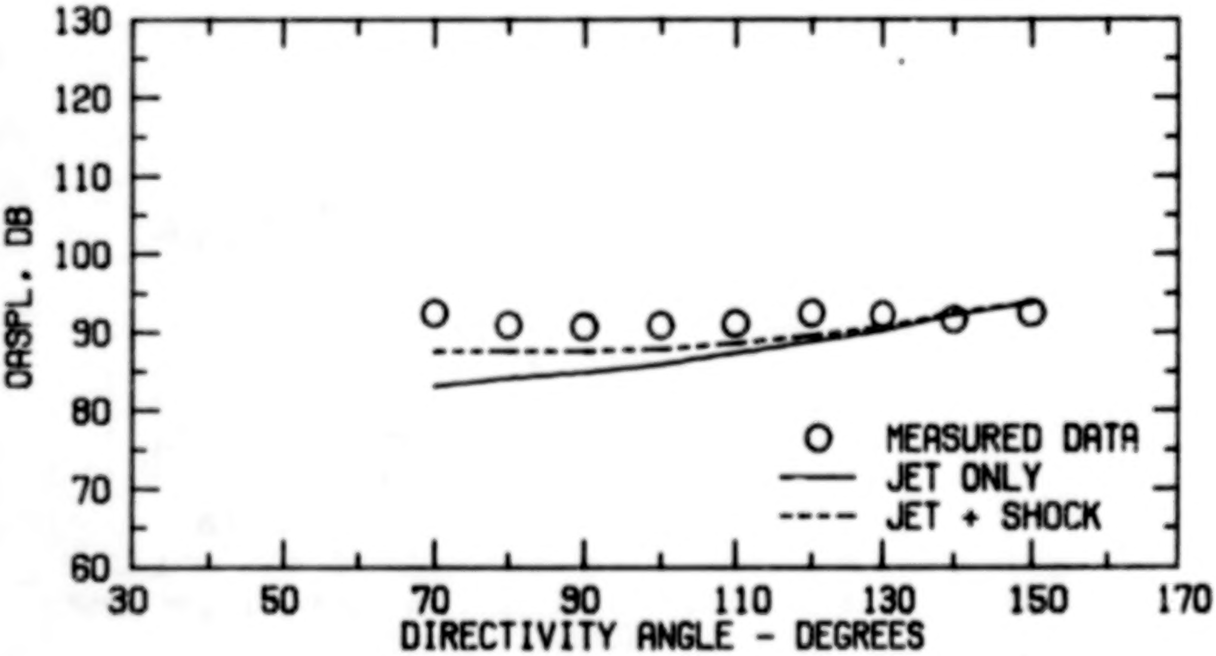

FIGURE B6 . SPECTRA COMPARISON FOR CASE 14
(A) FLOW PROPERTIES AND DIRECTIVITY PLOT

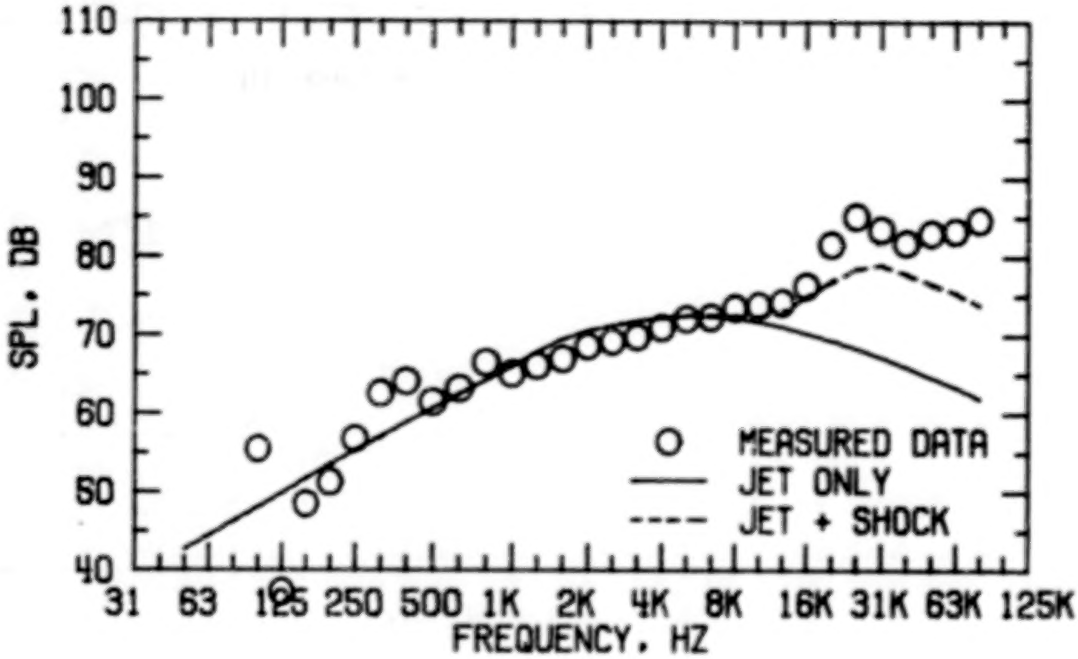

FIGURE B6 . SPECTRA COMPARISON FOR CASE 14
(B) DIRECTIVITY ANGLE = 70 DEGREES

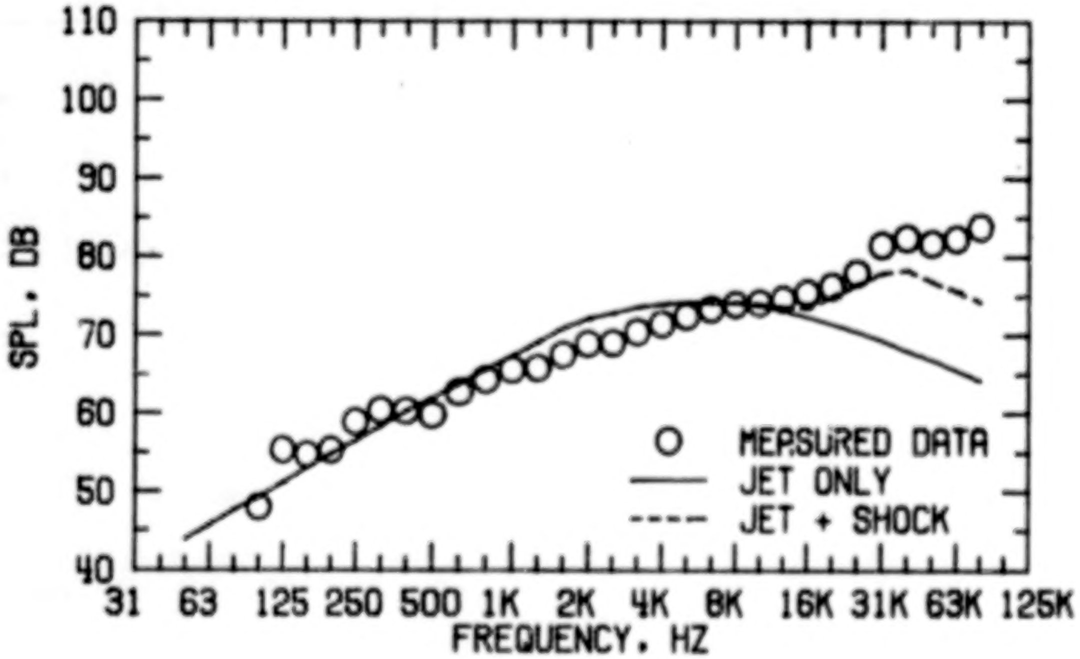

FIGURE B6 . SPECTRA COMPARISON FOR CASE 14
(C) DIRECTIVITY ANGLE = 90 DEGREES

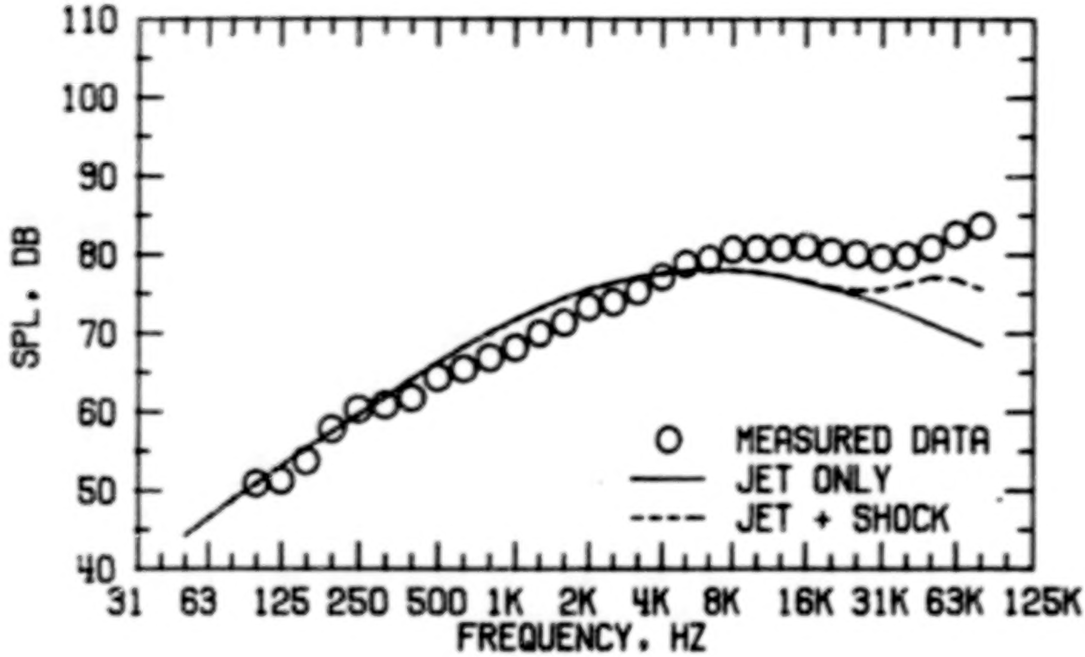

FIGURE B6 . SPECTRA COMPARISON FOR CASE 14
(D) DIRECTIVITY ANGLE = 120 DEGREES

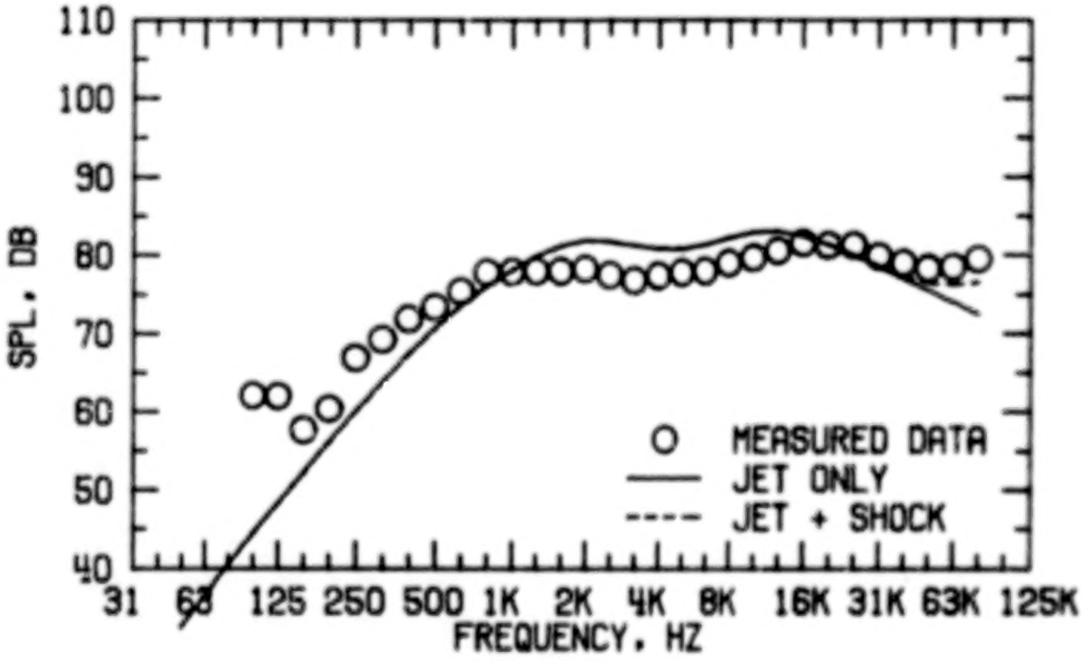

FIGURE B6 . SPECTRA COMPARISON FOR CASE 14
(E) DIRECTIVITY ANGLE = 150 DEGREES

FLOW PROPERTIES FOR CASE 18
NOZZLE MODEL 4

FORWARD FLIGHT VELOCITY.V_A = 103.6 M/S

	TEMPERATURE T_T, DEG K	VELOCITY V, M/S	MASS FLOW W, KG/S	P_T/P_A
PRIMARY	402.0	304.1	.3039	1.5300
SECONDARY	702.6	635.5	.5261	3.2060
EQUIVALENT	592.5	514.2	.8300	

REFERENCE RADIUS = 45.7 M

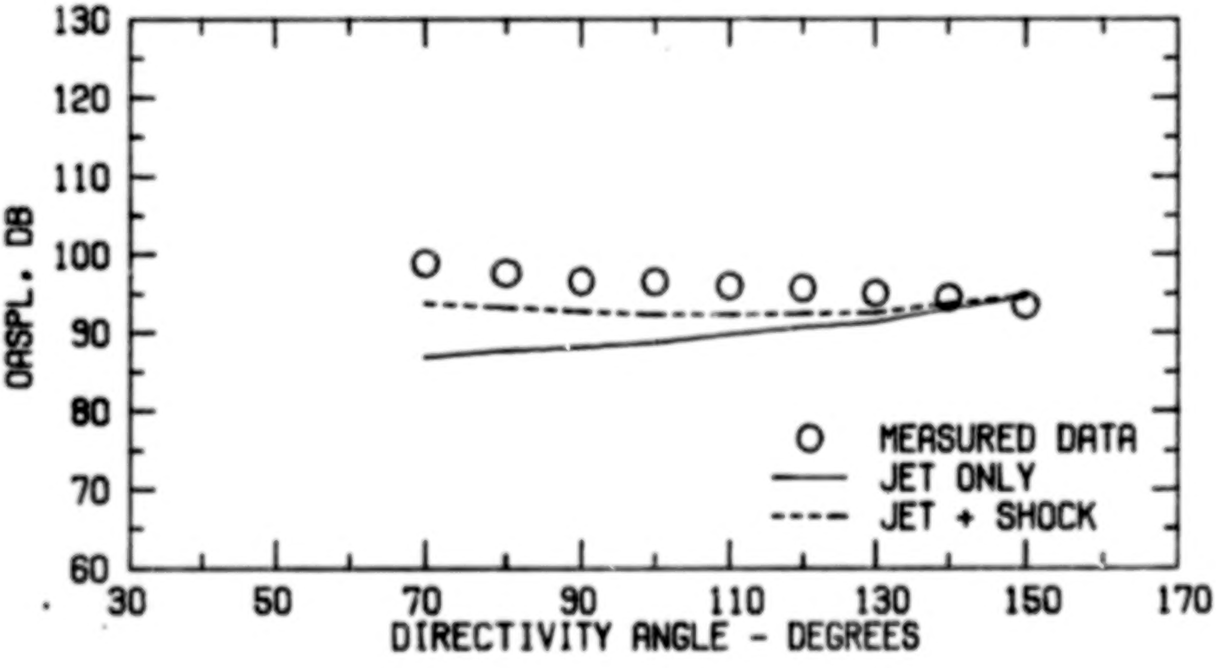

FIGURE B7 . SPECTRA COMPARISON FOR CASE 18
(A) FLOW PROPERTIES AND DIRECTIVITY PLOT

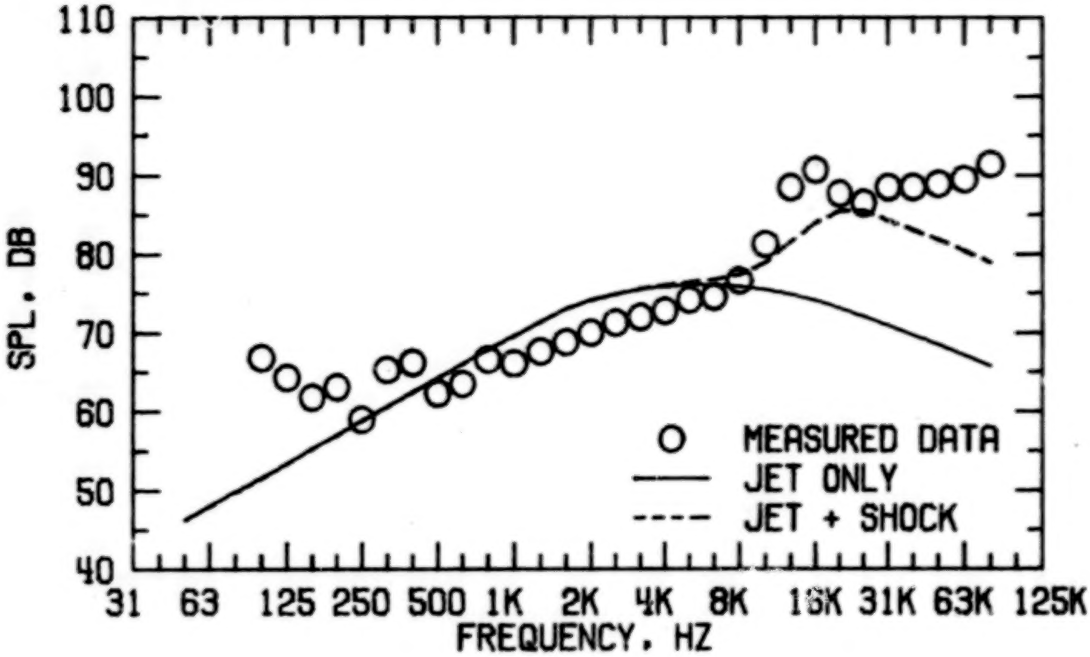

FIGURE B7 . SPECTRA COMPARISON FOR CASE 18
(B) DIRECTIVITY ANGLE = 70 DEGREES

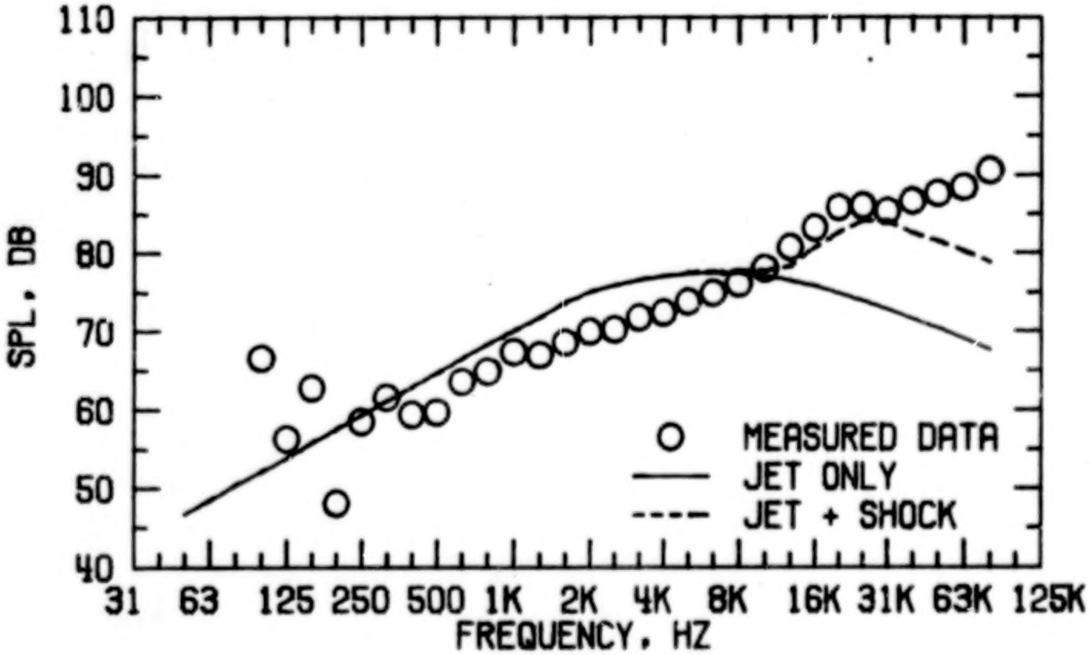

FIGURE B7 . SPECTRA COMPARISON FOR CASE 18
(C) DIRECTIVITY ANGLE = 90 DEGREES

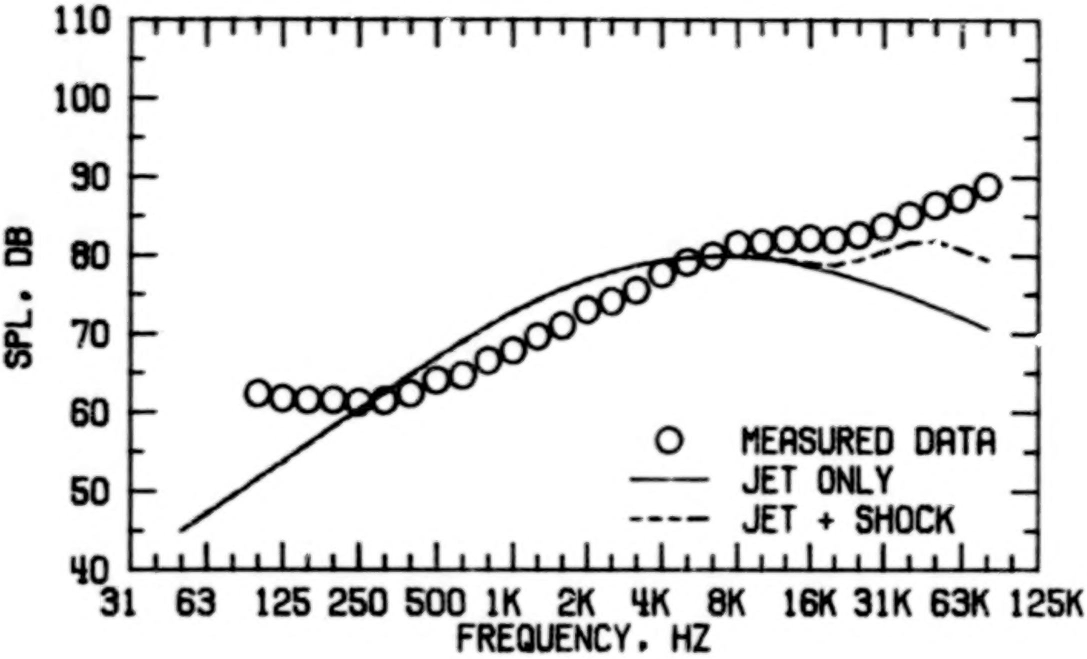

FIGURE B7 . SPECTRA COMPARISON FOR CASE 18
(D) DIRECTIVITY ANGLE = 120 DEGREES

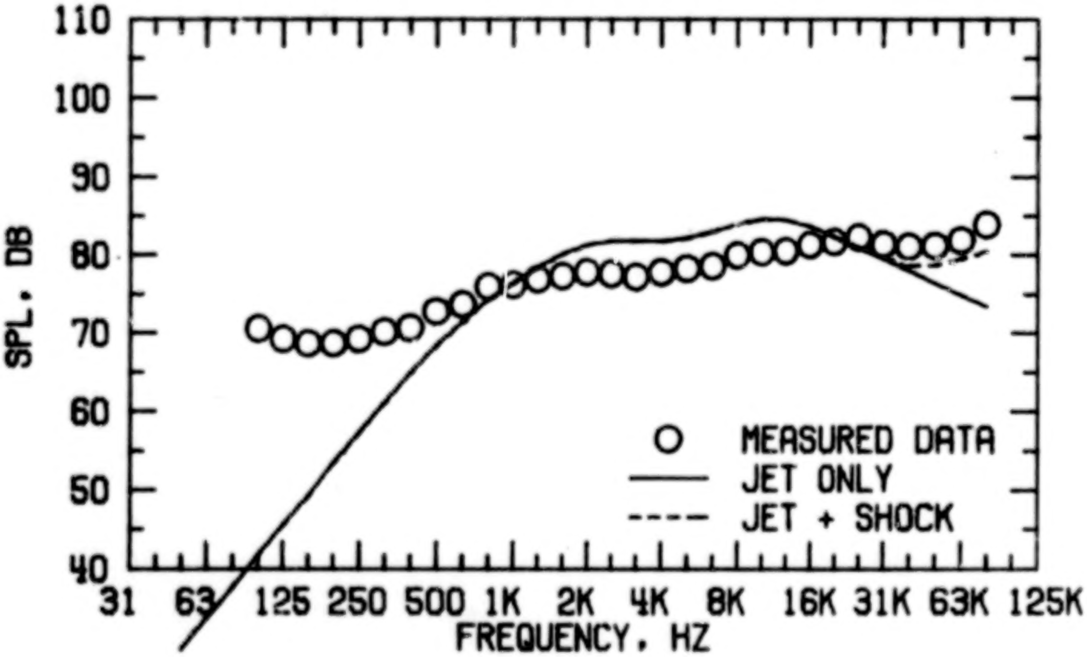

FIGURE B7 . SPECTRA COMPARISON FOR CASE 18
(E) DIRECTIVITY ANGLE = 150 DEGREES

FLOW PROPERTIES FOR CASE 20
NOZZLE MODEL 4

FORWARD FLIGHT VELOCITY, V_A = 129.8 M/S

	TEMPERATURE T_T, DEG K	VELOCITY V, M/S	MASS FLOW W, KG/S	P_T/P_A
PRIMARY	388.7	297.7	.2993	1.5250
SECONDARY	709.2	576.3	.3900	2.5110
EQUIVALENT	570.0	455.4	.6894	

REFERENCE RADIUS = 45.7 M

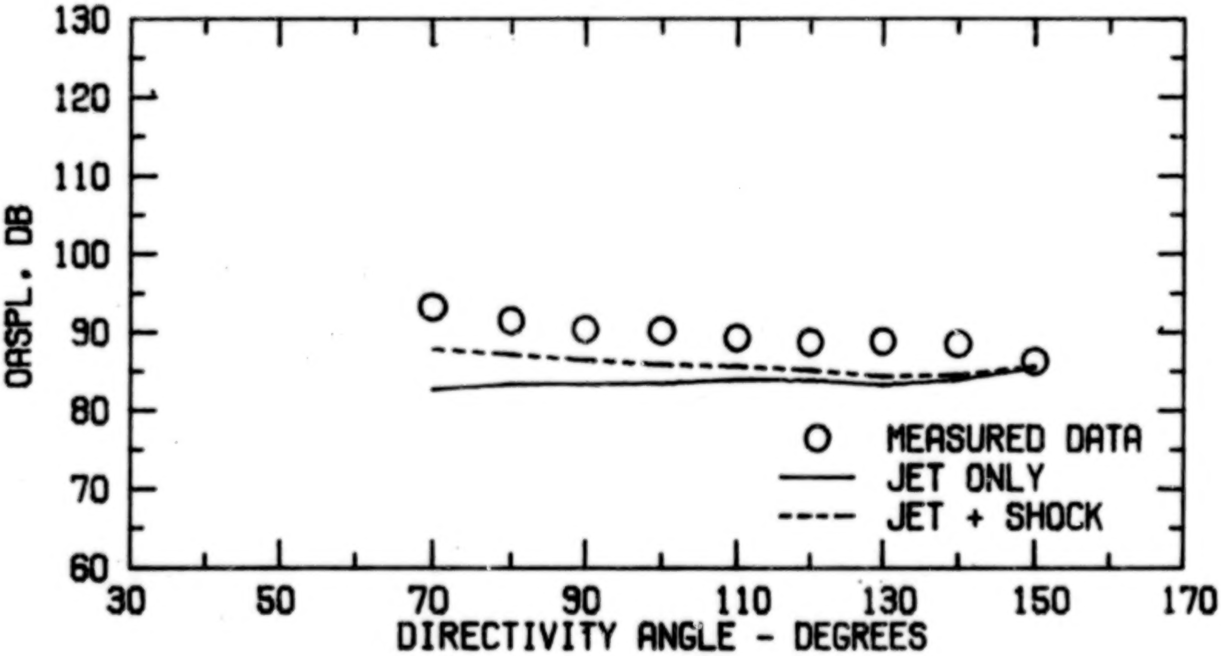

FIGURE B8 . SPECTRA COMPARISON FOR CASE 20
(A) FLOW PROPERTIES AND DIRECTIVITY PLOT

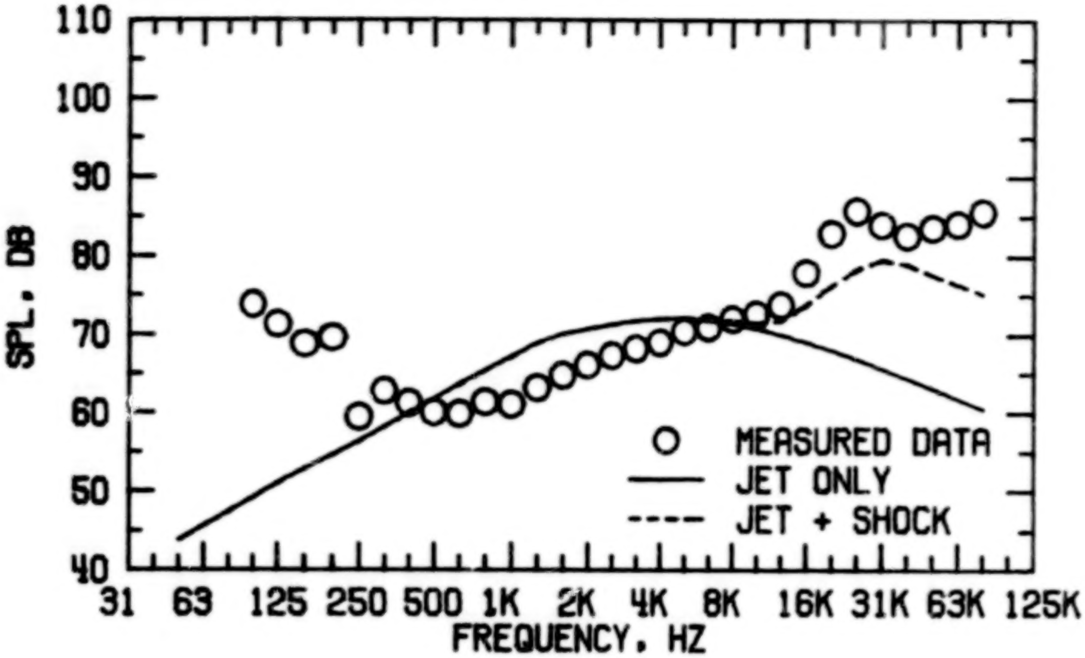

FIGURE B8 . SPECTRA COMPARISON FOR CASE 20
(B) DIRECTIVITY ANGLE = 70 DEGREES

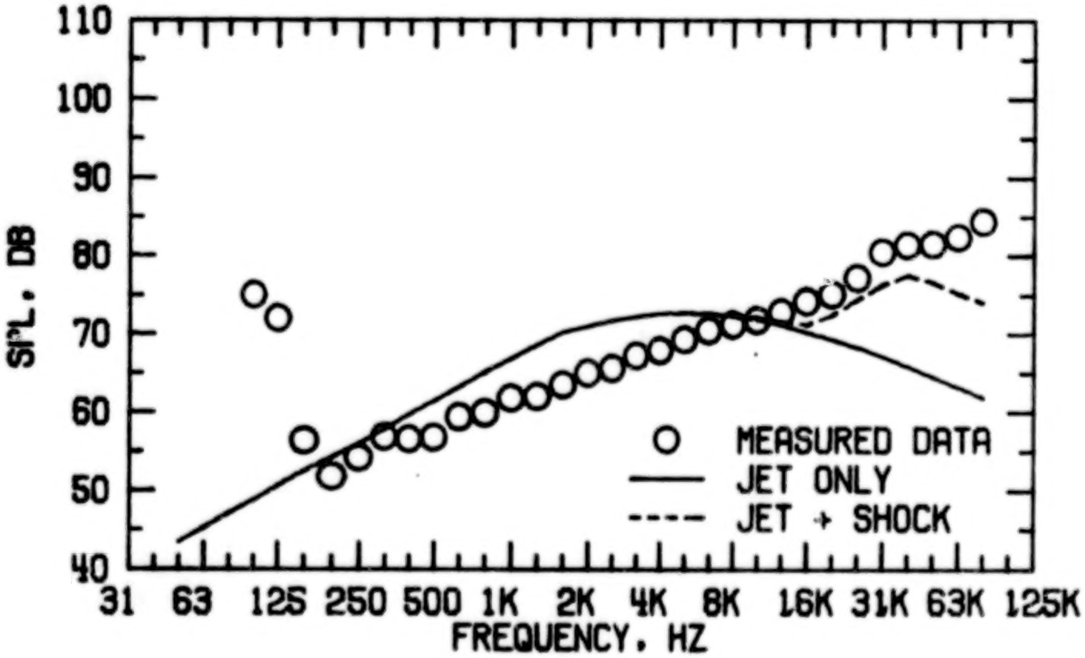

FIGURE B8 . SPECTRA COMPARISON FOR CASE 20
(C) DIRECTIVITY ANGLE = 90 DEGREES

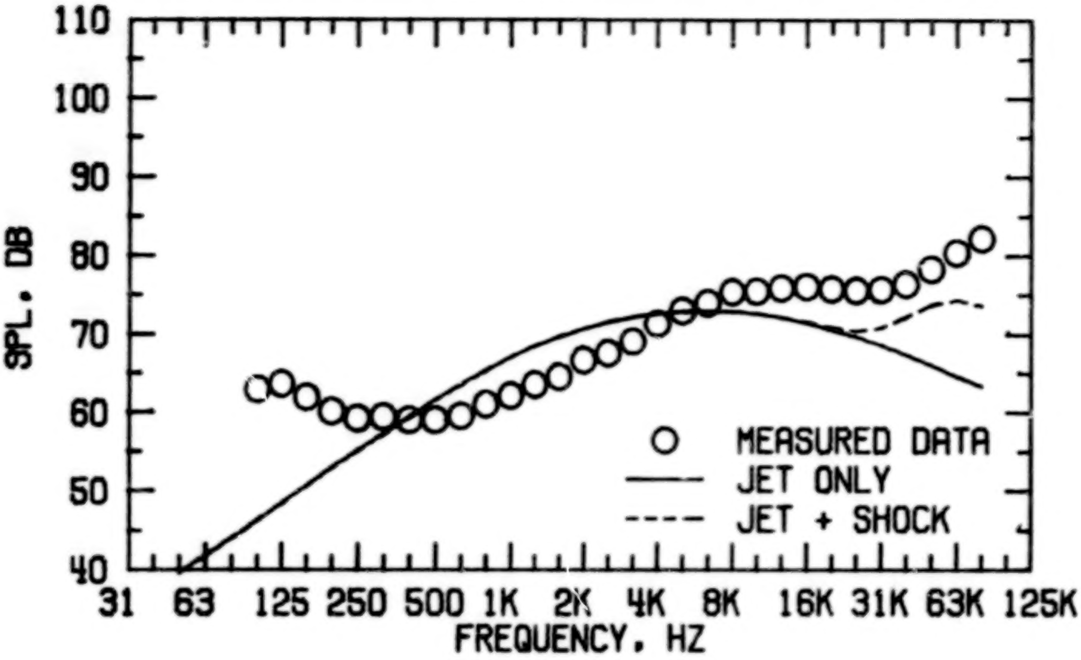

FIGURE B8 . SPECTRA COMPARISON FOR CASE 20
(D) DIRECTIVITY ANGLE = 120 DEGREES

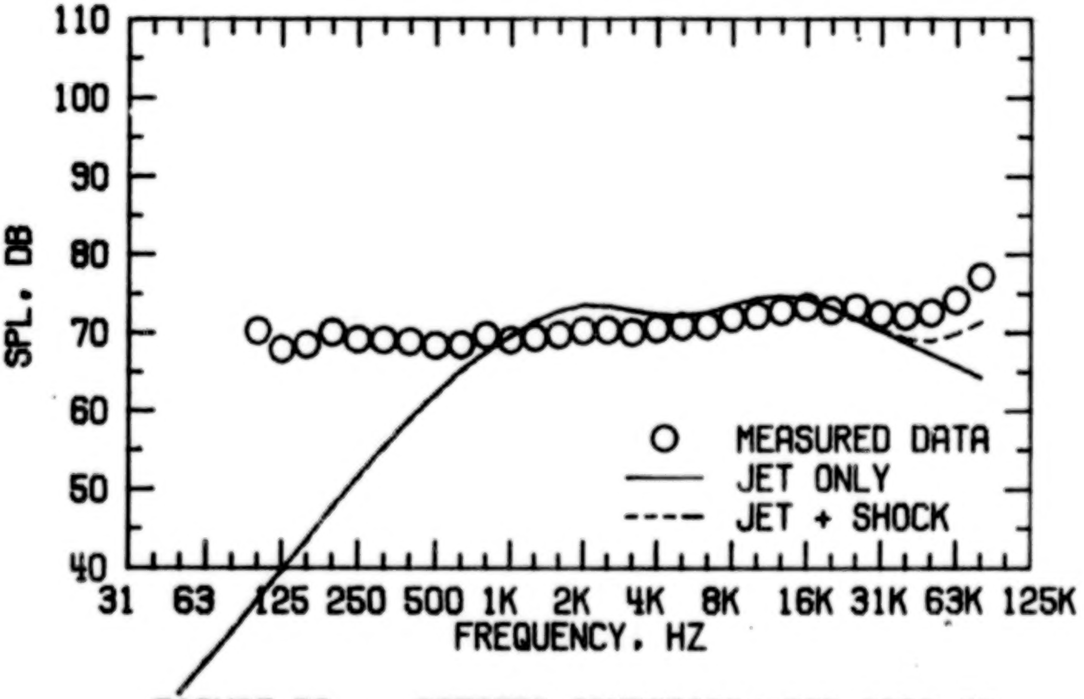

FIGURE B8 . SPECTRA COMPARISON FOR CASE 20
(E) DIRECTIVITY ANGLE = 150 DEGREES

*U.S. GOVERNMENT PRINTING OFFICE: 1979 - 635-004/31

1. Report No. NASA CR-3176	2. Government Accession No.	3. Recipient's Catalog No.

4. Title and Subtitle

A Method for Predicting the Noise Levels of Coannular Jets With Inverted Velocity Profiles

5. Report Date

October 1979

6. Performing Organization Code

7. Author(s)

James W. Russell

8. Performing Organization Report No.

9. Performing Organization Name and Address

Kentron International, Inc.
Hampton Technical Center
Hampton, Virginia 23666

10. Work Unit No.

11. Contract or Grant No.

NAS1-13500

12. Sponsoring Agency Name and Address

National Aeronautics and Space Administration
Washington, DC 20546

13. Type of Report and Period Covered

Contractor Report

14. Army Project No.

15. Supplementary Notes

Langley Technical Monitor: William E. Zorumski

Topical Report

16. Abstract

This report presents a method for predicting the noise characteristics of a coannular jet exhaust nozzle with an inverted velocity profile. The method equates the coannular jet to a single stream equivalent jet with the same mass flow, energy, and thrust. The acoustic characteristics of the coannular jet are then related to the acoustic characteristics of the single jet. The method also includes forward flight effects by incorporating a forward velocity exponent, a Doppler amplification factor, and a Strouhal frequency shift.

This prediction method was evaluated against model test data including 48 static cases and 22 wind tunnel cases. For the static cases and the low forward velocity wind tunnel cases the spectral mean square pressure correlation coefficients were generally greater than 90 percent and the spectral sound pressure level standard deviations were generally less than 3 dB. Also the correlation coefficient and standard deviation were not affected by changes in equivalent jet velocity.

The prediction method is limited to equivalent jet velocities which range from 0.85 to 2.5 times the local ambient speed of sound. The outer to inner stream nozzle exit area ratio should not be less than 0.4 or greater than 2.5. The outer to inner stream velocity ratio should not be less than 1.0. The prediction method is designed for obtaining free field unattenuated source noise levels.

17. Key Words (Suggested by Author(s))

Jet Noise
Noise Prediction
Variable Cycle Engine

18. Distribution Statement

Unclassified - Unlimited

Subject Category 71

19. Security Classif. (of this report) Unclassified	20. Security Classif. (of this page) Unclassified	21. No. of Pages 154	22. Price* $8.00

*For sale by the National Technical Information Service, Springfield, Virginia 22161

END

June 17, 1981